FINAL REPORT

A Practical Approach for Remediation Performance Assessment and Optimization at DNAPL Sites for Early Identification and Correction of Problems Considering Uncertainty

SERDP Project ER-2310

JULY 2018

Jack Parker
University of Tennessee

Ungtae Kim
Cleveland State University

Bob Borden
Water Resources & Environmental Engineering

Alyson Fortune
TerraTherm, Inc.

Distribution Statement A
This document has been cleared for public release

SERDP
DOD ▪ EPA ▪ DOE

Page Intentionally Left Blank

This report was prepared under contract to the Department of Defense Strategic Environmental Research and Development Program (SERDP). The publication of this report does not indicate endorsement by the Department of Defense, nor should the contents be construed as reflecting the official policy or position of the Department of Defense. Reference herein to any specific commercial product, process, or service by trade name, trademark, manufacturer, or otherwise, does not necessarily constitute or imply its endorsement, recommendation, or favoring by the Department of Defense.

Page Intentionally Left Blank

REPORT DOCUMENTATION PAGE

Form Approved
OMB No. 0704-0188

The public reporting burden for this collection of information is estimated to average 1 hour per response, including the time for reviewing instructions, searching existing data sources, gathering and maintaining the data needed, and completing and reviewing the collection of information. Send comments regarding this burden estimate or any other aspect of this collection of information, including suggestions for reducing the burden, to Department of Defense, Washington Headquarters Services, Directorate for Information Operations and Reports (0704-0188), 1215 Jefferson Davis Highway, Suite 1204, Arlington, VA 22202-4302. Respondents should be aware that notwithstanding any other provision of law, no person shall be subject to any penalty for failing to comply with a collection of information if it does not display a currently valid OMB control number.
PLEASE DO NOT RETURN YOUR FORM TO THE ABOVE ADDRESS.

1. REPORT DATE *(DD-MM-YYYY)*	2. REPORT TYPE	3. DATES COVERED *(From - To)*
07/01/2018	SERDP Final Report	9/26/2013 - 9/27/2017

4. TITLE AND SUBTITLE
A Practical Approach for Remediation Performance Assessment and Optimization at DNAPL Sites for Early Identification and Correction of Problems Considering Uncertainty

5a. CONTRACT NUMBER
Contract: 13-C-0069

5b. GRANT NUMBER

5c. PROGRAM ELEMENT NUMBER

6. AUTHOR(S)
Jack Parker

5d. PROJECT NUMBER
ER-2310

5e. TASK NUMBER

5f. WORK UNIT NUMBER

7. PERFORMING ORGANIZATION NAME(S) AND ADDRESS(ES)
University of Tennessee
62 Perkins Hall
Knoxville, TN 37996

8. PERFORMING ORGANIZATION REPORT NUMBER
ER-2310

9. SPONSORING/MONITORING AGENCY NAME(S) AND ADDRESS(ES)
Strategic Environmental Research and Development Program
4800 Mark Center Drive, Suite 17D03
Alexandria, VA 22350-3605

10. SPONSOR/MONITOR'S ACRONYM(S)
SERDP

11. SPONSOR/MONITOR'S REPORT NUMBER(S)
ER-2310

12. DISTRIBUTION/AVAILABILITY STATEMENT
Distribution A; unlimited public release

13. SUPPLEMENTARY NOTES

14. ABSTRACT
The objective of this project was to develop and test a methodology to periodically assess and optimize remediation and monitoring strategies at US Department of Defense (DoD) dense nonaqueous phase (DNAPL) contaminated sites with remedies in place (RIP). Methods were developed to model cost and performance of source zone and dissolved plume remediation technologies—including thermal treatment, chemical oxidation, enhanced bioremediation, and reactive barriers—and to optimize system operation and monitoring to meet user-defined cleanup criteria with minimum life-cycle cost, considering uncertainty in performance predictions using a stochastic optimization approach.

15. SUBJECT TERMS
Remediation Performance Assessment, Optimization, DNAPL Sites, Early Identification and Correction of Problems Considering Uncertainty

16. SECURITY CLASSIFICATION OF:			17. LIMITATION OF ABSTRACT	18. NUMBER OF PAGES	19a. NAME OF RESPONSIBLE PERSON
a. REPORT	b. ABSTRACT	c. THIS PAGE			Jack Parker
UNCLASS	UNCLASS	UNCLASS	UNCLASS	287	19b. TELEPHONE NUMBER *(Include area code)* 865-974-7718

Page Intentionally Left Blank

Acknowledgements

The idea for this project grew from a 2006 SERDP/ESTCP workshop on *Reducing the Uncertainty of DNAPL Source Zone Remediation,* which crystallized the need for an integrated approach to site remediation that couples an array of simulation models with calibration, error propagation, and stochastic optimization algorithms to rigorously assess complex tradeoffs and interactions among various remediation technologies and operational strategies, performance monitoring strategies, uncertainty in measurements and model predictions, and different approaches to the formulation of decision rules for terminating individual remediation technologies and site-wide compliance.

Substantial progress toward this goal was realized in SERDP project ER-1611 with implementation and field testing of the Stochastic Cost Optimization Toolkit (SCOToolit v.1). The current project (ER-2310) advanced the previous effort further by significantly enhancing the model capability, analyzing more field data, and undertaking tech transfer activities with help from many quarters.

Encouragement for the undertaking from Andrea Leeson (SERDP/ESTCP) and members of the SERDP Science Advisory Board have been helpful throughout the effort. Dave Becker (USACE), Dan Waddill (NAVFAC), and Phil Hunter (AFCEE) served as technical advisers and liaisons with the Army, Navy and Air Force, respectively.

The ultimate success of this project must be credited in large part to co-PI Ungtae Kim (Cleveland State University) who worked tirelessly, efficiently and patiently to implement and integrate the many program components and functions through many iterations as our understanding of the complex stochastic decision process grew, to obtain increased efficiency, improved remediation design reliability, and reduced costs.

As co-PI of ER-1611, Peter Kitanidis (Stanford University) and students under his direction (Mike Cardiff, Xiaoyi Liu and Jonghyun Lee) implemented initial versions of the coupled calibration and stochastic cost optimization code and investigated the statistical value of additional site characterization data. Dr. Kitanidis' involvement continued through collaboration between ER-2310 and ER-2313, including beta-testing of SCOToolkit v.2 and application to data from a high resolution "virtual sites." Other personnel from ER-2313 included Mike Kavanaugh, Dave Reynolds, Dave Majors, Cathy Crea and James Rayner (Geosyntec Inc.) and Bernard Kueper and Kevin Mumford (Queens University).

Bob Borden (North Carolina State University) and Michelle Crimi (Clarkson University) contributed to the development and testing of ISCO performance/cost model. Alyson Fortune, Steffen Griepke, Jim Galligan and Ralph Baker (TerraTherm Inc.) and Greg Beyke (TRS Group) provided invaluable guidance on operation procedures, costs and performance of thermal treatment methods for DNAPL sources.

Information on historical and ongoing remedial actions at Joint Base Fort Lewis McChord was provided by Bill Meyers, Jim Gillie, and Tom Lyncott (IMCOM), Mike Truex (PNNL), Mike Annable (University of Florida) and Tamzen Macbeth (CDM). Jean Chytil, Chuck Coyle, Dave Becker, Jeff Skogg, Delma Stoner, and Lynn Jenkins (USACE) collaborated on the analysis of remediation efforts at the Atlas Missile Site 11 in Nunn, Colorado. Aleisa Bloom and Bill Ahlers (ORNL) and Bob Lyon (USR Corp.) provided valuable practical insight, operational details and cost parameters on bioremediation using emulsified vegetable oil injection and its application at Dover AFB in Delaware.

This work was performed under contract number W912HQ-13-C-0069 administered by the U.S. Army Corps of Engineers.

Jack Parker
Knoxville, Tennessee

Abstract

Objective. The objective of this project was to develop and test a methodology to periodically assess and optimize remediation and monitoring strategies at US Department of Defense (DoD) dense nonaqueous phase (DNAPL) contaminated sites with remedies in place (RIP). Methods were developed to model cost and performance of source zone and dissolved plume remediation technologies—including thermal treatment, chemical oxidation, enhanced bioremediation, and reactive barriers—and to optimize system operation and monitoring to meet user-defined cleanup criteria with minimum life-cycle cost, considering uncertainty in performance predictions using a stochastic optimization approach. Physical, chemical and biological processes expected to significantly affect performance are incorporated in the model, including effects of back-diffusion from low permeability zones, such as clay layers or matrix zones in fractured rock.

Technical Approach. The capability of the Stochastic Cost Optimization Toolkit (SCOToolkit) developed under previous DoD funding was greatly extended in this project. The previous 2D contaminant transport model was rewritten simulate 3D transport with steady-state groundwater flow along linear or curvilinear streamlines with multiple DNAPL sources. A rigorous solution for resident and flux concentrations was derived and implemented that prevents physically-impossible counter-flow dispersion (which most solutions allow). In conjunction with an upscaled dispersion model, the solution enables efficient simulation of transport in dual-porosity media and associated back-diffusion phenomena.

Performance and cost functions were developed and stringently tested for thermal source reduction (TSR), source zone in situ chemical oxidation (ISCO), enhanced source zone mass transfer, and enhanced dissolved plume bioremediation involving electron donor injection in multiple galleries. Multiple remediation technologies may be operated concurrently or serially.

Site-wide no-further-action decisions are based on statistical criteria applied to compliance well data. For example, annual average concentrations must be less than a specified probability upper confidence limit of current concentration based on an *N*-year regression. Termination criteria for individual remediation system components are based on component-specific performance monitoring data. For example, individual injection galleries may be shut off when the contaminant concentration is less than a value that is optimized to meet compliance criteria with minimum cost.

Source zone TSR termination decisions are commonly predicated on soil sampling data and ISCO on dissolved concentration data. We developed and tested a method for estimating average soil concentration during thermal treatment from mass recovery measurements, which was found to be more reliable and less costly than soil sampling. Incorporating soil sampling during ISCO was found to reduce errors associated with slow rebound of groundwater concentrations after treatment termination.

These source zone performance monitoring options were incorporated into SCOToolkit, which also allows source regions to be divided into treatment zones (e.g., with different estimated levels of contamination) and subdivided further into monitoring zones (e.g., for soil or water sampling, cumulative mass recovery for thermal treatment). Statistical criteria were developed to allow termination of individual monitoring zones, treatment zones, or the entire system with equal decision reliability at all scales. SCOToolkit includes an inverse solution to obtain best estimates of model parameters and their uncertainty using available field and lab data as well as prior estimates of parameters and their uncertainty. A stochastic optimization technique is used to

determine optimum operational and monitoring variables to minimize the expected costs over multiple realizations of uncertain parameters and measurements.

Protocols were developed and implemented to periodically refine model calibration taking into consideration new data from monitoring, to assess the probability of the current operations to meet cleanup objectives, and to reoptimize (or redesign if necessary) remediation and monitoring variables to minimize expected cost-to-complete taking into consideration performance and cost uncertainty. Because prediction uncertainty generally decreases as additional data is used for calibration, predictions become more accurate and less overdesign is required to compensate for uncertainty. The SCOToolkit package also includes a number of Excel-based tools to pre-process data for input into calibration and optimization modules, as well as to analyze performance monitoring data to make real-time termination decisions based on the multi-scale statistical decision protocol.

Results. Case studies on hypothetical and field sites demonstrated that incremental re-optimization can greatly improve the likelihood of meeting remediation criteria within a target timeframe while reducing the expected cost by 10 to 20% or more over conventional approaches. Optimization of performance monitoring parameters (e.g., termination criteria, number of treatment zones and monitoring zones, type and number of samples per monitoring zone) was observed to reduce expected (probability-weighted average) cost-to-complete by 5 to 15% and to reduce 95% upper confidence limits of cost by up to 30% compared to conventional approaches.

Dividing thermal treatment areas into multiple zones with different soil concentration ranges and allowing individual zones to terminate early when local statistical criteria were met achieved site-wide criteria with 6% lower expected costs than a single zone. Optimizing confidence limit probability, local-scale cleanup level, and number of monitoring zones per treatment zone with three treatment zones, using mass recovery data instead of soil data, achieved an additional 10% cost reduction.

If confirmation of mass recovery-based results with soil sample data is desired or required, delaying each local termination decision until confirmed by soil sampling will increase cost. Therefore, if confirmatory soil sampling is required, we recommend waiting until all heating units have been stopped based on mass recovery data before performing site-wide soil sampling.

An optimized example problem using mass recovery data to make thermal termination decisions had a 16% lower expected cost than using soil concentration data following typical industry practice, while the 95% upper confidence limit of cost was 28% lower. Thus, the proposed methodology not only yields expected cost savings, but also sharply reduces worst case cost overruns.

Using multiple zones that are allowed to terminate independently based on statistical criteria provided similar cost savings for ISCO. Optimization of injected oxidant concentrations, treatment zone-level cleanup criteria, reinjection criteria, and performance monitoring variables yielded a failure-adjusted expected cost for an example problem 11% lower than a non-optimized case approximating best engineering practice. Furthermore, the cost probability distribution for the optimized design eliminated positive skew evident in the “best practice” case such that the worst case cost for the optimized design was 14% lower than that for the non-optimized design.

Following thermal treatment of three identified sources at Joint Base Lewis McChord in Washington State, SCOToolkit identified a fourth DNAPL source that had not been located during

site characterization studies. Stochastic optimization with interim calibration results did not favor undertaking thermal treatment of the fourth source. Final calibration results indicated that this decision resulted in an undiscounted cost savings equal to 46% of the total cost.

At Dover AFB in Delaware, an incremental stochastic optimization protocol yielded an expected cost savings of 29% with an 18-20 year earlier expected time-to-complete.

Optimization of an ISCO system at an Atlas missile site in Colorado indicated that increasing injected oxidant concentrations and the duration of annual oxidant injection periods predicted a decrease in the expected operating cost by 24% with a 90% probability of meeting the NFA date.

Benefits. Although most DoD sites have or should soon have remedial action plans in progress, many will not achieve regulatory closure quickly. Some planned remedies will likely not perform as expected and will require modification or, in some cases, implementation of a different remedial action plan. This project provides tools to periodically assess remediation performance, identify and rectify problems, and optimize remediation operations and monitoring to minimize life cycle costs while meeting remediation objectives. By explicitly optimizing operations to minimize probability-weighted cost-to-complete taking into account uncertainty in site characterization, model predictions, and remediation technology performance, as well as measurement "noise," numerous nonlinear interactions and tradeoffs are taken into account that conventional approaches would never consider. Results indicate that average savings in cost-to-complete across all sites of 10% to 30% can be readily achieved along with substantial decreases in remediation duration.

SCOToolkit Disclaimer and Terms of Use

The program SCOToolkit, including various accessory Excel worksheets is provided the User "as is" without warranty, implied or otherwise on the following terms and conditions:

1. The University of Tennessee, Cleveland State University, Stanford University, and the U.S. Department of Defense (hereafter, the "Developers") make no warranty of any kind, express or implied, with respect to the subject software products, and specifically make no warranty that said products shall be fit for any particular application. Furthermore, any description of said products shall not be deemed to create an express warranty that such products shall conform to the description.

2. The User assumes all risk and liability for loss, damage, claims or expense resulting from use, possession or resale of any of software products delivered subject to this agreement.

3. The User agrees to indemnify, defend and hold harmless the Developers and their agents and employees from and against any and all claims, liability, loss, damage or expense, including reasonable attorney's fees, arising from or by reason of receiver's use, possession or resale with respect to any of the software products furnished by the Developers pursuant to this agreement and such obligation shall survive acceptance of said products therefore by receiver.

4. This agreement constitutes the complete and final agreement of the parties hereto.

Table of Contents

4. DNAPL Source Remediation by Thermal Treatment

5. DNAPL Zone Treatment by In Situ Chemical Oxidation

6. Transport Model Calibration and Uncertainty Analysis

List of Figures

List of Tables

List of Acronyms and Symbols

AAB	accelerated anaerobic bioremediation
AFB	air force base
A_{TSRi}	areal extent of the thermal treatment zone [m^2]
A_L	longitudinal dispersivity [m]
A_T	transverse dispersivity [m]
AW	application well
BTEX	benzene, toluene, ethylbenzene, and xylene
B	lumped parameter defined as $B = J_{cal} / M_{cal}^{\beta}$
CDM	Camp Dresser McKee
CH	chlorinated hydrocarbon
COC	contaminants of concern
COD	chemical oxygen demand
C	dissolved concentration [µg/L]
$C'_{CH(mixed)}$	aqueous CH concentration after mixed reaction path [µg/L]
$C'_{CH(parallel)}$	aqueous CH concentration after parallel reaction path [µg/L]
$C'_{CH(serial)}$	aqueous CH concentration after serial reaction path [µg/L]
C_{EA}^{H}	background H-equivalent concentration all EA species in the aquifer [µg/L]
C_{ED}^{avail}	aqueous concentration of injected ED available for reactions [µg/L]
$C_{ED}^{H\ nat}$	background H-equivalent ED concentration in the aquifer [µg/L]
C_{ED}^{net}	aqueous ED concentration after reactions [µg/L]
C_{EDi}^{norx}	ED concentration associated with ED gallery *i* prior to reactions [µg/L]
C_{EDi}^{avail}	ED concentration associated with ED gallery *i* available for reactions [µg/L]
C_{EDstop}	annual average contaminant concentration in ED performance monitoring wells below which ED injection will be terminated
C_{NPV}^{all}	total NPV remediation and penalty cost [$K]
C_{NPV}^{SWtot}	total NPV site-wide cost [$K]
C_{NPV}^{EDtot}	total NPV ED injection system cost [$K]
C_{NPV}^{TRtot}	total NPV thermal remediation cost [$K]
C_{total}^{PTcap}	total PT fixed cost [$K]
C_{total}^{PTop}	total PT operating cost per year [$K/yr]
C_{NPV}^{pen}	NPV penalty cost [$K]
C_{NPV}^{SWcap}	total NPV site-wide fixed cost [$K]
C_{well}^{SWcap}	fixed cost for monitoring well construction [$K/well]
C_{other}^{SWcap}	any other site-wide fixed costs [$K]
C_{total}^{SWop}	total NPV operating cost for site-wide monitoring and reporting [$K]

C_{samp}^{SWop}	cost per sample for site-wide monitoring [$K/sample]
C_{other}^{SWop}	other annual site-wide operating costs [$K/yr]
C_{NPV}^{EDtot}	the total NPV cost for ED injection [$K]
C_{NPV}^{EDcap}	total NPV fixed ED cost [$K]
C_{width}^{EDcap}	fixed cost per ED gallery width [$K/m]
C_{mw}^{EDcap}	construction cost per operational ED monitoring well [$K/well]
C_{other}^{EDcap}	other fixed ED costs [$K]
C_{NPV}^{EDop}	total NPV operating cost for ED injection [$K]
C_{width}^{EDop}	operating cost per ED gallery width for maintenance etc. [$K/m]
C_{mass}^{EDop}	operating cost per unit ED mass injection [$K/kg]
C_{samp}^{EDop}	collection and analysis cost per ED monitoring sample [$K/sample]
C_{other}^{EDop}	other ED operating costs per gallery per year for reporting etc. [$K/gallery/yr]
C_{all}^{EDop}	other ED operating costs regardless of the number of galleries [$K/yr]
C_{NPV}^{TRtot}	total NPV cost for thermal treatment for all sources [$K]
C_{site}^{TR}	fixed cost for all sources at a site [$K]
$C_{vol_i}^{TR}$	cost multiplier per unit area of the treatment zone to reach design energy [$K/m^3]
$C_{area_i}^{TR}$	cost multiplier per unit area of the treatment zone to reach design energy [$K/m^2]
C_{mob}^{TR}	mobilization cost for each sampling event [$K/event]
$C_{well_i}^{TR}$	installation cost per monitoring well [$K/well]
C_{GWsamp}^{TR}	sampling and analysis cost per groundwater sample [$K/sample]
$C_{bore_i}^{TR}$	cost per soil boring [$K/boring]
$C_{SOILsamp}^{TR}$	cost per soil sample analyzed [$K/sample]
d	annual discount rate [-]
DNAPL	dense nonaqueous phase liquid
(E_0, N_0)	raw easting and northing field coordinates [m]
(E*, N*)	raw easting and northing field coordinates to evaluate [m]
EA	electron acceptor
ED	electron donor
EGDY	East Gate Disposal Yard
ERH	electrical resistance heating
ESTCP	Environmental Security Technology Certification Program
EVO	emulsified vegetable oil
EW	extraction well
EXV	extreme value compliance rule
E_{eff}	fractional energy yield for biologically-mediated reaction after energy for cell synthesis [-]
E_{frac}	ratio of actual energy consumed when TSR terminates versus the design estimate [-]

$E_{frac(init)}$	cumulative fraction of estimated total energy requirement at which the first samples are taken during TSR [-]
f'_{CH}	H-equivalent react with a unit contaminant concentration [-]
f'_{ED}	H-equivalents to react with a unit ED concentration [-]
f'_{EA}	H-equivalents to react with a unit EA concentration [-]
f_{samp}^{ED}	number of samples per well per year for ED operational monitoring
f_{samp}^{SW}	number of samples per well per year for site-wide monitoring [#/well/yr]
f_{mt}	mass transfer enhancement concentration coefficient [m^3/kg]
f_E	fraction of non-monitoring variable costs attributable to energy use [-]
F_i	total soil and/or groundwater samples divided by pre-treatment sampling number [-]
F_{mt}	mass transfer enhancement factor [-]
F_{miss}	fraction of pre-remediation mass outside thermal treatment zone [-]
F_{serial}	fraction of reductive dechlorination that follows serial pathway [-]
I_{pen}	1 if a penalty cost is triggered else 0 [-]
I_{PT}	1 if PT implementation is triggered else 0 [-]
I_i^{ED}	indicator that is 1 if gallery *i* is actually implemented else 0
IMCOM	US Army Installation Management Command
ISCO	in situ chemical oxidation
IWCD	Industrial waste collection drain
I_i^{TR}	1 if thermal treatment is performed for source i else 0 [-]
J_i	contaminant mass dissolution rate for source i [kg/d]
J_{cal}	contaminant mass dissolution rate for source on calibration date [kg/d]
$J_{treatment\ zone}$	discharge rate from mass within thermal treatment zone [kg/d]
L_z	aquifer thickness [m]
L_i^{ED}	width of ED gallery *i* perpendicular to the flow direction [m]
MCL	maximum contaminant level
M	contaminant mass in source [kg]
M_{cal}	contaminant mass on calibration date [kg]
M_{EDi}	mass injection rate of ED for gallery *i* [kg/d]
M_{miss}	initial mass outside the thermal treatment zone [kg]
M_{ref}	contaminant mass on reference date [kg]
M_{TSRo}	source mass at the commencement of thermal treatment [kg]
$M_{treatment\ zone\ o}$	initial mass within the thermal treatment zone [kg]
NC	non-compliance condition
NFA	no further action
N_{source}	number of individual source zones [-]
$N_{well_i}^{TR}$	number of source zone groundwater monitoring wells [-]
$N_{samp/well_i}^{TR}$	number of sampling depths per well [-]
$N_{bore_i}^{TR}$	number of soil boring locations for each sampling time [-]
$N_{samp/bore_i}^{TR}$	number of depth intervals sampled per boring [-]
N_{well}^{SW}	number of site-wide monitoring wells including compliance wells [-]
$N_{lookback}$	moving time window for compliance evaluation [yr]

N_{mw}^{ED}	number of operational monitoring wells [not injection wells] per ED gallery
N_{gal}^{ED}	number of potential ED galleries
O_{ti}^{ED}	indicator that is 1 if gallery *i* is operating in year t else 0
ORNL	Oak Ridge National Laboratory
PCE	tetrachloroethylene
PICT	permanent injection circulation transects
PNNL	Pacific Northwest National Laboratory
PT	conditional containment condition implemented (compliance condition)
q	darcy velocity [m/d]
R	retardation factor [-]
RCL	regression confidence limit compliance rule
$R_{TSR(gw)}$	target groundwater concentration reduction fraction for thermal treatment [-]
$R_{TSR(soil)}$	target soil concentration reduction fraction for thermal treatment [-]
SCOToolkit	Stochastic Cost Optimization Toolkit
SERDP	Strategic Environmental Research and Development Program
S_{lnC}	standard deviation of ln-transformed variable [-]
TCE	trichloroethene
TSR	thermal source reduction
t_{oi}^{ED}	start date for ED gallery *i* [yr]
t_o	source release date [yr]
t_{cal}	calibration date [yr]
t_{ref}	reference date for NPV adjustment [yr]
t_{max}	maximum simulation date [yr]
t_{nfa}	earliest date when no further action conditions may be met [yr]
t_{PT}	year that PT is triggered [yr]
t_{start}	first year capital costs are incurred [yr]
$t_{penalty}$	date when penalty cost is incurred [yr]
t_{ref}	basis date for present value [yr]
t_{ref}	reference date [yr]
t_{rem}	date remedial action commences [yr]
t_{TSRo}	date thermal treatment begins [yr]
t_{TSRf}	date when thermal treatment is completed [yr]
t_{TSR}	date that thermal treatment is performed [yr]
USACE	US Army Corps of Engineers
USDOE	US Department of Energy
UST	underground storage tank
VC	vinyl chloride
v	superficial pore water velocity [m/d]
X_i	binary switch [= 0 or 1] to select/deselect thermal treatment for source i [-]
(x, y)	local easting and northing coordinates along streamline from source origin [m]
Z_{TSR}	vertical extent of the thermal treatment zone [m]
β	source mass depletion exponent [-]
ΔE_{frac}	incremental energy fraction between thermal sampling events [-]
ϕ	aquifer porosity [-]
λ_i	first-order decay coefficient for zone *i* [d^{-1}]

1. Introduction

1.1 Background

There are more than 50,000 sites in the U.S. with contaminated groundwater, roughly half of which involve chlorinated solvents or other DNAPLs (Siegrist et al. 2006). Subsurface DNAPLs result in persistent long-term sources of groundwater contamination unless a very large fraction can be removed (Cohen and Mercer 1993, NRC 1994, Chapelle et al. 2003). Unfortunately, it is difficult and costly to reliably delineate the distribution of DNAPL in the subsurface prior to treatment, and source treatment costs per unit soil or aquifer volume are frequently high, resulting in a steep tradeoff between cost and probability of successful source remediation. Numerous other tradeoffs exist, such as between costs for aggressive source reduction strategies that (hopefully) decrease the time to reach regulatory compliance versus lower annual operating costs for less aggressive strategies that must be maintained for a much longer period. Most tradeoffs are neither binary nor linear, but rather involve nonlinear interactions of numerous natural and engineering variables. It is virtually impossible to optimize the cost performance of a system involving interactions of a complex engineered system with an even more complex, and imperfectly understood, natural system by conventional deterministic engineering methods.

The first efforts to develop methods to rigorously optimize groundwater remediation systems were reported by Gorelick et al. (1984), who linked a simulation model with a nonlinear optimization method to achieve plume containment while minimizing pump and treat operating costs. McKinney and Lin (1996) argued for incorporating fixed as well as operating costs, leading to solutions with fewer wells and higher pumping rates. Regulatory compliance criteria have been variously treated as optimization constraints (Wagner and Gorelick 1989, McKinney and Lin 1996), as a "penalty cost" for noncompliance (Rizzo and Dougherty 1996, Chan-Hilton and Culver 2005), or as a component in multi-objective programming (Erickson et al. 2002).

More recently, Teutsch et al. (2001) emphasized the need to combine physically based simulation models and economic models for quantitative decision-making. Minsker et al. (2003 and 2004) coupled global optimization methods (e.g., genetic algorithms) and groundwater transport models to evaluate cost-effective pumping strategies for existing pump and treat systems at DoD facilities. They demonstrated the proposed method could substantially reduce life cycle costs with range of uncertainty, compared to conventional trial and error methods. Becker et al. (2006) reported that simulation-optimization methods were able to identify solutions that cost 5% to 50% less than trial-and-error results, translating to cost savings of $600K to $10M for the sites studied. Abriola et al. (2008) developed an optimization tool to compare costs and benefits of several source zone treatment technologies in conjunction with post-treatment MNA. Liang et al. (2010) developed a probabilistic optimization framework to evaluate cost, source treatment performance, plume management, and risk, incorporating uncertainty in the decision process.

The design and operation of remediation systems is to a great degree a problem of managing uncertainty. Due to large uncertainties in source mass, aquifer properties, and many other variables, conventional remediation designs based on best estimates of system properties are likely to exhibit a high probability of failure to meet compliance requirements (Parker et al. 2010a), or overshoot expected budget or schedule based on unanticipated site conditions. On the other hand, designing for "worst case" parameters will lead to excessive cost. Stochastic optimization is the only means capable of taking into consideration the complex nonlinear interactions among uncertain physical properties, design variables, and compliance criteria.

In a previous project (SERDP ER-1611), we developed an integrated methodology for DNAPL site remedial design optimization using source zone electrical resistance heating (ERH), enhanced bioremediation with ED injection, and/or MNA that considers uncertainty in measurements and model predictions (Cardiff et al. 2010, Liu et al. 2010, Parker et al. 2010a, Parker et al. 2012) implemented in the Stochastic Cost Optimization Toolkit referred to as SCOToolkit (Parker et al. 2011). A forward model considers natural DNAPL source depletion, source reduction using ERH, and dissolved plume transport with enhanced bioremediation using ED injection. An inverse solution is used to estimate model parameters and their uncertainty as well as residual model error using all available site data. Monte Carlo (MC) simulations of remediation performance and cost are performed using equiprobable parameter realizations with residual error in simulated measurements based on model calibration results. A cost module computes NPV cost to meet specified objectives and constraints for each realization considering fixed and operating costs with a penalty cost for noncompliant realizations. A stochastic optimization algorithm identifies design variables that minimize "expected" cost (i.e., cost averaged over all MC realizations). Hypothetical and field applications of the methodology demonstrated its ability to reduce costs and improve the probability of successfully meeting remediation objectives (Lee et al. 2012, Kim et al. 2012).

As of FY2010, 86% of DoD installation restoration program (IRP) sites were reported as RIP or response complete (Leeson and Stroo 2011). As DoD transitions from development and implementation of remedial action plans to managing RIP sites, the focus must shift to optimizing operational variables and assessing progress towards remediation goals to achieve compliance and to minimize cost. Little attention seems to have been focused on this problem. However, the stochastic cost optimization methodology described above can be adapted for this purpose. As additional monitoring and performance data are collected, periodic recalibration will enable future performance to be predicted with less uncertainty. If projected performance is significantly better or worse than expected, remediation operation and monitoring variables may be reoptimized to minimize the remaining CTC. If the updated probability of failure is unacceptable, more substantial modifications in the remediation strategy may be evaluated to meet performance criteria while minimizing the remaining CTC. The cost utility of additional characterization data, as discussed further below, may also be evaluated in consideration of the revised model calibration results.

Considerable work has been performed on optimization of long-term monitoring (LTM) sampling locations and frequencies (Loaiciga et al. 1992, EPA 2000, Reed et al. 2000, Cameron and Hunter 2002, Reed and Minsker 2004, EPA 2005, Parsons 2005, EPA 2007). User-friendly LTM optimization (LTMO) tools have been developed by Aziz et al. (2003) and Harre et al. (2009 - ESTCP project ER-0629) that utilize statistical methods to eliminate redundant well locations and to reduce sampling frequency.

The handling of noisy data is a troublesome issue for compliance monitoring. Levine (2010) with the US EPA proposed to compute confidence limits on an N-year simple moving average (SMA) of measured concentrations to smooth noise. If the upper one-sided SMA confidence limit for a specified probability level (e.g., 95%) is less than the compliance concentration for each compliance well, regulatory closure criteria are deemed met. Parker et al. (2010b) reported stochastic simulation-optimization analyses using Levine's and other "noise management" approaches in SCOToolkit. The program provides broad flexibility in defining site specific performance objectives in terms of "compliance rules" and "operational rules," which are described in detail in Appendix B.

Results showed that increasing or decreasing monitoring frequency relative to an optimum value increased the expected CTC. Fewer samples lead to wider confidence limits, which increase the duration of LTM, and hence operating costs for the longer duration, more than the savings from reduced frequency. Effectively, more conservative operation is required to compensate for greater measurement uncertainty associated with fewer samples. Parker et al. demonstrate that the greatest net cost savings is achieved by simultaneously optimizing the moving average lookback period as well as monitoring frequency and remedial design variables. We infer from this study that while LTMO statistical methods may be useful for optimizing the number and location of monitoring wells, optimization of sampling frequency should be performed in the context of a more comprehensive stochastic optimization approach that considers cost tradeoffs. Furthermore, methods for handling measurement noise vis á vis compliance rules should be optimized to minimize CTC.

Site characterization efforts and monitoring can serve to reduce uncertainty and hence reduce the cost premium associated with overdesigning to compensate for uncertainty and to reduce the failure probability. However, characterization and monitoring efforts also incur direct costs, so the pertinent question to ask is whether the savings due to reduced uncertainty achieved by a given characterization or monitoring measure exceeds the direct cost of the measure itself. The cost savings due to reduced uncertainty is referred to as the value of information (VOI), defined more specifically as the difference between the total expected cost when the information in question is not used and that in which the information is used. The VOI concept has been applied in many areas, including medicine (Yokota and Thomson 2004), economics (Hanemann 1989), operation research (Gavirneni et al. 1999), and earth science (Dawdy 1979). Applications to groundwater management have been described by Reichard and Evans (1989), Wagner et al. (1992), James and Gorelick (1994), Borisova et al. (2005), and Feyen and Gorelick (2005). Liu et al. (2012) investigated VOI while optimizing remediation design to minimize cost considering parameter uncertainty.

EPA (2004) and Leeson and Stroo (2011) have noted that measurements are sometimes not performed in the belief that they will increase cost or delay completion, while in reality the additional information may enable a strategy to be implemented that decreases cleanup duration and life cycle cost. VOI is a powerful tool to evaluate whether a proposed measurement is warranted in terms of total CTC. The high computational cost of traditional VOI calculations has probably impeded their routine use, although more computationally efficient methods could ameliorate this obstacle.

A final factor we will address that contributes to uncertainty in predicted performance, and hence to higher expected total remediation cost, is intrinsic uncertainty in the model used to make predictions. After we calibrate a model to field measurements, residual deviations remain that are attributable to a combination of sampling/measurement error and intrinsic model error. These cannot be practically distinguished, although model error will usually dominate. Intrinsic error can be reduced by refining the model to account for more details of the real system. However, to the extent that the "refined" model requires more parameters that are imperfectly known, the reduction in intrinsic error may be offset by an increase in parameter uncertainty when calibrated to the same data (Parker et al. 2010b). The optimum model to minimize prediction uncertainty is ultimately limited by the data available for calibration.

Many field, laboratory and theoretical studies have shown that back-diffusion from low-permeability layers in heterogeneous aquifers can result in a long-term source of contamination at DNAPL sites (Sale et al. 2006, Wood et al. 2009, Leeson and Stroo 2011). Under conditions in which back-diffusion is a significant problem, large differences develop between "resident concentrations" and "flux concentrations," where the former represent volume-averaged concentrations in pore fluid and the latter represent flow-weighted averages (Parker and van Genuchten 1984). Recent field studies by Britt (2011) indicate that samples from normally purged or pumped wells approximate flow-averaged concentrations.

Models that explicitly treat the diffusion process between high and low permeability regions are readily available, but require additional parameters than conventional single-continuum models, and entail substantially greater computational effort. The latter issue is particularly problematic for incorporation within a calibration-stochastic optimization framework, which typically requires thousands of direct solution simulations. Explicit treatment of diffusion would thus render stochastic optimization analyses impractical without supercomputing capability. Unfortunately, these resources are generally not available to most environmental consultants.

A practical alternative method, described by Parker and Valocchi (1986), uses an upscaled dispersion model with boundary conditions that strictly enforce mass balance conditions pertinent for resident or flux concentrations, as needed. Although the solution approach is approximate, a comparison of results for an explicit diffusion model and the upscaled dispersion model agree quite closely. The upscaled dispersion coefficient can be computed theoretically from known parameters in the diffusion model, or the lumped coefficient can simply be calibrated to field data directly, without increasing the parameter vector dimension compared to a conventional dispersion model. Furthermore, the same approach is applicable to fractured rock aquifers, provided the fracture network is sufficiently dense that porosity and permeability are relatively uniform on the scale of average monitoring well spacing.

1.2 Project Objectives and Approach

The goal of the present project was to extend the capability of SCOToolkit to enable periodic assessment and optimization of the performance at remediation in progress (RIP) sites to minimize expected total NPV cost considering failure probability and measurement and prediction uncertainty, and to facilitate early identification and correction of problems associated with remediation technologies and/or goals. Considered remediation technologies that may be operated concurrently and/or sequentially include:

1. Electric resistance heating (ERH) DNAPL source remediation
2. Thermal conduction heating (TCH) DNAPL source remediation
3. Steam enhanced extraction (SEE) DNAPL source remediation
4. DNAPL source excavation
5. In situ chemical oxidation (ISCO) with recirculation for DNAPL source remediation
6. ISCO with pulsed injection for DNAPL source remediation
7. Electron donor (ED) injection for enhanced DNAPL source remediation
8. Electron donor (ED) injection for enhanced dissolved plume remediation
9. Reactive barriers or groundwater extraction for dissolved plume control

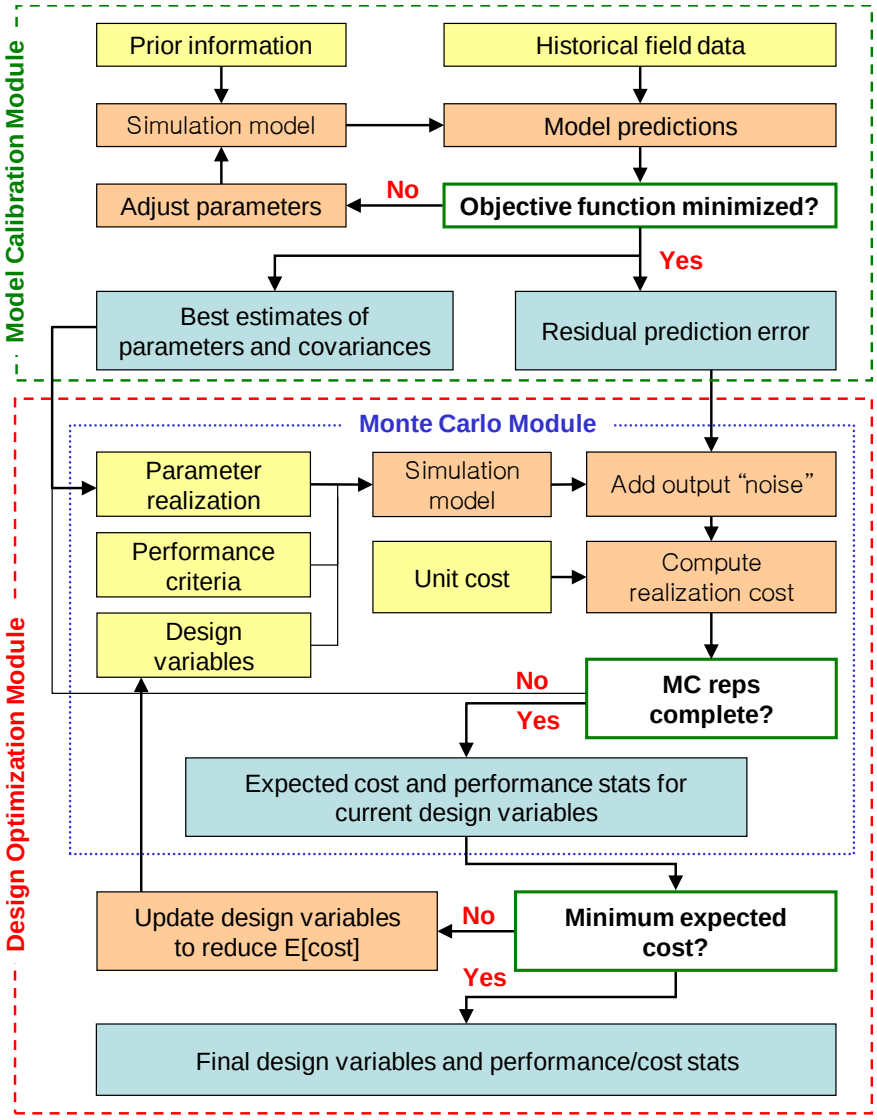

Figure 1.1 Flow chart for SCOToolkit program.

In addition to the expanded repertoire of remediation technologies and the capability to iteratively evaluate remediation progress and re-optimize operating parameters and/or strategies, enhancements to the transport model were undertaken to more accurately approximate complex site conditions. In particular, the solution was extended from a vertically-averaged two-dimensional model to a three-dimensional representation of finite vertical thickness with multiple DNAPL sources at different areal locations and/or depths. Additionally, the solution was modified to approximate effects of mass transfer limitations associated with diffusion into and out of low permeability zones (aka, "back diffusion"). The solution leads to differences between volume-averaged soil concentrations and flux-averaged monitoring well concentrations, both of which can be used in the revised program for model calibration.

Stochastic cost optimization is a computationally intensive iterative process that requires hundreds of evaluations of expected cost for different design and operation variables. Furthermore, each expected cost evaluation requires multiple simulations (typically 100) to represent uncertainty in

model predictions and measurements. As a result, tens of thousands of individual forward model simulations over a multi-decade time period are commonly required to solve a single optimization problem. Our overall objective has been to develop a practical tool to meet remediation objectives with the least possible cost. Due to uncertainty in future performance, this objective involves tradeoffs between the probability of successfully meeting remediation goals within a certain timeframe and the aggressiveness of the remediation strategy. Performance uncertainty arises from three sources. First, for a given model formulation, uncertainties in model parameters and boundary conditions over time produce prediction uncertainty. Second, field and lab measurements are subject to sampling and measurement uncertainty. And finally, there are inherent accuracy limitations associated with assumptions and simplifications – even for the most sophisticated models. SCOToolkit explicitly addresses errors from the first source. The last two sources or uncertainty are lumped together in the treatment of residual calibration error.

The foregoing considerations require a performance simulation model that is very robust and computationally efficient. This requires giving up some degree of model complexity to enable practical application with typically available computer hardware. Our experience indicates that the level of sophistication in the SCOToolkit performance models is adequate for most sites considering the magnitude of uncertainty from other sources.

The general approach for SCOToolkit described in this report is depicted in flowchart form in Figure 1.1. The central component of the method is a semi-analytical mathematical model to simulate DNAPL source depletion and dissolved phase transport of a target chlorinated hydrocarbon over time in response to natural and engineered conditions.

In the inverse modeling mode, historical site data is used to calibrate the simulation model and to estimate parameter covariances and residual prediction error. Forward predictions of remediation performance and cost are performed for defined remediation strategies, operating rules and remediation criteria. A Monte Carlo (MC) method is used to quantify uncertainty in performance and cost attributable considering uncertainty in model parameters, measurements employed for real-time decisions, and cost function variables.

Design optimization is performed to determine values of design variables that minimize the expected value (average over MC realizations) of NPV, which may include “penalty costs” for failure to achieve defined remediation objectives within a specified time period.

Chapter 2 of this report describes the basic 3-D transport model. Chapters 3 to 5 describe the enhanced bio, thermal and ISCO cost/performance models, respectively. Chapter 6 outlines calibration and uncertainty analysis methods. Chapter 7 presents the stochastic design optimization approach and Chapters 8 to 10 document applications of the program.

1.3 References

Abriola, L.M., P. Goovaerts, K.D. Pennell, and F.E. Löffler (2008) Development of Assessment Tools for Evaluation of The Benefits of DNAPL Source Zone Treatment. SERDP Project ER-1293. Final Report. Strategic Environmental Research and Development Program. US Department of Defense. 173p.

Aziz, J.J., M. Ling, H.S. Rifai, C.J. Newell, and J.R. Gonzales (2003) MAROS: A decision support system for optimizing monitoring plans. Ground Water 41(3): 355-367.

Becker, D.B., B. Minsker, R. Greeenwald, Y. Zhang, K. Harre, K. Yager, C. Zheng, and R. Peralta (2006) Reducing long-term remedial costs by transport modeling optimization, Ground Water 44: 864-875.

Borisova, T., J. Shortle, R.D. Horan, and A. David (2005) Value of information for water quality management. Water Resources Research 41:W06004.

Britt, S. (2011) Tools and techniques for long term groundwater monitoring cost reduction, SERDP/ESTCP Partners in Environmental Technology Symposium and Workshop, Nov 29-Dec 1, Washington DC.

Cardiff, M., X. Liu, P.K. Kitanidis, J. Parker, and U. Kim (2010) Cost optimization of DNAPL source and plume remediation under uncertainty using a semi-analytic model. Journal of Contaminant Hydrology 13: 24-43.

Chan-Hilton, A.B. and T.B. Culver (2005) Groundwater remediation design under uncertainty using genetic algorithms. Journal of Water Resources Planning and Management 131(1): 25-34.

Chapelle, F.H., M.A. Widdowson , J.S. Brauner , E. Mendez III, and C.C. Casey (2003) Methodology for Estimating Times of Remediation Associated with Monitored Natural Attenuation. US Geological Survey. Water Resources Investigations Report 03-4057. 58 pp.

Cohen, R.M. and J.W. Mercer (1993) DNAPL Site Evaluation. C.K. Smoley Publication, Boca Raton, FL, 384p.

Dawdy, D.R. (1979) The worth of hydrologic data. Water Resources Research 15(6): 1726–1732.

EPA (2000) Subsurface Remediation: Improving Long-Term Monitoring & Remedial Systems Performance. EPA/542/B-00/002. Conference Proceedings. June 8-11,1999. St. Louis, MI. US Environmental Protection Agency. 81 pp.

EPA (2004) Site Characterization Technologies for DNAPL Investigations. EPA 542-R-04-017. Report. US Environmental Protection Agency. 165 pp.

EPA (2005) Roadmap to long-term monitoring optimization. EPA 542-R-05-003. Report. US Environmental Protection Agency. 48 pp.

EPA (2007) Long-Term Groundwater Monitoring Optimization Newark, Muscoy, and Source Operable Units Newmark Superfund Sites San Bernardino, California. EPA 542-R-07-015. Report. US Environmental Protection Agency. 326 pp.

Erickson, M., A. Mayer, and J. Horn (2002) Multi-objective optimal design of groundwater remediation systems: application of the niched Pareto genetic algorithm (NPGA). Advances in Water Resources 25: 51-65.

Feyen, L. and S.M. Gorelick (2005) Framework to evaluate the worth of hydraulic conductivity data for optimal groundwater resources management in ecologically sensitive areas. Water Resources Research 41(3):W03019.

Gavirneni, S., R. Kapuscinski, and S. Tayur (1999) Value of information in capacitated supply chains. Management Science 45(1): 16–24.

Gorelick, S.M., C.I. Voss, P.E. Gill, W. Murray, and M.A. Saunders (1984) Aquifer reclamation design: The use of contaminant transport simulation combined with nonlinear programming. Water Resources Research 20(4): 415-427.

Hanemann, W.M. (1989) Information and the concept of option value. Journal of Environmental Economic Management 16(1): 23–37.

Harre, K., T. Chaundhry, R. Greenwald, W. Jian, C. Davis, M. Zavislak, and B. Minsker (2009) Adaptive Long-Term Monitoring at Environmental Restoration Sites. ESTCP Project ER-0629. TR-2317-ENV. Final Report. Environmental Security Technology Certification Program (ESTCP). US Department of Defense. 419 pp.

James, B.R. and S.M. Gorelick (1994) When enough is enough: The worth of monitoring data in aquifer remediation design. Water Resources Research 30(12):3499–3513.

Kim, U., J. Parker, P. Kitanidis, M. Cardiff, X. Liu, and J. Gillie (2012) Stochastic Cost Optimization of DNAPL Site Remediation: II. Field Application. Environmental Modeling and Software. DOI:10.1016/j.envsoft.2012.05.003, 2012.

Lee, J., X. Liu, P.K. Kitanidis, U. Kim, J. Parker, A. Bloom, and R. Lyon (2012) Cost optimization of DNAPL Remediation at Dover Air Force Base Site. Ground Water Remediation and Monitoring. DOI: 10.1111/j1745–6592.2011.01382.x.

Leeson, A. and H. Stroo (2011) SERDP and ESTCP Workshop on Investment Strategies to Optimize Research and Demonstration Impacts in Support of DoD Restoration Goals. Workshop Report. Environmental Research and Development Program (SERDP) and the Environmental Security Technology Certification Program (ESTCP). US Department of Defense, June 16 2011, Salt Lake City, UT. 59 pp.

Levine, H. (2010) EPA perspective on site closure: how clean is clean? US Dept of Defense SERDP/ESTCP Partners in Environmental Technology Technical Symposium and Workshop. Washington DC, Nov 30-Dec 2.

Liang, H., R.W. Falta, C.J. Newell, S.K. Farhat, P.S.C. Rao, and N. Basu (2010) Decision & Management Tools for DNAPL Sites: Optimization of Chlorinated Solvent Source and Plume Remediation Considering Uncertainty. ESTCP Project ER-200704. Final Report. Environmental Security Technology Certification Program (ESTCP). US Department of Defense. 88 pp.

Liu, X., J. Lee, P.K. Kitanidis, J. Parker, and U. Kim (2012) Value of Information as a context-specific measure of uncertainty in groundwater remediation. Water Resources Management. DOI: 10.1007/s11269-011-9970-3.

Liu, X., M. Cardiff, and P.K. Kitanidis (2010) Parameter estimation in nonlinear environmental problems. Stochastic Environmental Research and Risk Assessment 24(7): 1003-1022.

Loaiciga, H.A., R.J. Charbeneau, L.G. Everett, G.E. Fogg, B.F. Hobbs, and S. Rouhani (1992) Review of ground-water quality monitoring network design. Journal of Hydrologic Engineering 118(1): 11-37.

McKinney, D.C. and M.-D. Lin (1996) Pump-and-treat ground-water remediation system optimization. Journal of Water Resource Planning and Management 122(2): 128-136.

Minsker, B., Y. Zhang, R. Greenwald, R. Peralta, C. Zheng, K. Harre, D. Becker, L. Yeh, and K. Yager (2003) Application of flow and transport optimization codes to groundwater pump and treat systems. Final Report, Volume I. Environmental Security Technology Certification Program (ESTCP). US Department of Defense. 146 pp.

Minsker, B., Y. Zhang, R. Greenwald, R. Peralta, C. Zheng, K. Harre, D. Becker, L. Yeh, and K. Yager (2004) Application of flow and transport optimization codes to groundwater pump and treat systems. Final

Report, Volume III. Environmental Security Technology Certification Program (ESTCP). US Department of Defense. 226 pp.

National Research Council (1994) Alternatives for Ground Water Cleanup. National Academy Press, Washington D.C., 336p.

Parker, J.C. and A. J. Valocchi (1986) Constraints on the validity of equilibrium and first-order kinetic transport models in structured soils. Water Resources Research 22: 399-407.

Parker, J.C, U. Kim, P.K. Kitanidis, M. Cardiff, M., and X. Liu (2010a) Stochastic cost optimization of multi-strategy DNAPL site remediation. Groundwater Monitoring & Remediation 30(3): 65-78.

Parker, J., U. Kim, M. Widdowson, P. Kitanidis, and R. Gentry (2010b), Effects of model formulation and calibration data on uncertainty in DNAPL source dissolution predictions, Water Resources Research, 46:W12517.

Parker, J.C, U. Kim, P.K. Kitanidis, M. Cardiff, X. Liu, and G. Beyke (2012) Stochastic Cost Optimization of DNAPL Site Remediation: I. Method Description and Sensitivity Studies. Environmental Modeling and Software. 38: 74-88, 2012.

Parsons (2005) Keesler Air Force Base U.S. Installation Restoration Final Quality Program Plan, Environmental Monitoring at Seven Sites. Prepared for U.S. Air Force. EPA ID No. MS2 570 024 164. Atlanta, Georgia.

Reed, P.M., B.S. Minsker, and A.J. Valocchi (2000) Cost-effective long-term groundwater monitoring design using a genetic algorithm and global mass interpolation. Water Resources Research 36(12): 3731-3741.

Reed, P. and B.S. Minsker (2004) Striking the balance: Long-term groundwater monitoring design for conflicting objectives. Journal of Water Resources Planning and Management 130(2): 140-149.

Reichard, E.G. and J.S. Evans (1989) Assessing the value of hydrogeologic information for Risk-Based remedial action decisions. Water Resources Research 25(7):1451–1460.

Rizzo, D.M. and D.E. Dougherty (1996) Design optimization for multiple management period groundwater remediation. Water Resources Research 32(8): 2549-2561.

Sale, T.C., L.A. Doner, and E.S. Seger (2006) Storage and release of contaminants in low flow zones in source and plumes, American Geophysical Union Fall Meeting Abstracts, San Francisco, 12 Dec 2006.

Siegrist, R.L., M. Crimi, J. Munakata-Marr, and T. Illangasekare (2006) Reaction and Transport Processes Controlling In Situ Chemical Oxidation of DNAPLs. SERDP Project CU-1290. Final Report. Strategic Environmental Research and Development Program (SERDP). US Department of Defense. 235 pp.

Teutsch, G., H. Rugner, D. Zamfirescu, M. Finkel, and M. Bittens (2001) Source remediation vs. plume management: critical factors affecting cost-efficiency. Land Contamination and Reclamation 9: 128-142.

Wagner, B.J. and S.M. Gorelick (1989) Reliable aquifer remediation in the presence of spatially variable hydraulic conductivity: From data to design. Water Resources Research 25: 2211-2225.

Wood, A.L., M.D. Annable, J.W. Jawitz, R.W. Falta, M.C. Brooks, C.G. Enfield, P.S.C. Rao, and M.N. Goltz (2009) Impacts of DNAPL Source Treatment: Experimental and Modeling Assessment of the Benefits of Partial DNAPL Source Removal. EPA 600/R-09/096 supported by SERDP Project ER-1295. US Environmental Protection Agency. 177 pp.

Yokota, F. and K.M. Thompson (2004) Value of information analysis in environmental health risk management decisions: Past, present, and future. Risk Analysis 24(3):635–650.

2. DNAPL Source and Dissolved Transport Model

2.1 Background

The aqueous plume model in SCOToolkit is driven by one or more DNAPL sources that deplete over time at rates controlled by natural and/or engineered processes. Mass transfer kinetics are treated as a power function of source mass remaining. The transport model itself distinguishes between resident and flux concentrations. The importance of this distinction when dealing with heterogeneous aquifers is well established (Kreft and Zuber 1978, Parker 1984, Parker and van Genuchten 1984, van Genuchten and Parker 1984, Batu and van Genuchten 1990, Roth and Jury 1993, Toride et al. 1999, Zhang et al. 2006), although the practical implications are often not fully appreciated and the distinction is not considered in field modeling efforts.

The physical distinction between resident and flux concentrations is illustrated in Figure 2.1 for a well screened across two zones with groundwater discharge rates Q_1 and Q_2, screened lengths L_1 and L_2 and local concentrations C_1 and C_2. A water sample obtained from the well using usual field methods would approximate a flow-weighted average ("flux concentration" C_F) along the length of the well screen. Alternatively, a water sample extracted from a composite soil sample over the same depth interval would yield a volume-weighted average ("resident concentration" C_R). For the hypothetical example in Figure 2.1, which corresponds to aquifer flushing after the primary contaminant source has largely dissipated, the average resident concentration over the well bore length is 17 times greater than the flux concentration due slow back-diffusion from the low velocity zone.

Resident and flux concentrations can be shown to follow equations that are identical in mathematical form but subject to different boundary conditions. Details regarding boundary conditions for correctly distinguishing between resident and flux concentrations using analytical as well as numerical solution methods, and practical implications of such distinctions, are discussed by Parker and Kim (2015).

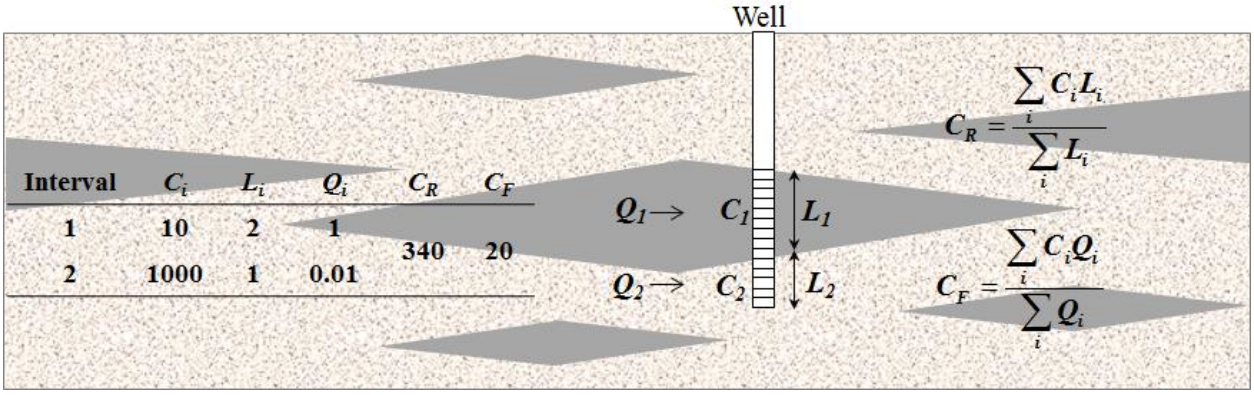

Figure 2.1. Illustration of flow-averaged concentration (C_F) observed in well screened over high and low permeability zones and volume-averaged concentration (C_R) that would be determined in fluid extracted from adjacent soil samples aggregated over the same length.

2.2 DNAPL Source Model

Field-scale DNAPL source dissolution and mass depletion over time is described by a widely accepted power function model (Rao et al. 2001, Zhu and Sykes 2004, Parker and Park 2004, Park and Parker 2005Jawitz et al. 2005, Falta et al. 2005, Christ et al. 2006, Fure et al. 2006, Basu et al. 2007, Saenton and Illangasekare 2007). Considering the possibility of engineered manipulation in mass transfer kinetics, we describe the contaminant mass dissolution rate, $\dot{m}$ [MT^{-1}], in an individual source zone as a function of time, t, by

$$\dot{m}(t) = F_{mt} J_{cal} \left(\frac{M(t)}{M_{cal}} \right)^{\beta} \tag{2.1}$$

where $J_{cal} = \dot{m}\,(t{=}t_{cal})$ and $M_{cal} = M(t{=}t_{cal})$ in which t_{cal} denotes a reference time selected for model calibration, $M(t)$ is the contaminant source mass remaining at time t, β is a depletion exponent that reflects the DNAPL source "architecture" (Parker and Park, 2004) [-], and F_{mt} is a dimensionless mass transfer enhancement factor, discussed further in Chapters 3 and 5.

Integration of the source mass balance equation as described by Park and Parker (2005) yields source mass remaining versus time after an instantaneous release of mass M_o at time t_o

$$M(t) = \left[\max\left(0, M_{ref}{}^{1-\beta} - F_{mt} B (1-\beta)(t - t_{ref})\right) \right]^{1/(1-\beta)} \tag{2.2}$$

where $B = J_{cal} / M_{cal}^{\beta}$. Note (2.2) is valid for $\beta \neq 1$. If $\beta = 1$, the value is internally set to 0.9999. The effects of β on source mass remaining and mass discharge rate versus time based on (2.1) and (2.2) are illustrated in Figure 2.2. Discharge rate decreases linearly with time when $\beta = 0.5$ and logarithmically for $\beta = 1$. For $\beta < 1$, the log discharge rate is concave downwards and discharge rate and mass remaining become zero at a finite time. For $\beta \geq 1$, log discharge rate is convex downward and the discharge rate and mass remaining approach zero asymptotically with time. For $\beta < 1$, mass remaining reaches zero at a finite time. Based on high resolution simulations, Parker and Park (2004) associated $\beta \geq 1$ with residual DNAPL and $\beta < 1$ with DNAPL pools and lenses.

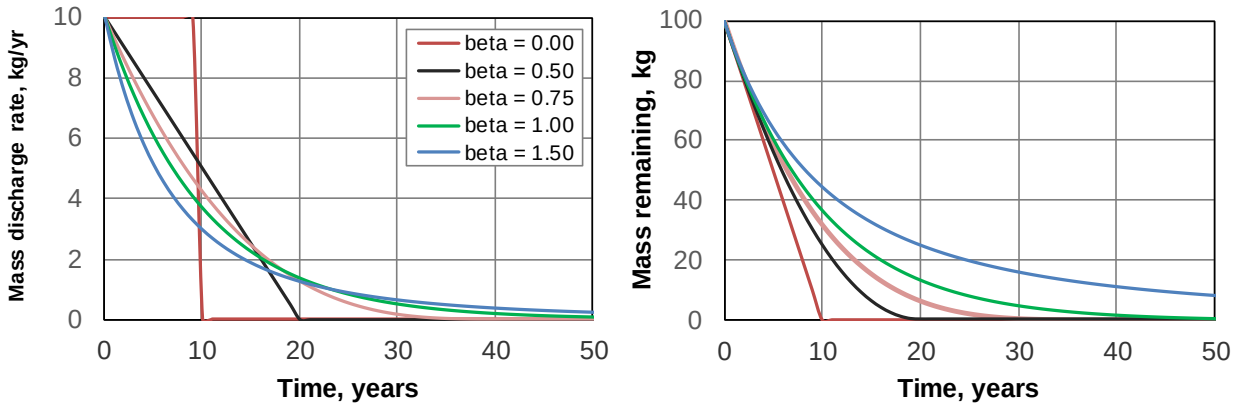

Figure 2.2. Effect of β on source mass remaining and discharge rate versus time for M_o = 100 kg and J_o = 10 kg/day. Note: with a log-scale y-axis, β = 1 curves are linear.

In some cases, it may be necessary to consider multiple DNAPL sources to be contributing to groundwater contamination at a site. Obvious cases include multiple known or inferred historical disposal areas at different locations. Large vertical variability in DNAPL saturations may be important to consider in some cases (e.g., thick aquifer, low vertical dispersivity, short plume). A more common, but overlooked, problem is the existence of subregions characterized by source architectures that exhibit different mass transfer characteristics. For example, DNAPL pools are characterized by β values <1, while residual DNAPL sources exhibit larger β values. Since the composite behavior of multiple sources with different β values cannot be accurately described by a single function with a single average β value, two (or more) modeled sources may be necessary to capture the behavior of sources with significant DNAPL with both pools and residual architectures. Also, sources in saturated and unsaturated zones will likely have different parameters that cannot be accurately represented by single lumped parameterizations.

However, it must be recognized that more source functions require more parameters to calibrate from available field data. If one attempts to calibrate more parameters than the quality and/or quantity of data can support, overall model reliability will suffer rather than improve (Parker et al. (2010). Optimum model parameterization may be identified by trial and error to obtain the smallest total prediction uncertainty (see Chapter 7).

Considering remedial actions at dates $t_{rem\,1}$, $t_{rem\,2} \ldots t_{rem\,n}$ when partial source mass removal and/or step changes in F_{mt} occur and stipulating that $t_o < t_{cal} < t_{rem\,1}$, values of M_{ref}, t_{ref} and F_{mt} in (2.2) are assumed to vary with time as described in Table 2.1.

Table 2.1. Definitions of F_{mt}, t_{ref} and M_{ref} as functions of time.

Time Period	F_{mt}	t_{ref}	M_{ref}
$t_o < t \leq t_{rem\,1}$	$F_{mt\,0} = 1$	$t_{ref\,0} = t_{cal}$	$M_{ref\,0} = M_{cal}$
$t_{rem\,1} < t \leq t_{rem\,2}$	$F_{mt\,1}$	$t_{ref\,1} = t_{rem\,1}$	$M_{ref\,1}$
$t_{rem\,n-1} < t \leq t_{rem\,n}$	$F_{mt\,n-1}$	$t_{ref\,n-1} = t_{rem\,n-1}$	$M_{ref\,n-1}$
$t > t_{rem\,n}$	$F_{mt\,n}$	$t_{ref\,n} = t_{rem\,n}$	$M_{ref\,n}$

Values of $M_{ref\,n}$ in Table 2.1 for $n > 0$ are given by

$$\begin{aligned} M_{ref\ n} &= M_{remo\ n} - \Delta M_{rem\ n} \\ M_{remo\ n} &= \left[M_{rem\ n-1}^{\,1-\beta} - F_{mt\ n-1} B(1-\beta)(t_{rem\ n} - t_{rem\ n-1}) \right]^{1/(1-\beta)} \end{aligned} \tag{2.3}$$

where $\Delta M_{rem\,n}$ is the mass removed from the source at time $t_{rem\,n}$ regarded as instantaneous. The source mass at time t_o may be computed as

$$M_o \equiv M(t_o) = \left[M_{cal}^{\,1-\beta} - B(1-\beta)(t_o - t_{cal}) \right]^{1/(1-\beta)} \tag{2.4}$$

for an instantaneous release at t_o, $M = 0$ and $J = 0$ for $t < t_o$. For a finite duration DNAPL release event from start date t_s to a release termination date t_o with a linear net increase in DNAPL source mass over time

$$M(t) = \frac{t - t_s}{t_o - t_s} M_o \qquad \text{for } t_s < t \leq t_o \tag{2.5}$$

The mass dissolution rate between t_s and t_o may be computed from (2.1) and (2.5) and the total mass released, including mass dissolution prior to t_o, obtained by integrating (2.1) with (2.5) as

$$M_{total} = M_o + \frac{J_{cal} M_o^{\beta} \left(t_o - t_s\right)}{(1+\beta) M_{cal}^{\beta}} \tag{2.6}$$

Note that dissolution of DNAPL mass will usually continue long after the final DNAPL release date t_o unless remedial action is undertaken to reduce or eliminate the remaining DNAPL mass.

Discharge rate decreases linearly with time if $\beta = 0.5$ (Figure 2.2). For $\beta > 0.5$, discharge rate approaches zero asymptotically but (theoretically) never reaches zero, while for $\beta < 0.5$, discharge rate reaches zero abruptly after a definable period. Residual or "ganglia" type DNAPL exhibit low β values (< 0.5-1.0), while pools and lenses will exhibit higher values (Parker and Park 2004).

Sorenson (2006) reported that enhanced source zone biodecay caused dissolution rate coefficients to increase by factors of 2 to 6 in laboratory studies and 3 to 8 in field studies. Parker and Park (2004) also have shown that field-scale dissolution rate coefficients will vary inversely with changes in source zone darcy flux (e.g., due to engineered or inadvertent permeability decreases due to amendment injection). Changes in F_{mt} due to ED injection upgradient of DNAPL sources are described in Chapter 3. Effects of in situ chemical oxidation are described in Chapter 5.

2.3 Mapping the Groundwater Flow Field

SCOToolkit considers multiple chlorinated hydrocarbon (CH) sources that may occur within an aquifer characterized by a Cartesian coordinate system in field mapping units (E, N) – i.e, easting and northing. Flow paths may be approximated as linear or nonlinear cubic polynomial functions. To apply the semi-analytical solution for contaminant transport in a planar flow field to mildly nonlinear flow fields, we define a coordinate transformation for each DNAPL source (and also for ED injection galleries that will be discussed later) to convert from field coordinates to linearized local coordinates (x, y) and back.

For each source we define the origin of the local coordinate system to be at the center of the downgradient plane of the source: e.g., (E_0, N_0) in field coordinates. A streamline may be drawn through (E_0, N_0) using water level contours, dissolved plume data, and user discretion. Coordinates of selected points along the inferred streamline are used to fit a streamline function. Detailed procedures for fitting nonlinear streamline functions are described in Chapter 6 (section 6.2.3).

For nonlinear streamlines, a polynomial function is used to define the (E, N)→(x, y) mapping, where x is the distance along the centerline and y is the transverse distance orthogonal to the centerline. Given the source origin in field coordinates (E*, N*), local coordinates oriented with the streamline can be found as follows (Figure 2.3):

1) The orthogonal line that passes through (E*, N*) and intersects the streamline at $E = E_{cross}$ may be described by $N = A+BE$ where $A = N^* + BE_{cross}$ and $B = -(a+2b+3cx^2)^{-1}$,
2) Solve recursively for E_{cross} using $E_{cross} = E^*$ initially then solve the cubic equation for E where the orthogonal line intersects the streamline,
3) Compute y' as the distance from (E*, N*) to (E_{cross}, N_{cross}),

4) Compute x as the distance along the streamline from (E_0, N_0) to (E_{cross}, N_{cross}) by integrating $[1 + N'(E)^2]^{1/2}dE$ from E_0 to E_{cross} where $N'(E)=dN/dE$. Calculate numerically using dE = 10 m.

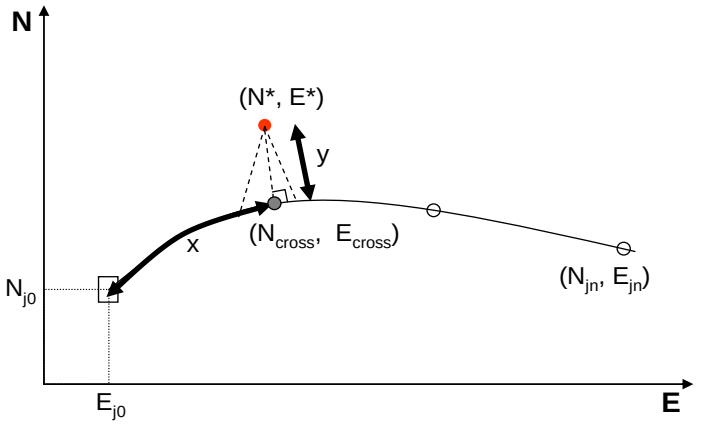

Figure 2.3. Curvilinear streamline in (E, N) field coordinates and mapping to local (x, y) coordinates for source j.

To estimate streamline parameters *a*, *b*, and *c*, it is necessary first to manually sketch the streamline and digitize northing-easting coordinates for a number of points along the streamline. These coordinates can be input into the provided Excel program ***Streamline calculation.xlsx*** to fit model parameters (Appendix A).

2.4 Dissolved Plume Transport

2.4.1 Analytical solutions for resident and flux concentrations

In the following, we present 3-D solutions for resident and flux concentrations in an aquifer of finite thickness L_{aq} with a steady-state planar flow field with a contaminant source on a vertical plane centered at $x = 0$, $y = 0$, $z = 0$. The x-dimension is treated as infinite in the positive (downstream) direction, the y-direction is infinite, and the z-direction may be semi-infinite or finite as discussed later. Dissolved phase transport is commonly described by the advection-dispersion equation (ADE), which for a planar flow field takes the form

$$R\frac{\partial C}{\partial t} = A_x v\frac{\partial^2 C}{\partial x^2} + A_y v\frac{\partial^2 C}{\partial y^2} + A_z v\frac{\partial^2 C}{\partial z^2} - v\frac{\partial C}{\partial x} - \lambda C \tag{2.7}$$

where A_x, A_y and A_z are dispersivities [L] in longitudinal, transverse horizontal, and vertical directions, respectively; R is a retardation actor for linear sorption [L^0], $v = q/\phi$ is the pore velocity with darcy velocity q [MT^{-1}] and porosity ϕ [L^0], λ is a first-order decay coefficient [T^{-1}] x is distance from the source in the direction of flow [L]; y is lateral distance from the center of the source perpendicular to flow [L]; z is vertical distance [L]; t is time since the initial release [T]; and C [ML^{-3}] may represent resident or flux concentration depending on the boundary conditions applied.

An arbitrarily time-dependent contaminant source with mass discharge rate $\dot{m}(t)$ [MT^{-1}] distributed uniformly over a vertical plane perpendicular to flow of width L_y and height L_z with its center at $x = 0$ and $y = 0$. The location of $z = 0$ depends on various cases described later. Zero concentration gradients for resident and flux solutions are assumed in the z-direction to the top and bottom of the aquifer, in the y-direction at $y = \pm\infty$, and in the x-direction at $x = +\infty$ and at $x = 0$ other than vertical plane source area. Note that the boundary conditions at x=0 preclude upstream migration of contaminant. The boundary condition on the source plane area for the resident concentration solution of (2.4) is

$$q\left(C_R - A_L \frac{\partial C_R}{\partial x}\right) = \frac{\dot{m}(t)}{L_x L_y} \tag{2.8a}$$

and the boundary condition for the flux concentration solution is

$$qC_F = \frac{\dot{m}(t)}{L_x L_y} \quad . \tag{2.8b}$$

The solution of (2.7) for resident or flux boundary conditions with an arbitrary contaminant mass discharge rate as a function of time can be obtained by convolution using

$$C(x,y,z,t) = \frac{1}{L_y L_z \phi} \int_0^t \dot{m}(\tau)\, f_x(x,t-\tau)\, f_y(y,t-\tau)\, f_z(z,t-\tau) d\tau \tag{2.9}$$

where τ is a dummy time integration variable [T], $f_x(x,t)$ is the x-direction solution for a dirac pulse (i.e., instantaneous unit mass injection) subject to (2.8a) or (2.8b) as applicable [L^{-1}], $f_y(y,t)$ is the dispersion solution in the y-direction [-], and $f_z(z,t)$ is the z-direction dispersion solution [-]. Equation (2.6) is integrated numerically.

Toride et al. (1995, Table 2.2) present 1-D solutions for instantaneous unit mass injection in time for resident and flux concentrations for an unbounded solution domain in the positive x-direction, which yield the following solutions for $f_x(x,t)$

$$f_x^F(x,\tau) = \frac{Rx}{v\tau\left(4\pi R A_x v\tau\right)^{1/2}} \exp\left(\frac{-\lambda\tau}{R} - \frac{\left(Rx - v\tau\right)^2}{4RA_x v\tau}\right) \tag{2.10a}$$

$$f_x^R(x,\tau) = \exp\left(\frac{-\lambda\tau}{R}\right)\left\{\begin{array}{l} \dfrac{1}{\left(\pi A_x v R\tau\right)^{1/2}} \exp\left(-\dfrac{(Rx - v\tau)^2}{4A_x v R\tau}\right) \\ -\dfrac{1}{2A_x R} \exp\left(\dfrac{x}{A_x}\right) \operatorname{erfc}\left(\dfrac{Rx + v\tau}{\left(4A_x v R\tau\right)^{1/2}}\right) \end{array}\right\} \tag{2.10b}$$

where f_x^R and f_x^F are functions for resident and flux solutions, respectively. An alternative formulation in lieu of (2.6), which can be integrated more efficiently for locations near the source, is

$$C(x,y,z,t) = \frac{1}{L_y L_z q} \int_0^{\dot{m}(t)} g_x(x,t-\tau)\, f_y(y,t-\tau)\, f_z(z,t-\tau)\, d\dot{m}(\tau) \tag{2.11}$$

where $g_x(x,t)$ represents the solution for continuous injection at a constant unit rate. Note that since $\dot{m}(t)$ is a function of time, numerical integration of (10) can be performed either by (i) integrating over a specified Δt and computing $\Delta\dot{m}(t)$ corresponding to each time-step using (2.9), or (ii) integrating over a specified $\Delta\dot{m}(t)$ and back-calculating t for each step for use in g_x and other terms in (2.11). Resident and flux solutions for g_x are

$$g_x^F(x,\tau) = \frac{1}{2}\exp\left(\frac{(v-u)x}{2A_x v}\right)\operatorname{erfc}\left(\frac{Rx-u\tau}{2(RA_x v\tau)^{1/2}}\right) + \frac{1}{2}\exp\left(\frac{(v+u)x}{2A_x v}\right)\operatorname{erfc}\left(\frac{Rx+u\tau}{2(RA_x v\tau)^{1/2}}\right) \tag{2.12a}$$

$$g_x^R(x,\tau) = \frac{1}{v+u}\exp\left(\frac{(v-u)x}{2A_x v}\right)\operatorname{erfc}\left(\frac{Rx-u\tau}{2(RA_x v\tau)^{1/2}}\right) + \frac{1}{v-u}\exp\left(\frac{(v+u)x}{2A_x v}\right)\operatorname{erfc}\left(\frac{Rx+u\tau}{2(RA_x v\tau)^{1/2}}\right) + \frac{v}{2\lambda A_x v}\exp\left(\frac{vx}{A_x v}-\frac{\lambda\tau}{R}\right)\operatorname{erfc}\left(\frac{Rx+v\tau}{2(RA_x v\tau)^{1/2}}\right) \quad \text{for } \lambda > 0 \tag{2.12b}$$

$$g_x^R(x,\tau) = \frac{1}{2}\operatorname{erfc}\left(\frac{Rx-v\tau}{2(RA_x v\tau)^{1/2}}\right) + \left(\frac{v^2\tau}{\pi RA_x v}\right)^{1/2}\exp\left(-\frac{(Rx-v\tau)^2}{4RA_x v\tau}\right) - \frac{1}{2}\left(1+\frac{vx}{A_x v}+\frac{v^2\tau}{RA_x v}\right)\exp\left(\frac{vx}{A_x v}\right)\operatorname{erfc}\left(\frac{Rx+v\tau}{2(RA_x v\tau)^{1/2}}\right) \quad \text{for } \lambda = 0$$

where g_x^R and g_x^F are functions for resident and flux concentrations [L^0], respectively, and $u = \left(v^2 + 4\lambda A_x v\right)^{1/2}$. It may be noted that (2.10a) and (2.10b) will yield nearly identical results (hence $C_R \approx C_F$) when $A_x/x << 1$. This is also the case for (2.12a) and (2.12b).

The horizontal spreading terms in (2.9) and (2.11) for an aquifer unbounded laterally is given by

$$f_y(y,\tau) = \frac{1}{2}\left[\operatorname{erf}\left(\frac{|y|+L_y/2}{2(A_y v\tau/R)^{1/2}}\right) - \operatorname{erf}\left(\frac{|y|-L_y/2}{2(A_y v\tau/R)^{1/2}}\right)\right] \tag{2.13}$$

Note that symmetry about the center line yields the same function values for positive or negative y-values having the same absolute magnitude.

To account for different vertical source configurations, three conditions are distinguished for vertical dispersion terms as described below.

Condition 1. Fully penetrating source (2-D solution)

If the source thickness, L_z, is equal to the aquifer thickness, L_{aq}, then a 2-D solution strictly applies for which $f_z(z,t) = 1$. A 2-D solution may also be applicable at distances sufficiently far downstream from the source that vertical dispersion yields essentially uniform mixing over the aquifer thickness.

Condition 2. Partially penetrating source adjacent to top or bottom aquifer boundary
For this condition, the top of the source zone may coincide with the aquifer upper boundary defined at $z = 0$ (e.g., water table) and the bottom of the source is substantially above the aquifer lower boundary with z increasing downwards. Alternatively, the bottom of the source coincides with the aquifer lower boundary defined locally as z=0 with z increasing upwards.

The Condition 2 vertical dispersion function for an aquifer of infinite thickness is given by

$$f_z^{\infty}(z,\tau) = \frac{1}{2}\left[\text{erf}\left(\frac{z + L_z}{2(A_z v\tau / R)^{1/2}} \right) - \text{erf}\left(\frac{z - L_z}{2(A_z v\tau / R)^{1/2}} \right) \right] \tag{2.14a}$$

An image boundary technique (e.g., Galya 1987) is employed to correct for effects of plume interaction with finite vertical boundaries as follows

$$\begin{aligned} f_z(z,\tau) = {} & f_z^{\infty}(z,\tau) + f_z^{\infty}(2L_{aq} - z,\tau) + f_z^{\infty}(2L_{aq} + z,\tau) + \\ & f_z^{\infty}(4L_{aq} - z,\tau) + f_z^{\infty}(4L_{aq} + z,\tau) + \\ & f_z^{\infty}(6L_{aq} - z,\tau) + f_z^{\infty}(6L_{aq} + z,\tau) + \ldots \end{aligned} \tag{2.14b}$$

Three subsidiary conditions may be distinguished for computing the Condition 2 dispersion function:

Condition 2a. $x < x_{\infty} = (L_{aq}\text{-}L_z)^2 F_{\infty} / A_z$

At distances closer than x_{∞} from the source, the plume has not intercepted the opposite aquifer boundary opposite the source. Therefore, no correction terms need to be applied and (2.14a) alone can be used to compute $f_z(z,\tau) = f_z^{\infty}(z,\tau)$. The factor F_{∞} = 0.001 was determined by comparing 3-D solution results with and without correction terms.

Condition 2b. $x > x_{2D} = (L_{aq}\text{-}L_z)^2 F_{2D} / A_z$

At distances greater than x_{2D} from the source, vertical mixing yields negligible vertical concentration gradients and a 2-D approximation may be adopted as described above with $f_z(z,t) = 1$. The factor $F_{2D} = 10$ was determined by comparing 3-D and 2-D solution results.

Condition 2c. $x_{\infty} < x < x_{2D}$

For this case, (2.14b) is employed using a sufficient number of correction terms to obtain desired accuracy. After computing the first two terms in (2.11b), the series is terminated when the last computed term is less than 0.1% of the sum of all terms computed to that point.

Condition 3. Source NOT immediately adjacent to top or bottom of aquifer

Finally, we consider the instance in which the source does not lie immediately adjacent to the top or bottom of the aquifer. The center of the source of thickness L_z is located at an elevation denoted locally as $z = 0$ with positive z above the source and negative below. The top of the source is at $z = L_z/2$ and the aquifer upper boundary is at $z = L_u \geq L_z/2$. The bottom of the source is at $z = -L_z/2$ and the aquifer lower boundary is at $z = L_b \leq L_z/2$. Note that if the top of the source is designated

as L_{top} below the water table, then $L_u = L_{top} - L_z/2$ and $L_b = L_{aq} - L_u$. The vertical dispersion function for an unbounded aquifer is

$$f_z^{\infty}(z,\tau) = \frac{1}{2}\left[\operatorname{erf}\left(\frac{|z| + L_z/2}{2(A_z v\tau / R)^{1/2}} \right) - \operatorname{erf}\left(\frac{|z| - L_z/2}{2(A_z v\tau / R)^{1/2}} \right) \right] \tag{2.15a}$$

Note that although the function defined by (2.12a) is symmetric about z = 0, corrections for finite aquifer thickness will be asymmetric unless the source lies exactly midway between the upper and lower aquifer boundaries. If corrections for finite aquifer thickness are required and $L_u - |z| < L_b - |z|$, the series with terms in order of decreasing magnitude is

$$\begin{aligned} f_z(z,\tau) = {} & f_z^{\infty}(z,\tau) + f_z^{\infty}(2L_b + z, t) + f_z^{\infty}(2L_u - z, t) + \\ & f_z^{\infty}(2L_b + 2L_u - z, t) + f_z^{\infty}(2L_u + 2L_b + z, t) + \\ & f_z^{\infty}(4L_b + 2L_u + z, t) + f_z^{\infty}(4L_u + 2L_b - z, t) + \\ & f_z^{\infty}(4L_b + 4L_u - z, t) + f_z^{\infty}(4L_u + 4L_b + z, t) + \\ & f_z^{\infty}(6L_b + 4L_u + z, t) + f_z^{\infty}(6L_u + 4L_b - z, t) + \\ & f_z^{\infty}(6L_b + 6L_u - z, t) + f_z^{\infty}(6L_u + 6L_b + z, t) + \ldots \end{aligned} \tag{2.15b}$$

otherwise, the computational sequence is

$$\begin{aligned} f_z(z,t) = {} & f_z^{\infty}(z,t) + f_z^{\infty}(2L_u - z, t) + f_z^{\infty}(2L_b + z, t) + \\ & f_z^{\infty}(2L_u + 2L_b + z, t) + f_z^{\infty}(2L_b + 2L_u - z, t) + \\ & f_z^{\infty}(4L_u + 2L_b - z, t) + f_z^{\infty}(4L_b + 2L_u + z, t) + \\ & f_z^{\infty}(4L_u + 4L_b + z, t) + f_z^{\infty}(4L_b + 4L_u - z, t) + \\ & f_z^{\infty}(6L_u + 4L_b - z, t) + f_z^{\infty}(6L_b + 4L_u + z, t) + \\ & f_z^{\infty}(6L_u + 6L_b - z, t) + f_z^{\infty}(6L_b + 6L_u + z, t) + \ldots \end{aligned} \tag{2.15c}$$

The series is truncated after the last computed term is less than 0.1% of the sum of all terms to that point. Sub-conditions analogous to those for Condition 2 may be distinguished as follows.

Condition 3a. If $x < x_{\infty} = (L_{min} - L_z/2)^2 F_{\infty}/A_z$ where $L_{min} = \min(L_u, L_b)$ then (2.15a) with no corrections is used to compute $f_z(z,\tau) = f_z^{\infty}(z,\tau)$.

Condition 3b. If $x > x_{2D} = (L_{max} - L_z/2)^2 F_{2D}/A_z$ where $L_{max} = \max(L_u, L_b)$ then a 2-D approximation with $f_z(z,t) = 1$ is employed.

Condition3c. If $x_{\infty} < x < x_{2D}$ then (2.15b) or (2.15c) is used to compute correction terms until the truncation criteria is met.

2.4.2 Aqueous concentration upgradient of source plane

Since the transport solution assumes no counterflow dispersion and the source is treated as a plane at the downgradient edge of the source zone, the solution predicts no contaminant for $x<0$. To compute reasonable concentrations within the source zone from $-x_{source} < x < 0$, we adopt the following approximation

$$\begin{aligned} C(x,y,z,t) &= C(0,y,z,t)\left(1+\frac{x}{x_{source}}\right) && -x_{source} < x < 0 \\ C(x,y,z,t) &= 0 && x < -x_{source} \end{aligned} \tag{2.16}$$

where x_{source} is the source length.

2.4.3 Variable decay coefficients with distance from source

Spatially-variable decay within an aquifer can be described with up to three "zones" at specified distances from a source characterized by different decay coefficients. Zone 1 represents the region $x < L_{12}$ with a decay coefficient of λ_1; Zone 2 is from $L_{12} < x \leq L_{23}$ with a decay coefficient of λ_2; and Zone 3 is located at $x > L_{23}$ with a decay coefficient of λ_3.

The solution for Zone 1 is computed as described in section 2.3.2 with $\lambda = \lambda_1$ and actual best estimates of the source parameters J_{cal} and M_{cal}. For Zone 2, λ_2 is used in the solution and $\dot{m}(t)$ is computed from (2.1) using values for J_{cal} and M_{cal} multiplied by a scaling factor S_2 defined as

$$S_2(t) = \frac{C(x=L_{12}, y=0, t; \lambda_1, J_{cal}, M_{cal})}{C(x=L_{12}, y=0, t; \lambda_2, J_{cal}, M_{cal})} \tag{2.17a}$$

For Zone 3 $\lambda = \lambda_3$ and J_{cal} and M_{cal} values are scaled by a factor S_3 defined as

$$S_3(t) = \frac{C(x=L_{23}, y=0, t; \lambda_2, S_2(t)J_{cal}, S_2(t)M_{cal})}{C(x=L_{23}, y=0, t; \lambda_{3,cal}, J_{cal}, M_{cal})} \; . \tag{2.17b}$$

Extension of the model to simulate ED-limited biodecay is discussed in Chapter 3.

2.4.4 Modeling dissolved plumes from multiple DNAPL sources

Contaminant concentrations resulting from multiple sources are computed by superposition of the individual source solutions after reverting back to field coordinates as

$$C(E,N,t) = \sum_{j=1}^{N_{source}} C_j(E,N,t) \tag{2.18}$$

Note that function calls on the RHS of (2.18) require mapping of global (E, N) coordinates to local (x, y) coordinates for each source as illustrated in Figure 2.4.

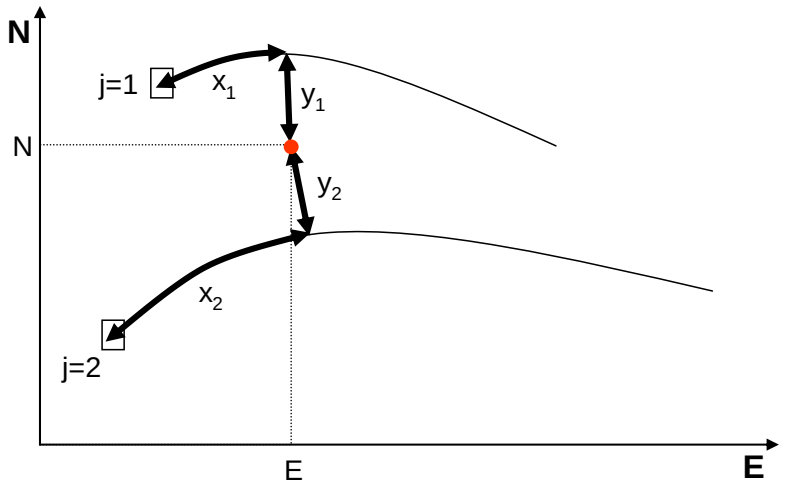

Figure 2.4. Mapping of well location to linearized coordinates for two adjacent nonlinear streamlines in field coordinates for solution superposition.

2.5 Diffusion-limited Mass Transfer

2.5.1 Upscaled back-diffusion model

Many mathematical models have been presented for transport in media characterized by "mobile" regions in which contaminants move primarily by advection and "immobile" regions where contaminants move primarily by diffusion. We consider here the interpretation of resident and flux concentrations obtained from the analytical model described in section 2.4 in terms of a mobile-immobile model quantified by the following parameters:

q_m = mobile zone darcy velocity [LT^{-1}]
F_m = ratio of mobile zone volume to total aquifer volume [L^3L^{-3}]
A_m = mobile zone longitudinal dispersivity [L]
L_{im} = average immobile zone diffusion path length[L]
D_{im} = immobile zone effective molecular diffusion coefficient [L^2T^{-1}]
ϕ_m = mobile zone water volume as fraction of total mobile zone volume [L^3L^{-3}]
ϕ_{im} = immobile zone water volume as fraction of total immobile zone volume [L^3L^{-3}]
ρ_m = dry soil mass in mobile zone as fraction of total mobile zone volume [$M\ L^{-3}$]
ρ_{im} = dry soil mass in immobile zone as fraction of total immobile zone volume [$M\ L^{-3}$]
k_m = mobile zone adsorption coefficient [L^3M^{-1}]
k_{im} = immobile zone adsorption coefficient [L^3M^{-1}]
λ_m = mobile zone first-order decay coefficient [T^{-1}]
λ_{im} = immobile zone first-order decay coefficient [T^{-1}]
γ = dimensionless factor reflecting mobile-immobile zone geometry

A number of studies (Bolt 1979, Passioura 1971, Raats 1981, Parker and Valocchi 1986, van Genuchten 1985, van Genuchten and Dalton 1986) have shown that diffusion-limited mobile-immobile model solutions can be approximated by the simple ADE solved subject to boundary conditions that distinguish between resident and flux concentrations using the following upscaling relationships between dispersion model parameters and mobile-immobile model parameters:

$$\hat{A}_x = f_m A_m + \frac{(1-f_m)\hat{v}L_{im}^2 R_{im}^2}{\gamma D_{im} R^2} \tag{2.19a}$$

$$\hat{v} = \frac{\hat{q}}{\hat{\phi}} = \frac{F_m q_m}{F_m \phi_m + (1-F_m)\phi_{im}} \tag{2.19b}$$

$$R = f_m R_m + (1-f_m) R_{im} \tag{2.19c}$$

$$\hat{\lambda} = f_m \lambda_m + (1-f_m)\lambda_{im} \tag{2.19d}$$

where

$$R_m = 1 + \frac{\rho_m k_m}{F_m \phi_m} \tag{2.19e}$$

$$R_{im} = 1 + \frac{\rho_{im} k_{im}}{(1-F_m)\phi_{im}} \tag{2.19f}$$

$$f_m = \frac{F_m \phi_m}{F_m \phi_m + (1-F_m)\phi_{im}} \tag{2.19g}$$

In which variables depicted with a "hat" (e.g., $\hat{A}_x$) represent field-scale "effective" or "upscaled" model parameters. Values of the geometry factor γ for various mobile-immobile zone configurations based on van Genuchten and Dalton (1986) are shown in Table 2.2.

Table 2.2. Geometry factors for upscaled dispersion model.

Geometry of media	Geometry factor, γ	L_{im}
Spherical aggregates in mobile matrix	15	Sphere radius
Solid cylindrical aggregates in mobile matrix	8	Cylinder radius
Planar sheets in mobile matrix	3	Sheet half-thickness
Hollow cylinders with "wormhole" [1]	$\left[0.5\ln\left(\frac{b}{a}\right)-0.25\right]^{-1}$	$b - a$

[1] a = outer radius and b = "wormhole" radius for hollow cylinder case

Simulations using upscaled parameters given by (2.16) will yield first and second moments of flux concentration versus time for a Dirac injection equal to those for the bi-continuum model of specified fracture-matrix geometry (Parker and Valochchi 1986).

To the extent mobile-immobile model parameters can be directly estimated from field and/or lab data, the foregoing relationships can be used to estimate upscaled model parameters, which can then be refined, if necessary, by calibration to field data. Potential types of field data and their interpretations include the following.

Monitoring well data

Dissolved concentrations from well samples should be regarded as upscaled model flux concentrations, C_F. This is true regardless of whether immobile zones occur or not, since immobile zones, by definition, do not contribute to flux concentration.

Small-scale dissolved concentration samples

If dissolved concentration samples are obtained using suction devices (e.g., in conjunction with geoprobe equipment) at a scale smaller than the spacing between mobile and immobile zones, the values can best be interpreted as local scale resident concentrations. To obtain average resident concentrations, C_R, at a scale that encompasses mobile and immobile zones, local concentrations within an appropriate distance can be averaged and used for calibration. Alternatively, local values may be used directly for calibration using a least squares objective. However, residual deviations will be much larger due to the scale mismatch.

Soil concentration data averaged over mobile and immobile zones

If the spacing between mobile and immobile zones is small compared to the length over which soil samples are taken, measurements of total soil concentration (dissolved and sorbed contaminant mass per dry soil mass, S_{all}) can be interpreted as

$$S_{all} = \frac{R\phi C_R}{\rho} \tag{2.20a}$$

where all variables represent upscaled model values.

Soil concentrations from mobile zone samples

If soil samples are taken from identifiable mobile zones within the aquifer, measured mobile zone soil concentrations, S_m, can be interpreted as

$$S_m = \frac{R_m \phi_m C_F}{\rho_m} \tag{2.20b}$$

assuming that the mobile zone dissolved concentration is approximately equal to the upscaled model flux concentration since mobile zone dispersivity is generally small. The aqueous + sorbed mobile zone contaminant mass per total (mobile + immobile zone) soil mass, $S_{m/t}$, is

$$S_{m/t} = f_m R_m \phi_m C_F \tag{2.20c}$$

Soil concentrations from immobile zone samples

If soil samples are taken from identifiable low permeability zones, the measured immobile zone contaminant mass per dry mass of immobile zone soil, S_{im}, can be interpreted as

$$S_{im} = \frac{\rho S_{all} - f_m \rho_m S_m}{(1 - f_m)\rho_{im}} \tag{2.20d}$$

while the aqueous + sorbed immobile zone contaminant mass per total (mobile + immobile zone) soil mass, $S_{im/t}$, can be interpreted as

$$S_{im/t} = \rho S_{all} - f_m \rho_m S_m \,. \tag{2.20e}$$

Note that interpretation of mobile and immobile zone soil concentrations depends on both upscaled and bi-continuum model parameters. SCOToolkit includes the capability to employ any of the above types of data in input files used for model calibration.

2.5.2 Verification of the upscaled back-diffusion model

The upscaling relations given by (2.16) may be derived by equating certain characteristics of the mono- and bi-continuum models, such as their first- and second-moments, which will yield equality of the matched characteristic, but not equality at every point in time or space. In this section, we investigate applications of the upscaled dispersion model to previously published studies of media with significant mass transfer limitations that exhibit early breakthrough and extended tailing to assess the accuracy of the upscaling relationships.

The first problem involves a laboratory study of 190 mm long columns with an outer diameter of 52 mm consisting of a sand/clay/grout mixture with a 1.7 mm diameter hole in the center extending axially from the inlet of the column to the outlet of the column intended to simulate a root or worm channel (Parker, 1984). The porosity was 0.365. A 0.65 pore volume bromide solution was added to two essentially identical columns under positive pressure at a flow rate of 4.65×10^{-4} m/s. One column was sectioned immediately following tracer injection, cut into 19 mm long sections and extracted pore fluid was analyzed for bromide. Bromide-free solution was added to the second column for another 1.15 pore volumes and effluent samples were collected and analyzed. No measurement of the effective diffusion coefficient was available. However, Promentilla et al. (2006) report tortuosities for cement samples over a range of porosities, which in conjunction with a literature value for the bromide diffusion coefficient in bulk water yield an effective diffusion coefficient of 7.4×10^{-9} m^2/s. Disregarding mobile zone dispersivity, an effective dispersivity of 167 m was computed for the column from (2.16a) using the "hollow cylinder" geometry factor.

The experimental data reveal breakthrough within a small fraction of one pore volume and extended "tailing" albeit at very low concentrations due slow back-diffusion from the matrix and high dilution in mobile region (Figure 2.5a). Except for the sample closest to the inlet, measured resident concentrations after the injection period and prior to flushing are less than 3% of the effluent concentration magnitude at the time of sampling (Figure 2.5b). The higher concentration in the sample close to the inlet is attributable to longitudinal diffusion from the upper surface of the column rather than radial diffusion from the "wormhole."

Simulated flux concentrations using model parameters computed using (2.19) with no calibration agree closely with measured effluent data (Figure 2.5a) and simulated resident concentrations agree well with the sectioned column data (Figure 2.5b). Note that simulated and measured flux concentrations at the end of the injection period are much greater than measured and simulated resident concentrations. The importance of distinguishing between resident and flux concentrations and of employing the correct governing equation and boundary conditions for heterogeneous media should be self-evident. This example provides compelling evidence that the upscaled dispersion model solved for appropriate boundary conditions is capable of describing transport behavior in media characterized by highly preferential flow paths.

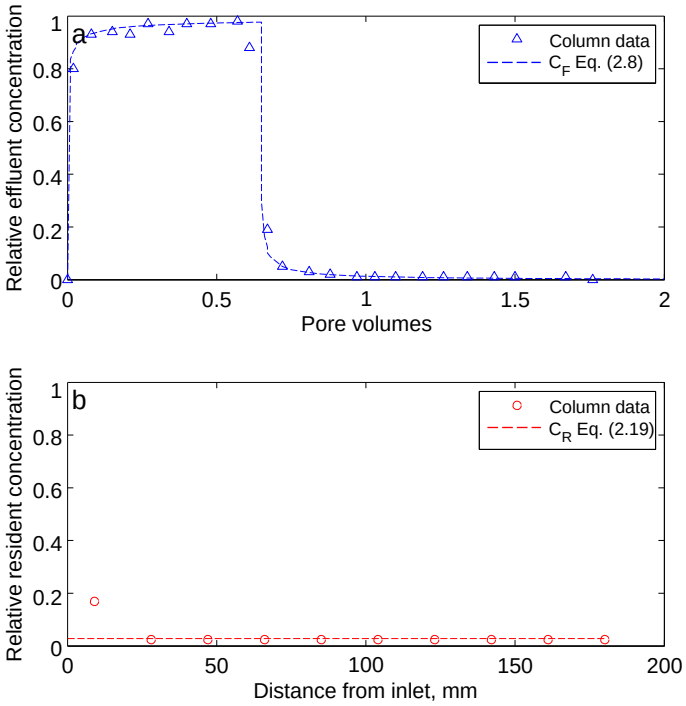

Figure 2.5. Observed and simulated transport for column experiment with "wormhole". (a) Measured breakthrough curves and simulated flux concentrations, and (b) measured and simulated resident concentrations versus distance following 0.65 pore volume tracer injection.

The second problem we consider involves a high resolution 2-D numerical simulation by Beth Parker and colleagues (2008) of chlorinated solvent in a permeable aquifer with discontinuous clay layers underlain by a clay aquitard. The model was used to simulate advection-dominated transport in the permeable material and diffusion in low permeability zones (Figure 2.5). Due to the large contrast between advective and diffusive time scales, a high-resolution grid and small time steps were required. Pools of TCE were assumed to occur on clay lenses as constant concentration sources for 30 years, after which sources were completely removed. Since mobile zone dispersivity is small, local scale resident and flux concentrations will be essentially identical and high-resolution model results will be insensitive to the type of boundary condition employed. A multi-level monitoring well was assumed near the downgradient boundary about 160 m from the sources. Numerically simulated TCE concentrations remained above 1 μg/L at most depths 200 years after source removal as a result of back-diffusion from clay layers (Figure 2.6).

Since contaminant sources are distributed more or less uniformly over the aquifer thickness, the 2-D numerical simulation may be reasonably approximated as a vertically-averaged 1-D problem. If we approximate the model domain as a system consisting of horizontal mobile and immobile layers, a flux concentration solution of the upscaled dispersion model may be obtained using parameters given by (2.19) to simulate samples taken from the entire well length. The model domain is taken as the 15 m thickness that includes the aquifer and aquitard. The well is not screened below the top of the aquitard and the well bore does not intersect any clay lenses within the aquifer. Therefore, the arithmetic average of numerically computed concentrations over all well intervals within the 10 m thick aquifer represent a flow-weighted concentration over the 15 m deep model domain.

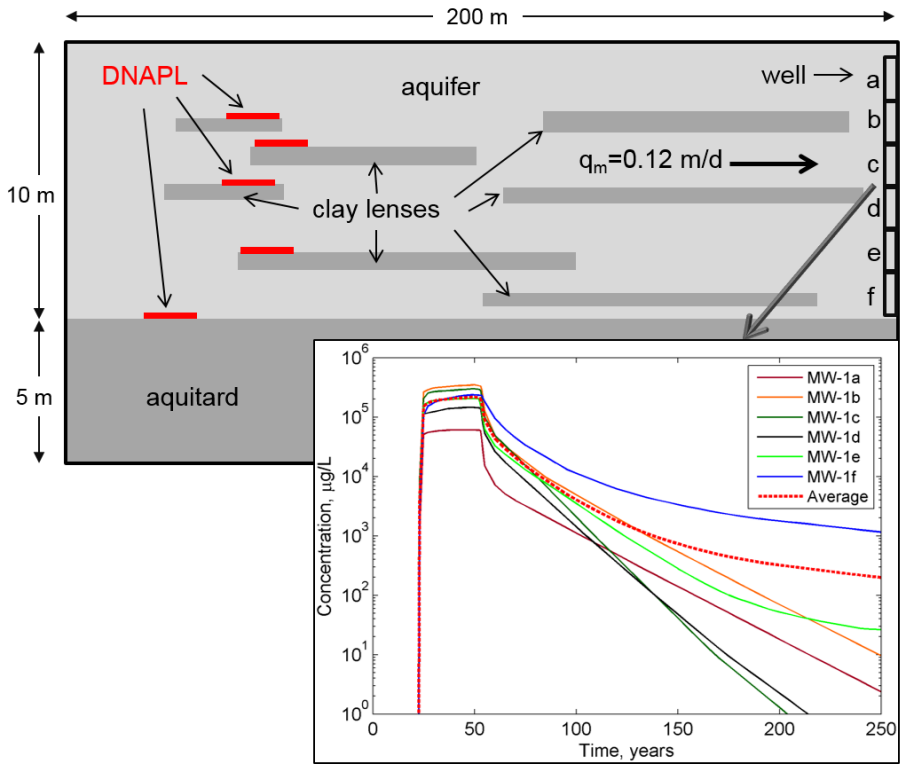

Figure 2.6. Domain for high resolution numerical model and numerically simulated TCE concentrations at different depths plus depth-averaged concentration in downgradient well over time (Parker et al., 2008).

Mobile and immobile zone porosities for this problem were assumed to be 0.4. Retardation factors were 1 in mobile zones, 5 in clay lenses within the aquifer and 3 in the aquitard. The mobile zone darcy velocity is 0.12 m/d and the effective TCE diffusion coefficient in all clay units was assumed to be 3.9×10^{-5} m^2/d. If we consider only effects of mass transfer involving clay lenses within the aquifer, the mobile pore fraction, f_m, over the 10 m thick aquifer is 0.85 and the average diffusion path length, L_{im}, is 0.25 m. Plugging the foregoing values into (2.19) gives an effective longitudinal dispersivity of 201 m. The retarded pore velocity (averaged over the full 15 m depth) is 58 m/yr. Average flux concentration at the monitoring well simulated with these model parameters dropped below 1 µg/L about 85 years after source removal (results not shown). Since the high resolution numerical model showed average concentrations exceeding 100 µg/L after 200 years, it is evident that the thin clay layers within the aquifer are relatively minor contributors to back-diffusion processes.

If we include the 5 m thick aquitard in the tally of immobile zones, the average mobile pore fraction over the 15 m model thickness drops to 0.57 and the volume-weighted diffusion path length increases to 3.9 m. Note that the diffusion path length for the aquitard is equal to its thickness, not its half thickness, because it contacts the aquifer on only one side. Although the aquitard retardation factor is smaller than that for the thin clay lenses, the average aquitard is about 5 times more voluminous resulting in a lower average pore velocity of 31 m/yr. (2.19a) gives a longitudinal dispersivity of 27,000 m for this system. With this exceedingly high dispersivity, the upscaled model predicts earlier breakthrough than the high-resolution model and exhibits a faster drop in

concentration following source removal compared to the high resolution numerical model (Figure 2.7). However, the late-time rate of concentration change for the upscaled model closely parallels the numerical model.

The early time deviations in the upscaled model likely reflect shorter effective diffusion path lengths at times when contaminant has only penetrated a fraction of the low permeability zones. To account for this, we investigated the simple and widely-used approximation of diffusion path length time-dependence (Crank 1975)

$$L_{im}(t) \approx \min\left(L_{im}^{max}, \left(\frac{2D_{im}t}{R_{im}} \right)^{1/2} \right) \tag{2.21}$$

where L_{im}^{max} is the maximum diffusion path length (5 m), t is time since the initial release, and other variables are as previously defined. Substitution of (2.21) into (2.19a) yields a linear increase in dispersivity with time to a maximum value of 6,800 m in 230 years. Simulated flux concentrations using the time-dependent diffusion length and dispersivity in the upscaled model follow the high resolution numerical results fairly well except for moderate under-prediction between 30 and 100 years (Figure 2.7). The maximum error during this period is about 65%, which would likely be within the range of "noise" in field data and the limits of reliability that can be reasonably expected even with sophisticated models at such a complex site. In any case, the upscaled model appears to offer a practical and efficient approach to evaluating the effects of back-diffusion that arise at heterogeneous sites, especially considering the demonstrated feasibility of quantifying dispersivity from physically meaningful site parameters with little or no calibration.

Comparisons between upscaled model C_R solutions and numerical model results were not possible since simulated aquitard concentrations were not given by Parker et al. (2008). However, a few observations may be made. The analytical model indicates that resident concentrations are less than flux concentrations prior to source removal and greater after source removal. Further, the magnitude of the difference between C_R and C_F is found to increase with dispersivity.

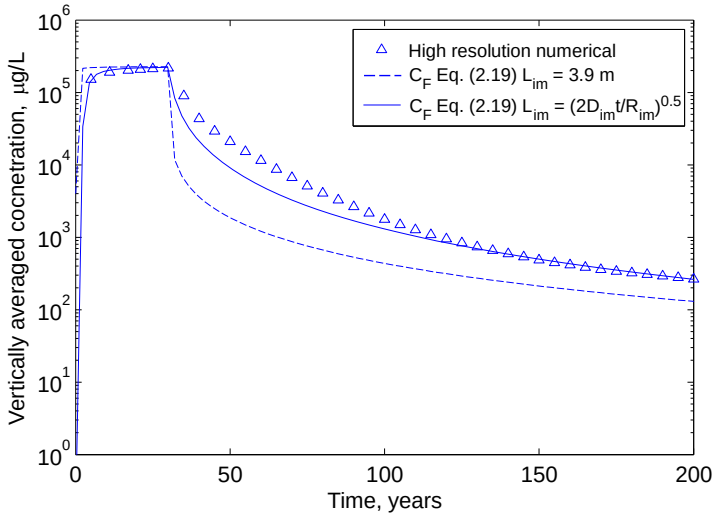

Figure 2.7. Vertically-averaged flux concentrations in aquifer with clay layers at well location based on Parker et al. high resolution numerical simulation and results for upscaled dispersion model with a constant diffusion path length, L_{im}, of 3.9m, or with a time-varying $L_{im}(t)$.

These observations are readily explained in the context of the mobile-immobile model. When the source is active, concentrations are higher in mobile zones than adjacent immobile zones, resulting in higher volume-averaged than flow-averaged concentrations, while the reverse is true after source removal as back-diffusion occurs. Also, the magnitude of concentration differences between mobile and immobile zones will increase as diffusive mass transfer resistance increases, which corresponds to increasing dispersivity according to (2.19a).

As a final point of interest, consider the fact that the well in the numerical model is located within a "window" in the aquifer where no clay layers intersect the well bore over the 10 m aquifer thickness. As a result, volume- and flow-averaged concentrations over the 10 m aquifer thickness (i.e., excluding the aquitard) are essentially equal at this location. In spite of the absence of clay lenses at the monitoring location, the flux concentration solution for the upscaled model with time-dependent dispersion provides a reasonable approximation of the high resolution numerical results. This reflects the relative insensitivity of flux concentrations to local variations in the immobile fraction, since the later have zero contribution to flux concentration. This reflects the fact that flux concentrations are controlled by cumulative upgradient transport processes (Figure 2.8).

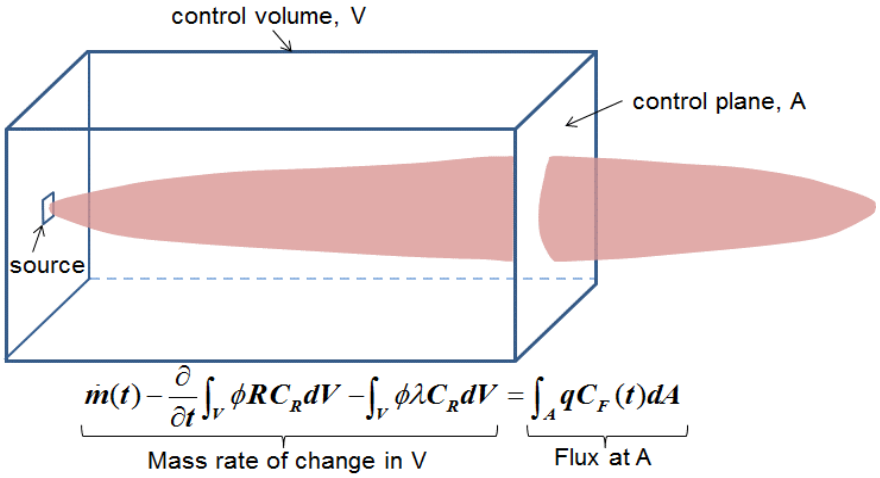

Figure 2.8. Illustration of the dependence of flux concentration at a control plane on integral of upgradient transport processes.

In contrast, local resident concentrations will exhibit large variance in response to local spatial variability in the distribution of low permeability material. For these reasons, well measurements, if properly interpreted as flux concentrations, are expected to exhibit less variance and hence be more valuable, in general, for model calibration than resident or soil concentration data. Nevertheless, a limited number of soil samples may provide valuable additional information for model calibration.

2.6 Summary

Depending on how samples are taken, fluid may be obtained equally from all pores (volume-averaged resident concentrations) or in proportion to local permeability (flow-averaged flux concentrations). Water samples from wells or suction sampling devices should generally be regarded as flux concentrations, while soil samples that are mixed and extracted in their entirety may be regarded as resident concentrations after correcting for dilution and sorption. The scale of measurements versus that of significant heterogeneities must be carefully considered for upscaled models in order to properly interpret field data.

Heterogeneous aquifers frequently exhibit much earlier breakthrough downgradient of a source than expected for purely advective transport and show extended tailing to long travel times. It is commonly assumed that simple advection dispersion models are not capable of describing such systems. We have shown this to be a misconception. While the ADE may not describe every detail of such systems exactly, when distinctions between resident and flux concentration solutions, dispersion upgradient of sources, and time-dependence of diffusion path length are addressed, the ADE is capable of representing rapid breakthrough and extended tailing with reasonable accuracy even in quite extreme cases.

2.7 References

Ball, W.P., C. Liu, G. Xia, and D.F. Young, (1997) A diffusion-based interpretation of tetrachloroethene and trichloroethene concentration profiles in a groundwater aquitard. *Water Resour. Res. 33*, 2741-2757.

Barker, J.A. (1985) Block-geometry functions characterizing transport in densely fissured media. *J. Hydrol. 77*, 263-279.

Barry, D.A. and J.C. Parker (1987) Approximations for solute transport through porous media with flow transverse to layering. *Transp. Porous Media. 2*, 65-82.

Basu, N.B, P.S.C. Rao, R.W. Falta, M. D. Annable, J. W. Jawitz, K. Hatfield (2007) Temporal evolution of DNAPL source and contaminant flux distribution: Impacts of source mass depletion, J Contam Hydrol., 95, 93-109.

Batu, V. and M. Th. van Genuchten (1990) First- and third-type boundary conditions in two-dimensional solute transport modeling. *Water Resour. Res. 26*, 339-350.

Batu, V. (1996) A generalized three-dimensional analytical solute transport model for multiple rectangular first-type sources. *J. Hydrol. 174*, 57–82.

Berkowitz, B., A. Cortis, M. Dentz, and H. Scher (2006) Modeling non-Fickian transport in geological formations as a continuous time random walk. *Rev. Geophys. 44*, DOI: 10.1029/2005RG000178

Bolt, G.H. (1979) Movement of solutes in soil: principles of adsorption/exchange chromatography. In: G.H. Bolt (ed.), *Soil Chemistry, B. Physico-Chemical Models.* Developments in Soil Science 5B, Elsevier, Amsterdam, 295-348.

Bromly, M. and C. Hinz (2004) Non-Fickian transport in homogeneous unsaturated repacked sand. *Water Resour. Res*. W07402. doi:10.1029/2003WR002579.

Chapman, S.W. and B.L. Parker (2005) Plume persistence due to aquitard back diffusion following dense nonaqueous phase liquid source removal or isolation. *Water Resour. Res. 41*, W12411. doi:10.1029/2005WR004224

Christ, J. A., C. A. Ramsburg, K. D. Pennell, and L. M. Abriola (2006) Estimating mass discharge from dense nonaqueous phase liquid source zones using upscaled mass transfer coefficients: An evaluation using multiphase numerical simulations, Water Resour. Res., 42, W11420, doi:10.1029/2006WR004886.

Cleary, R.W. and M.J Ungs (1978) Analytical methods for groundwater pollution and hydrology. *Water Resour. Prog. Rep. 78-WR-15*, Princeton University, Princeton, New Jersey.

Coats, K.H. and B.D. Smith (1964) Dead-end pore volume and dispersion in porous media. *Soc. Petroleum Eng. J. 4*, 73-84.

Crank, J. (1975) *The Mathematics of Diffusion.* 2nd ed. Oxford University Press London, 414 pp.

Dentz, M., T. Le Borgne, A. Englert, and B. Bijeljic (2011) Mixing, spreading and reaction in heterogeneous media: A brief review. *J. Contam. Hydrol. 120–121*, 1–17.

De Smedt, F. and P.J. Wierenga (1979) A generalized solution for solute flow in soils with mobile and immobile water. *Water Resour. Res. 15,* 1137-l 141, 1979.

Domenico, P.A. (1987) An analytical model for multidimensional transport of a decaying contaminant species. *J. Hydrol. 91*, 49–58.

Falta, R. W., P. S. Rao, and N. Basu (2005) Assessing the impacts of partial mass depletion in DNAPL source zones: I. Analytical modeling of source strength functions and plume response, J. Contam. Hydrol., 78, 259-280.

Falta, R., N. Basu, and R. Rao (2005) Assessing impacts of partial mass depletion in DNAPL source zones: II. Coupling source strength functions to plume evolution. *J. Contam. Hydrol. 79*, 45–66.

Fure, A.D., J. W. Jawitz, and M. D. Annable (2006) DNAPL source depletion: Linking architecture and flux response, J Contam Hydrol, 85, 118-140.

Galya, D.P. (1987) A horizontal plane source model for ground-water transport. *Ground Water 25*, 733-739.

Gelhar. L.W., C. Welty, and K.R. Rehfeldt (1992) A critical review of data on field-scale dispersion in aquifers. *Water Resour. Res. 28*, 1955-1974.

Gillham, R.W., E.A. Sudicky, J.A. Cherry, and E.O. Frind (1984) An advection-diffusion concept for solute transport in heterogeneous unconsolidated geological deposits. *Water Resour. Res. 20*, 369-378.

Guyonnet, D. and C. Neville (2004) Dimensionless analysis of two analytical solutions for 3-D solute transport in groundwater. *J. Contam. Hydrol. 75*, 141–153.

Huyakorn, P., M. Ungs, L. Mulkey, and E. Sudicky (1987) A three-dimensional analytical method for predicting leachate migration. *Ground Water 25*, 588–598.

Jawitz, J. W., A. D. Fure, G. G. Demmy, S. Berglund, and P. S. C. Rao (2005) Groundwater contaminant flux reduction resulting from nonaqueous phase liquid mass reduction, Water Resour. Res., 41, W10408, doi:10.1029/2004WR003825.

Kreft, A. and A. Zuber (1978) On the physical meaning of the dispersion equation and its solution for different initial and boundary conditions. *Chem. Eng. Sci. 33*, 1471-1480.

Leij, F., T. Skaggs, and M.Th. van Genuchten (1991) Analytical solutions for solute transport in three-dimensional semi-infinite porous media. *Water Resour. Res. 27*, 2719–2733.

Leij, F.J. and J.H Dane (1990) Analytical solution of one-dimensional advection equation and two- and three-dimensional dispersion equation. *Water Resour. Res., 26*, 1475-1482.

Levy, M. and B. Berkowitz (2003) Measurement and analysis of non-Fickian dispersion in heterogeneous porous media. *J. Contam. Hydrol. 64*, 203–226.

Liu, C. and W.P. Ball (1998) Analytical modeling of diffusion-limited contamination and decontamination in a two-layer porous medium. *Adv. Water Res. 21*, 297–313.

Liu, C. and W.P. Ball (2002) Back diffusion of chlorinated solvent contaminants from a natural aquitard to a remediated aquifer under well-controlled field conditions: predictions and measurements. *Ground Water 40*, 175-84.

Liu, C., J.E. Szecsody, J.M. Zachara, and W.P. Ball (2000) Use of the generalized integral transform method for solving equations of solute transport in porous media. *Adv. Water Res. 23*, 483-492.

Liu, C., W.P. Ball, and J.H. Ellis (1998) An analytical solution to one-dimensional solute advection-dispersion equation in multi-layer porous media. *Transport Porous Med. 30*, 25–43.

Neuman, S.P. and D.M. Tartakovsky (2009) Perspective on theories of non-Fickian transport in heterogeneous media. *Adv. Water Res. 32*, 670–680.

Ogata, A., and R. Banks (1961) A solution of the differential equation of longitudinal dispersion in porous media. *Prof. Pap. No. 411A*, USGS, Reston, Virginia.

Parker, B.L., S.W. Chapman, and M.A. Guilbeault (2008) Plume persistence caused by back diffusion from thin clay layers in a sand aquifer following TCE source-zone hydraulic isolation. *J. Contam. Hydrol. 102*, 86–104.

Parker, J.C. (1984) Analysis of solute transport in column tracer studies. *Soil Sci. Soc. Amer. J. 48*, 719-724.

Park, E. and J. C. Parker (2005) Evaluation of an upscaled model for DNAPL dissolution kinetics in heterogeneous aquifers, Adv. in Water Resources., 28, 1280-1291.

Parker, J. C. and E. Park (2004) Field-scale DNAPL dissolution kinetics in heterogeneous aquifers, Water Resources Research, 40, W05109, doi:10.1029/2003WR002807.

Parker, J.C. and M.Th. van Genuchten (1984) Flux-averaged and volume-averaged concentrations in continuum approaches to solute transport. *Water Resour. Res. 2*0, 866-872.

Parker, J.C. and A.J. Valocchi (1986) Constraints on the validity of equilibrium and first-order kinetic transport models in structured soils. *Water Resour. Res. 22*, 399-407.

Parker, J.C., U. Kim, P. Kitanidis, M. Cardiff, X. Liu, and J. Lee (2011) Practical Cost-Optimization of Characterization and Remediation Decisions at DNAPL Sites with Consideration of Prediction Uncertainty. SERDP Project ER-1611, Final Report, May 2011.

Parker, J., U. Kim, M. Widdowson, P. Kitanidis, and R. Gentry (2010) Effects of model formulation and calibration data on uncertainty in DNAPL source dissolution predictions, Water Resour. Res., 46, W12517.

Passioura, J.B. (1971) Hydrodynamic dispersion in porous media. I. Theory. *Soil Sci. 111,* 339-344.

Promentilla, M.A., T. Sugiyama, T. Hitomi, and N. Takeda (2009) Quantification of tortuosity in hardened cement pastes using synchrotron-based X-ray computed microtomography. *Cement Concrete Res. 39*, 548-557.

Raats, P.A.C. (1981) Transport in structured porous media. *Proc. Euromech. 143,* Sept 2-4, Delft, 221-226.

Rao, P.S.C., J.W. Jawitz, C.G Enfield, R. Falta, M.D. Annable, A.L. Wood (2001) Technology integration for contaminated site remediation Rasmuson, A. and I. Neretnieks, 1980. Exact solution for diffusion in particles and longitudinal dispersion in packed beds. *Am. Inst. Chemical Eng. J. 26*, 686-690.

Roth, K., and W.A. Jury (1993) Linear transport models for adsorbing solutes. *Water Resour. Res. 29*, 1195– 1203.

Rubin, S., I. Dror, and B. Berkowitz (2012) Experimental and modeling analysis of coupled non-Fickian transport and sorption in natural soils. *J. Contam. Hydrol. 132*, 28-36.

Saenton, S. and I. Illangasekare (2007) Upscaling of mass transfer rate coefficient for the numerical simulation of dense nonaqueous phase liquid dissolution in heterogeneous aquifers. Water Resour. Res., 43, doi: 10.1029/2005WR004274.

Sagar, B. (1982) Dispersion in three dimensions: Approximate analytical solutions. *ASCE J. Hydraul. Div. 108,* 47–62.

Seyedabbasi, M.A. C.J Newell, D.T. Adamson, and T.C. Sale (2012) Relative contribution of DNAPL dissolution and matrix diffusion to the long-term persistence of chlorinated solvent source zones. *J. Contam. Hydrol. 134-135*, 69-81. doi:10.1016/j.jconhyd.2012.03.010.

Starr, R.C., R.W. Gillham, and E.A. Sudicky (1985) Experimental investigation of solute transport in stratified porous media 2. The reactive case. *Water Resour. Res. 2*1, 1043-1050.

Sudicky, E.A., R.W. Gillham, and E.O. Frind (1985) Experimental investigation of solute transport in stratified porous media 1. The nonreactive case. *Water Resour. Res. 21*, 1035-1041.

Tang, D.H., E.O. Frind, and E.A. Sudicky (1981) Contaminant transport in fractured porous media: Analytical solution for a single fracture. *Water Resour. Res. 17,* 555-564.

Toride, N., F.J. Leij, and M.Th. van Genuchten (1999) *CXTFIT code for estimating transport parameters from laboratory or field tracer experiments. Version 2.1*. U.S. Salinity Laboratory Research Report No. 137, USDA, ARS, Riverside, CA.

van Genuchten, M.Th. (1985) A general approach to modeling solute transport in structured soils. *Proc. 17th Int. Congress on Hydrogeology of Rocks of Low Permeability, Memoires Int. Assoc. of Hydrogeologists. 17,* 513-526.

van Genuchten, M.Th. and F.N. Dalton (1986) Models for simulating salt movement in aggregated field soils. *Geoderma 30,* 165-183.

van Genuchten, M.Th. and J.C. Parker (1984) Boundary conditions for displacement experiments through short laboratory soil columns. *Soil Sci. Soc. Amer. J. 48*, 703-708.

Wexler, E.J. (1992) Analytical solutions for one- two- and three-dimensional solute transport in ground-water systems with uniform flow. *U.S. Geological Survey Techniques of. Water-Resources Investigations,* Book 3, Chap. Series 03-B7B7, 190 p., U.S. Geological Survey.

Yeh, G.T. and Y.-J Tsai (1976) Analytical three-dimensional transient modeling of effluent discharges. *Water Resour. Res. 12*, 533-540.

Zhang, Y., B. Baeumer, and D.A. Benson (2006) Relationship between flux and resident concentrations for anomalous dispersion. *Geophys. Res. Lett. 33,* L18407. doi:10.1029/2006GL027251.

Zhu, J. and J.F. Sykes (2004) Simple screening models of NAPL dissolution in the subsurface, J. Contam. Hydrol., 72, 245-258.

3. Enhanced Bioremediation and Dissolved Plume Control

3.1 Overview

In this chapter, we address technologies for the control or attenuation of aqueous phase contamination. Three such technologies are considered in SCOToolkit. They are electron donor (ED) enhanced bioremediation, pump-and-treat, and reactive barriers. The last two methods are treated by SCOToolkit as contingency measures that can be implemented to prevent or limit plume migration beyond a designated location if the primary remediation methods fail to perform as expected. ED enhanced bioremediation is treated as a primary remediation method with optimizable design variables. In this chapter, we discuss the ED model first, followed by contingency control methods.

Streamlines that pass through the center of each electron donor injection gallery or reactive barrier are characterized using a linear or polynomial model in the same manner discussed for contaminant transport in Chapter 2.

3.2 Electron donor enhanced bioremediation

3.2.1 Electron donor transport

SCOToolkit simulates effects of ED injection in one or more injection well galleries of width Y_i^{ED} for gallery *i* perpendicular to the groundwater flow direction, with the top of the injection zone a depth $z = Z_i^{ED}$ below the water table for gallery *i* and with the bottom at $z = Z_i^{ED} + H_i^{ED}$ below the water table. The flow field for each ED gallery is characterized in the same manner as for contaminant transport – i.e., linear or linearized by mapping a nonlinear field to local coordinates for each ED gallery as described in Chapter 2. Needless to say, streamlines for all ED galleries and DNAPL sources should be consistent with each other – i.e. parallel or with mild convergence/divergence.

The ED injection rate, $\dot{m}_{EDi}$ [MT^{-1}], for injection gallery *i* is approximated by a step function

$$\begin{aligned} \dot{m}_{EDi}(t) &= 0 && \text{for } t < t_{EDio} \\ \dot{m}_{EDi}(t) &= M_{EDi} && \text{for } t_{EDio} < t < t_{EDif} \\ \dot{m}_{EDi}(t) &= 0 && \text{for } t > t_{EDif} \end{aligned} \tag{3.1}$$

where t_{EDio} is the ED injection start date and t_{EDif} is the stop date for gallery *i*. Actual aqueous phase ED injection will commonly be pulsed to reduce well fouling problems and injection of nonaqueous phase ED will be performed with a frequency that depends on the dissolution rate of ED material. As a result, temporal variations in ED concentrations will occur near injection galleries. However, since these variations will diminish markedly with distance from the galleries, modeling ED injection with a time-averaged rate will generally not greatly affect ED available to drive biodecay through most of the aquifer.

ED concentrations attributable to injection gallery *i* before reactions with contaminants, denoted $C_{EDi}^{norx}(x, y, z, t)$, are computed using the transport model described in Chapter 2 but with the step function ED injection rate used in lieu of the DNAPL source function. Aquifer porosity, velocity

and dispersivity values will be the same for ED and contaminants. Sorption coefficients for ED transport will be specific to the ED and first order decay for ED is assumed to be zero, as ED reactions will be modeled explicitly.

Resident or flux concentration solutions for ED transport are employed corresponding to the solution type specified for the contaminant model at a given location and time, depending on the applicable type of measurement, as specified by the user.

Kinetics of ED reactions with dissolved contaminant is approximated assuming the fraction of injected ED concentration that is reactive varies exponentially with travel time as

$$C_{EDi}^{avail}(x,y,z,t) = \left(1 - \exp\frac{-\alpha_{ED} x R_{ED}}{v}\right) C_{EDi}^{norx}(x,y,z,t) \tag{3.2}$$

where (x, y, z) are local coordinates of the computational point downgradient of ED gallery i, α_{ED} is a reaction rate coefficient [T^{-1}], v is groundwater pore velocity [$L\ T^{-1}$], and R_{ED} is the ED retardation factor [-].

For multiple ED galleries, the total ED concentration prior to reactions C_{ED}^{norx} at a given field location and time is computed by superposition in field coordinates as

$$C_{ED}^{norx}(E,N,z,t) = \sum_i C_{EDi}^{norx}(E,N,z,t) \tag{3.3}$$

and the total ED concentration available for reactions is computed similarly as

$$C_{ED}^{avail}(E,N,z,t) = \sum_i C_{EDi}^{avail}(E,N,z,t) \tag{3.4}$$

where i denotes solutions for individual ED injection galleries.

The foregoing implicitly treats introduced ED as an aqueous phase material. However, nonaqueous or emulsified ED (e.g., various vegetable oil formulations) can be approximated by suitable adjustment of α_{ED} and R_{ED} – e.g. by calibration to pilot test data.

3.2.2 Electron donor reactions with electron acceptors and contaminants

Biodecay of CH species is assumed to be limited by the quantity of ED species relative to electron acceptor (EA) species (Kamanth et al., 2006). To estimate the attenuation of CH due to ED addition, a superposition method is used that is analogous to that described by Borden and Bedient (1986). If redox reactions occur serially in order of decreasing reaction free energy (e.g., O_2 > NO_3 > SO_4 > Fe(III) > CH), then an electron balance yields

$$C'_{CH(\text{serial})} = \max\left[0, C_{CH(norx)} - \max\left(0, \frac{R_{ED} f'_{ED} C_{ED}^{avail} + R_{ED} C_{ED}^{H\ nat} - C_{EA}^{H}}{R_{CH} f'_{CH}}\right)\right] \tag{3.5}$$

where $C'_{CH(\text{serial})}$ is the aqueous CH concentration after serial ED reactions, $C_{CH(norx)}$ is the computed CH concentration before ED reactions as described in Chapter 2, C_{ED}^{avail} is the aqueous concentration of injected ED available for reactions, $C_{ED}^{H\ nat}$ is the background H-equivalent ED concentration in the aquifer, C_{EA}^{H} is the background H-equivalent concentration of each EA species in the aquifer, f'_{CH} is the ratio of H-equivalent to actual contaminant concentration, f'_{ED} is the ratio

of H-equivalent to actual injected ED concentration, R_{CH} is the CH retardation factor, and R_{ED} is the ED retardation factor (note that R=1 is assumed for EA species).

H-equivalent ratios (H_{stoch}) for common groundwater ED, EA, and solvent species are summarized in Table 3.1. H-equivalent ratios for EAs are estimated as $f'_{EA} = f_{EA}/E_{eff}$ where f_{EA} is the stoichiometric ratio for complete EA reduction and E_{eff} is fractional energy yield for the biologically-mediated reaction after deducting energy consumed for cell synthesis. The H-equivalent ratio for CH is similarly computed as $f'_{CH} = f_{CH}/E_{eff}$, while H-equivalent ratios for ED species are computed as $f'_{ED} = f_{ED}E_{eff}$, since ED occurs on the opposite side of the EA-ED balance ledger.

If reductive dechlorination of CH is assumed to occur under anaerobic conditions with competition among microbial populations responsible for reduction of NO_3, SO_4, etc., an electron balance yields

$$C'_{CH(parallel)} = \min\left[1, \max\left(0, \frac{R_{CH} f'_{CH} C_{CH(norx)} + C^H_{EA} - R_{ED} f'_{ED} C^{avail}_{ED} - R_{ED} C^{H\ nat}_{ED}}{R_{CH} f'_{CH} C_{CH(norx)} + C^H_{EA} - C^H_{O2}}\right)\right] C_{CH(norx)} \tag{3.6}$$

where no retardation is assumed for O_2. Assuming that actual biodecay can be approximated as a linear combination of the foregoing pathways, then

$$C'_{CH(mixed)} = F_{serial} C'_{CH(serial)} + (1 - F_{serial}) C'_{CH(parallel)} \tag{3.7}$$

where F_{serial} is the fraction of reductive dechlorination that follows the serial pathway. The ED concentration remaining in solution after reactions with EA and CH may be computed by

$$C^{net}_{ED} = C^{norx}_{ED} - \frac{\min\left(R_{ED} f'_{ED} C^{avail}_{ED} + R_{ED} C^{H\ nat}_{ED}, C^H_{EA} + R_{CH} f'_{CH}\left(C_{CH} - C'_{CH(\text{mixed})}\right)\right)}{R_{CH} f'_{CH}} \tag{3.8}$$

which is used to determine effects of ED injection on mass transfer enhancement.

3.2.3 DNAPL source mass transfer enhancement by ED injection

SCOToolkit considers changes in DNAPL mass transfer rate by a factor F_{mt} due to ED injection upgradient of DNAPL sources as described in Chapter 2. Whey injection studies at the Fort Lewis, Washington East Gate Disposal Yard (EGDY) DNAPL site by Macbeth and Sorenson (2008) indicate an approximately linear mass transfer enhancement with ED concentration in the source zone (measured as COD). This observation is consistent with a theoretical analysis of NAPL dissolution rate enhancement associated with reactions between the NAPL constituents and other aqueous phase species by Reitsma and Dai (2001). For mass transfer with an instantaneous irreversible reaction described by eqs. (1), (4) and (5) of Reitsma and Dai and assuming a bulk aqueous phase contaminant concentration much less than its solubility, we obtain

$$F_{mt} = 1 + f_{mt} \frac{C_{rx}}{C_{CHsol}} \tag{3.9a}$$

$$f_{mt} = \frac{D_{rx}}{n_{rx} D_{CH}} \tag{3.9b}$$

where F_{mt} is the ratio of mass transfer rate with reaction to that without reaction defined by (2.1) [-], f_{mt} is an enhancement coefficient [-], C_{CHsol} is the molar aqueous solubility of contaminant [mol

L^{-3}], C_{rx} is the bulk aqueous phase molar concentration of reactant [mol L^{-3}], D_{CH} is the contaminant aqueous diffusion coefficient [L^2T^{-1}], D_{rx} is the reactant aqueous diffusion coefficient [L^2T^{-1}], and n_{rx} is the stoichiometric ratio of reactant to contaminant for the reaction. While the value of f_{mt} may be calculated from (3.9b) as a first approximation, given the simplistic nature of the rate enhancement model, calibration to field data is desirable if feasible.

For the case of mass transfer enhancement by aqueous phase ED, $C_{rx} = C_{ED}^{net}$, which we compute at coordinates corresponding to the center of the DNAPL source zone at the injection start date plus a lag time to allow the ED concentration to approach a steady-state value estimated as $t_{lag} = xR/v + 3(2RxA_x)^{1/2}/v$ where x is the travel distance from the ED injection gallery to the center of the DNAPL source, R is the ED retardation factor, v is the mean groundwater pore velocity, and A_x is the aquifer longitudinal dispersivity.

Table 3.1. H-equivalent conversion factors for selected ED, EA and CH.

Species	H_{stoch} [1]	E_{eff} [2]	f' [3]
Chlorinated solvents[4]			
PCE (tetrachloroethene)	0.058	0.9	0.064
TCE (trichloroethene)	0.046	0.9	0.051
DCE (cis-1,2-dichloroethene)	0.042	0.9	0.038
VC (vinyl chloride)	0.032	0.9	0.024
Electron donors			
Acetate	0.13	0.6	0.078
Butyrate	0.21	0.6	0.126
Ethanol	0.26	0.6	0.156
HRC	0.12	0.6	0.072
Lactate	0.13	0.6	0.078
Methanol	0.19	0.6	0.114
Molasses	0.14	0.6	0.084
Propionate	0.18	0.6	0.108
Vegetable oil	0.39	0.6	0.234
Whey	0.13	0.6	0.078
Electron acceptors			
Oxygen	0.125	0.51	0.245
Sulfate	0.081	0.43	0.188
Nitrate	0.083	0.92	0.091
Iron (II)	0.018	0.9	0.020

[1] H_{stoch} is the H-equivalent ratio computed for the simple chemical redox reactions (Kamanth et al., 2006)

[2] E_{eff} is the energy conversion efficiency to adjust yield for cell synthesis for relevant microbial populations (Rittman and McCarty, 2001)

[3] f' is the net H-equivalent mass ratio = $H_{stoch}E_{eff}$ for electron donors and H_{stoch}/E_{eff} for electron acceptors.

[4] Stoichiometry based on conversion to ethene.

3.2.4 Electron donor gallery termination criteria and design variables

SCOToolkit can model multiple ED injection galleries. Each gallery can have different gallery coordinates (northing and easting at center of gallery), width, depth, start and stop dates, and ED injection rates. Termination of injection galleries may be specified at fixed dates or (more realistically) the end date may be defined conditionally based on performance monitoring of contaminant concentrations in a specified well or wells as described below.

For ED galleries placed downgradient of a DNAPL source, intended to enhance dissolved plume remediation ("dissolved plume ED galleries"), ED injection may be terminated when

a. the annual average of contaminant concentration measurements in a designated ED performance monitoring well or wells upgradient of the gallery is less than a specified value C_{EDstop}, and

b. optionally, when the annual average concentration in a designated site-wide compliance monitoring well downgradient of the gallery is also less than the site-wide compliance concentration C_{nfa} (see Chapter 7), and

c. optionally, if there are no ED injection galleries currently operating upgradient of the gallery in question (i.e., multiple galleries can only terminate sequentially form up- to downgradient).

For ED galleries placed immediately upgradient of a DNAPL source to enhance source zone remediation ("source zone ED galleries"), ED performance monitoring wells are located immediately downgradient of the source to monitor total solvent species and decay products ("total contaminant concentration"). In this case, injection is terminated when the annual average total contaminant concentration is less than C_{EDstop}.

SCOToolkit generates "measurements" for ED performance monitoring wells by applying lognormal noise to simulated average annual contaminant concentrations. For dissolved plume ED galleries, simulated values of $C'_{CH(mixed)}$ are used to represent noise-free contaminant concentrations after ED-enhanced biodecay. For source zone ED galleries, simulated $C_{CH(norx)}$ are used to represent contaminant concentrations prior to ED reactions, corresponding to field measurements of total contaminants and daughter products. Measurement "noise" applied to simulated values has a ln-standard error equal to $S_{lnCED}\, f_{samp}^{ED\ 1/2}$ where S_{lnCED} is the user specified ln-error for single measurements from ED performance monitoring wells and f_{samp}^{ED} is the number of measurements per year (number of ED monitoring wells per decision gallery times annual sampling frequency).

Design variables that may warrant optimization for ED injection include the following:

M_{EDi} is the ED mass injection rate for gallery i (kg/d),

Y_i^{ED} is the width of gallery i (m),

H_i^{ED} is the vertical thickness of the injection zone i (m),

t_{oi}^{ED} is the start date for ED injection in gallery i (days),

$C_{EDstop\ i}$ is the target annual average contaminant concentration in ED performance monitoring wells below which ED injection will be terminated, and

f_{samp}^{ED} is the number of measurements per gallery per year for ED monitoring.

When optimizing multiple potential ED injection galleries, if the optimized value of M_{EDi} is below a specified lower cutoff, the gallery is treated as inoperative and no capital or operating costs are applied to it, thus allowing the number (and locations) of injection galleries may be optimized.

3.2.5 Electron donor injection cost function

Capital and operating costs for implementation of enhanced bioremediation by injection of ED and other amendments in injection well galleries are described as follows:

$$
\begin{aligned}
C_{NPV}^{EDtot} &= C_{NPV}^{EDcap} + C_{NPV}^{EDop} \\
C_{NPV}^{EDcap} &= C_{width}^{EDcap} \sum_{i=1}^{N_{gali}^{ED}} I_i^{ED} Y_i^{ED} (1-d)^{t_{oi}^{ED} - t_{ref}} + C_{mw}^{EDcap} N_{mw}^{ED} \sum_{i=1}^{N_{gali}^{ED}} I_i^{ED} (1-d)^{t_{oi}^{ED} - t_{ref}} \\
&\quad + \max_i \left(I_i^{ED} \right) C_{other}^{EDcap} (1-d)^{\min_i (t_{oi}^{ED}) - t_{ref}} \\
C_{NPV}^{EDop} &= \sum_{t=t_{ref}}^{t_{max}} \left(\begin{array}{l} C_{width}^{EDop} \sum_{i=1}^{N_{gali}^{ED}} O_{ti}^{ED} Y_i^{ED} + C_{mass}^{EDop} \sum_{i=1}^{N_{gali}^{ED}} O_{ti}^{ED} M_{EDi} \\ + C_{samp}^{EDop} f_{samp}^{ED} \sum_{i=1}^{N_{gali}^{ED}} O_{ti}^{ED} N_{mw}^{ED} + C_{other}^{EDop} \sum_{i=1}^{N_{gali}^{ED}} O_{ti}^{ED} + C_{all}^{EDop} \max_i \left(O_{ti}^{ED} \right) \end{array} \right) (1-d)^{t-t_{ref}}
\end{aligned}
\tag{3.10}
$$

where the time summation is over integer values of time in years and

C_{NPV}^{EDtot} is the total NPV cost for ED injection ($K),

C_{NPV}^{EDcap} is the total NPV fixed ED cost ($K),

C_{width}^{EDcap} is the fixed cost per ED gallery width ($K/m),

C_{mw}^{EDcap} is the construction cost per operational ED monitoring well ($K/well),

C_{other}^{EDcap} is any other fixed ED costs,

C_{NPV}^{EDop} is the total NPV operating cost for ED injection ($K),

C_{width}^{EDop} is the operating cost per ED gallery width for maintenance etc. ($K/m),

C_{mass}^{EDop} is the operating cost per unit ED mass injection ($K/kg),

C_{samp}^{EDop} is the collection and analysis cost per ED monitoring sample ($K/sample),

C_{other}^{EDop} is other ED operating costs per gallery per year for reporting etc. ($K/gallery/yr),

C_{all}^{EDop} is other ED operating costs regardless of the number of galleries ($K/yr),

d is the annual discount rate (fraction),

f_{samp}^{ED} is the number of samples per well per year for ED operational monitoring,

I_i^{ED} is an indicator that is 1 if gallery i is actually implemented else 0,

Y_i^{ED} is the width of ED gallery i perpendicular to the flow direction (m),

M_{EDi} is the mass injection rate of ED for gallery i (kg/yr),

N_{mw}^{ED} is the number of operational monitoring wells (not injection wells) per ED gallery,

N_{gal}^{ED} is the number of potential ED galleries,

O_{ti}^{ED} is an indicator that is 1 if gallery *i* is operating in year t else 0,

t_{oi}^{ED} is the start date for ED gallery *i* (yr),

t_{ref} is the reference date for NPV adjustment (yr), and

t_{max} is the maximum simulation date (yr).

3.3 Hydraulic control and reactive barriers

3.3.1 Pump-and-treat for plume control

Pump-and-treat (PT) systems have a long history. They were once the sole means for treatment of groundwater contamination until it was recognized in the 1970s that slow dissolution of DNAPL sources may require hundreds or thousands of pore volumes before the source was fully dissipated. This led to the realization that pump-and-treat for DNAPL plumes is often more reasonably regarded as a plume control measure rather than as a remediation technology per se.

SCOToolkit treats pump-and-treat as a means of limiting dissolved plume migration beyond a certain distance downgradient, which may be used in conjunction with natural attenuation, source reduction methods, and/or other dissolved plume technologies. If SCOToolkit implements a pump-and-treat system at a given location, any monitoring wells downgradient of the pump-and-treat system are assumed to be "clean." In other words, the pump-and-treat system is assumed to be implemented at or near the distal edge of the dissolved plume. The steady state flow field upgradient of the pump-and-treat system is assumed to be unaffected and the analytical transport model is used to compute upgradient concentrations.

SCOToolkit does not assess pumping rates or well locations needed to ensure plume capture, nor does it determine construction or unit operating costs. Many other tools are available to perform such calculations. If pump-and-treat is considered as an option at a given site, design personnel must independently perform calculations to estimate PT capital costs and annual operating costs. SCOToolkit can treat implementation of pump-and-treat technology as a conditional decision contingent on the magnitude of contaminant concentration in a designated "PT trigger well."

If simulated concentrations at the trigger well exceed a value C_{PT} based on specified statistical criteria over time, capital costs for implementation are triggered and annual operating costs are accrued until site-wide remediation requirements are met. Statistical criteria to initiate PT and to achieve site wide "no further action" (NFA) status are discussed in Chapter 7.

The total net present value (NPV) pump-and-treat system cost for a given simulation of remediation performance is computed as

$$C_{NPV}^{PT} = I_{PT} C_{total}^{PTcap} (1-d)^{t_{PT}-t_{ref}} + I_{PT} \sum_{t=t_{PT}}^{t_{nfa}} C_{total}^{PTop} (1-d)^{t-t_{ref}} \qquad (3.11)$$

where I_{PT} is a value equal to 1 if PT is implemented and 0 if not, t is time (yrs), t_{PT} is the time PT is implemented (yrs), t_{ref} is the reference date for NPV adjustment (yrs), d is the annual discount rate, C_{total}^{PTcap} is the undiscounted PT fixed cost ($K), and C_{total}^{PTop} is the undiscounted PT operating cost per year ($K/yr).

3.3.2 Reactive barrier model

Consider a reactive barrier (RB) of width Y_{rb} perpendicular to the flow direction extending from the water table to depth H^{RB} below the water table. The contaminant mass flux versus time entering the barrier area ($=Y^{RB}H^{RB}$) is $J_{in}^{RB}(t)$ and that leaving the area is $J_{out}^{RB}(t)$. We assume the removal efficiency of the barrier is E^{RB} over the operating period from t_o to t_f, such that the contaminant flux leaving the barrier is $J_{out}^{RB}(t) = (1 - E^{RB}) J_{in}^{RB}(t)$ and the mass removal rate within the barrier is $J_{loss}^{RB}(t) = E^{RB} J_{in}^{RB}(t)$. Note that even if E^{RB}=1, upstream contamination can still move downgradient around the sides and beneath the barrier.

To model the dissolved plume at a location downgradient of a reactive barrier, we first compute $J_{loss}^{RB}(t)$ for the barrier. Assuming E^{RB} is known, $J_{loss}^{RB}(t)$ can be computed using the flux concentration solution for contaminant transport for all sources upgradient of a given barrier at discretized locations on the barrier face in the Y and Z directions (e.g., red dots in Figure 3.1). The average of the latter values as a function of time is denoted $C_{avg}^{CH}(t)$. The loss rate is computed as

$$J_{loss}^{RB}(t) = E^{RB} q Y^{RB} H^{RB} C_{avg}^{CH}(t) . \tag{3.12}$$

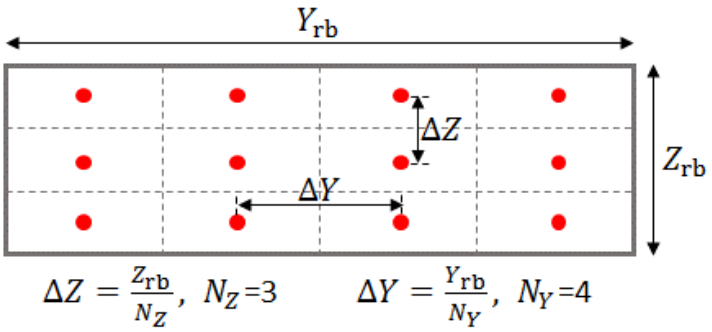

Figure 3.1. Schematic of reactive barrier face in flow direction for computing $C_{avg}^{CH}(t)$.

To compute contaminant concentrations at a given location downgradient of the barrier, we first compute a pseudo contaminant concentration, $C_{loss\ i}^{CH}(t)$ at the location of interest using the contaminant transport model with a source mass function equal to $J_{loss}^{RB}(t)$ and source coordinates and dimensions corresponding to the RB. Now, we can compute the contaminant concentration at the downgradient location of interest corrected for mass lost in the reactive barrier, $C_{RB}^{CH}(t)$, as

$$C_{RB}^{CH}(t) = C_{noRB}^{CH}(t) - C_{loss}^{CH}(t) \tag{3.13}$$

where $C_{noRB}^{CH}(t)$ is the contaminant concentration at the location downgradient of the RB computed with the transport solution disregarding effects of the reactive barrier, and $C_{RB}^{CH}(t)$ is the solution corrected for mass removed by the RB. Note that the solution type (i.e., resident or flux) for $C_{noRB}^{CH}(t)$ and $C_{loss}^{CH}(t)$ must be consistent with each other and with the desired type for $C_{RB}^{CH}(t)$.

3.4 Summary

Dissolved plume control and attenuation are important components of DNAPL remediation strategies. While monitored natural attenuation (MNA) can be an effective strategy in some cases, engineered systems to enhance natural attenuation mechanisms and/or to limit further migration to buy time for other system components to work are often necessary. Enhanced reductive dechlorination of common chlorinated solvents is the most commonly used and cost-effective strategy for accelerating dissolved plume remediation. The modeling approach presented here is physically based yet computationally efficient and requires minimal empirical parameters that must be calibrated using pilot tests or field scale data.

3.5 References

Kamanth, R. K., C. J. Newell, B. B. Looney, K. M. Vengelas, and J. Perex (2006) Biobalance: A Mass Balance ToolKit for Evaluating Source Depletion, Competition Effects, Long-Term Sustainability and Plume Dynamics. GSI Environmental Inc., 61 p.

Borden, R. C. and P. B. Bedient (1986) Transport of dissolved hydrocarbons influenced by oxygen limited biodegradation - theoretical development. Water Resources Research 22, 1973-1982.

Rittman, B. E. and P. L. McCarty (2001) Environmental Biotechnology: Principles and Applications. McGraw-Hill, 754 p.

Reitsma, S. and Q. L. Dai (2001) Reaction-enhanced mass transfer and transport from non-aqueous phase liquid source zones, J. Contam. Hydrol. 49, 49-66.

4. DNAPL Source Remediation by Thermal Treatment

4.1 Overview

In situ thermal technologies for DNAPL source remediation have largely evolved from methods developed for enhanced oil recovery applications (Schumacher 1980, U.S. EPA 2004, Kingston et al. 2010). These technologies have been used to treat a wide range of volatile organic chemicals (VOCs) including chlorinated solvents, non-chlorinated volatile organic compounds, petroleum hydrocarbons, and semi-volatile organic compounds (Vinegar et al. 1999, Beyke and Fleming 2005, Truex et al. 2007). Thermal methods are often used to treat contaminant source regions containing low solubility non-aqueous phase liquids (NAPLs), which are recalcitrant to many other methods. Thermal technologies utilize heat to enhance the removal of contaminants from the subsurface primarily by increasing the contaminant vapor pressure for VOCs and by decreasing the viscosity of low volatility NAPL. Heating may also enhance contaminant removal by increasing aqueous solubility, aqueous and vapor phase diffusion coefficients, and/or biotic and abiotic decay rates. Depending on the operating temperature and contaminant properties, heating may also decrease soil-water sorption coefficients and/or NAPL interfacial tension and liquid viscosities.

In situ thermal technologies in common commercial use include thermal conductive heating (TCH) that employs heating elements in wells to heat soil primarily by thermal conduction (Fan and Udell 1995, Hansen et al. 1998), electrical resistive heating (ERH) involving application of electrical current to an electrode network to heat soil by resistive energy dissipation (Heron et al. 1998a and 1998b, Beyke and Fleming 2005, Powell et al. 2007), and steam enhanced extraction (SEE) which heats the aquifer by steam injected into a network of injection wells with vapor and liquid phase recovery from multiphase extraction wells (Wu 1977, Itamura and Udell 1993, Davis 1997, Davis 1998). Mass recovery rates during thermal treatment can be measured by monitoring mass recovery rates in extracted vapor and liquid phases as applicable to the various technologies.

The total energy input required to achieve a specified cleanup objective is strongly dependent on the boiling point of the contaminant(s) of concern, which depends on the chemical composition of NAPL (if present) and boiling point(s) of the pure contaminant(s). Chlorinated solvents and other chemicals can exhibit heterogeneous azeotropic behavior in which the boiling point of a NAPL-water mixture is less than the boiling point of solvent or water alone (Gmehling and Onken 1997, U.S. EPA 2004, Ponton 2009). The heterogeneous mixture boiling point may be estimated from Dalton's law of partial pressures as the temperature when solvent vapor pressure plus water vapor pressure equals the ambient (atmospheric plus hydrostatic) pressure. After the co-boiling point is reached, mole fractions of water and solvent in liquid and vapor phases will remain constant (in the absence of mass transfer limitations) until the NAPL phase is depleted. Azeotropic boiling points and mole fractions for several chlorinated solvents are shown in Table 4.1. For azeotropic systems with a boiling point less than 100°C, the water-NAPL system boils first when the co-boiling point is reached. After NAPL is boiled off, dissolved and adsorbed solvent will continue to volatilize as the temperature gradually increases to the aqueous phase boiling point. Thus, most solvent may be volatilized well before water reaches a full boil (contingent on spatial variability in temperature and contaminant distribution), which may substantially reduce the energy requirements in the absence of co-boiling behavior. However, if very low residual soil concentrations are targeted, heating above the co-boiling point to the free water boiling point, and/or holding the system at the target temperature longer may be necessary.

Table 4.1. Azeotropic properties of selected chemicals in water (Ponton 2009).

Solvent	Pure substance Boiling Point, °C	Heterogeneous Azeotrope with Water	
		Azeotropic Boiling Point, °C	Mass fraction of solvent in water
Tetrachloroethene	121	86	0.83
Trichloroethene	87	73	0.94
1,1,2-Trichlorethane	114	86	0.84
Carbon tetrachloride	77	67	0.96
Methylene chloride	40	39	0.99
Benzene	80	69	0.91
Ethylbenzene	136	92	0.67
Toluene	111	85	0.80
m-Xylene	140	94	0.60

After a specific technology suited to site conditions is selected, heat balance calculations are typically performed considering treatment zone geometry, well configurations, subsurface heat transfer characteristics (heat capacity, thermal conductivity, advection rates), and cost and remediation time tradeoffs associated with well spacing, heating rates and energy required to reach the target temperature. Operational monitoring is employed to determine when remediation objectives have been met and operation can be terminated. The most common criteria for thermal system termination are maintaining a specified aquifer temperature for a defined period or reducing the average contaminant soil concentration below a target level. We will focus on the latter because knowledge of contaminant mass remaining after thermal treatment is an important variable to predict effects of thermal treatment on downgradient dissolved plume attenuation (Rao et al. 2001). Thermal system monitoring also commonly utilizes measurements of contaminant mass recovery rates based on fluid flow rates and concentrations from recovery wells.

The design and operation of all in situ remediation systems is complicated by the high degree of spatial and temporal variability inherent to geologic systems and by the hard reality that characterization of this variability is difficult and costly. It is imperative to come to terms with uncertainty and to design and operate systems with due consideration of uncertainty so that desired outcomes can be achieved with acceptable probability. To manage noisy data, Levine (2010) proposed comparing the upper confidence limit of a moving aquifer average of aquifer concentration at a specified probability level with the compliance concentration as a criterion for regulatory closure.

Remediation system design is to a great degree a problem of managing uncertainty. Conventional approaches based on best estimates of system properties have a potential likelihood of failure to meet remediation targets, to overshoot budgets or both. Considerable work has been performed on optimization of long-term monitoring to trade off costs against the value of information (Loaiciga et al. 1992, U.S. EPA 2000, Reed et al. 2000, U.S. EPA 2007). Stochastic optimization methods employ Monte Carlo models to define probability distributions of remediation performance and cost for a given design and use optimization algorithms to determine design variables that minimize probability-weighted cost subject to performance constraints (Cardiff et al. 2010, Parker et al. 2011).

4.2 Thermal treatment model

4.2.1 Model formulation

In this section, we will describe a simple and computationally efficient model to estimate average soil concentration of contaminant within a defined thermal treatment volume from field measurements of cumulative mass recovery over time. The approach is applicable to most thermal systems, with the exception of those involving high temperature thermal decomposition or chemical destruction by oxidation, hydrolysis or other mechanisms. For SEE, estimation of contaminant mass recovery rates over time requires monitoring and analysis of total fluids recovered from multiphase extraction wells. For TCH and ERH, periodic measurements of gas concentrations and flow rates from vapor extraction wells are required, although mass recovery in extracted liquids may be necessary if groundwater extraction is performed to control advective heat losses or to maintain hydraulic control. Total volatiles in extracted gas can be monitored economically using photoionization detector and flame ionization detector sensors with occasional sample analyses using more accurate gas chromatography units to provide speciation information to calibrate sensor data. Time integration of mass recovery rates provides an accurate and cost-effective means of determining cumulative mass recovery. Although commonly used to monitor integrated recovery rates over entire thermal systems, subsets of recovery wells or even individual recovery wells may be monitored separately to measure mass recovery from different areas within a site at relatively low cost compared to soil sampling.

Thermal mass recovery versus time is often approximated using a normal probability distribution model with a mean equal to the time when recovery rate is at a maximum (Δt_{peak}), which corresponds closely to the mixture boiling point. However, since the normal distribution model is symmetrical about the mean while elapsed time cannot be negative, a normal distribution that fits data prior to Δt_{peak} must predict essentially 100% recovery within 2 x Δt_{peak}. For many sites, this will significantly underestimate treatment duration. To describe recovery curves more accurately, we propose to use a lognormal cumulative distribution function (CDF) in the form

$$M(t) = M_o \mathrm{N}\left[\ln(t); \ln(\Delta t_{peak}), S_{therm}\right] + M'_{ext} t \tag{4.1}$$

where $M(t)$ is the cumulative mass recovered from the treated region after operating duration t, M_o is the initial mass in the monitored volume, Δt_{peak} is the time to reach maximum recovery rate, N[x;m, S] is the normal CDF of x with mean m and standard deviation S, S_{therm} is the standard deviation of the lognormal distribution, and M'_{ext} is a steady-state mass inflow rate to the monitored zone from adjacent soil, e.g., due to groundwater flow. For small S_{therm} values (<0.2), the lognormal model closely approximates a normal distribution, but exhibits increasingly positive skewness as S_{therm} increases. Mass recovery rate, $M'(t)$, can be computed by differentiating eq. (4.1). Making use of the normal probability density function (PDF), $\mathrm{N}'[x;m,S]$ = dN[x;m, S]/dx, yields

$$M'(t) = \frac{dM(t)}{dt} = \frac{M_o}{t} \mathrm{N}'\left[\ln(t); \ln(\Delta t_{peak}), S_{therm}\right] + M'_{ext}. \tag{4.2}$$

Normalized cumulative mass recovery and recovery rate versus time curves for the above model with M'_{ext} = 0 are illustrated in Figure 4.1 for a range of S_{therm} values. As S_{therm} increases, the curves become increasingly skewed to larger times.

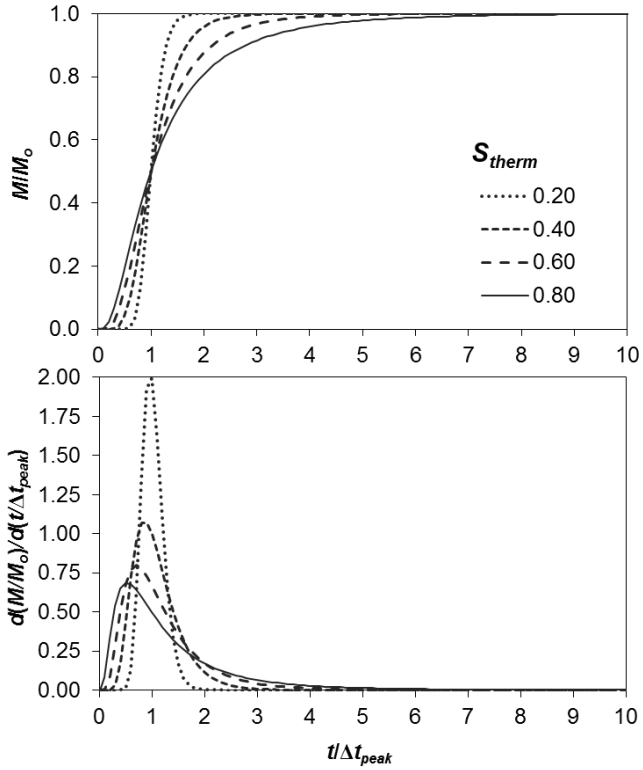

Figure 4.1. Normalized cumulative mass recovery (top) and recovery rate (bottom) curves for proposed model with a range of S_{therm} values.

The cumulative mass recovered and average soil concentration at a given time may be computed from eq. (4.1) assuming no net accumulation due to M'_{ext} (i.e., M'_{ext} is truly steady-state) as

$$M_{rem}(t) = M_o - M(t)$$
$$C_{avg}^{soil}(t) = \frac{M_{rem}(t)}{\rho_{soil} V_{soil}} \tag{4.3}$$

where $M_{rem}(t)$ is mass remaining at time t, ρ_{soil} is soil bulk density, and V_{soil} is the treated soil volume. The rate of change of average soil concentration may be derived from eq. (4.3) as

$$\frac{dC_{avg}^{soil}(t)}{dt} = \frac{-M'(t)}{\rho_{soil} V_{soil}} . \tag{4.4}$$

An alternative method of estimating soil concentration from recovery data, independent of the lognormal model, is to extrapolate the current recovery rate forward in time assuming a constant rate reduction factor (i.e., second derivative of ln recovery curve) as

$$C_{avg}^{soil}(t) = -\int_0^{\infty} \frac{M'(t)\left(1+M''_{\ln}\right)^{\tau}}{\rho_{soil} V_{soil}} d\tau = \frac{-M'(t)}{\rho_{soil} V_{soil} \ln\left(1+M''_{\ln}\right)} \tag{4.5}$$

where $M'(t)$ is the current observed mass recovery rate, $M''_{\ln} = d(\ln M')/dt$ is the rate reduction factor, an τ is a dummy integration variable. We will address the magnitude and variability of $M''_{\ln}$ later.

4.2.2 Calibration of thermal mass recovery model

To apply the lognormal mass recovery model, values for M_o, Δt_{peak}, S_{therm} and M'_{ext} must be determined. A preliminary estimate of M_o may be taken as the product of the treatment zone volume and average measured soil concentration or by more sophisticated geostatistical integration methods. An estimate of Δt_{peak} may be obtained from heat balance calculations during the design process as the time to reach the contaminant co-boiling point. Refined estimates of Δt_{peak} and M_o as well as S_{therm} may be made by nonlinear regression of measured and model predicted cumulative recovery and recovery rate versus time. We do not recommend attempting to estimate M'_{ext} by nonlinear regression, due to the high likelihood of solution non-uniqueness, and suggest that a non-zero M'_{ext} be considered only if the recovery curve clearly exhibits a non-zero asymptotic rate.

Since we are interested in behavior as soil concentration approaches the cleanup target, we disregard data prior to reaching the peak recovery rate. Mass recovery data is analyzed as follows:

(1) Tabulate cumulative mass recovered and recovery rate versus operating time up to the most recent measurement date. If operation is intermittent due to maintenance etc., deduct downtime from calendar time to obtain operating time.

(2) Compute squared deviations between natural logarithms of measured and model-computed cumulative recovery $M(t)$ and of measured and model-computed recovery rates $M'(t)$ for each measurement date used for calibration.

(3) Sum squared cumulative mass recovery deviations multiplied by a weighting factor w_{mass} and squared rate deviations multiplied by $(1-w_{mass})$ to obtain an objective function.

(4) Apply a nonlinear regression algorithm (e.g., Excel Solver) to estimate M_o, S_{therm} and Δt_{peak} values that minimize the objective function. If multiple inflections in the recovery curve are observed, fit parameters for each curve segment.

(5) Compute average soil concentrations from eqs. (4.3) and (4.5) using calibrated parameter values. Stop if termination criteria are met. Otherwise repeat steps 1-5 for the next measurement date.

For real-time performance monitoring, regression analyses need not be commenced until the rate of change of average soil concentration per day from eq. (4.4) is less than the target concentration. Theoretically, optimal regression weights for cumulative mass recovery and recovery rate data should be inversely proportional to their variances (Kool et al. 1987) as

$$w_{mass} = \frac{S_{\ln mass}^{-2}}{S_{\ln mass}^{-2} + S_{\ln rate}^{-2}} \tag{4.6}$$

with a weight of $1- w_{mass}$ for rate data where $S_{\ln\, mass}$ is the computed standard deviation between ln measured and ln model-predicted cumulative mass recovery, and $S_{\ln\, rate}$ is the value for measured and predicted recovery rates. If subcategories of soil data were identifiable with different variances (e.g., certain geologic facies), eq. (4.6) may be generalized as $w_i = S_{lni}^{-2} / \Sigma_j S_{lnj}^{-2}$.

Due to the large "noise" in rate measurements, model calibration is best performed using a two-step procedure. For the step (or the first monitoring date that regression is performed), we advise fitting only to cumulative recovery data using w_{mass}=1. For the second step (or for regressions at subsequent ending dates), we recommend fitting M_o and S_{therm} values with Δt_{peak} fixed at its initial calibrated value using only the most recent 20-30 days of cumulative recovery with w_{mass}=0.5.

An Excel spreadsheet ***Thermal treatment model calibration.xlsx*** is available for calibrating lognormal mass recovery model parameters (Appendix A).

4.2.3 Field verification of model

Data from eight thermal treatment sites (Table 4.2) were used to evaluate the lognormal recovery model. PCE was the primary contaminant at all sites except Site 6 for which TCE was the main contaminant. Nonlinear weighted regressions were performed to fit lognormal model parameters to cumulative mass recovery and recovery rate data for each field site. Weights for mass recovery and recovery rate data were taken as inversely proportional to data "noise."

Due to much greater "noise" in rate measurements, relative weights for cumulative recovery data (w_{mass}) were generally greater than 0.99. Given the low weight applicable to rate data and the observation that rate data, even with low weights, tended to make convergence of the nonlinear regression more difficult, we used w_{mass}=1 for initial calibrations.

Initial calibrations were performed by fitting M_o, Δt_{peak} and S_{therm} to a single mass recovery function for the entire treatment duration for each field site. Fitted parameter values are summarized in Table 2 along with $S_{\ln mass}$ and $S_{\ln rate}$ values computed using the calibrated parameters. The results (Table 4.2, Figure 4.2) show reasonably good agreement. Estimated S_{therm} values range from 0.2 to 0.8 for the various sites and appear to be uniformly distributed with an equal number of sites having S_{therm} values above and below 0.5.

The lognormal model predicts thermal treatment duration (Δt_{rem}) to be a function of S_{therm}, Δt_{peak}, M_o and target mass remaining M_{rem}. Figure 4.3 illustrates this relationship normalized as $\Delta t_{rem}/\Delta t_{peak}$ versus M_{rem}/M_o for S_{therm} values from 0.2 to 0.8. To obtain a mass reduction of 99% to 99.99% (i.e., M_{rem}/M_o from 0.01 to 0.0001), $\Delta t_{rem}/\Delta t_{peak}$ ranges from approximately 1.6 to 2.1 for S_{therm} = 0.2, from 2.5 to 4.4 for S_{therm} = 0.4, from 4.0 to 9.3 for S_{therm} = 0.6, and from 6.4 to 19.6 for S_{therm} = 0.8. Note that M_{rem}/M_o is equivalent to the ratio of target average soil concentration to initial average soil concentration. The results emphasize the strong dependence of thermal treatment duration on S_{therm} as well as initial and target soil concentrations.

Of the sites studied, half had S_{therm} values less than 0.5 with actual treatment termination between 2 to 3 times Δt_{peak} at model-estimated mass recovery ratios averaging 99.8%. The other half of the sites, with S_{therm} values greater than 0.5, exhibited marked positive skew in the recovery curves and terminated at model-estimated mass recovery ratios averaging only 95% after operating for 2 to 4.5 times Δt_{peak}. The results demonstrate the relative difficulty of achieving high recovery ratios at sites with high S_{therm} values.

Closer inspection of observed and simulated mass recovery curves indicates multiple inflection points for many sites, reflecting multiple recovery rate peaks. This may be attributed to operations initiated on different treatment zones at various times, e.g., incremental startup of component systems including pilot tests, to variations in well spacings or geologic properties that affect heat or mass transfer rates, or to spatial variability in co-contaminants that affect boiling point. The

behavior of multi-inflection sites may be modeled by superposition of multiple lognormal recovery events – that is, by modeling each "event" by a different parameterization of eq. (4.1) and then summing results for all events at each date (after converting from operating time to calendar time) to obtain site-wide mass recovery curves, recovery rate curves, and average soil concentrations.

Table 4.2. Summary of $M(t)$ model results for eight field sites.

Site ID	Thermal Method	Treatment zone volume (m^3)	Actual mass recovery (kg)	t_{start} (d)	t_{stop} (d)	Initial calibration					Final calibration				
						M_o (kg)	Δt_{peak} (d)	S_{therm}	$S_{\ln\, mass}$	$S_{\ln\, rate}$	M_o (kg)	Δt_{peak} (d)	S_{therm}	$S_{\ln\, mass}$	$S_{\ln\, rate}$
1	TCH	11,100	2,353	0	210	2,353	73	0.25	0.011	1.692	2,353	73	0.34	0.053	0.870
2	TCH	6,039	5,248	0	147	5,248	55	0.40	0.024	0.710	5,390	55	0.52	0.048	0.604
3	TCH	78,000	75,331	0	244	75,332	118	0.20	0.039	1.079	75,332	118	0.24	0.030	0.832
4	TCH	2,523	3,400	0	100	3,408	42	0.25	0.023	0.909	3,401	42	0.26	0.024	0.888
4a		*a*		0	100	739	16	0.40	0.012	0.645	800	18	1.00	0.039	0.396
4b		*a*		10	100	1,183	26	0.20	*b*	*b*	1,209	24	0.26	*b*	*b*
4c		*a*		24	100	1,478	27	0.22	*b*	*b*	1,400	25	0.20	*b*	*b*
5	TCH	1,180	349	0	76	356	21	0.63	0.019	0.412	356	21	0.68	0.023	0.391
5a		*a*		0	76	95	8	0.90	0.023	0.356	95	8	0.90	0.023	0.356
5b		*a*		17	76	270	8	0.70	*b*	*b*	205	7	0.70	*b*	*b*
5c		*a*		33	76	205	25	0.99	*b*	*b*	71	25	0.99	*b*	*b*
6	ERH	13,340	528	0	200	570	78	0.65	0.035	0.504	568	76	0.74	0.043	0.495
6a		*a*		0	200	100	23	0.80	0.021	0.505	95	23	0.60	0.021	0.504
6b		*a*		23	200	280	40	0.63	*b*	*b*	280	40	0.63	*b*	*b*
6c		*a*		83	200	155	40	0.70	*b*	*b*	160	40	0.70	*b*	*b*
7	TCH	10,703	1,250	0	108	1,270	23	0.80	0.083	0.813	1,341	19	0.93	0.079	0.793
7a		*a*		0	20	250	4	0.61	0.014	0.566	250	4	0.50	0.031	0.515
7b		*a*		7	60	835	17	0.37	*b*	*b*	835	17	0.44	*b*	*b*
7c		*a*		54	108	201	22	1.02	*b*	*b*	195	22	0.87	*b*	*b*
8	SEE	5,248	10,959	0	450	12,300	155	0.60	0.068	0.529	12,500	155	0.56	0.085	0.530
8a		*a*		0	305	7,100	105	0.45	0.021	0.386	7,100	100	0.40	0.021	0.368
8b		*a*		110	305	2,800	100	0.30	*b*	*b*	2,700	105	0.25	*b*	*b*
8c		*a*		190	305	1,600	81	0.20	*b*	*b*	1,600	100	0.25	*b*	*b*

a Total treatment zone volume for multiple "event" model is the same as that shown for single "event" model.
b $S_{\ln\, mass}$ and $S_{\ln\, rate}$ values for multiple "event" model are aggregate values for the combined event model.

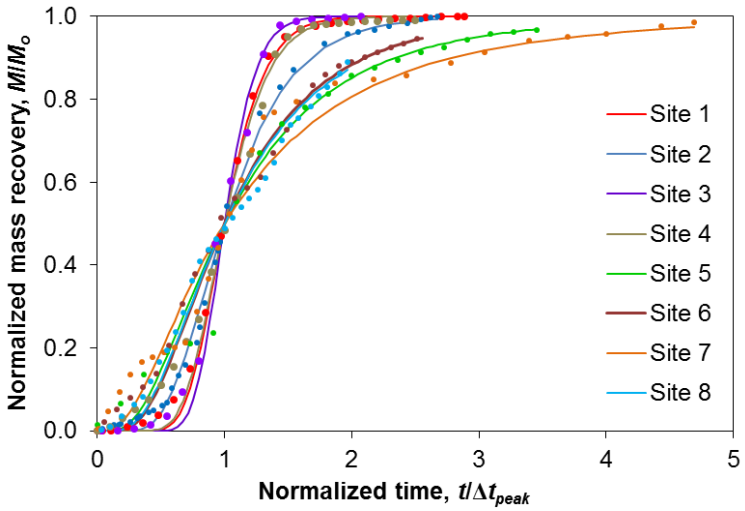

Figure 4.2. Observed normalized cumulative mass recovery versus normalized time for eight thermal treatment sites (data points) and model predictions (smooth curves) for single lognormal distribution function.

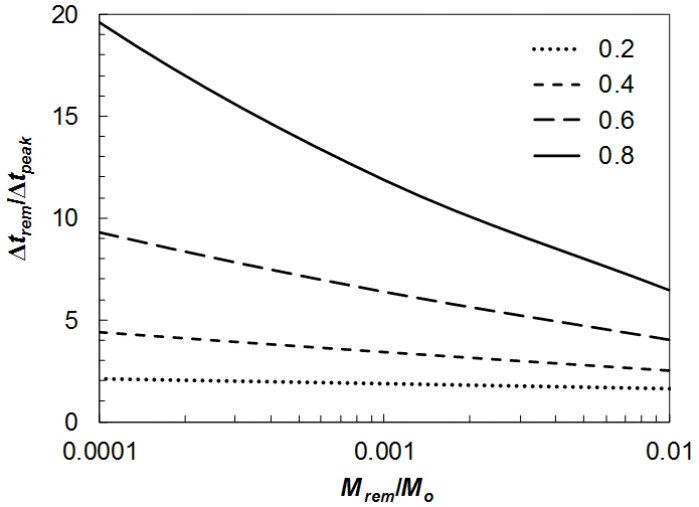

Figure 4.3. Normalized duration of thermal remediation vs. mass remaining for various S_{therm} values.

For each added event, two additional model parameters are introduced to align calendar and operating times, namely the stop time for the prior event t_{stop} and the start time for the following event t_{start}. We take t_{stop} and t_{start} values relative to the first start time (designated as zero), while Δt_{peak} values are given relative to t_{start} for each separate event. Values for these parameters may be operationally known. If not, they may be estimated during the calibration process.

Initial calibrations with w_{mass}=1 were repeated using multi-lognormal models for five sites that exhibited multiple inflections. Results for these calibrations are given in Table 4.2 with letters following the site number to identify each lognormal event (e.g., 4a, 4b, 4c). A graphical

illustration of cumulative mass recovery and recovery rate curves versus time for single- and multi-inflection calibrations is given for Site 7 (Figure 4.4).

Initial calibration results reveal a tendency for calibrated parameters to under-predict recovery rates at late times. Because small deviations in recovery curve tails may result in significant errors in inferred final average soil concentrations, a final round of calibrations was performed to refine asymptotic tail behavior. Only data from the last 20–30 days of recovery operations were used in these regressions and more weight was given to recovery rate data using $w_{mass} = 0.5$. This procedure resulted in small increases in S_{therm} values (Table 4.2). For single-event calibrations, S_{therm} values ranged from 0.2 – 0.8 for initial calibrations and 0.24 – 0.93 for final calibrations across all sites. For multi-event calibrations, the range in average S_{therm} values between sites was from 0.27 to 0.86 for initial calibrations and from 0.30 to 0.86 for final calibrations. Within multi-event sites, the difference between maximum and minimum S_{therm} values for the same site varied from a relatively narrow 0.30 to a high of 0.86, indicating that while S_{therm} values for different areas within a site are likely to be less variable than differences between sites, differences within sites may sometimes be as great as differences between sites.

Uncertainty in estimated mass remaining using the recovery model depends on uncertainty in the computed mass recovered as well as the asymptotic recovery, M_o. Standard deviations in ln model-predicted mass, $S_{\ln\, mass}$, and ln recovery rate, $S_{\ln\, rate}$, were computed from deviations between ln predicted and ln measured quantities and are tabulated for each calibration in Table 4.2. As an overall measure of model uncertainty, the root mean square error (RMSE) in ln cumulative mass recovery and ln recovery rate was computed as

$$S_{\ln\, rmse} = \left(\frac{S_{\ln mass}{}^2 + S_{\ln rate}{}^2}{2} \right)^{1/2} . \qquad (4.7)$$

Average values of $S_{\ln\, mass}$, $S_{\ln\, rate}$, and $S_{\ln rmse}$ are summarized in Table 4.3 for initial and final calibrations of sites with single inflection points, for multi-inflection sites modeled with a single inflection model and for multi-inflection sites modeled with a multi-inflection model. Not surprisingly, the multi-inflection sites exhibited lower uncertainty when a multi-inflection model was used. Final calibrations that used rate as well as mass recovery data to refine the initial calibrations reduced uncertainty for all cases. We recommend using the two-step calibration method as it is more robust than attempting to calibrate in a single step with rate and mass data. The second calibration using mass and rate data produced a small increase in $S_{\ln\, mass}$ and a larger decrease in $S_{\ln\, rate}$ yielding a net decrease in $S_{\ln\, rmse}$. Curiously, single inflection sites had significantly higher error than multi-inflection sites calibrated with a single inflection model. We attribute this to the small sample size and unique features of the individual sites. Across all formulations, average $S_{\ln\, rmse}$ is about 0.50 with mass data only and 0.41 after calibration refinement using rate and mass data.

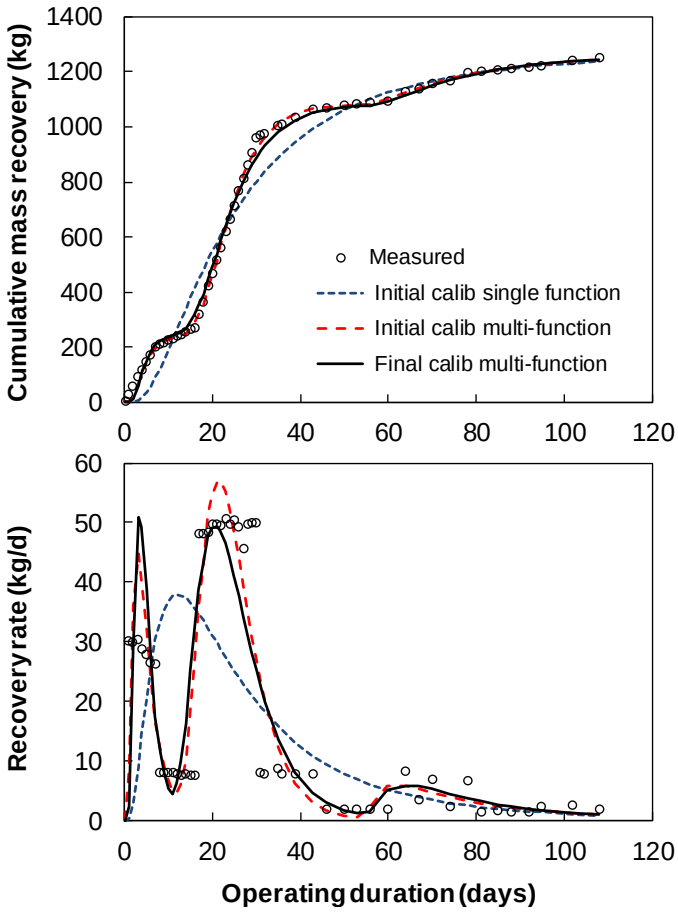

Figure 4.4. Cumulative mass recovery (top) and recovery rate (bottom) curves for Site 7 for single- and multi-function calibrations.

Table 4.3. Mass recovery model calibration error for various cases.

	Initial calibration			Final calibration		
Calibration case	$S_{\ln\ mass}$	$S_{\ln\ rate}$	$S_{\ln\ rmse}$	$S_{\ln\ mass}$	$S_{\ln\ rate}$	$S_{\ln\ rmse}$
a. Single inflection sites	0.025	1.160	0.821	0.044	0.769	0.544
b. Multi-inflection site treated as single	0.046	0.633	0.449	0.051	0.619	0.440
c. Multi-inflection site treated as multi	0.018	0.492	0.348	0.027	0.428	0.303
d. Best site model (cases a and c)	0.021	0.742	0.525	0.033	0.556	0.394

4.3 Performance monitoring

4.3.1 Soil monitoring data accuracy and uncertainty

Three of the study sites (1, 4, and 5) had soil concentration measurements before and after thermal treatment that can be used to estimate initial and final contaminant mass and its uncertainty for comparison with estimates from mass recovery data. Prior to undertaking this comparison, we wish to consider the estimation of mean concentration and its confidence limits from soil concentration data, as there are many factors that must be considered to avoid, or at least limit, errors.

The following methods were used to compute two-sided 95% confidence limits for initial (pre-remediation) and final (post-remediation) average soil concentration.

Method 1 – Normal distribution model. This approach is well known and is often used by remediation contractors. Confidence limits are computed as

$$m_{\pm CL\ \alpha} = m \pm t(\alpha, n_{smp}) \frac{S}{\sqrt{n_{smp}}} \tag{4.8}$$

where m = average(x_1,...,x_{nsmp}) and S= stdev(x_1...,x_{nsmp}) are the arithmetic average and standard deviation of soil concentration measurements on n_{smp} soil samples, $m_{LCL\ \alpha} = m_{\pm CL\ \alpha}$ is the lower confidence limit of the mean value computed with a negative sign on the right hand side, $m_{UCL\ \alpha} = m_{\pm CL\ \alpha}$ is the upper confidence limit computed with a positive sign, and $t(\alpha, n)$ is the two-sided t-value for probability level α.

Method 2 – Lognormal distribution model. This approach accommodates the asymmetric nature of positively skewed high variance populations. Confidence limits of the arithmetic mean concentration are computed from the lognormal model as

$$m_{\pm CL\ \alpha} = \exp\left(\ln m \pm t(\alpha, n_{smp}) \frac{S_{\ln}}{\sqrt{n_{smp}}} \right) \tag{4.9}$$

where m is the arithmetic average concentration computed as $m = \exp(m_{\ln} + 0.5S_{\ln})$ where $m_{\ln}$ = average($\ln x_1$,...,$\ln x_{nsmp}$) and $S_{\ln}$ = stdev($\ln x_1$,..., $\ln x_{nsmp}$).

Method 3 – Alternate lognormal model. Although the lognormal model is a more realistic approximation of high variance populations, estimates of the arithmetic mean from lognormal model parameters can be sensitive to deviations from the lognormal model especially in the tail (Reiman and Filzmoser 2000) or to truncation of non-detects (Helsel 2010). Method 3 uses eq. (4.8), but instead of computing the arithmetic mean m from lognormal parameters, it is computed as in Method 1.

Omitting non-detect values from statistical calculations can result in overestimation of the sample mean and underestimation of variance (Helsel 2010). Including non-detects for statistical calculations with values set at the detect limits will somewhat attenuate errors in sample means, but may do little to attenuate underestimation of variance. Setting non-detects below the detection limit will reduce lognormal statistics errors for analyses involving single contaminants as in the present case. Normal distribution means (arithmetic averages) and standard deviations are less sensitive to the treatment of non-detects than lognormal statistics.

Analyses of synthetic lognormal datasets with an $S_{\ln}$ of about 2.5 (typical for field sites) were performed to evaluate handling of samples below detection limits by assigning nondetects a numerical value equal to the detection limit times a factor *F*. For datasets with about 20% nondetects, arithmetic averages were insensitive to *F*, while S_{ln} values were most accurately estimated using *F* values between 0.1 and 0.5 (0.2 was optimal). With 40% nondetects, average values remained insensitive, while the sensitivity of S_{ln} values to *F* increased. The most accurate results were obtained using *F*=0.1 (S_{ln} was underestimated by 25% using *F*=0.5). For greater than 50% nondetects, it was not possible to obtain accurate averages and S_{ln} values using a single *F* value. With 80% nondetects, the best compromise was obtained using *F*=0.001, which underestimated the average value and overestimated S_{ln}, but yielded similar 95% confidence limits. For the present study, *F*=0.1 was used to assign numerical values to all reported nondetects.

Average soil concentrations from soil sampling rounds prior to thermal treatment for the three sites were computed by each of the above methods and multiplied by estimates of dry soil mass within the treatment volumes to determine total pre-remediation contaminant mass (M_o) and their confidence limits. Confidence limits of pre-remediation mass estimates were also computed from the $M(t)$ model for comparison with soil-sample–based values by

$$M_{\pm CL\ \alpha} = \exp\left(\ln M_{\ o} \pm t(\alpha,\infty) S_{\ln rmse}\right) \tag{4.10}$$

where $M_{LCL\ \alpha} = M_{\pm CL\ \alpha}$ is the lower confidence limit of the mean value computed with a negative sign on the right hand side, $M_{UCL\ \alpha} = M_{\pm CL\ \alpha}$ is the upper confidence limit computed with a positive sign, M_o is the calibrated pre-remediation mass summed across all treatment zones, and $S_{\ln\ rmse}$ is the RMSE for the final single inflection model calibration for Site 1 and the final multi-inflection model calibrations for Sites 4 and 5.

Estimates of M_o and its confidence limits for the above methods are tabulated in Table 4.4 along with measured total mass recovered during thermal treatment. Not surprisingly, the $M(t)$ model yields estimates of pre-remediation mass with narrow confidence limits consistent with actual recovery data from which model results are derived. Best estimates of contaminant mass using soil concentration data with Method 1 consistently underestimate actual recovery. Upper and lower confidence limits appear to have a downward bias compared to actual recovery, as expected for data with positive skew. Method 2 best estimates consistently over-predict actual recovery by 6 to 450%. Lower and upper confidence limits appear to be biased high. The lower confidence limit for Site 1 using Method 2 exceeds actual recovery by a factor of nearly 3. Method 3 shows the least erratic behavior with confidence limits that bracket actual recovery.

The results suggest that the soil data exhibit greater positive skew than the lognormal model accommodates, resulting in an inconsistency between the actual arithmetic mean soil concentration and the mean inferred from lognormal model parameters. Method 3 largely avoids this discrepancy by using the actual arithmetic mean. Some of the observed differences in mass estimates may be due to averaging data with equal weights for all data points. Geostatistical methods might reduce such errors, although it was not possible for the data sets considered, since sample coordinate information was not available. It is also possible that the selection of sampling locations itself was biased.

Table 4.4. Comparison of pre-remediation contaminant mass estimated using various methods of averaging soil concentration data versus estimates from cumulative mass recovery.

			Estimated mass in treatment zone prior to remediation (kg)				
			Soil data			Final Calibration	Actual
Site	No. samples	Parameter	Method 1	Method 2	Method 3	Eq. (4.3)	recovery
1	78	Mean value or best estimate	1,645	13,122	1,645	2,353.5	2,353.4
		95% LCL of mean	1,004	6,877	862	2,353.4	-
		95% UCL of mean	2,286	25,038	3,139	2,353.7	-
4	124	Mean value or best estimate	1,616	3,617	2,417	3,401.6	3,400.6
		95% LCL of mean	463	2,113	1,412	3,401.2	-
		95% UCL of mean	2,769	6,189	4,137	3,402.4	-
5	46	Mean value or best estimate	282	445	354	349.2	349.2
		95% LCL of mean	2	226	180	351.9	-
		95% UCL of mean	561	876	697	356.3	-

Table 4.5. Estimates of post-remediation average soil contaminant concentrations based on various methods.

			Average soil concentration (mg/kg)					
			Soil data			*M*(*t*) model		
Site	No. samples	Parameter	Method 1	Method 2	Method 3	Initial Calibration	Final Calibration	Recovery rate extrapolation
1	58	Mean value or best estimate	2.407	0.256	2.407	0.009	0.093	0.123
		95% LCL of mean	-1.398	0.147	1.383	0.002	0.028	0.023
		95% UCL of mean	6.212	0.446	4.191	0.045	0.307	0.654
4	14	Mean value or best estimate	2.600	110.071	2.600	0.044	1.042	0.978
		95% LCL of mean	-0.657	12.038	0.284	0.004	0.603	0.250
		95% UCL of mean	5.857	120.694	13.223	0.476	1.800	3.824
5	85	Mean value or best estimate	0.286	0.077	0.286	9.707	4.383	2.102
		95% LCL of mean	-0.013	0.046	0.171	5.921	2.718	0.542
		95% UCL of mean	0.584	1.211	1.420	15.915	7.067	8.150

For example, if sampling focused on identification of "hot spots" upward bias would likely occur. Unintended bias may be avoided using pseudo-random sampling algorithms (ITRC 2012).

Post-remediation average soil concentrations and confidence limits are tabulated in Table 4.5 for the same sites based on the three soil data analysis methods, the $M(t)$ model (eq. 4.3), and the rate extrapolation method (eq. 4.5) Calculations for the rate extrapolation method were performed using moving averages of measured recovery rates to attenuate noise. Values of $M''_{\ln}$ in eq. (4.5) at termination dates ranged from about -0.5 to -0.01, which were used to estimate a range of C_{avg}^{soil} roughly interpreted as 95% confidence limits at the time thermal treatment ceased.

Although the $M(t)$ model and recovery rate extrapolation method are based on the same underlying data, the assumptions and computational approaches are very different. Reasonable agreement between the $M(t)$ model and the recovery rate extrapolation method support the validity and accuracy of both methods. The difference between the initial and final calibration results indicates that model refinement to weight late time mass and recovery rates is important to obtain accurate estimates of mass remaining.

Method 1 confidence limits are clearly unreliable as all three cases show physically impossible negative lower confidence limits. Method 2 results are erratic. The Method 2 lower confidence limit for Site 1 exceeds the value based on mass recovery, while the Site 5 upper confidence limit is less than the concentration estimated from mass recovery methods. Site 4 confidence limits using Method 2 are far above the value inferred from mass recovery data. Method 3 results do not appear to be much better.

All three methods of analyzing soil concentration data yield final average soil concentrations that are at least an order of magnitude lower than those obtained from mass recovery data for Site 5. It is tempting to conjecture that the mass recovery methods are overestimating the final average concentration for Site 5 rather than the converse. However, a quick look at the mass recovery curve for Site 5 (Figure 4.2) reveals that the curve was still climbing rather steeply at the time treatment was terminated and would likely have taken another several weeks to flatline. The measured recovery rate on the last day of operation for Site 5 was just under 0.5 kg PCE per day, suggesting on the order of 5 kg of PCE was remaining in the system at termination. Dividing this by the estimated soil mass in the treatment zone (9.5×10^5 kg) indicates the average soil concentration was about 5 mg/kg when terminated, which is far greater than the average concentration of 0.067 mg/kg estimated from soil data by Method 3.

Surprisingly, the reliability of average soil concentration results shows no evident relationship with the number of soil samples. While confidence interval widths increase substantially from Site 5, which had 85 samples, to Site 4 with only 14 samples, the most egregiously erroneous best estimate occurred for Site 5, which had the most samples. Results based on soil concentration data indicate that while numerical precision improves with more samples, the accuracy does not necessarily converge to full-scale reality. For confidence limits of Site 5 to bracket the average soil concentration estimated from mass recovery data, a residual ln error of about 2 would need to be added to $S_{\ln}/n_{smp}^{1/2}$ in eq. (4.9). In most cases, a term of this magnitude would be greater than $S_{\ln}/n_{smp}^{1/2}$ even with a small number of samples. Perhaps Site 5 is an anomaly, but the large number of eccentric results for the three sites (Sites 1, 4, and 5) do not engender confidence in the reliability of contaminant mass estimates based on soil sample data.

The foregoing indicates that estimates of average soil concentration from soil sample data exhibit large uncertainty. Uncertainty associated with estimates based on mass recovery data is generally lower, but still significant. Furthermore, S_{therm} values exhibit significant a priori uncertainty which has a large effect on treatment duration to reach a given cleanup objective. While S_{therm} values can be progressively refined by regression analyses as treatment progresses, uncertainty in treatment duration, and hence cost, associated with both measurement and model uncertainties should be factored into treatment design, as discussed in the following sections.

4.3.2 Monitoring strategies and termination criteria

As stated previously, the objective we adopt for thermal treatment is the commonly used criteria that contaminant mass in the source zone should be reduced below a value corresponding to a specified average soil concentration, which may be stated as

$$C_{avg}^{soil} \le C_{stop}^{soil} \tag{4.11}$$

where C_{avg}^{soil} is the arithmetic average soil concentration in the source zone and C_{stop}^{soil} is a stipulated cleanup target. In practice, difficulties arise in the application of eq. (4.11) because the true value of C_{avg}^{soil} is never known exactly. If we compute the average value of soil concentration from a number of soil samples, $C_{avg\ smp}^{soil}$, and substitute this value for the <u>true</u> C_{avg}^{soil} in eq. (4.11), there will be a substantial likelihood of erroneously terminating treatment before the target criterion is met owing to deviations between $C_{avg\ smp}^{soil}$ and C_{avg}^{soil}.

A practical way to contend with this uncertainty is to employ the statistical termination criteria

$$C_{UCL\ \alpha}^{soil} \le C_{stop}^{soil} \tag{4.12}$$

where $C_{UCL\ \alpha}^{soil}$ is the upper confidence limit of estimated average soil concentration at exceedance probability α (i.e., significance level). Since $C_{UCL\ \alpha}^{soil} > C_{avg\ smp}^{soil}$ for any α>0.5, eq. (4.12) is a more stringent stop criterion than eq. (4.11) when $C_{avg\ smp}^{soil}$ is implicitly substituted for C_{avg}^{soil}. The difference between $C_{UCL\ \alpha}^{soil}$ and $C_{avg\ smp}^{soil}$ is a safety factor to reduce the likelihood of an erroneous decision to terminate early.

High variance properties of quantities that are physically constrained to be non-negative, such as contaminant concentration, necessarily exhibit positively skewed distributions. Normal probability distributions cannot describe such behavior. Lognormal distributions capture the major features of such data and are commonly used as a mathematically expedient approximation. If the average concentration is estimated from n_{smp} soil samples, then

$$C_{UCL\ \alpha}^{soil} = \exp\left(\ln\left(C_{avg\ smp}^{soil}\right) + t_1\left(\alpha, N\right) S_{\ln smp}^{soil} \Big/ \sqrt{n_{smp}}\right) \le C_{stop}^{soil} \tag{4.13a}$$

which may be rearranged to yield a termination criterion in terms of $C_{avg\ smp}^{soil}$ for n_{smp} soil samples

$$C_{avg\ smp}^{soil} \le \exp\left(\ln\left(C_{stop}^{soil}\right) - t_1\left(\alpha, N\right) S_{\ln smp}^{soil} \Big/ \sqrt{n_{smp}}\right) \tag{4.13b}$$

where $C_{avg\ smp}^{soil}$ is the arithmetic average for n_{smp} samples, $S_{\ln smp}^{soil}$ is the standard deviation of ln concentration values, and $t_1\left(\alpha, N\right)$ is the *t*-value for one-sided significance level α with *N* degrees

of freedom. If $S_{\ln smp}^{soil}$ is computed from the n_{smp} samples then $N=n_{smp}-1$, while if $S_{\ln smp}^{soil}$ is based on prior site characterization data or experience with other sites, then $N=\infty$. Note that for $\alpha = 0.05$, which denotes the 95% upper confidence limit, t_1 is 1.64 with $N=\infty$, while for $\alpha = 0.5$ t_1 is 0, in which case $C_{UCL}^{soil} = C_{avg\ smp}^{soil}$ indicating an equal probability of over- or under-estimating the average value. Eqs. (4.13a) and (4.13b) are approximate because the actual probability distribution will not exactly follow a lognormal curve (Reimann and Filzmoser 2000) and because they assume uncertainty in the arithmetic average concentration has the same variance as the geometric mean.

As an example, consider a site with a cleanup target C_{stop}^{soil} of 1 mg/kg. It is planned to take n_{smp}=20 soil samples to assess whether the objective has been met. Assume a prior estimate of $S_{\ln smp}^{soil} = 2.9$. If we want a 95% probability ($\alpha = 0.05$) that the actual average soil concentration will be less than 1 mg/kg when we terminate treatment, then t_1=1.64 and eq. (4.13) indicates that the average concentration $C_{avg\ smp}^{soil}$ computed from 20 samples needs to be less than 0.345 mg/kg to achieve the desired reliability. If we increase the number of samples to 50, we could terminate with the same confidence when $C_{avg\ smp}^{soil} \le 0.510$ mg/kg.

An alternative to termination based on soil sample measurements is to estimate average soil concentration from cumulative mass recovery data as described by eq. (4.3). Since mass recovery data is intrinsically integrated over a defined bulk soil volume V_{soil}, no sample averaging operation is required and eq. (4.13) can be modified as

$$C_{UCL\ \alpha}^{soil} = \exp\left(\ln\left(\frac{M_{rem}}{\rho_{soil} V_{soil}} \right) + t_1(\alpha,\infty) S_{\ln}^{rec} \right) \le C_{stop}^{soil} \tag{4.14}$$

where $M_{rem} = M(t) - M_o$ is the best estimate of mass remaining based on recovery data, and $S_{\ln}^{rec}$ is the standard error of the natural log of mass remaining.

An important aspect of the statistical stop criteria is that $C_{UCL\ \alpha}^{soil}$ decreases with decreasing measurement uncertainty ($S_{\ln smp}^{soil}$ for soil data and $S_{\ln}^{rec}$ for mass recovery data) and with increasing number of soil samples, which allows earlier termination of heating at a given confidence level. As we have shown, $S_{\ln}^{rec} << S_{\ln smp}^{soil}$, which lends a significant advantage to mass recovery data for termination decisions. For decisions based on soil data, increasing the number of samples reduces uncertainty in principle (assuming unbiased sampling), which allows earlier termination and reduces heating costs. However, this benefit must be balanced against higher sampling costs.

The foregoing statistical stop criteria may be applied to an entire thermal treatment volume to terminate operation of all heating units simultaneously. Alternatively, since time to reach C_{avg}^{soil} will vary spatially, it may be possible to reduce operating costs by applying stop criteria independently to smaller regions to terminate heating earlier in areas that reach cleanup objectives sooner. For example, anticipating that regions with higher initial contaminant concentrations are likely to take longer to cleanup, a system designer may consider dividing a site into multiple treatment zones (TZ) based on ranges of pre-remediation soil concentrations determined from soil boring data. It may also be cost advantageous to further divide TZs into multiple monitoring zones (MZ). The

total number of MZs may thus range from 1 to a value equal to the number of MZs per TZ summed over all TZs.

Tradeoffs will arise when trying to optimize the number of TZs and MZs. Specifically, while more TZs and/or MZs offer the possibility of cost savings by terminating heating earlier for areas that clean up more quickly, more total soil samples and/or more mass recovery measurements (and associated plumbing) will be needed to make reliable decisions at smaller scales. The potential savings from early termination may thus be offset by additional monitoring costs.

UCL values at each decision scale will increase as the number of soil samples per sampling event increases, making it easier to meet stop criteria at a prescribed probability level. Increasing the number of soil samples thus enables earlier system termination, but there will be a trade-off between the cost for additional samples versus operating cost reductions for earlier termination. Similarly, increasing the frequency of sampling will enable heating to be terminated earlier on average, which is likely to produce some savings, but at the expense of greater sampling costs. However, sampling and analytical costs are typically small relative to other operating costs, making a net cost reduction likely. Increasing the number of MZs also has the potential to reduce operating costs by terminating some areas sooner at the cost of more measurements. Additional performance monitoring variables that will affect decision uncertainty and cost include the number of MZs per TZ, the number of locations sampled per sampling event within each MZ, the number of depths sampled per boring during each sampling event, the initial date for soil sampling, the time interval between sampling events, and the choice of measurement methods (i.e., soil samples, mass recovery data, or both). Optimization of performance monitoring parameters may be used to minimize total cost for specific site conditions, as discussed in the following section.

MZ stop criteria that apply when soil and/or mass recovery data are used to make individual MZ termination decisions may be obtained by statistically pooling information from both soil and mass recovery data. If mass recovery data is employed, then mass recovery must be monitored independently for each MZ. The standard deviation of individual ln soil concentration measurements within TZ*i* is characterized by $S^{smp}_{\ln TZi}$ and we assume that all MZs within a given TZ have the same uncertainty (assuming random sampling locations). Different measurement types are weighted inversely proportional to their variance (Kool et al. 1987) and the pooled standard deviation is computed as a weighted root mean square.

The pooled data termination criteria for an entire TZ can be computed from the volume-weighted average MZ soil concentrations within the TZ and its pooled standard deviation and site-wide termination criteria may be obtained by upscaling TZ statistical parameters in the same manner, as described in the following section.

4.3.3 Statistical criteria for pooled data

The protocol proposed for making equal reliability site-wide, treatment zone and monitoring zone termination decisions is

IF $C^{pool}_{UCL\ global} \le C^{soil}_{stop\ global}$, THEN terminate all zones
ELSE
  FOR TZ $i = 1 \ldots N_{TZ}$
    IF $C^{pool}_{UCL\ TZ\,i} \le C^{soil}_{stop\ local}$, THEN stop treatment for TZi
    ELSE
      FOR MZ $j = 1 \ldots N_{MZ}$
        IF $C^{pool}_{UCL\ MZ\,ij} \le C^{soil}_{stop\ local}$, THEN stop treatment for MZj in TZi
      CONTINUE
  CONTINUE

where $C^{pool}_{UCL\ global}$ is a site-wide upper confidence limit based on statistically pooled soil sampling and mass recovery data (discussed below) across all TZs and MZs, $C^{pool}_{UCL\ TZ\,i}$ is the value computed using pooled data from all MZs within TZi, $C^{pool}_{UCL\ MZ\,ij}$ is the value from pooled data from a single MZj within TZi, $C^{soil}_{stop\ global}$ is a site-wide cleanup criteria specified by the site owner in consultation with regulators, and $C^{soil}_{stop\ local}$ is a termination criteria for individual TZs or MZs that may be equal to or less than $C^{soil}_{stop\ global}$. Specifying $C^{pool}_{stop\ local} = 0$ effectively disables local termination criteria, in which case no individual zones will be terminated early.

The MZ stop criteria that apply when soil and/or mass recovery data are used to make individual MZ termination decisions may be obtained by statistically pooling information from both soil and mass recovery data. If mass recovery data is employed, then mass recovery must be monitored independently for each MZ. The standard deviation of individual ln soil concentration measurements within TZi is characterized by $S^{smp}_{\ln TZi}$ and we assume that all MZs within a given TZ have the same uncertainty (assuming random sampling locations). Different measurement types are weighted in inverse proportion to their variance (Kool et al. 1987) and the pooled standard deviation is computed as the weighted root mean square, yielding the following criteria for termination of MZj within TZi

$$C^{pool}_{UCL\ MZij}(\alpha) = \exp\left(\ln C^{pool}_{avg\ MZij} + t_1(\alpha,\infty)\, S^{pool}_{\ln MZij}\right) \le C^{soil}_{stop\ local} \tag{4.15a}$$

where

$$\ln C^{pool}_{avg\ MZij} = w^{smp}_{MZij} \ln C^{smp}_{avg\ MZij} + (1 - w^{smp}_{MZij}) \ln\left(\frac{M^{rec}_{MZij}}{\rho_{soil} V_{MZij}}\right) \tag{4.15b}$$

$$S^{pool}_{\ln MZij} = \left(\frac{n^{smp}_{MZij}}{\left(S^{smp}_{\ln TZi}\right)^2} + \frac{I_{rec}}{\left(S^{rec}_{\ln}\right)^2}\right)^{-1/2} \tag{4.15c}$$

$$w^{smp}_{MZij} = \frac{\dfrac{n^{smp}_{MZij}}{\left(S^{smp}_{\ln TZi}\right)^2}}{\dfrac{n^{smp}_{MZij}}{\left(S^{smp}_{\ln TZi}\right)^2} + \dfrac{I_{rec}}{\left(S^{rec}_{\ln}\right)^2}} \tag{4.15d}$$

in which $C^{smp}_{avg\ MZij}$ is the average concentration for n^{smp}_{MZij} soil samples from MZ*ij*, M^{rec}_{MZij} is the estimated mass remaining in MZ*ij* from mass recovery data with uncertainty $S^{rec}_{\ln}$, V_{MZij} is the bulk volume of MZ*j* within TZ*i*, w^{smp}_{MZij} is the relative weight (certainty) for soil data and thus (1-w^{smp}_{MZij}) for mass recovery, $S^{smp}_{\ln TZi}$ is the prior estimate of standard deviation for ln concentration data applicable to TZ*i*, and I_{rec} is an indicator equal to 1 if mass recovery data is used or 0 otherwise. Note that when only soil data is employed, w^{smp}_{MZij} = 1 and when only mass recovery data is used w^{smp}_{MZij} = 0. Values of $S^{smp}_{\ln\ TZ}$ may be estimated from samples within individual treatment zones collected during source characterization as the standard deviation of ln measured concentrations. In rough terms, if about 2/3 of measurements (i.e., ± one standard deviation) in a TZ are within a factor of 10 (e.g., 1–10, 10–100), $S^{smp}_{\ln\ TZ} \approx \ln(10)/2 = 1.15$. For measurements within a factor of 100, $S^{smp}_{\ln\ TZ} \approx \ln(100)/2 = 2.30$.

The pooled data termination criteria for an entire TZ can be computed from the volume-weighted average MZ soil concentrations within the TZ and its pooled standard deviation as

$$C^{pool}_{UCL\ TZi}(\alpha) = \exp\left(\ln C^{pool}_{avg\ TZi} + t_1(\alpha,\infty)\, S^{pool}_{\ln TZi}\right) \le C^{soil}_{stop\ local} \tag{4.16a}$$

$$C^{pool}_{avg\ TZi} = \frac{\sum_{j=1}^{N_{MZi}} \rho_{soil} V_{MZij} C^{pool}_{avg\ MZij}}{\sum_{j=1}^{N_{MZi}} \rho_{soil} V_{MZij}} \tag{4.16b}$$

$$S^{pool}_{\ln TZi} = \left(\sum_{j=1}^{N_{MZij}} \left(S^{pool}_{\ln MZij}\right)^{-2}\right)^{-1/2} \tag{4.16c}$$

Note that the summation in eq. (4-16b) includes MZs in which heating may have terminated earlier, in which case $C^{pool}_{avg\ MZij}$ is the value from eq. (4.16b) for the last sampling date prior to termination.

Finally, the site-wide termination criteria may be obtained by upscaling TZ statistical parameters in the same manner as eqs. (4.16a) – (4.16c) yielding

$$C^{pool}_{UCL\ global}(\alpha) = \exp\left(\ln C^{pool}_{avg\ global} + t_1(\alpha,\infty)\, S^{pool}_{\ln global}\right) \le C^{soil}_{stop\ global} \tag{4.17a}$$

$$C^{pool}_{avg\ global} = \frac{\sum_{i=1}^{N_{TZ}} \rho_{soil} V_{TZi} C^{pool}_{avg\ TZi}}{\sum_{i=1}^{N_{TZ}} \rho_{soil} V_{TZi}} \tag{4.17b}$$

$$S^{pool}_{\ln\ global} = \left(\sum_{i=1}^{N_{TZ}} \left(S^{pool}_{\ln TZi}\right)^{-2}\right)^{-1/2} \tag{4.17c}$$

where V_{TZi} is the bulk volume of TZ*i*.

In addition to termination decisions at the MZ level (smallest decision level), we may concurrently apply termination rules at the TZ level to terminate all MZs within a TZ based on their aggregated data, or at the site level to terminate all TZs (and their MZs) based on aggregated data for the entire site. Note that since n_{smp} for an entire TZ is equal to the sum of n_{smp} values for its MZs, $C^{soil}_{UCL\ \alpha}$ for a TZ based on soil data will always be lower than that for the individual MZs. Therefore, it may be possible for an entire TZ to meet its aggregated termination criteria before the individual MZs, or likewise for site-wide criteria to be met before individual TZs.

The following decision logic is proposed for making termination decisions at various scales after each measurement/sampling event:

1. Tabulate and analyze the most recent sampling/monitoring data
2. If $C^{pool}_{UCL\ global} \le C^{soil}_{stop\ global}$ then terminate treatment in all TZs and MZs
3. If $C^{pool}_{UCL\ TZi} \le C^{soil}_{stop\ local}$ then terminate treatment for TZ*i*
4. If TZ*i* has multiple MZs and $C^{pool}_{UCL\ MZij} \le C^{soil}_{stop\ local}$ then terminate treatment for MZ*j*
5. Repeat step 4 for all MZs in TZ*i*
6. Repeat steps 3-5 for all TZs
7. Repeat step 1-6 for next sampling/monitoring event until all treatment is terminated

where $C^{pool}_{UCL\ global}$ is a site-wide upper confidence limit based on statistically pooled soil sampling and mass recovery data across all TZs and MZs, $C^{pool}_{UCL\ TZ\ i}$ is the value computed using pooled data from all MZs within TZ*i*, $C^{pool}_{UCL\ MZ\ ij}$ is the value from pooled data from a single MZ*j* within TZ*i*, $C^{soil}_{stop\ global}$ is a site-wide cleanup criteria specified by the site owner in consultation with regulators, and $C^{soil}_{stop\ local}$ is a termination criteria for individual TZs or MZs that may be equal to or less than $C^{soil}_{stop\ global}$.

An Excel spreadsheet, ***Thermal treatment termination decisions using real time data.xlsx,*** is available to track performance monitoring data and make real time MZ, TZ and site-wide termination decisions using mass recovery and/or soil concentration data measured in MZs based on the above statistical upscaling protocol. The spreadsheet also implements methods to incrementally calibrate thermal mass recovery models for each MZ (Appendix A).

4.4 Design optimization

4.4.1 Optimization approach and cost function

We have identified various factors that will affect the performance reliability and cost of thermal remediation—some of which are inherent properties of the site and others that can be manipulated and hence treated as design variables. Due to the large number of factors, uncertainty in true values of many properties, and complexity of interactions, *ad hoc* design approaches are likely to be suboptimal in terms of performance and/or cost. We wish to evaluate potential performance improvement and cost reductions for thermal treatment associated with various monitoring strategies by application of SCOToolkit to perform optimization analyses to determine design parameters that minimize expected (i.e., probability-weighted) total cost to meet specified remediation criteria taking into consideration uncertainty in measurements and model predictions.

Our focus here will be on optimization of monitoring parameters to meet specified source cleanup objectives without explicit consideration of downstream plume behavior.

Each Monte Carlo simulation considers equally probable realizations of thermal model parameters (e.g., M_o and S_{therm}) with termination decisions based on "noisy" data. At the termination of each realization, the performance and cost is evaluated and an optimization algorithm is used to iteratively adjust specified design variables to minimize the "expected" (i.e., probability-weighted average) cost.

To encourage the optimization algorithm to identify design parameter values that have a high probability of meeting remediation objectives, the optimization objective function adds a user-defined "penalty cost" for each Monte Carlo realization if the "true" site-wide average soil concentration (i.e., with "noise free" measurements) exceeds the global stop criteria. The penalty cost may be a real cost, for example the anticipated cost to implement "Plan B" if the initially proposed approach fails (e.g., a plume containment system) or it may be a fictitious value selected to yield a desired probability of success. Design parameters are determined to minimize the expected cost including any penalty costs. However, the penalty cost is not included in reported expected costs for optimized designs.

The total cost $\$_{total}$ for thermal treatment for each realization is computed as

$$\$_{total} = \$_{cap} + \$_{op} + \$_{mon} \tag{4.18a}$$

$$\$_{op} = M_{rec}\$_{mass} + \Delta t_{site}\left(\$_{SiteOp/day} + \sum_{i=1}^{N_{TZ}} f_{op\ i}\$_{TZop/day\ i}\right) \tag{4.18b}$$

$$\begin{aligned}\$_{mon} = \sum_{i=1}^{N_{TZ}} \Big\{ & N_{MZi}\$_{MZcap} + N_{MZi}\Delta t_{site} f_{op\,i}\$_{MZ/day} \\ & + \sum_{j=1}^{N_{MZi}} N_{smp\ events\ ij} N_{boring/MZi}\left(\$_{boring} + N_{smp/boring}\$_{soil\ smp}\right)\Big\}\end{aligned} \tag{4.18c}$$

where $\$_{cap}$ is the capital cost excluding fixed costs for monitoring equipment ($k), $\$_{op}$ is operating costs excluding performance monitoring, $\$_{mon}$ is monitoring cost ($k), Δt_{site} is the site treatment duration (site-wide max duration for all MZ values in days), $\$_{SiteOp/day}$ is the site-wide operating cost per day ($k/d) for activities that depend on the total treatment duration (e.g., vapor treatment system operation), M_{rec} is the total mass of contaminant recovered (kg), $\$_{mass}$ is the treatment cost per unit mass ($k/kg), $\$_{TZop/day\ i}$ is the operating cost per day for TZ*i* when all heating wells are operating ($k/d), $\$_{MZcap}$ is the cost per MZ for equipment to monitor cumulative mass recovery ($k), $\$_{MZ/day}$ is the cost per day per MZ to monitor cumulative mass recovery ($k/d), $\$_{boring}$ is the cost per soil boring ($k), $\$_{soil\ smp}$ is the cost per soil sample taken from a given boring ($k), N_{TZ} is the number of TZs, N_{MZi} is the number of MZs in TZ*i*, $N_{smp\ events\ ij}$ is the number of soil sampling events for MZ*j* in TZ*i*, $N_{boring/MZi}$ is the number of soil borings per MZ in TZ*i* for each sampling event, $N_{smp/boring}$ is the number of soil samples per boring, and $f_{op\ i}$ is a cost reduction factor for TZ*i* due to incremental MZ termination computed as

$$f_{op\ i} = \frac{\sum_{j=1}^{N_{MZi}} \Delta t_{ij} V_{MZij}}{\Delta t_{site} V_{TZi}} \tag{4.18d}$$

where Δt_{ij} is the duration of heating for MZ*j* in TZ*i*. After a decision is made to terminate heating site-wide or in a MZ or TZ, fluid recovery operations will generally be continued for some time.

To compute operating costs during optimization simulations, a user-specified lag time is added to modeled termination signal dates to account for delays in shutdown of all relevant system components.

Unit cost values may be determined from cost analyses performed by a thermal remediation contractor. Based on soil and aquifer characteristics, contaminant type and contaminant distributions from site characterization studies, the contractor will first identify the most appropriate thermal technology (ERH, TCH, SEE) and configurations of heating and vapor and liquid extraction wells for ERH, TCH or steam injection for each TZ. Unit costs for performance monitoring ($\$_{MZcap}$, $\$_{MZ/day}$, $\$_{boring}$, $\$_{soilsmp}$) and treatment ($\$_{mass}$) can be estimated directly. The remaining cost variables ($\$_{cap}$, $\$_{SiteOp/day}$, $\$_{TZop/day}$) can be determined from sensitivity analyses. For example, for a site with two potential TZs, the following cost estimates may be made.

(1) Compute cost $\$_{aAll}$ to design, implement and operate a system with two TZs for a duration Δt_a (e.g., Δt_{peak}) with all heating units and recovery wells operating continuously,

(2) Compute cost $\$_{bAll}$ in the same manner as step 1 but for a longer duration Δt_b (e.g., $2\Delta t_{peak}$),

(3) Compute cost $\$_{b1}$ in the same manner as step 2 except with a fraction f_{off} of heating units turned off in TZ_1 after Δt_a,

(4) Compute cost $\$_{b2}$ in the same manner as step 2 except with a fraction f_{off} of heating units turned off in TZ_2 after Δt_a,

where all costs exclude performance monitoring. Unit costs may be computed from the cost sensitivity results as

$$\$_{cap} = \$_a - \Delta t_a \frac{\$_{bAll} - \$_{aAll}}{\Delta t_b - \Delta t_a} \tag{4.19a}$$

$$\$_{TZop/day\,i} = \frac{\$_{bAll} - \$_{bi}}{f_{off}(\Delta t_b - \Delta t_a)} \tag{4.19b}$$

$$\$_{SiteOp/day} = \frac{\$_{bAll} - \$_{aAll}}{\Delta t_b - \Delta t_a} - \sum_{i=1}^{N_{TZ}} \$_{TZop/day\,i} \tag{4.19c}$$

The logic may be extended for additional TZs by performing additional cost sensitivities in the manner of steps 3 and 4 above. A spreadsheet, ***Thermal treatment unit cost calcs.xlsx***, is provided to compute unit costs from the foregoing cost sensitivity results (Appendix A).

4.4.2 Example problem description

We consider a hypothetical problem involving thermal treatment of a DNAPL PCE source in an unconfined aquifer using TCH. The site consists of 1.5 m of gravelly fill over interbedded silt and clay with some sand lenses to a depth of 9.1 m, and with clay from 9.1 to 12.2 m over bedrock. A water table occurs at 4.5 m with an average darcy velocity of 0.2 m/yr. Three treatment zones were identified based on site characterization data (Figure 4.5, Table 4.6). Thermal treatment is planned using TCH from the surface to the maximum observed PCE depth of 4.6 m.

The site cleanup objective ($C^{soil}_{stop\ global}$) is to achieve average soil concentration over the entire treatment volume <1 mg/kg. Optimization analyses that couple thermal treatment and dissolved plume migration could be used to determine the most cost-effective approach to meet groundwater criteria (Parker et al. 2010, 2012). However, we focus here solely on optimizing thermal treatment operational variables based on a specified soil cleanup criterion.

Contaminant mass in each TZ (M_{oTZ}) for each Monte Carlo realization prior to commencing thermal treatment is generated assuming a lognormal distribution as

$$M_{o\,TZ} = \rho_{soil} V_{TZ} \exp\left(m_{\ln soil\ TZ} + S_{\ln Mo} N_{rand}(0,1)\right) \tag{4.20}$$

where V_{TZ} is the bulk TZ volume, $m_{\ln soil\ TZ}$ is the mean ln soil concentration in the TZ computed as (ln C_{max} + ln C_{min})/2 based on values in Table 4.6 assuming C_{max} and C_{min} represent +/- one standard deviation confidence limits of a lognormal population, $S_{\ln Mo}$ is the ln standard deviation of M_o which is assumed to be 0.7, and N_{rand}(0,1) is a normally distributed random variable with zero mean and unit standard deviation. If TZs are divided into multiple MZs, the initial mass in the j^{th} MZ is generated such that the total equals M_{oTZ}. Based on results from the eight field sites discussed previously, S_{therm} uncertainty is characterized by a uniform distribution with a range from 0.2 to 0.8.

The number of heating and vapor recovery wells and related infrastructure for the example problem were determined based on heat balance calculations taking into consideration capital and operating cost tradeoffs with continuous heating. The number of heating wells (N_{HW}) and vapor recovery wells (N_{VW}) for each TZ and unit cost values computed from cost sensitivity analyses (see Appendix 4.3) are summarized in Table 4.6. The estimated time to reach the PCE azeotropic boiling point, Δt_{peak}, for the design was 65 days, which is treated as deterministic in Monte Carlo simulations. Vapor recovery is assumed to continue for 2 weeks following termination of heating at all wells.

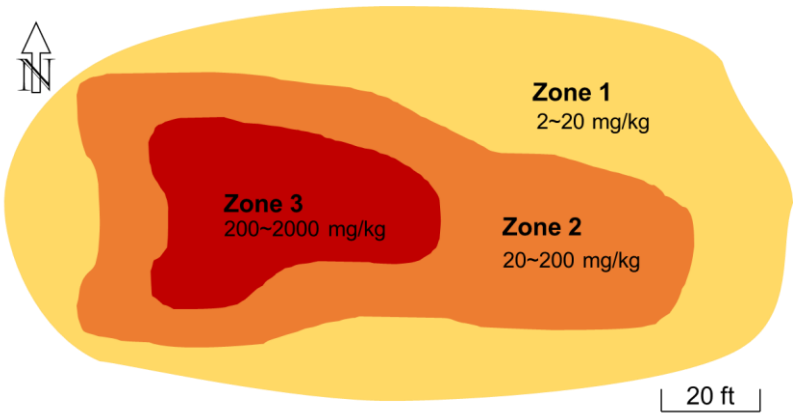

Figure 4.5. Plan view of treatment zones for optimization problem.

Table 4.6. PCE soil concentration ranges, numbers of heating and recovery wells and unit costs multiple TZ and single TZ cases for example problem.

Variable	TZs for multi-TZ cases 1	2	3	Single TZ cases
TZ area (m^2)	609	288	121	1018
C_{min} (mg/kg) *	2	20	200	2
C_{max} (mg/kg) *	20	200	2000	2000
Number of heating wells	54	25	13	92
Number of recovery wells	18	9	5	32
$\$_{TZ\ op/day}$ ($k)	2.015	0.933	0.485	3.433
	Costs independent of TZ			
$\$_{cap}$ ($k)	1,953.0			
$\$_{SiteOp/day}$ ($k)	2.137			
$\$_{mass}$ ($k/kg)	0.0055			
$\$_{MZcap}$ ($k)	0.200			
$\$_{MZ/day}$ ($k/d)	0.020			
$\$_{boring}$ ($k)	2.175			
$\$_{soil\ smp}$ ($k)	0.280			

* C_{min} and C_{max} are regarded as +/- one standard deviation confidence limits

In addition to considering cases with the site divided into three TZs with approximately known contaminant levels, we also consider the entire site treated as a single TZ. For consistency with the multi-TZ analyses, M_o values for the single "lumped" TZ realizations are computed as the sum of values for the multi-TZ analyses.

Three performance monitoring strategies are considered:

(1) Soil data only. Soil sampling is assumed to commence at a time Δt_{mon1} after beginning thermal treatment and is repeated at time intervals *of* Δt_{mon2}. At each sampling event, $N_{boring/MZ}$ borings per MZ are advanced with $N_{smp/boring}$ samples taken per boring at different depths. The total number of samples per sampling event per MZ is thus $N_{boring/MZ}\, N_{smp/boring}$.

(2) Mass recovery data only. Cumulative mass recovery data for each MZ is used to estimate mass remaining and average soil concentration is computed from eqs. (4.1) to (4.3) using calibrated model parameters. Mass recovery data is assumed to be available weekly to conservatively account for time to process data and implement decisions.

(3) Mass recovery and soil data. Method 2 is used to make preliminary termination decisions, which are not implemented until soil sampling data confirm the decision. Soil sampling commences one week after mass recovery termination signals for the signaled regions only and is repeated at time intervals Δt_{mon2} until pooled soil concentration data and mass recovery measurements satisfy termination criteria.

To generate "noisy" measurement data and to compute confidence limits for termination decisions, estimates of $S_{\ln TZ}^{smp}$ for soil measurements and $S_{\ln}^{rec}$ for mass recovery measurements are needed in eq. (4.13). Based on RMSE estimates for the eight field sites discussed above, we assume that mass recovery data have an uncertainty of $S_{\ln}^{rec} = 0.4$. For field sites with soil sample datasets, site-wide $S_{\ln}^{smp}$ values computed from the raw data ranged from 2.11 to 3.86. Based on anomalous behavior observed for average soil concentration confidence limits for the field sites discussed earlier, a considerably larger site-wide $S_{\ln}^{smp}$ value may be appropriate. We use a site-wide value of 3.5 for example cases that involve a single lumped TZ. For cases with the site divided into three TZs with approximately equal variances, $S_{\ln TZ}^{smp}$ should be smaller than the site-wide value by a factor of about $(1/3)^{1/2}$, which yields an estimate of $S_{\ln TZ}^{smp} \approx 2.0$ for each TZ in the multiple TZ cases.

Stochastic cost optimization analyses for the hypothetical site were performed for six cases with the site treated as a single TZ or divided into multiple TZs, with fixed or optimized values for the exceedance probability α and local stop criteria ($C_{stop\ local}^{soil}$), and with design variables for the three monitoring strategies described above optimized. The maximum number of MZs for each TZ is taken equal to the number of recovery wells in the TZ. Our objective is to evaluate effects of various operational monitoring strategies and associated optimized variables on thermal treatment performance and cost. Six optimization cases are considered, which are summarized in Table 4.7.

4.4.3 Design optimization results

Probability-weighted average ("expected") total costs for the various cases ranged from $3,247k to $4,099k with 95% upper confidence limits (UCL_{95}) from $3,247k to $4,987k considering all quantifiable sources of uncertainty (Table 4.7). Expected durations ranged from 289 to 411 days. The 95% upper confidence limit of total cost, considering all quantifiable sources of uncertainty, ranged from $3,247k to $4,987k. Total costs are divided into monitoring costs, other operating costs (including energy), and fixed costs for design and construction. The latter were constant at $1,953k for all cases. Expected monitoring costs ranged from $29k to $189k, and other operating costs from $1,265k to $1,957k.

It may be noted that expected values for corresponding costs from the stochastic optimization analyses are higher than those reported in the literature (Baker et al. 2016, Heron et al. 2016). Costs are similar if normalized for treatment duration. Longer probability-weighted average treatment durations in the present study may be partly attributed to a publication bias in favor of sites with low S_{therm} values that are mostly completed within about 2–3 times Δt_{peak}. Based on data from the sites reported here, the frequency of sites with S_{therm} values >0.5 is about equal to that of lower S_{therm} sites. However, average remediation duration to achieve 99% mass reduction for low S_{therm} sites (0.5-0.8) is about 2.4 times Δt_{peak} compared to 4.8 times Δt_{peak} for high S_{therm} sites (0.5-0.8). To reach 99.9% mass reduction, these ratios climb to 3.3 times Δt_{peak} for low S_{therm} sites and 8.3 times for high S_{therm} sites. A second factor may be that high S_{therm} sites tend to be terminated at lower mass recovery ratios owing to durations exceeding time and budget expectations. For the sites reported here, the average mass reduction ratio computed for low S_{therm} sites was 99.8% versus only 95% for high S_{therm} sites. A third factor contributing to longer treatment durations and costs

is that design optimizations were formulated to achieve a high probability (in most cases > 99%) that remediation criteria will be met. It is likely that most system designs are not this stringent. For these reasons, we believe the expected durations and costs from the stochastic optimization results are realistic considering the full range in S_{therm} values that may occur and assuming comparable cleanup levels are met with a high probability of success regardless of site recalcitrance.

Results for the various cases are discussed below.

Opt1. The first four cases utilize soil data only to make termination decisions for thermal treatment and treat the entire treatment volume as a single TZ. For Opt1 $\alpha = 0.5$ (hence $C^{soil}_{UCL\,\alpha} = C^{soil}_{avg\ smp}$) and $C^{soil}_{stop\ local} = C^{soil}_{stop\ global}$, indicating that heating in individual MZs and individual TZs is terminated when the measured average soil concentration within the respective area is below the site-wide stop criteria. These operating procedures are typical of industry practice. The number of MZs in the TZ ($N_{MZ/TZ}$), soil borings per MZ for each sampling event ($N_{boring/MZ}$), and soil sample depths per boring ($N_{smp/boring}$), time at which soil monitoring commences (Δt_{mon1}), and the time between successive sampling events (Δt_{mon2}) were optimized.

The fixed α value of 0.5 in conjunction with the condition that $C^{soil}_{stop\ local} = C^{soil}_{stop\ global}$ made it difficult to find a set of design variables that could reliably achieve the remediation target. The best that could be managed by optimization still suffered an 8% probability that the true average concentration will exceed the target value of 1 mg/kg. No exceedances greater than 10 mg/kg were predicted. With optimized values of only one MZ in the single TZ, 10 borings in the MZ with 4 sampling depths per boring, this case employs a total of 50 soil samples per sampling event, yielding reasonable monitoring costs that are consistent with industry practice ($67k).

The expected total cost is $3,764k with $1,745k for operating costs other than monitoring with the UCL_{95} of total cost equal to $4,808. The expected treatment duration of 310 days is 4.8 times Δt_{peak}, which is consistent with the range in S_{therm} values and remediation times inferred from the field sites discussed earlier in this paper. Aside from the consideration of risks from higher S_{therm} values, we regard Opt1 as a reasonable approximation of typical industry practice.

Opt2. This case is the same as Opt1 except that $C^{soil}_{stop\ local}$ is optimized subject to the constraint that it be no greater than $C^{soil}_{stop\ global}$. The optimized value of 0.094 mg/kg requires individual TZs to reach a significantly lower concentration than the site-wide target to terminate early, which permits site-wide termination to occur when remaining areas are at a higher average concentration. This flexibility allowed probability of failure to decrease to <1%, which enabled improved reliability as reflected by a lower total cost UCL_{95} of $4,525 compared to $4,808 for Opt1. However, improved reliability was achieved at the expense of a significantly longer expected remediation duration (411 days), and higher expected total cost ($4,099k), monitoring cost ($189k) and other operating cost ($1,957k).

Opt3. This case is the same as Opt2 except that α is also optimized to a value of 0.120. The resulting design also achieves an exceedance probability of <1% but with a shorter expected duration (320 days) and lower expected monitoring, other operating and total costs ($79k, $1,802k and $3,834k, respectively) using only one MZ with 7 borings per MZ sampled at 4 depths. However, the total cost UCL_{95} for Opt3 ($4.987k) is greater than that for Opt1 or Opt2.

Opt4. This case is identical to Opt3, except that the site is divided into three TZs that have less uncertainty in average soil concentration than the site as a whole. The optimized value of α for this case is a stringent 0.017 while the value of 0.948 mg/kg for $C^{soil}_{stop\ local}$, which is essentially the same as the site-wide criteria and less aggressive than the values for Opt 2 (0.094) and Opt 3 (0.390). The two largest and least contaminated TZs (TZ1 and TZ2) are each divided into two MZs and TZ3 is divided into three MZs for a total of 7 MZs. Two borings per sampling event are taken from each MZ and TZ if they have not already terminated. Four depths are sampled per all borings.

Although the expected treatment duration is slightly longer than that for Opt3 at 332 days, energy savings from early termination of MZs or TZs resulted in significantly lower expected non-monitoring operating costs ($1,530k), expected total cost ($3,612k) and total cost UCL_{95} ($4,100k). Opt4 has a lower expected total cost and UCL_{95} of total cost, as well as a significantly higher probability of success than Opt1.

Table 4.7. Results of stochastic cost optimization analyses for example problem. Bold values are fixed during optimization. Italic values are optimization results.

	Opt1	Opt2	Opt3	Opt4	Opt5	Opt6
Monitoring method	Soil	Soil	Soil	Soil	Recovery	Both
Probability of failure (%)	8	<1	<1	<1	<1	<1
Expected duration* (d)	310	411	320	332	290	289
Costs* ($k)						
Expected total cost	3,764	4,099	3,834	3,612	3,247	3,580
95% UCL of total cost	4,808	4,525	4,987	4,100	3,752	4,289
Expected monitoring cost	67	189	79	129	29	48
Expected other op. cost	1,745	1,957	1,802	1,530	1,265	1,580
Design variables						
N_{TZ}	**1**	**1**	**1**	**3**	**3**	**3**
Significance level (α)	**0.500**	**0.500**	*0.120*	*0.017*	*0.025*	*0.003*
$C^{soil}_{stop\ local}$ (mg/kg)	**1**	*0.094*	*0.390*	*0.948*	*0.701*	*0.783*
$N_{MZ/TZ}$	*1*	*19*	*1*	*2,2,3*	*6,1,1*	*3,1,1*
$N_{boring/MZ}$	*10*	*1*	*7*	*2,2,2*	-	*1,3,4*
$N_{smp/boring}$	*4*	*4*	*4*	*4*	-	*4*
Δt_{mon1} (d)	*245*	*168*	*168*	*182*	-	-
Δt_{mon2} (d)	*70*	*70*	*63*	*35*	-	*28*

* Expected costs and durations are probability-weighted averages. See text for discussion.

Opt5. This case is the same as Opt4 with three TZs, except that mass recovery measurements for each MZ are used to make termination decisions (Method 2). No soil sampling is performed during thermal treatment or for confirmation after treatment. The results achieve an exceedance probability of less than 1% with an optimized α value of 0.025 and $C^{soil}_{stop\ local}$ of 0.701 mg/kg. The number of MZs per TZ is 6 for TZ1 (the largest, least contaminated zone) and only one for TZ2 and TZ3, for a total of 8 MZs. Expected monitoring costs for Opt5 ($29k) are much lower than for any of the soil monitoring cases (Opt1-Opt4). Because mass recovery data have lower measurement uncertainty and are available with much higher frequency (weekly is assumed), termination decisions can be made much sooner on average than with soil sample data. This is evidenced by a lower expected treatment duration (289 days) than Op1 – Opt4, hence sharply lower expected non-monitoring operating costs ($1,265k) and total cost ($3,247k). The expected total cost is 10% lower than the best case using soil data only (Opt4) with the same probability of success. The expected total cost is also 14% lower than that for Opt1, the surrogate for "typical practice" that has the additional liability of an 8% probability of failure. Furthermore, the UCL_{95} for Opt5 total cost ($3,752k) is significantly less than corresponding values for all soil monitoring cases (Opt1-Opt4) and less than the expected total cost for all but Opt4.

Opt6. This case is similar to Opt4 and Opt5, except that monitoring is performed using Method 3, which employs mass recovery data by itself until a termination signal is obtained for site-wide, TZ or MZ termination, after which soil data is collected periodically until pooled soil and recovery data confirm the decision. The results achieve an exceedance probability of less than 1% with a $C^{soil}_{stop\ local}$ of 0.783 mg/kg and a stringent α value of 0.003. The number of MZs per TZ is three for TZ1 (largest, least contaminated) and one MZ for each of TZ2 and TZ3, for a total of five MZs. Only one boring per MZ is specified for TZ1 with three for TZ2 and four for TZ3 sampling 4 depths per boring for each location. The frequency of soil sampling after a termination signal based on mass recovery data is 28 days. Monitoring costs ($48k) are not much higher than for Opt5 and the operating time of 289 days is essentially the same as for Opt5. However, other operating costs for Opt6 ($1,580) are 25% higher than for Opt5, which is attributable to a 39% higher average energy utilization for Opt6 due to fewer early terminations of individual MZs and/or TZs. Relatively large uncertainty in soil data result in wider pooled confidence limits for Opt6 termination and a significantly higher UCL_{95} of total cost.

4.5 Summary and conclusions

Thermal treatment methods are effective technologies for remediation of DNAPL source zones due to their relatively low sensitivity to aquifer heterogeneity and DNAPL distributions. Nevertheless, significant uncertainty exists in the duration of heating required to meet remedial goals for a given system design. Normal distribution models for mass recovery as a function of time are unable to capture the positive skew of actual recovery data, which can lead to significant underestimation of the treatment duration necessary to reach cleanup objectives. We introduced a lognormal distribution model with recovery time duration characterized by the standard deviation in ln recovery time, S_{therm}, with values ranging from about 0.2 to 0.8 on a site-wide basis for field sites studied. For S_{therm} = 0.2, remediation duration can range from 1.6 × Δt_{peak} (time to reach effective boiling point) to achieve a mass reduction of 99% to 2.4 × Δt_{peak} for 99.99% reduction, while for S_{therm} = 0.8, treatment durations from about 6 to 20 × Δt_{peak} are predicted for the same mass reduction percentages.

We were unable to identify any significant correlations between S_{therm} values and geologic complexity, DNAPL source complexity, or initial contaminant concentration of the sites. Furthermore, since differences in S_{therm} values within a given site were as variable as differences between sites, estimates of S_{therm} from pilot tests may not be predictive of the whole site. A priori uncertainty in S_{therm} can result in significant uncertainty in site-wide treatment times. Iterative calibration of lognormal model parameters from mass recovery data provides incrementally refined estimates of S_{therm} and other model parameters which enable extrapolation of contaminant mass remaining for use in making reliable real-time termination decisions. Uncertainty in S_{therm} and other factors affecting treatment duration are taken into consideration in the design process using stochastic optimization methods.

We have proposed a strategy to turn the liability of uncertainty in time to reach cleanup objectives into a potential advantage by dividing the contaminated soil volume into treatment zones (TZ) that exhibit different average contamination levels based on site characterization data and (optionally) further dividing TZs into monitoring zones (MZ) for purposes of making termination decisions. We also allow target soil concentrations for regions smaller than the full site (local stop criteria) to be specified at a value less than the site-wide stop criterion. Cleaning up *less* recalcitrant regions (lower initial soil concentration and/or S_{therm}) to a lower average concentration enables *more* recalcitrant regions (higher initial soil concentration and/or S_{therm}) to be terminated at a higher average concentration to achieve the same site-wide average, which offers the possibility of reducing overall treatment duration and total operating cost. The multi-level monitoring and termination strategy allows for site-wide termination as well as early termination of individual TZs or MZs within TZs.

Thermal system termination decisions are commonly made by comparing the average concentration computed from a round of soil samples directly with a cleanup target. However, averages from soil data are subject to large uncertainty even when the number of soil samples is large. An alternative method, which estimates average soil concentration from mass recovery measurements during thermal treatment using the lognormal mass recovery model, has been demonstrated that exhibits less uncertainty and lower cost than soil sampling. To explicitly account for uncertainty in average soil concentrations estimated from soil and/or mass recovery data, the multi-level termination strategy stops treatment when an upper confidence limit of estimated mean concentration at a specified probability is below the target concentration. We employ a statistical methodology for computing confidence limits at site-wide, treatment zone and monitoring zone levels that allows termination decisions to be made at all scales with equal reliability.

To identify cost-optimal performance monitoring strategies to guide termination decisions, we incorporated the multi-scale thermal treatment performance monitoring protocol into the stochastic cost optimization program SCOToolkit to identify design variables that minimize probability-weighted total cost considering uncertainty in site properties, model predictions, and monitoring data while maintaining a high likelihood of meeting remediation objectives.

Results for an example problem indicate that the practice of using computed average soil concentration (as opposed to an upper confidence limit) cannot achieve a high probability of meeting the target average soil concentration. Optimizing the confidence limit probability, local scale cleanup level, number of monitoring zones per treatment zone, soil borings per monitoring zone for each sampling event, sample depths per boring, date for first sampling event, and time interval between sampling events for a site treated as a single treatment zone using only soil sampling data achieved cleanup objectives with a higher probability of success than a more

conventional approach. Dividing the site into three treatment zones with different soil concentration ranges and optimizing the same variables reduced total cost by 6%. Optimizing confidence limit probability, local-scale cleanup level, and number of monitoring zones per treatment zone with three treatment zones while using mass recovery data instead of soil data, achieved an additional 10% cost reduction. If confirmation of mass recovery-based results with soil sample data is desired or required, delaying each local termination decision until confirmed by soil sampling will increase the cost. Therefore, if confirmatory soil sampling is required, we recommend waiting until all heating units have been stopped based on mass recovery data before performing site-wide soil sampling.

In addition to computing the probability-weighted average cost for optimized designs, the method gives cost probability distributions that reflect uncertainty in measurements and calculations. An optimized example problem using only mass recovery data to make termination decisions (Opt5) had a 16% lower expected total cost than a case that approximates typical industry practice (Opt1), while the 95% upper confidence limit of total cost for the former was 28% lower. Thus, the proposed methodology not only yields "expected" cost savings, but also sharply reduces the magnitude of potential cost overruns.

4.6 References

Baker, R.S., S.G. Nielsen, G. Heron, and N. Ploug (2016) How effective is thermal remediation of DNAPL source zones in reducing groundwater concentrations? *Groundwater Monitoring & Remediation*, 36, 38-53.

Beyke, G. and D. Fleming (2005) In situ remediation of DNAPL and LNAPL using electrical resistance heating. *Remediation* 15: 5–22.

Cardiff, M., X. Liu, P. K. Kitanidis, J. Parker, and U. Kim (2010) Cost optimization of DNAPL source and plume remediation under uncertainty using a semi-analytic model. *Journal of Contaminant Hydrology* 13: 24-43.

Davis, E.L. (1997) How Heat Can Enhance In Situ Soil and Aquifer Remediation: Important Chemical Properties and Guidance on Choosing the Appropriate Technique. U.S. EPA Issue paper, EPA/540/S-97/502.

Davis, E.L. (1998) Steam Injection for Soil and Aquifer Remediation. U.S. EPA Issue paper, EPA/540/S-97/505.

Fan, Y.H. and K.S. Udell (1995) An analysis of the vaporization of volatile organic contaminants from porous media by conductive heating. *In Proceedings of ASME Heat Transfer and Fluids Engineering Divisions*, HTD-32: 715-721.

Gmehling, J. and U. Onken (1997) Vapor-Liquid Equilibrium Data Collection. *DECHEMA Chemistry Data Series*, Vol. 1 Parts 1-10. Frankfort.

Hansen, K.S., D.M. Conley, H.J. Vinegar, J.M. Coles, J.L. Menotti, and G.L. Stegemeier (1998) In situ thermal desorption of coal tar. In *Proceedings of Institute of Gas Technology/Gas Research Institute International Symposium on Environmental Biotechnologies and Site Remediation Technologies*. Orlando, Florida, December 7-9.

Helsel, D. (2010) Much ado about nothing: incorporating nondetects into science. *The Annals of Occupational Hygiene* 54(3): 257-262.

Heron, G., J. Bierschenk, R. Swift, R. Watson and M. Kominek (2016) Thermal DNAPL source zone treatment impact on a CVOC plume, *Groundwater Monitoring & Remediation*, 36, 26-37.

Heron, G., M. van Zutphen, T.H. Christensen, C.G. Enfield (1998a) Soil heating for enhanced remediation of chlorinated solvents: A laboratory study on resistive heating and vapor extraction in a silty, low-permeable soil contaminated with trichloroethylene. *Environmental Science and Technology* 32: 1474-1481.

Heron, G., T.H. Christensen, and C.G. Enfield (1998b) Henry's law constant for trichloroethylene between 10 and 95 C. *Environmental Science and Technology* 32: 1433–1437.

Itamura, M.T., and K.S. Udell (1993) Experimental clean-up of a dense nonaqueous phase liquid in the unsaturated zone of a porous medium using steam injection. *Multiphase Transport in Porous Media* HTD-265: 57-62.

ITRC, 2012, Technical and Regulatory Guidance Incremental Sampling Methodology, Interstate Technology & Regulatory Council Incremental Sampling Methodology Team, 417 p.

Kim, U., J.C. Parker, P.K. Kitanidis, M. Cardiff, X. Liu, and J. Gillie (2012) Stochastic Cost Optimization of DNAPL Remediation - Field Application. *Environmental Modeling & Software* 38: 74-88.

Kingston, J.T., P.R. Dahlen, P.C. Johnson, E. Foote, and S. Williams (2010) Critical Evaluation of State-of-the-Art In Situ Thermal Treatment Technologies for DNAPL Source Zone Treatment. SERDP Project ER-0314, Final Report, SERDP-ESTCP, U.S. Department of Defense, 1270 p.

Kool, J.B., J.C. Parker and M.Th. van Genuchten (1987) Parameter estimation for unsaturated flow and transport models: A review. *Journal of Hydrology* 91: 255-293.

Lee, J., X. Liu, P.K. Kitanidis, U. Kim, J. Parker, A. Bloom, and R. Lyon (2012) Cost optimization of DNAPL remediation at Dover Air Force Base. *Ground Water Remediation and Monitoring* 32: 48–56.

Levine, H. (2010) EPA perspective on site closure: how clean is clean? U.S. Department of Defense SERDP/ESTCP Partners in Environmental Technology Technical Symposium and Workshop. Washington D.C., Nov 30-Dec 2.

Loaiciga, H.A., R.J. Charbeneau, L.G. Everett, G.E. Fogg, B.F. Hobbs, and S. Rouhani (1992) Review of ground-water quality monitoring network design. *Journal of Hydrologic Engineering* 118(1): 11-37.

Parker, J., U. Kim, P. Kitanidis, M.Cardiff, X. Liu, and J. Lee (2011) Practical Cost-Optimization of Characterization and Remediation Decisions at DNAPL Sites with Consideration of Prediction Uncertainty. SERDP Project ER-1611, Final Report, SERDP-ESTCP, U.S. Dept. of Defense, 92p.

Ponton, J.W. (2009) Edinburgh Collection of Open Software for Simulation and Education. Edinburg University, http://homepages.ed.ac.uk/jwp/Chemeng/azeotrope/hetero.html.

Powell, T., G. Smith, J. Sturza and K. Lynch, and M. Truex (2007) New advancements for in situ treatment using electrical resistance heating. *Remediation* 17(2): 51-70. DOI: 10.1002/rem.20124

Rao, P.S.C., J.W. Jawitz, C.G Enfield, R. Falta, M.D. Annable, A.L. Wood (2001) Technology integration for contaminated site remediation, in Cleanup goals and performance metrics. Ground Water Quality, Sheffield UK: 410-412.

Reed, P.M., B.S. Minsker, and A.J. Valocchi (2000) Cost-effective long-term groundwater monitoring design using a genetic algorithm and global mass interpolation. *Water Resources Research* 36(12): 3731-3741.

Reimann, C. and P. Filzmoser (2000) Normal and lognormal data distribution in geochemistry: death of a myth. Consequences for the statistical treatment of geochemical and environmental data. *Environmental Geology* 39: 1001-1014.

Schumacher, M.M. (1980) Enhanced Recovery of Residual and Heavy Oils. Second Edition, Noyes Data Corporation, Park Ridge, New Jersey, 378 p.

Truex, M., T. Powell, and K. Lynch (2007) In situ dechlorination of TCE during aquifer heating. *Ground Water Monitoring and Remediation* 27: 96–105.

U.S. EPA (2000) Subsurface Remediation: Improving Long-Term Monitoring & Remedial Systems Performance. EPA/542/B-00/002. Conference Proceedings. June 8-11, 1999. St. Louis, MI. U.S. Environmental Protection Agency, 81 pp.

U.S. EPA (2004) In Situ Thermal Treatment of Chlorinated Solvents: Fundamentals and Field Applications. EPA 542-R-04-010. U.S. Environmental Protection Agency, 145 p.

U.S. EPA (2007) Long-Term Groundwater Monitoring Optimization Newark, Muscoy, and Source Operable Units Newmark Superfund Sites San Bernardino, California. EPA 542-R-07-015. Report. U.S. Environmental Protection Agency, 326 pp.

Vinegar, H.J., G.L. Stegemeier, F.G. Carl, J.D. Stevenson, and R.J. Dudley (1999) In situ thermal desorption of soils impacted with chlorinated solvents. *In Proceedings of Annual Meetings of the Air and Waste Management Association*, Paper No. 99-450.

Wu, C.H. (1977) A critical review of steamflood mechanisms. In Proceedings of *Society of Petroleum Engineers California Regional Meeting*, 13-15 April, Bakersfield, California. Paper SPE 6550-MS.

5. DNAPL Zone Treatment by In Situ Chemical Oxidation

5.1 Overview

In situ chemical oxidation (ISCO) involves injection of a chemical reagent into the subsurface to chemically oxidize contaminants. The technology has been studied since the early 1990s and has been used extensively in the field for a variety of contaminants. The most common reagents are potassium or sodium permanganate although others have also been used, including persulfate, ozone, hydrogen peroxide, and modified Fenton's reagent (H_2O_2 plus ferrous iron). The most common delivery method involves injection of a pulse of oxidant into an injection well network, followed by a period with natural gradient conditions in which oxidant reacts with contaminants and migrated with groundwater. This method is well adapted to the treatment of DNAPL source zones in relatively low permeability aquifers. In permeable aquifers, low residence times in the target zone diminish the cost effectiveness of this delivery method. An alternative delivery approach is to inject oxidant continuously at lower flow rates, capture unreacted reagent downgradient of the treatment zone and reinject it with additional oxidant to maintain a more or less constant oxidant concentration in the treatment zone over time.

ISCO is a mature technology with well documented design protocols (Huling and Pivetz 2006, Siegrist et al 2006) including useful software tools for system design and cost estimation (Siegrist et al. 2010). These guidance documents and design tools provide a starting point for the tools described here. In particular, we assumed that the individual who wishes to undertake cost optimization of ISCO design, has used the aforementioned guidance and tools to develop a draft design that is suited to his site conditions. This will serve as the starting point for stochastic design optimization using SCOToolkit to refine selected operating variables and performance monitoring details taking into consideration effects of measurement and prediction uncertainty, coupling between ISCO performance and plume scale processes, and complex interactions and tradeoffs that affect performance and cost.

5.2 DNAPL mass decrease during ISCO

We consider a DNAPL source zone of volume V_o [L^3] to which we wish to apply ISCO. The total contaminant mass prior to ISCO is M_o [M] and the corresponding discharge rate is J_o [MT^{-1}]. In general, we expect ISCO efficiency to improve if DNAPL source zones are divided into smaller operational units that are monitored and managed independently. For example, field data may indicate one or more "hot spots" having high soil concentrations, with adjacent areas of moderate concentrations, and peripheral zones of lower concentrations. Since lower concentration zones will likely require fewer oxidant injections, earlier termination will be possible and less aggressive design variables may more cost effective. Therefore, we consider division of the source zone into $i = 1, \ldots, N_{TZ}$ treatment zones (TZ). For each TZ, source discharge to groundwater downgradient of the source for the transport model is described by a modified form of eq. (2.1) as

$$J_i(t) = F_{mti}(t) F_{ki}(t) J_{oi} \left(\frac{M_i(t)}{M_{oi}} \right)^{\beta} \tag{5.1}$$

where $J_i(t)$ is the discharge rate of contaminant from the source zone for TZ i as a function of time [MT^{-1}], $M_i(t)$ is the DNAPL mass remaining versus time [M], M_{oi} is the mass just prior to ISCO

[M], J_{oi} is the initial dissolution rate [MT^{-1}], β is an empirical depletion exponent, $F_{mt\,i}$ is a mass transfer enhancement factor [-], and $F_{k\,i}$ is a mass transfer inhibition factor [-]. In the following, we drop TZ subscripts, *i*, for brevity. The enhancement factor is estimated based on Reitsma and Dai (2001) as

$$F_{mt}(t) = 1 + f_{mt}\,\frac{C_{ox}(t)W_{CH}}{S_{CH}W_{ox}}$$
$$f_{mt} = \frac{D_{ox}}{n_{ox/CH}D_{CH}} \tag{5.2}$$

where $C_{ox}(t)$ is the current aqueous oxidant concentration [ML^{-3}], S_{CH} is the effective solubility of contaminant in the DNAPL [ML^{-3}], W_{ox} is the molecular weight of oxidant [M mol^{-1}], W_{CH} is the molecular weight of contaminant [M mol^{-1}], D_{OX} is the aqueous diffusion coefficient of oxidant [L^2T^{-1}], D_{CH} is the contaminant aqueous diffusion coefficient [L^2T^{-1}], and $n_{ox/CH}$ is the stoichiometric ratio of oxidant to contaminant for the redox reaction. Diffusion coefficient ratios for permanganate are about 1.12 for PCE, 1.03 for TCE, and 0.95 for DCE. yielding f_{mt} values of 1.49 for PCE and 2.1 for TCE with permanganate. Values for $n_{ox/CH}$ will be discussed later.

Mass transfer inhibition due to MnO_2 precipitation during permanganate addition has been studied by West et al. (2007) and West and Keuper (2012), modeled as

$$F_k(t) = 1 - S_{rind}\;C_{precip}(t) \tag{5.3}$$

where $C_{precip}(t)$ is the mass of precipitated MnO_2 per treatment zone pore volume [ML^{-3}] as a function of time (computed from the cumulative mass of injected oxidant and the reaction stoichiometry) and S_{rind} = 4.6 x 10^{-6} L/mg based on West and Keuper studies, although site-specific measurements may be advisable as this value may vary with site conditions. If precipitation reactions are expected for other oxidants, lab or field pilot studies would need to be conducted to quantity C_{precip} and S_{rind}.

The initial mass M_{oi} in each TZ_i is generated in the model from user-specified minimum and maximum soil concentrations C_{soil}^{min} and C_{soil}^{max} within each TZ from site characterization data. Mass conservation requires that

$$\sum_{i=1}^{N_{TZ}} M_{oi} = M_o,\;\; \sum_{i=1}^{N_{TZ}} J_{oi} = J_o,\;\text{ and }\;\sum_{i=1}^{N_{TZ}} V_{oi} = V_o \tag{5.4}$$

To satisfy the above constraints the following two-step method is used to generate TZ parameters.

Step 1. Assuming minimum and maximum soil concentrations represent 95% confidence levels of a log-normal distribution, generate initial mass estimates for each TZ by

$$M_{1i} = \exp\left(m_{\ln i} + S_{\ln i}\;\mathrm{N}(0,1)\right) \tag{5.5a}$$

$$\text{where}\quad \begin{cases} m_{\ln i} = 0.5\;(\ln C_{max} + \ln C_{min}) \\ S_{\ln i} = 0.25\;(\ln C_{max} - \ln C_{min}) \end{cases} \tag{5.5b}$$

Step 2. Adjust estimates for consistency with M_{oi} as

$$M_{oi} = M_{1i} \frac{M_o}{\sum_{i=1}^{N_{TZ}} M_{1i}} \tag{5.5c}$$

In addition to characterization of the source mass discharge function for the entire DNAPL source to be treated by ISCO (see Chapter xx on model calibration), potential treatment zones should be identified and key characteristics determined, including the depth, width and volume, minimum and maximum soil concentrations, and mean oxidant travel length.

5.3 ISCO reaction model

A mass balance model is solved for each ISCO treatment zone to compute average soil and groundwater concentrations within treatment zone volumes. The model accommodates boundary conditions for both pulsed and continuous oxidant injection conditions. Each treatment zone is modeled as a stirred tank reactor with five components, namely

- Contaminant occurring as DNAPL
- Aqueous and adsorbed contaminant
- Rapidly oxidizable natural oxidant demand ("fast" NOD or NOD_f)
- Slowly oxidizable natural oxidant demand ("slow" NOD or NOD_s)
- Aqueous phase oxidant

DNAPL serves as a rate-limited source of aqueous contamination described by eqs. (5.1) – (5.5). Direct oxidation of DNAPL contaminant is assumed to be negligible. However, DNAPL dissolution rate is coupled with aqueous oxidant concentration via (5.2). Following Cha and Borden (2012), oxidant is assumed to react instantaneously with aqueous and adsorbed contaminant and with NOD_f. Oxidation of NOD_s is modeled as a second-order kinetic reaction. Equilibrium is assumed to occur between aqueous and sorbed contaminants. The reaction of chlorinated solvent with an O_2-equivalent oxidant (O_{2eq}) is given by

$$C_aH_bCl_c + n_{O2eq}O_{2eq} + n_{H_2O}H_2O \longrightarrow aCO_2 + cHCl \tag{5.6}$$

with stoichiometry coefficients n_{O_2eq} = a-(c-b)/4 and n_{H_2O} = (c-b)/2. For PCE (C_2Cl_4), TCE (C_2HCl_3), and DCE ($C_2H_2Cl_2$), as an example, the reactions become

$$\begin{aligned} C_2Cl_4 + 2H_2O + O_{2eq} &\longrightarrow 2CO_2 + 4HCl \\ C_2HCl_3 + H_2O + \frac{3}{2}O_{2eq} &\longrightarrow 2CO_2 + 3HCl \\ C_2H_2Cl_2 + 2O_{2eq} &\longrightarrow 2CO_2 + 2HCl \end{aligned} \tag{5.7}$$

indicating that n_{O_2eq} = 1 mol-O_{2eq} of oxidant per mole of PCE, 1.5 mol-O_{2eq} per mole of TCE, and 2 mol-O_{2eq} per mole for DCE.

Common oxidizing agents include permanganate (MnO_4^-), ozone (O_3), hydrogen peroxide (H_2O_2), and persulfate ($S_2O_8^{-2}$) that have theoretical oxygen equivalents (O_{2eq}) of 0.75, 1.5, 0.5, and 1.0, respectively, although actual field values can vary with pH and other geochemical conditions, other added reactants (e.g., ferrous iron with hydrogen peroxide or persulfate) or heat (e.g., thermal activation of persulfate to produce the stronger oxidant SO_4^-). As an example, the oxidation of TCE by MnO_4^- may be written as

$$2MnO_4^- + C_2HCl_3 \longrightarrow 2CO_2 + 2MnO_2(s) + 3Cl^- + H^+ \quad (5.8)$$

indicating complete oxidation of one mole of TCE by $n_{ox/CH}$ = 2 moles of permanganate. Note that the overall stoichiometry ratio $n_{ox/CH} = n_{O_2eq} / O_{2eq} = 1.5/0.75 = 2$. Overall baseline stoichiometries for oxidation of PCE, TCE and DCE by the afore-mentioned oxidants are summarized in Table 5.1. Theoretical values for other contaminants and oxidants may be easily derived. However, it is advisable to confirm (or refine) values based on results of bench- or field-scale pilot tests under conditions approximating those planned.

NOD is characterized by the total NOD per dry soil mass (C_{soil}^{NODtot}), the ratio of fast to total NOD (f_{NODf}), and the second order rate coefficient for NODs (k_{NODs}). NOD parameters may be determined on soil samples using the laboratory protocol described by ASTM method D7262-07 (ASTM 2007). Since potassium permanganate is the oxidant in this lab test, the quantity of NOD is typically reported as moles of $KMnO_4$. These values are converted to mol-O_2eq in SCOToolkit. Typical ranges for NOD parameters are given in Table 5.2.

Table 5.1 Stoichiometry factors $n_{O_2eq} / O_{2eq} = n_{ox/CH}$ for PCE, TCE and DCE oxidation by MnO_4^-, O_3, H_2O_2, and $S_2O_8^{-2}$.

	MnO_4^-	O_3	H_2O_2	$S_2O_8^{-2}$
PCE	1.0 / 0.75 = 1.5	1.0 / 1.5 = 0.67	1.0 / 0.5 = 2.0	1.0 / 1.0 = 1.0
TCE	1.5 / 0.75 = 1.5	1.5 / 1.5 = 1.0	1.5 / 0.5 = 3.0	1.5 / 1.0 = 1.5
DCE	2.0 / 0.75 = 2.67	2.0 / 1.5 = 1.33	2.0 / 0.5 = 4.0	2.0 / 1.0 = 2.0

Table 5.2 Typical natural oxygen demand (NOD) parameter ranges (Cha 2012).

Parameter	10% LCL [1]	Median	90% UCL [1]	Unit [2]
Total NOD per soil mass (C_{soil}^{NODtot})	2	28	158	mmol kg^{-1}
Fraction of "fast" NOD (f_{NODf})	0.028	0.126	0.361	-
"slow" NOD rate constant (k_{NODs})	0.003	0.018	0.395	L $mmol^{-1}$ d^{-1}

[1] LCL and UCL = lower and upper confidence limits, respectively
[2] reported as mmol of MnO_4^{-1-} (to obtain mmol O_2eq multiply by O_{2eq} (e.g., 0.5 for H_2O_2)

For generality in performing model calculations, all reactant species are expressed in mol-O_{2eq}. The model may be used to simulate any oxidant species by specification of appropriate stoichiometric coefficients. The reaction sequence solved for each TZ over time is:

- Compute quantity of contaminant releases from DNAPL over current time step. Update mass remaining in DNAPL and dissolved plus equilibrium adsorbed contaminant mass.
- Solve mass balance for oxidant reactions with aqueous and adsorbed contaminant.
- Compute oxidant loss by downgradient outflow and dilution by upgradient inflow.
- If aqueous oxidant mass > 0, compute mass balance for oxidation of NOD_f.
- If aqueous oxidant mass > 0, solve second-order equation for oxidation of NOD_s.
- Update values of F_{mt} and F_k.

Initial contaminant quantities in DNAPL, dissolved and adsorbed phases are obtained from the plume scale transport model. Prior to commencing ISCO, zero oxidant species is assumed to be present in treatment zones. Initial quantities of total, fast and slow NOD are computed as

$$m_{NODtot} = 0.75\, C_{soil}^{NODtot} \rho V_{TZ} \tag{5.9a}$$

$$m_{NODf} = f_{NODf}\, m_{NODtot} \tag{5.9b}$$

$$m_{NODs} = (1 - f_{NODf})\, m_{NODtot} \tag{5.9c}$$

where m_{NODtot}, m_{NODf} and m_{NODs} are total, fast and slow NOD in moles O_2eq, C_{soil}^{NODtot} is the total NOD quantity per soil mass in mol-$KMnO_4$ per kg, ρ is soil bulk density (kg m^{-3}), V_{TZ} is the TZ volume (m^3) and the factor 0.75 is the oxidation potential ratio in mol-O_2eq per mol-$KMnO_4$. The rate equation for slow NOD is

$$\frac{dm_{NODs}}{dt} = -k_{NODs} \frac{m_{OXs} m_{NODs}}{\phi V_0} \tag{5.10}$$

where m_{OXs} is mol-O_2eq of oxidant after fast and slow NOD reactions and k_{NODs} is the second-order rate coefficient. By assuming $m_{OXf} = m_{OXs} = m_{OX}$ in the first time-step, m_{OXs} can be iteratively computed for each time step (dt) using the following relationships

$$m_{OXs} = m_{OXf} + dm_{NODs} \tag{5.11a}$$

$$m_{NODs} = m_{NODs*} + dm_{NODs} \tag{5.11b}$$

where $m_{OXf} = m_{OX} - m_{NODf}$ to consider instantaneous reaction of fast NOD. Variables subscripted with * represent values returned from the previous time step.

As dm_{NODs} is on both sides of (5.10) after replacing m_{OXs} and m_{NODs} with eq. (5.11), an implicit approach was used to find dm_{NODs} assuming its initial value is same as m_{NODs} computed in the

previous time step. The mol-O_{2eq} of oxidant (m_{OX}) at the current time step can be determined by accounting gains and losses as follows.

For pulsed oxidant injection

$$m_{OX} = m_{OX\,0} = \frac{C_{OX\,0} V_{OX}}{k_{OX-O_2eq}} \quad \text{during injection, otherwise}$$

$$m_{OX} = m_{OXs*} - \left(J_{m*} + F_{k*} \frac{m_{OXs*} q A_{vert}}{\phi V_0} \right) dt - m_{CH*}^{aq+s} \tag{5.12a}$$

And for continuous injection

$$m_{OX} = 0 \quad \text{for the first time step, otherwise}$$

$$m_{OX} = m_{OXs*} + F_{k*} \left(m_{OX\,0} - (1 + f_{lost}) \frac{C_{OX*} Q_{OX}}{k_{OX-O_2eq}} \right) dt - m_{CH*}^{aq+s} \tag{5.12b}$$

where $m_{OX\,0}$ is the m_{OX} value during injection, $k_{OX-O_{2eq}}$ is the oxidant mass per mol-O_2eq, C_{OX0} is the concentration of injected oxidant [ML^{-3}], V_{OX} is the volume of injected oxidant computed as $f_v \phi V_0$ using a well overlap factor (f_v) ranging typically between 1.1 and 1.3, J_m is mol-O_{2eq} contaminant flux [mol-$O_{2eq}T^{-1}$] computed from (5.1) with F_{rb}=1 multiplied by n_{O_2eq}, f_{lost} is the fraction of the groundwater flux recovered by extraction wells (0 for pulsed injection, maximum of 1 for recirculation system with complete capture else <1), C_{OX*} is the oxidant concentration in the previous time step [ML^{-3}], Q_{OX} is the oxidant injection rate [L^3T^{-1}], and m_{CH}^{aq+s} is mol-O_{2eq} of contaminant in aqueous + sorbed phases within the treatment zone computed as follows

$$m_{CH}^{aq+s} = \frac{J_{mo} \phi V_o}{q A_{vert}} \quad \text{during injection or for the first time step,}$$

otherwise (5.13)

$$m_{CH}^{aq+s} = m_{CH*}^{aq+s} + \left(J_{m*} - m_{CH*}^{aq+s} \frac{(1 - E_{ISCO}) F_{k*} q A_{vert}}{\phi V_o} \right) dt - m_{OX_*}$$

where q is the average darcy velocity [LT^{-1}], A_{vert} is the vertical area [L^2] of a treatment zone perpendicular to flow, and E_{ISCO} is the fraction of flow though the TZ captured by recovery wells (0 for typical pulsed flow system, max value of 1 for recirculation system). Note that eq. (5.13) accounts for slow rebound of dissolved contaminant concentration following depletion of oxidant in the treatment zone. C_{OX} at the current time step is then obtained as

$$C_{OX} = \left(\frac{m_{OXs} k_{OX-O_2eq}}{V_{OX}} \right) \tag{5.14}$$

and the mol-O_{2eq} DNAPL contaminant in the TZ is computed by

$$m_{CH}^{DNAPL} = m_{CH*}^{DNAPL} - J_{m*}dt$$
$$m_{CH*}^{DNAPL} = \frac{n_{O_2eq} M_{i*}}{W_{CH}} \tag{5.15}$$

where W_{CH} is the contaminant molecular weight [M mol^{-1}].

If the number of injection wells in the treatment zone is N_{IW} but a smaller number of wells N_{block} are injected at a given time, then the number of serial injection events or "splits" to be performed to complete injection in all wells is N_{split} = roundup(N_{iw} / N_{block}). The total duration of each oxidant injection event is

$$\Delta t_{inj} = \frac{V_{OX} N_{split}}{Q_{OX} N_{IW}} \tag{5.16}$$

where Q_{ox} is the average volumetric injection rate per well [L^{3}T^{-1}]. Since the injection duration is generally short compared to the monitoring interval between injections, we treat each injection as an instantaneous event at a time $\Delta t_{inj}/2$ following the actual start of an injection event.

Average chloride concentration in each treatment zone is also computed from the cumulative moles of solvent oxidized and the mole fraction of chloride in the solvent, considering advection losses and dilution.

Mass balance equations for DNAPL contaminant, aqueous and sorbed contaminant, oxidant, chloride, and NOD_f for each treatment zone are solved using forward difference solutions. The NOD_s mass balance equation is solved using an implicit backwards difference method described by eqs. (5.10) - (5.12). Advective losses of aqueous phase oxidant and contaminant are assumed to occur in proportion to the product of the average darcy velocity and current average concentration. DNAPL and NOD are assumed to be immobile.

5.4 ISCO performance monitoring

Our objective here is to formulate performance monitoring protocols to facilitate reliable real-time operational decisions to be made. To minimize decision lags due to travel times to downgradient locations, performance monitoring needs to focus on measurements within or near the aquifer volume being treated. Remediation progress is commonly monitored by measuring contaminant concentrations in soil and/or groundwater samples. But what is the relationship between these two types of measurements to each other and to the downgradient plume? To answer this question, consider a DNAPL source zone of volume V [L^3], with an area A_{vert} perpendicular to flow downgradient of the source [L^2], mean darcy velocity q [LT^{-1}], retardation factor R_{CH}, source dissolution rate versus time $J(t)$ [MT^{-1}], and contaminant mass remaining in the source versus time $M(t)$ [M]. The flow-averaged groundwater concentration C_{avg}^{gw} [ML^{-3}] on the downgradient plane is

$$C_{avg}^{gw}(t) = \frac{J(t)}{qR_{CH}A_{vert}} \tag{5.17a}$$

while the average soil concentration C_{avg}^{soil} [MM^{-1}], within the source volume is

$$C_{avg}^{soil}(t) = \frac{M(t)}{\rho V} \tag{5.17b}$$

where ρ is the soil dry density [ML^{-3}]. Combining eqs. (5.17a) and (5.17b) with eq. (5.1) assuming no effects of oxidant (F_{mt}=F_k=1), yields

$$C_{avg}^{soil} = \frac{M_0}{\rho V}\left(\frac{qR_{CH}A_{vert}C_{avg}^{gw}}{J_0}\right)^{1/\beta} \tag{5.18}$$

which allows us to compute "equivalent" average soil or groundwater concentrations.

A complicating factor for using groundwater concentration data to monitor ISCO performance (and in using eq. 5.18) is that aqueous contaminant concentrations will be negligible as long as dissolved phase permanganate oxidant is present. Following oxidant injection, aqueous phase oxidant will deplete over time due to reactions and advection and aqueous contaminant concentrations will subsequently rebound. However, full rebound can take many months, depending on the DNAPL dissolution rate and groundwater velocity. Therefore, measurements of dissolved contaminant within or near the downgradient edge of a source zone will provide limited information on the progress of remediation until rebound occurs. This will require longer waiting times between oxidant injection events to make termination and reinjection decisions than if soil sample data were used.

Since pre-existing groundwater monitoring wells will generally be present within the ISCO treatment area, which are required to be monitored at a specified interval (e.g., quarterly, semi-annual), we assume that groundwater concentration will be measured at all such wells at the regulatory-mandated intervals. Additional numbers of groundwater monitoring locations may be stipulated strictly for ISCO performance monitoring (i.e., "temporary" wells or push-probe water samples). All groundwater sampling locations will be sampled at no less than the regulatory-mandated frequency. At each groundwater sampling date following oxidant injection, oxidant concentration will be measured until oxidant concentration drops below a practical detection value ($C_{ox\ min}$). Prior to reaching this level, contaminant concentrations will not be measured and afterwards, oxidant concentration will not be monitored until after the next injection event.

In addition to mandated and optional water samples, we also consider collection of soil samples for ISCO performance monitoring. Decision logic soil and groundwater data or groundwater data only are described below.

5.5 Decision logic for ISCO termination and reinjection

The criterion for terminating ISCO treatment is commonly specified as

$$C_{avg}^{type} \le C_{stop}^{type} \tag{5.19}$$

where $C_{avg}^{type} = C_{avg}^{soil}$ [MM^{-1}] or C_{avg}^{gw} [ML^{-3}] represents average soil or groundwater concentrations, respectively, and $C_{stop}^{type} = C_{stop}^{soil}$ or C_{stop}^{gw} represents corresponding termination criterion. In practice, we never know true values of C_{avg}^{type}, but only estimates of the average $C_{avg\ smp}^{type}$ calculated from a

finite number of samples. If we substitute $C_{avg\ smp}^{type}$ for the true average C_{avg}^{type} in eq. (5.19), resulting termination decisions will have a significant probability of erroneously terminating treatment before the target criterion is actually met due to differences between $C_{avg\ smp}^{type}$ and C_{avg}^{type}.

A more conservative approach that explicitly accounts for this uncertainty is to modify the termination criteria as

$$C_{UCL}^{type} \le C_{stop}^{type} \tag{5.20}$$

where C_{UCL}^{type} is the upper confidence limit of the estimated average concentration at significance level α (e.g., 0.1 for a 90% upper confidence limit). Since $C_{UCL}^{type} > C_{avg\ smp}^{type}$ for $0<\alpha<0.5$, eq. (5.20) is a more stringent criterion than eq. (5.19). The ratio of C_{UCL}^{type} and $C_{avg\ smp}^{type}$ represents a safety factor that reduces the likelihood of erroneous decisions that terminate too early. Note that $\alpha=0.5$ corresponds to $C_{UCL}^{type} = C_{avg\ smp}^{type}$.

High variance properties of quantities that are physically constrained to be non-negative, such as contaminant concentrations, necessarily exhibit positively skewed distributions. Normal probability distributions cannot describe such behavior. Lognormal distributions capture the major features of such data and are commonly used as a reasonable and mathematically expedient approximation. If the average concentration is estimated from n_{smp}^{type} samples and a log-normal distribution is assumed, then

$$C_{UCL}^{type} = \exp\left(\ln\left(C_{avg\ smp}^{type}\right) + t_1\left(\alpha, N\right) S_{\ln avg}^{type}\right) \le C_{stop}^{type} \tag{5.21a}$$

where

$$S_{\ln avg}^{type} = \frac{S_{\ln}^{type}}{\sqrt{n_{smp}^{type}}} \tag{5.21b}$$

in which $C_{avg\ smp}^{type}$ is the arithmetic average of n_{smp}^{type} samples, $S_{\ln}^{type}$ is the population standard deviation of ln concentration, $S_{\ln avg}^{type}$ is the standard deviation of $\ln C_{avg\ smp}^{type}$, and $t_1\left(\alpha, N\right)$ is the one-sided *t*-value for significance level α with N degrees of freedom (Snedecor and Cochran 1967). If $S_{\ln}^{type}$ is computed from n_{smp}^{type} samples then $N= n_{smp}^{type} -1$, while if $S_{\ln}^{type}$ is based on prior site characterization data or experience with other sites, then $N=\infty$. Eq. (5.21) may also be written

$$C_{avg\ smp}^{type} \le C_{stop\ SF}^{type} = \frac{C_{stop}^{type}}{\exp\left(t_1\left(\alpha, N\right) S_{\ln avg}^{type}\right)} \tag{5.22}$$

where $C_{stop\ SF}^{type}$ is the "true" stop criterion divided by a safety factor to account for uncertainty. Note that decreasing population uncertainty $S_{\ln}^{type}$ and/or increasing the number of samples n_{smp}^{type} will yield lower C_{UCL}^{type} and higher $C_{stop\ SF}^{type}$ values at a given confidence level, which enable earlier ISCO termination at the specified confidence level. Alternatively, if the same termination criteria (C_{UCL}^{type}

and $C^{type}_{stop\ SF}$) are employed, more reliable data will result in a lower probability of erroneously terminating before actual concentrations meet the desired levels.

As an example, consider a source zone with a cleanup target of C^{soil}_{stop} = 1000 µg/kg. It is planned to take n^{soil}_{smp} =15 soil samples to assess whether the objective has been met. Assume a prior estimate of $S^{soil}_{\ln} = 2.9$. If we want a 95% probability ($\alpha = 0.05$) that the actual average soil concentration will be less than 1000 µg/kg when we terminate treatment, then t_1=1.646 and eq. (5.22) indicates that the average concentration computed from 15 samples needs to be less than $C^{type}_{stop\ SF} = 291$ µg/kg to achieve the desired reliability. If the number of samples is increased to 30, we could terminate earlier with the same decision confidence when $C^{soil}_{avg\ smp} < 418$ µg/kg.

Since the time to reach C^{type}_{stop} or $C^{type}_{stop\ SF}$ will vary spatially, it may be possible to reduce operating costs by applying the foregoing criteria independently to sub-regions to terminate injection earlier in areas that reach cleanup objectives before site-wide termination criteria are met. Alternatively, we could treat less contaminated zones longer to reach a local C^{type}_{stop} that is less than the site-wide value, allowing earlier termination of more contaminated areas when the site-wide criteria is met.

Anticipating that regions with higher initial contaminant concentrations are likely to take longer to cleanup, a system designer may divide a site into multiple treatment zones (TZ) based on ranges of pre-remediation contaminant concentrations observed during site characterization. When independent TZ termination is considered, the criteria for ISCO termination in a single TZ is taken as

$$C^{type}_{avg\ smp\ TZi} \le \frac{C^{type}_{stop\ TZi}}{\exp\left(t_1(\alpha, N) S^{type}_{\ln avg\ TZi}\right)} = C^{type}_{stop\ SF\ TZi} \tag{5.23a}$$

$$S^{type}_{\ln avgTZi} = \frac{S^{type}_{\ln\ TZi}}{\sqrt{n^{soil}_{smp\ TZi}}} \tag{5.23b}$$

where all variables are for TZ *i*. Criteria for simultaneous termination of all currently operating TZs are formulated in a similar fashion, while taking into consideration that site-wide statistical properties can be described by upscaling individual TZ statistics as follows

$$C^{type}_{avg\ smp\ all} = \frac{\sum_{i=1}^{N_{TZ}} V_{TZi} C^{type}_{avg\ TZi}}{\sum_{i=1}^{N_{TZ}} V_{TZi}} \le \frac{C^{type}_{stop\ all}}{\exp\left(t_1(\alpha, N) S^{type}_{\ln avg\ all}\right)} = C^{type}_{stop\ SF\ all} \tag{5.24a}$$

$$S^{type}_{\ln avg\ all} = \frac{\sum_{i=1}^{N_{TZ}} n^{type}_{smp\ TZi}}{\left(\sum_{i=1}^{N_{TZ}} \frac{n^{type}_{smp\ TZi}}{\left(S^{type}_{\ln\ TZi}\right)^2}\right)^{1/2}} \tag{5.24b}$$

where V_{TZi} is the bulk volume of TZ *i*. Note that the stop criterion for individual TZs is permitted to differ from that for site-wide termination, subject to the constraint that $C^{type}_{stop\ TZi} \le C^{type}_{stop\ all}$, i.e., the TZ stop criteria cannot exceed the site-wide stop criteria. When evaluating eq. (5.24) for TZs that have previously terminated operation, the average concentration and number of samples from the last sampling event prior to termination are conservatively assumed to apply.

In addition to determining when oxidant injection can be terminated, a corollary decision must be made regarding if or when reinjection should be initiated must be made. The reinjection criteria for a given TZ is specified as

$$C^{type}_{UCL\ smp\ TZi} > C^{type}_{reinject\ TZi} \tag{5.25}$$

where $C^{type}_{reinject\ TZi}$ is the average concentration above which reinjection is indicated ($C^{type}_{reinject\ TZi} \ge C^{type}_{stop\ TZi}$), and $S^{type}_{\ln\ avg\ TZi}$ is defined by eq. (5.23b). Due to the inconvenience and cost of commencing injection in TZs at different times, reinjection is not initiated until criterion for either reinjection or termination has been met for all TZs.

The time interval Δt^{gw}_{mon} between potential groundwater sampling events for ISCO monitoring is assumed to be equal to or an integer fraction (e.g., 1, 1/2, 1/3) of the regulatory mandated interval. Following an oxidant injection event, oxidant concentration will be monitored prior to taking samples for contaminant analysis. If the oxidant concentration exceeds its detection limit for the method utilized ($C_{ox\ min}$), samples for contaminant analysis are not taken, as values would not be meaningful. Subsequently, average contaminant concentrations from groundwater samples are not deemed to represent full rebound conditions until the current average value is less than or equal to the previous value for the TZ or site-wide depending on the level for which the termination decision is to be made. A minimum number of groundwater sampling rounds N^{gw}_{min} is stipulated before a termination decision is allowed, where N^{gw}_{min} is at least 2. If Δt^{gw}_{mon} is very short and/or rebound is very slow, larger N^{gw}_{min} values may be necessary to avoid erroneous early termination due to multiple rounds below detection limits prior to exhibiting rebound. The minimum number of sampling rounds is not applicable for making reinjection decisions.

To coordinate soil monitoring (when utilized) with groundwater monitoring, the period between soil sampling events Δt^{soil}_{mon} is constrained to be an integer fraction or multiple (notated as $F_{soil/gw}$) of Δt^{gw}_{mon} (e.g., 1/3, 1/2, 1, 2, 3). Since rebound is not an issue with soil data, termination or reinjection decisions do not require a minimum number of soil sampling rounds. Operational decisions may be based on groundwater data only, soil data only, or on statistically-pooled soil and groundwater data (Appendix B) for the site as a whole or for individual TZs at the specified confidence level α. However, to maintain site-wide coordination of injection events, reinjection in individual TZs is not implemented until all TZs have met either reinjection or termination criteria following each injection event. A flowchart of the performance monitoring and decision-making protocol given in Figure 5.1.

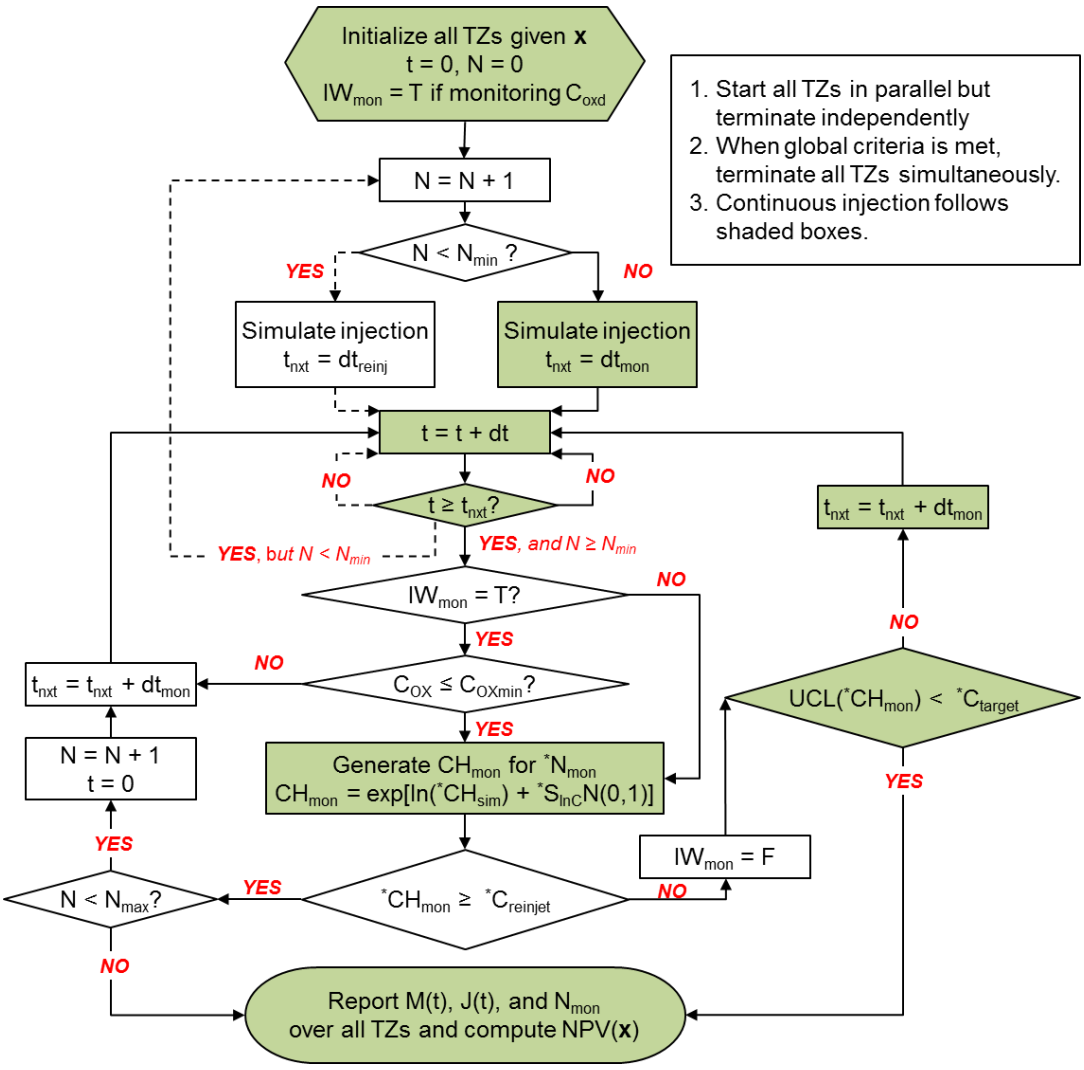

Figure 5.1. Flowchart for ISCO operational decisions.

5.6 Statistical criteria for pooled data

In the previous section, decision criteria were formulated based on a single type of monitoring data (e.g. water samples from monitoring wells or geoprobes, soil samples from borings or geoprobes composited over specified core lengths). To pool multiple types of soil and/or groundwater data with different measurement uncertainties, all measurements must first be converted to a consistent basis as a soil or groundwater concentration via eq. (5.18). In the following, we assume all values are converted to "equivalent" soil concentrations in this manner.

To pool across different measurement types, we weight average values inversely proportional to their variances (Kool et al. 1987) and compute the pooled standard deviation is the weighted root mean square, yielding the following criteria for TZ termination:

$$C_{avgTZi}^{pool} \le C_{stop\ SF\ TZi}^{pool} = \frac{C_{stop\ TZi}^{pool}}{\exp\left(t\left(\alpha,\infty\right)S_{\ln TZi}^{pool}\right)} \tag{5.26a}$$

$$\ln C_{avgTZi}^{pool} = \sum_{type=1}^{N_{type}} w_{TZi}^{type} \ln C_{avgTZi}^{type} \tag{5.26b}$$

$$S_{\ln\ TZi}^{pool} = \left(\frac{1}{N_{type}} \sum_{type=1}^{N_{type}} \frac{w_{TZi}^{type}\left(S_{\ln TZi}^{type}\right)^2}{n_{TZi}^{type}} \right)^{1/2} = \left(\sum_{type=1}^{N_{type}} \frac{n_{TZi}^{type}}{\left(S_{\ln TZi}^{type}\right)^2} \right)^{-1/2} \tag{5.26c}$$

$$w_{TZi}^{type} = \frac{\dfrac{n_{TZi}^{type}}{\left(S_{\ln TZi}^{type}\right)^2}}{\displaystyle\sum_{k=1}^{N_{type}} \frac{n_{TZi}^{k}}{\left(S_{\ln TZi}^{k}\right)^2}} \tag{5.26d}$$

where $C_{stop\ SF\ TZi}^{pool}$ is the "true" stop criteria $C_{stop\ TZi}^{pool}$ divided by a safety factor to account for uncertainty, N_{type} is the number of different sample types (e.g., water samples from monitoring wells, soil or water samples from geoprobes, etc.) with ln standard deviations for individual measurements $S_{\ln TZi}^{type}$ and arithmetic average soil concentrations $C_{avg\ TZi}^{type}$ (or average groundwater concentrations expressed in "equivalent" soil concentrations) for each type in TZ *i*, $S_{\ln\ TZi}^{pool}$ is the uncertainty of pooled data that was weighted by the uncertainty ($S_{\ln TZi}^{type}$) of each data type in TZ *i*, and n_{TZi}^{type} is the number of samples taken in TZ *i* of specified type. Values of $S_{\ln\ TZi}^{type}$ may be estimated using data from samples within individual treatment zones collected during source characterization as the standard deviation of ln measured concentrations. In rough terms, if about 2/3 of measurements (±1 standard deviation) in a TZ are within range of *F = upper limit/lower limit* then $S_{\ln\ TZ}^{soil} \approx \ln(F)/2$.

The pooled site-wide termination criteria may be obtained by upscaling TZ statistics as

$$C_{avg\ all}^{pool} \le C_{stop\ SF\ all}^{pool} = \frac{C_{stop\ all}^{pool}}{\exp\left(t\left(\alpha,\infty\right)S_{\ln all}^{pool}\right)} \tag{5.27a}$$

$$C_{avg\ all}^{pool} = \frac{\sum_{i=1}^{N_{TZ}} V_{TZi} C_{avg\ TZi}^{pool}}{\sum_{i=1}^{N_{TZ}} V_{TZi}} \tag{5.27b}$$

$$S_{\ln\ all}^{pool} = \left(\sum_{i=1}^{N_{TZ}} \left(S_{\ln TZi}^{pool} \right)^{-2} \right)^{-1/2} \tag{5.27c}$$

where $C_{stop\ SF\ all}^{pool}$ is the "true" stop criteria $C_{stop\ all}^{pool}$ divided by a safety factor to account for uncertainty, N_{type} is the number of different sample types (e.g., water samples from monitoring wells, soil or water samples from geoprobes, etc.) with ln standard deviations $S_{\ln TZi}^{type}$ per individual measurement and arithmetic average soil or groundwater concentrations C_{avg}^{type} expressed as "equivalent" soil concentrations for each type of measurement in TZ *i*, and $S_{\ln\ all}^{pool}$ is the site-wide uncertainty of pooled data that was weighted by the pooled uncertainty ($S_{\ln TZi}^{pool}$) of each TZ *i*.

An Excel spreadsheet, ***ISCO treatment termination decisions using real time data.xlsx***, is provided to enable site personnel to make real-time termination decisions from performance monitoring data based on the foregoing decision logic (Appendix A).

5.7 ISCO cost model and design variables

ISCO costs are computed for each forward simulation (i.e., Monte Carlo realizations) of ISCO performance. Since ISCO applications are typically conducted over relatively short time periods, costs are discounted for the time difference between the average julian date while the system was operating to the discounting reference date, rather than discounting for each in operation. The ISCO cost model is formulated as follows:

$$\begin{aligned} \$_{NPV} = \Big(& \$_{base} + M_{ox}\$_{mass} + V_{ox}\$_{vol} + \Delta t_{ISCO}\$_{time} + N_{MWnew}\$_{MWnew} \\ & + I_{pulse} N_{inj}\$_{inj\ mob} + N_{OXsmp}\$_{OXsmp} + N_{mon\ mob}\$_{mon\ mob} \\ & + \sum_{type=1}^{N_{type}} \$_{smp}^{type} \Big) (1-d)^{(t_{start} + 0.5\Delta t_{ISCO} - t_{ref})} \end{aligned} \tag{5.28a}$$

$$\$_{smp}^{type} = \left(\$_{smp0}^{type} + \$_{smp1}^{type} \max\left(0, N_{smp/loc} - 1\right) \right) \sum_{i=1}^{N_{mon}} \sum_{j=1}^{N_{TZ}} I_{active\ ij} N_{loc/TZ\ j} \tag{5.28b}$$

where *type* denotes the options for monitoring soil and groundwater concentrations in TZs which are soil concentration from soil borings (SB_{soil}) or geoprobe samples (GP_{soil}), groundwater concentrations from monitoring wells (MW_{gw}) or geoprobe samples (GP_{gw}), or measurements of both soil and groundwater from geoprobe samples taken from the same hole at the same sampling event ($GP_{soil+gw}$). Descriptions of variables in the cost function are summarized below.

$\$_{NPV}$ total net present value ISCO cost ($K),
$\$_{base}$ base fixed cost excluding other itemized cost variables ($K),

N_{MWnew} *t*otal number of new (not pre-existing) monitoring wells,
$\$_{MWnew}$ installation and decommissioning cost per monitoring well ($K/well),
M_{ox} cumulative mass of oxidant injected - internally computed (kg),
$\$_{mass}$ cost per unit oxidant mass utilized ($K/kg),
V_{ox} cumulative fluid volume injected - internally computed (m^3),
$\$_{vol}$ cost per volume of injected fluid excluding $\$_{mass}$ ($K/$m^3$),
I_{pulse} indicator for pulse injection (1 if true else 0),
N_{inj} total number of injection events - internally computed,
$\$_{inj\ mob}$ mobilization cost for each injection event ($K/injection event),
Δt_{ISCO} total duration of the ISCO operation - internally computed (days),
$\$_{time}$ cost per unit time for project management, reporting, etc. ($/day),
N_{OXsmp} total number of oxidant measurements ($K)
$\$_{OXsmp}$ cost per oxidant measurement ($K)
$N_{mon\ mob}$ total number of performance monitoring events - internally computed,
$\$_{mon\ mob}$ mobilization cost for each performance monitoring event ($K/event),
d annualized discount rate (yr^{-1})
t_{start} ISCO system start date (Julian yrs),
t_{ref} reference date for present value discounting (julian yrs),
N_{TZ} number of treatment zones
$I_{active\ ij}$ indicator = 1 if TZ *j* active during sampling event *i* else 0 (internally computed)
$N_{loc/TZ\ j}$ number of holes sampled per sampling event in TZ *j* (user input or optimized)
$N_{smp/loc}$ number of depths sampled per hole per event (user input or optimized)
$\$^{type}_{smp0}$ cost to collect, analyze, etc first sample depth for data of *type* ($/sample)
$\$^{type}_{smp1}$ cost to collect, analyze, etc each additional sample depth at same time ($/sample)

Note that $\$^{type}_{smp1}$ is relevant only if $N_{smp/loc} > 1$ and is applicable to soil borings, geoprobe data or multilevel monitoring wells, but not to conventional monitoring wells. For each data type, there will be a tradeoff between the sampling cost and uncertainty in average concentrations computed from the data and hence on treatment duration and the likelihood of mistakenly terminating treatment too early resulting in failure to achieve the expected source discharge reduction. Injection and monitoring events are assumed to be synchronized across treatment zones to minimize mobilization costs.

Estimation of unit cost parameters in eq. (5.28) should be performed by or in cooperation with an ISCO design engineer. The number and locations of injection wells, and extraction wells if required, will be generally be determined based on hydraulic modeling. The design engineer should be able to directly estimate all unit cost parameters for terms beyond the third term in eq. (5.28), i.e., $\$_{time}$, $\$_{MWnew}$, $\$_{inj\ mob}$, $\$_{mon\ mob}$, and unit sampling costs. To estimate the remaining three cost variables $\$_{base}$, $\$_{mass}$ and $\$_{vol}$, the following cost sensitivity calculations should be performed.

(1) Compute cost for single pulsed injection of specified volume or for injection for a fixed duration for a continuous injection-recirculation system with an assumed oxidant injection concentration.

(2) Compute cost for same conditions as (1) but for two pulsed injections or double the injection duration for continuous injection.

(3) Compute cost for same conditions as (1) but double the injected oxidant concentration.

All of the above cost calculations must exclude all monitoring and other costs in terms beyond the first three in eq. (5.28). The cost, total injection fluid volume and total injected oxidant mass for the three cases should be tabulated and a regression performed to a three-term truncated form of eq. (5.29) to determine $\$_{base}$, $\$_{mass}$ and $\$_{vol}$.

Spreadsheets are available to determine ISCO unit costs from the foregoing cost sensitivity protocol for pulsed and continuous injection: ***ISCO unit cost calcs for pulsed injection.xlsx*** and ***ISCO unit cost calcs for continuous injection. xlsx*** (Appendix A).

In addition to unit cost parameters, measurement uncertainty must be characterized for each sample type at local and global scales. Sample types considered for ISCO and designations of their local and global standard deviations are

- Soil concentrations from conventional soil borings ($S_{\ln local}^{SBsoil}$ and $S_{\ln global}^{SBsoil}$)
- Groundwater samples from monitoring wells ($S_{\ln local}^{MWgw}$ and $S_{\ln global}^{MWgw}$)
- Soil concentrations from geoprobe samples ($S_{\ln local}^{GPsoil}$ and $S_{\ln global}^{GPsoil}$)
- Groundwater concentrations from geoprobe samples ($S_{\ln local}^{GPgw}$ and $S_{\ln global}^{GPgw}$)
- Soil and groundwater collected concurrently with geoprobe ($S_{\ln local}^{GPsoil+gw}$ and $S_{\ln global}^{GPsoil+gw}$).

Values for the first four data types, $S_{\ln local}^{type}$ and $S_{\ln global}^{type}$ are direct user inputs, which may be quantified by analyzing pre-remediation source characterization data as

$$S_{\ln\ local}^{type} = \frac{1}{N_{TZ}} \sum_{i=1}^{N_{TZ}} STDEV\left(\ln C_{TZi}^{type}\right) \tag{5.29a}$$

$$S_{\ln\ global}^{\text{type}} = \text{STDEV}\left(\ln C_{all}^{type}\right) \tag{5.29b}$$

where STDEV is a standard deviation operator, C_{TZi}^{type} denotes data of the specified *type* within TZ*i*, and C_{all}^{type} denotes combined data of the same type from all TZs.

- Oxidant concentration in injected fluid per TZ, C_{ox0}
- Target average groundwater or soil concentration for TZ termination, $C_{stop\ TZi}^{type}$
- Average groundwater or soil concentration above which reinjection begins, $C_{reinject}^{type}$
- Number of sampling locations and depths per TZ for each data type
- Time intervals between groundwater and soil sampling events $F_{soil/gw}$, $\Delta t_{mon}^{soil} / \Delta t_{mon}^{gw}$, and
- Minimum number of groundwater sampling rounds following injection before termination or reinjection decision can be made, N_{min}^{gw}.

Our objective is to identify operational and monitoring strategies to minimize total expected (i.e., probability-weighted) cost to reliably achieve cleanup objectives.

5.8 Example applications

5.8.1 Example 1 - Sensitivity to aquifer parameters

Several simulations are investigated to evaluate sensitivity of ISCO performance to various aquifer parameters. All simulations consider a PCE DNAPL source with a single treatment zone having a plan view area of 1,125 m^2 and a thickness of 5.5 m yielding a total treatment volume of 6,188 m^3. The TZ width perpendicular to flow is 75 m resulting in a vertical plane area of 413 m^2. Base case site parameters are summarized in Table 5.3. A source zone remediation target of C_{stop}^{gw} =100 μg/L is used, which is assumed to yield concentrations below regulatory standards at downgradient receptors. This level corresponds to C_{stop}^{soil} = 26 μg/kg via eq. (5.18). A total of 18 injection wells is used with oxidant solution injected at 16.35 m^3/d (3 gallons per minute) in each well until about 1.25 pore volumes of oxidant solution is injected per well to ensure overlapping injection zones. Since there is only a single TZ, all injection wells are utilized during each reinjection event until the cleanup criteria is met. For all simulations in Example 1, average groundwater concentration in each TZ was determined quarterly (i.e., Δt_{mon}^{gw} = 90 days) with a minimum of two monitoring events (N_{min}^{gw} = 2). Groundwater sampling commences after the oxidant concentration drops below $C_{ox\,min}$ of 50 mg/L and continues until C_{avg}^{gw} exceeds 200 μg/L, in which case oxidant reinjection is performed, or until C_{avg}^{gw} is less than or equal to C_{stop}^{gw} and the previous sampling round C_{avg}^{gw}.

Deterministic simulations were performed to evaluate the effect of groundwater velocity and injected oxidant concentration for the following cases:

(a) q = 0.008 m/d and C_{ox0} = 5 g/L,
(b) q = 0.008 m/d and C_{ox0} = 25 g/L,
(c) q = 0.08 m/d and C_{ox0} = 5 g/L,
(d) q = 0.08 m/d and C_{ox0} = 25 g/L.

Table 5.3 Base case model parameters for example problems.

Parameter	Best Estimate	Log uncertainty (S_{ln})
Initial source mass, M_o	100 kg	0.2
Initial dissolution rate, J_o	0.1 kg/d	0.1
Depletion coefficient, β	0.75	0.1
Groundwater velocity, q	0.008 m/d	0.05
Porosity, ϕ	0.3	-
Bulk density, ρ_b	1855 kg/m^3	-
Total NOD concentration, C_{soil}^{NODtot}	2.0 g/kg	0.3
Fast NOD fraction, f_{NODf}	0.15	0.3
NOD rate coefficient, k_{NODs}	0.02 L/mmol MnO_4^{-1}/day	0.3

Average concentrations versus time were computed for oxidant, "observed" (i.e., nonequilibrium) and asymptotic (equilibrium rebound) dissolved PCE, and soil PCE. These are shown in Figure 5.2 without consideration of pore clogging as relative concentrations computed as $C_{ox}(t)/ C_{ox0}$ for oxidant and as $\left(C_{avg}^{type}(t) - C_{stop}^{type}\right) / \left(C_{avg}^{type}(t_0) - C_{stop}^{type}\right)$ for soil and groundwater contaminant concentrations, where t_0 is the time immediately prior to ISCO such that $C_{avg}^{soil}(t_0)$ is 9000 μg/kg and $C_{avg}^{gw}(t_0)$ is 7000 μg/L for Cases (a) and (b) and 700 μg/L for Cases (c) and (d).

Time series curves for Case (a) indicate that soil and groundwater concentrations met the remediation objectives in about 16 months following three oxidant injections (open circle in Figure 5.2a). However, because high oxidant concentrations persisted in the treatment zone much longer due to the low velocity, the groundwater monitoring protocol was unable to confirm completion until month 41. Comparison of equilibrium and nonequilibrium groundwater contaminant concentrations (solid and dashed blue lines) reveals about 10% of full rebound is reached in 3 months following the first injection. For the second injection about the same percent rebound was not reached until 9 months after injection. This is expected, because rebound rate will diminish as source dissolution rate decreases with DNAPL mass. This phenomenon will contribute to the delay between actually reaching the remediation objective and confirmation by groundwater monitoring. The higher oxidant concentration for Case (b) is predicted to reduce the time to reach the cleanup objective more than 50% to about 7 months with only a single oxidant injection (Figure 5.2b), although the groundwater monitoring protocol does not confirm termination until 30 months, again due largely to slow flushing of excess oxidant from the TZ.

Case (c) with a high velocity and low oxidant concentration (Figure 5.2c) exhibits more robust rebound than Case (a), with about 85% rebound in 3 months for the first injection and 17% in 3 months for the second injection – about 8 times faster than Case (a). The faster rebound allows the third injection to be implemented sooner than for Case (a) resulting in actual attainment of the cleanup goal in only 12 months. However, the monitoring protocol triggered a fourth injection shortly before this, which extended the duration of monitoring to about 21 months. Due to more rapid flushing of excess oxidant at the higher velocity, the extended monitoring period was much shorter than for Cases (a) and (b). Enhanced mass transfer rates associated with a higher oxidant concentration for Case (d) sharply accelerated remediation with actual attainment occurring in less than 2 months with confirmation from groundwater monitoring in 9 months (Figure 5.2d).

The foregoing simulations were repeated with pore clogging. The mass transfer inhibition factor (F_k) in eq. (5.3), representing pore clogging effects, was computed to range from 0.96 (slow flow) to 0.97 (fast flow), indicating that mass transfer was minimally affected. Remediation duration did not increase by more than 2 days for any of the cases. These observations agree with results of Huling and Pivetz (2006) and West and Kueper (2012).

It should be noted that our results are based on a value for S_{rind} in eq. (5.3) of -4.6 x 10^{-6} L/mg reported by West et al. (2007) for a test column. However, the value of S_{rind} is likely to vary for different aquifer materials, so pore clogging effects may be larger or smaller than indicated by the simulations if S_{rind} exhibits substantial variability. Localized pore clogging effects have been reported in DNAPL zones and near well screens at field sites (Reitsma and Randhawa 2002). If pore clogging is a concern, it would be advisable to calibrate S_{rind} from laboratory or field pilot test data.

Another geochemical factor that can affect the availability of oxidant during ISCO is the rate constant for NOD oxidation (eq. 5.10). Table 5.4 presents remediation times and numbers of injection events for simulations with different groundwater velocities and NOD rate constants (k_{NODs}) with C_{ox0} = 5 g/L. The range of k_{NODs} values is based on Yan and Schwartz (2000) and Waldemer and Tratnyek (2006).

Table 5.4 Time in months to attain an aqueous PCE concentration less than 100 μg/L for Example 1 with various NOD rate coefficients (k_{NODs}) and groundwater velocities with C_{ox0} = 5 g/L. Values in parentheses indicate the number of injection events.

Darcy velocity	k_{NODs}, L/mmol MnO_4^{-1}/day		
	0.002	0.02	0.2
0.008 m/d	30.48 (3)	16.27 (3)	12.16 (3)
0.08 m/d	9.93 (3)	11.90 (4)	11.93 (4)

NOD rate exerts a greater effect on remediation period than pore clogging especially at lower oxidant injection concentrations for the cases simulated. The NOD rate coefficient and groundwater velocity have a complex effect on remediation duration. At low groundwater velocities, advective oxidant loss is slow and higher NOD rates allow NOD to be depleted more quickly so contaminant oxidation can proceed. However, at high groundwater velocities, oxidant losses due to flushing become predominant and higher NOD rates scavenge more oxidant before it is flushed from the TZ leaving less for contaminant oxidation, increasing remediation duration.

The above simulations considered the use of groundwater sampling only to make reinjection and termination decisions. We now reconsider Case (a) using soil and groundwater samples, which are assumed to be taken on the same schedule. Comparing the results of Case (a) with groundwater data only (Figure 5.2a) with that for soil and groundwater data (Figure 5.3) indicate that the second oxidant injection is initiated at the same time (3 months-after-start) for both cases. However, soil monitoring triggers the third and final injection only 3 months later (6 months-after-start), while using the groundwater data only delayed the third injection to 12 months after start.

Actual concentrations met cleanup criteria 16 months-after-start with groundwater data only, but only 11.5 months-after-start with soil data. Monitoring was required to continue to only 12 months-after-start with soil data, but 41 months-after-start with groundwater data only due to slow attenuation of oxidant concentrations. Cost savings may or may not result depending on the savings from less groundwater sampling versus additional costs for soil sampling. However, in circumstance where remediation duration is important, soil data should be strongly considered.

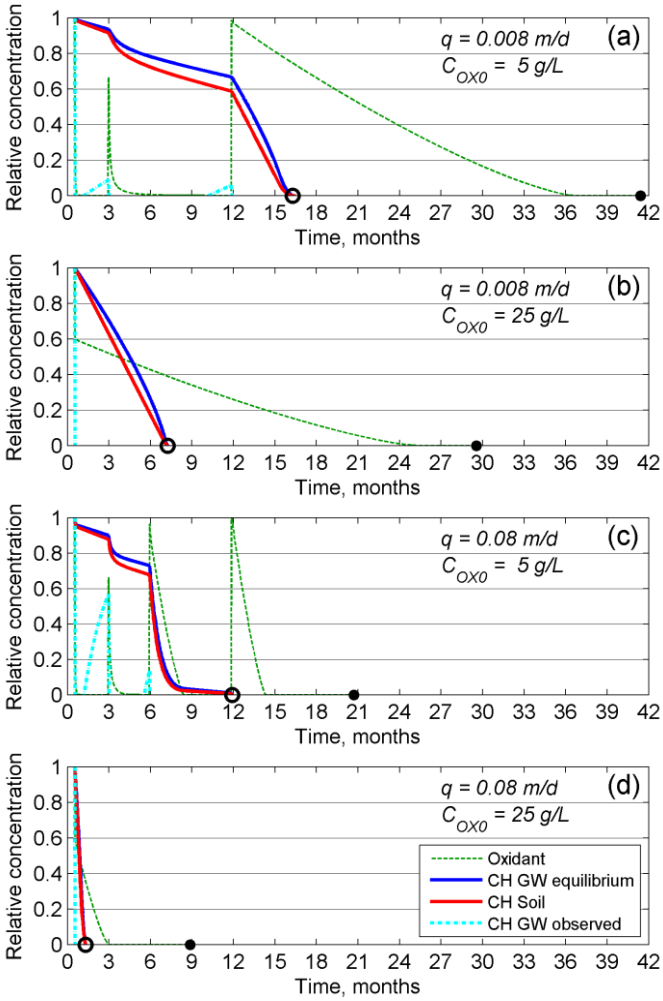

Figure 5.2. Example 1 results with groundwater monitoring only and no pore clogging for (a) q = 0.008 m/d with 5 g/L oxidant, (b) q = 0.008 m/d with 25 g/L oxidant, (c) q = 0.08 m/d fast flow with 5 g/L oxidant, and (d) q = 0.08 m/d conditions with 25 g/L oxidant. Empty circle (○) indicates the time when groundwater concentration is less than C^{gw}_{stopTZ} =100 µg/L and solid circle (●) indicates the termination time based on the monitoring protocol.

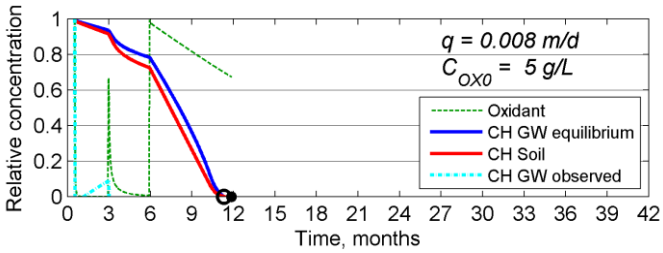

Figure 5.3. Results for Figure 5.2a except using soil and groundwater monitoring data. Empty circle (○) indicates the time when groundwater concentration is less than C^{gw}_{stopTZ} =100 µg/L (equivalent corresponding $C^{soil}_{stop\ all}$ = 26 µg/kg) and solid circle (●) indicates the termination time based on monitoring protocol.

5.8.2 Example 2 – Monte Carlo simulations and stochastic optimization

In this series of problems, we evaluate effects of selected design variables and design approaches on ISCO performance and cost. Performance and cost uncertainty is represented by 100 Monte Carlo realizations of site parameters generated using log-normal distributions based on best estimates (taken as the geometric mean) and ln standard deviations (Table 5.2). Measurement uncertainty (S_{ln}) for individual groundwater samples was assumed to be 0.5 and the corresponding value for soil samples, when taken, was 1.15. These values were used to simulate "noisy" soil and groundwater performance monitoring data. For all cases, groundwater samples were assumed to be taken quarterly (Δt_{mon}^{gw} =90 d) from existing compliance monitoring wells (4 per TZ). Following each oxidant injection, oxidant concentration was determined on the quarterly schedule. Contaminant samples were not collected until the oxidant concentration dropped below $C_{ox\ min}$ taken to be 50 mg/L for all cases. Soil sampling and additional groundwater sampling were considered for selected cases.

Three potential TZs, A, B and C from most to least contaminated, were identified from site characterization data (Table 5.5 and Figure 5.4). For unoptimized cases, ISCO treatment was terminated independently for each TZ with termination criteria $C_{stop\ TZ}^{gw}$ =100 μg/L. For optimized cases, site-wide termination was also considered with $C_{stop\ all}^{gw}$ =100 μg/L (independent of contaminant distribution among TZs). Individual TZ termination was allowed with optimized values of $C_{stop\ TZ}^{gw}$ constrained to be $\leq$100 μg/L. For cases with soil sampling, the corresponding C_{stop}^{soil} value was computed from eq. (5.18). The C_{stop}^{soil} value corresponding to best estimates of model parameters is 26 μg/kg. Note, however, that C_{stop}^{soil} will vary for each Monte Carlo realization depending on stochastic values for source parameters and groundwater velocity (eq. 5.18). The oxidant reinjection criterion $C_{reinject}^{gw}$ was taken as 200 μg/L for unoptimized cases and was optimized for other cases. The concentrations of injected oxidant C_{ox0} were assumed to be 10 g/L for all TZs for unoptimized cases, but were optimized for the optimized cases. Assumed unit costs for all simulations are summarized in Table 5.6.

Table 5.5 Treatment zones and initial PCE concentrations for Example 2.

TZ	Area (m^2)	Width (m)	Thickness (m)	Soil concentration (mg/kg)
A	200	25	5.5	10-100
B	460	60	5.5	1-10
C	465	75	5.5	0.1-1
all	1125	75	5.5	0.1-100

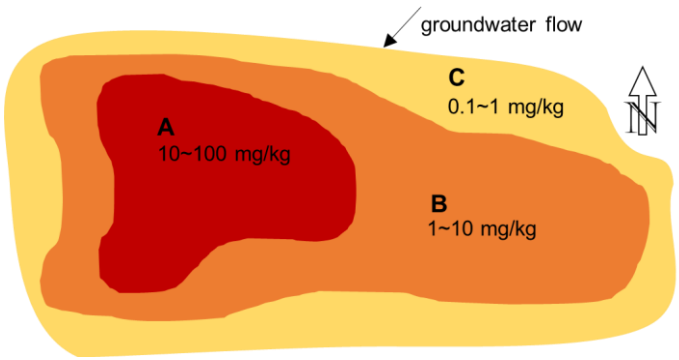

Figure 5.4. Configuration of treatment zones for Example 2.

Table 5.6 Unit costs for Example 2.

Parameter	Unit cost		Parameter	Unit cost	
$\$_{base}$	108.16	\$k	$\$_{smp\,0}^{GPsoil}$	0.90	\$k/sample
$\$_{mass}$	0.0055	\$k/kg	$\$_{smp\,1}^{GPsoil}$	0.30	\$k/sample
$\$_{vol}$	0.02076	\$k/ m^3	$\$_{OXsmp}$	0.10	\$k/event/TZ
$\$_{time}$	0.30	\$k/day	$\$_{penalty}$	10^6	\$k/failure

A total of 8 cases was investigated with 4 unoptimized Monte Carlo simulations (NoOpt1-NoOpt4) and 4 stochastic optimization cases (Opt1-Opt4). Design variables for NoOpt1 were selected to be representative of typical engineering practice for ISCO sites. NoOpt2, NoOpt3, and NoOpt4 investigate the use of more stringent criteria for making termination decisions. Opt1 – Opt 4 investigate the effects of stochastic optimization of ISCO design parameters with or without risk-adjusted termination criteria and with or without employing soil concentration data to condition operational decisions.

A summary of design variables that were fixed (bold values) or optimized (underlined) and of performance metrics (normal text) for each scenario is given in Table 5.7. The expected (probability-weighted) net present value (ENPV) cost, probability of average groundwater concentration failing to meet the target value, failure-adjusted ENPV cost, expected average groundwater concentration, expected treatment duration, expected total volume of oxidant solution, and expected total mass of injected $KMnO_4$ are also summarized in Table 5.6. ENPV cost is the probability-weighted total cost excluding penalty costs. Also tabulated is an adjusted ENPV cost, which is the ENPV cost divided by the probability of successful completion (=1–failure probability). The latter is a normalized measure of cost to compare design alternatives with the probability of failure taken into account. Probability distributions of NPV cost excluding penalty costs are illustrated in Figure 5.5 for all NoOpt and Opt cases.

Table 5.7 Results for Example 2 unoptimized design (NoOpt1 – NoOpt4) and stochastic optimization scenarios (Opt1 – Opt4).

Case		NoOpt1	NoOpt2	NoOpt3	NoOpt4	Opt1	Opt2	Opt3	Opt4
ENPV ($k)		1034	1062	1035	1066	955	959	952	957
Adjusted ENPV ($k) [1]		1077	1073	1067	1066	955	959	952	957
Failure probability (%)		4	1	3	< 1	< 1	< 1	< 1	< 1
Expected C_{gw} (μg/L)		50	2	49	1	6	5	11	4
Expected duration (yrs)		4.20	4.29	4.16	4.29	3.93	3.89	4.07	4.20
Expected oxidant vol (m^3)		5260	5344	5335	5410	4293	4680	3952	3845
Expected oxidant mass (kg)		52.6	53.4	53.3	54.1	46.2	46.1	47.6	48.0
Expected number of injection events	TZ_A	4.7	4.8	4.8	4.9	4.5	4.6	3.7	3.5
	TZ_B	1.9	1.9	1.9	1.9	1.4	1.6	1.3	1.4
	TZ_C	1.6	1.6	1.7	1.7	1.2	1.3	1.3	1.1
Number of monitoring wells per TZ	TZ_A	**4**	**4**	**4**	**4**	4	4	4	4
	TZ_B	**4**	**4**	**4**	**4**	4	4	4	4
	TZ_C	**4**	**4**	**4**	**4**	4	4	4	4
Number of soil borings per TZ	TZ_A	**0**	**0**	**0**	**0**	**0**	**0**	0	0
	TZ_B	**0**	**0**	**0**	**0**	**0**	**0**	1	1
	TZ_C	**0**	**0**	**0**	**0**	**0**	**0**	2	1
Soil samples per boring		**0**	**0**	**0**	**0**	**0**	**0**	1	2
Min. sampling events		**2**	**3**	**2**	**3**	**2**	**2**	**2**	**2**
Soil sampling frequency ($F_{soil/gw}$)		**0**	**0**	**0**	**0**	**0**	**0**	3	3
Significance level, α		**0.50**	**0.50**	**0.05**	**0.05**	**0.50**	**0.05**	**0.50**	**0.05**
$C^{gw}_{stop\ TZ}$ (μg/L)		**100**	**100**	**100**	**100**	95	25	47	94
$C^{gw}_{reinject}$ (μg/L)		**200**	**200**	**200**	**200**	306	269	344	339
C_{ox0} (g/L)	TZ_A	**10.0**	**10.0**	**10.0**	**10.0**	7.0	6.4	9.2	8.4
	TZ_B	**10.0**	**10.0**	**10.0**	**10.0**	13.2	11.6	15.5	14.5
	TZ_C	**10.0**	**10.0**	**10.0**	**10.0**	14.1	13.0	12.2	15.5

[1] Adjusted ENPV = no penalty ENPV / (1-Failure probability/100).
Bold = fixed variables, underlined = optimized variables, others = computed results

NoOpt1 Results. We regard NoOpt1 as a reasonable approximation of current "best engineering practice." The termination criteria compares average groundwater concentrations to the cleanup target without adjustment for measurement uncertainty using the significance level $\alpha = 0.5$ using data from 12 existing monitoring wells (4 in each TZ). Reinjection and termination decisisions are made indepdndently for each of the three TZs. A minimum of two sampling rounds after each injection is stipulated before a termination or reinjection decision can be made. Termination decisions require that the UCL of current TZ average concentration is less than the stop criteria

and less than or equal to the average for the previous sampling date. Termination decisions are allowed after a minimum of two sampling rounds N_{min}^{gw} after each injection.

NoOpt1 had a 4% failure probability (i.e., probability of $C_{avg\ all}^{gw}$ > 100 μg/L) with an ENPV cost of $1,034k and an adjusted ENPV cost of $1,077k. Inspection of the 4 NoOpt1 Monte Carlo realizations that failed to meet actual remediation criteria (based on "true" noise-free simulations) indicated that three of the four failures occurred because observed aqueous concentrations in one TZ remained at non-detect for the required minimium of two quarterly sampling events, thus triggering ISCO termination for that TZ. However, the actual full rebound concentration was much above the cleanup target. The erroneous early terminations were thus attributable to slow rebound.

NoOpt2 Results. This case is identical to NoOpt1, except that the minimum number of sampling rounds following each injection event was increased from 2 to 3 to avoid erroneous early termination decisions noted in NoOpt1. Increasing the minimum number of sampling rounds eliminated the three erroneous early termination decisions associated with slow rebound in the NoOpt1 case, leaving only 1 noncompliant realization (1% failure probability). The reduced failure probability comes at the expense of an increase in the ENPV cost to $1,062k with a slightly lower adjusted ENPV cost of $1,073k.

NoOpt3 and NoOpt4 Results. These two cases are identical to NoOpt1 and NoOpt2, respectively, except that a significance level α of 0.05 was used rather than 0.5 – i.e., the 95% UCL of average measured concentration rather than the average itself was compared with the target level to make termination decisions. NoOpt3 with a minimum of 2 sampling rounds has a 3% failure, which corresponds to the three Monte Carlo realizations that failed in NoOpt1 due to slow rebound. Using the lower α value of 0.05 in NoOpt3 eliminated the single NoOpt2 failure case, which was attributable to average measured concentrations substantially less than actual averages because of measurement "noise." NoOpt4, with a minimum of three sampling rounds, has a failure probability <1% (i.e., less than the resolution of 100 Monte Carlo realizations). Using a higher minimum number of sampling events for NoOpt4 eliminated the remaining failure realizations associated with slow rebound. The ENPV and adjusted ENPV costs for NoOpt4 were $1,066k.

Opt1 and Opt2 Results. These simulations optimize the number of groundwater monitoring wells from a minimum of 4 in each TZ (currently available compliance wells) to a maximum of 10 in each TZ. Quarterly sampling is assumed. No soil sampling is considered. A fixed value of two is specified for the minimum number of groundwater sampling rounds following each injection before termination or reinjection decisions can be made. Fixed values of α = 0.5 for Opt1 and α = 0.05 for Opt2 are assumed. Additional optimized variables for these cases are injected oxidant concentrations for each TZ, average groundwater concentration below which ISCO can be terminated for an individual TZ C_{stopTZ}^{gw}, and average groundwater concentration above which oxidant reinjection will be intitated for a TZ $C_{reinject}^{gw}$. Note that since α and $C_{stop\ TZ}^{gw}$ are explicitly related via eq. (5.22), both cannot be optimized. Results for Opt1 indicate a failure probability of <1% (Table 5.6). The ENPV cost is $955k, which is $79k (7.6%) lower than that for NoOpt1, the "best engineering practice" case, which had a 4% failure probability. The adjusted NPV cost for Opt1 is $122k (11.3%) lower than that for NoOpt1. Compared to NoOpt4, which had a failure probability <1%, the Opt1 ENPV cost is $111k (10.4%) lower. Savings for Opt1 are achieved by a 3 month shorter expected duration, 18% lower total oxidant volume, and 12% lower oxidant mass utilized compared to NoOpt1.

Optimization of the number of monitoring wells for Opt1 kept the number at their initial values of four per TZ. The optimized oxidant concentration was 7 g/L for TZ A (the smallest, most contaminanted zone) and about 14 g/L for TZs B and C. The TZ stop criteria C^{gw}_{stopTZ} was slightly more aggressive (95 μg/L) compared to the site-wide value $C^{gw}_{stop\ all}$ (100 μg/L) and the optimized $C^{gw}_{reinject}$ value of 306 μg/L was significantly more aggressive than the value used for the NoOpt cases (200 μg/L). The probability-weighted average number of oxidant injection events was 4.5 for TZ A, 1.4 for TZ B and 1.2 for TZ C.

Results for Opt2 with $\alpha = 0.05$ differ little from Opt1. The failure probabilities were both <1% and the ENPV cost of Opt2 was only $4k higher than Opt1. The more stringent α value used for Opt2 was offset by slightly less aggressive optimized TZ oxidant concentrations and a less aggressive $C^{gw}_{reinject}$, while the optimized value of C^{gw}_{stopTZ} was more aggressive than for Opt1. Interactions among the optimized variables are clearly complex and nonlinear.

Opt3 and Opt4 Results. These cases are the same as Opt1 and Opt2, except that soil sampling is considered in addition to groundwater monitoring. We still assume existing groundwater monitoring wells will be sampled and allow additional wells (up to 10 per TZ) to be installed. From 0 to 10 soil borings are also allowed for each TZ with up to 2 sample depths per boring. The frequency of soil sampling as a multiple of the quarterly frequency of groundwater sampling was also optimized between once a quarter to once every 4 quarters.

Opt3 with $\alpha = 0.5$ yielded a failure probability <1% and an ENPV cost of $952k, just $3k less than Opt1. Opt4 with $\alpha = 0.05$ also had a failure probability <1%. Its ENPV cost was $957k, slightly higher than Opt1 and slightly lower than Opt2. The optimized number of monitoring wells for both Opt3 and Opt4 was 4 for each TZ, correponding to the initial wells available. The optimized number of soil borings was zero in TZ A and one in TZ B for both cases. The optimized number of soil borings for TZ C was two for Opt3 and one for Opt4. In addtion, the optimized frequency of soil sampling ($F_{soil/gw}$) was once every three groundwater samplings for both Opt3 and Opt4, i.e., optimized $F_{soil/gw} = 3$ indicating $\Delta t^{soil}_{mon} = 3\,\Delta t^{gw}_{mon}$.

Optimized oxidant concentrations for each TZ were higher for Opt3 and Opt4 than for Opt1 and Opt2, resulting in fewer oxidant injections for Opt3 and Opt4 compared to Opt1 and Opt2. However, the average treatment duration for Opt 3 and Op4 were longer due to longer intervals between injection events to perform additional sampling. As observed for Opt1 and Opt2, similar cost and performance was achieved for Opt3 and Opt4 by optimizing $C^{gw}_{stop\ TZ}$, $C^{gw}_{reinject}$, C_{ox0}, and performance monitoring variables, regardless of the assumed fixed value of α. We regard Opt4 as the best case for optimization as it permits soil sampling to the extent justified by performance and cost and uses a conservative significance level which reduces failure probability.

Inspection of cost probability distributions for the various cases (Figure 5.5) reveals a distinct positive skew for all NoOpt cases as evidenced by expected values that are significantly greater than the medians. This is much less the case for optimized simulations, which exhibit essentially zero skew for Opt3 and Opt4, slightly negative skew for Opt2, and positive skew for Opt1 (which was largely constrained by NoOpt assumptions).

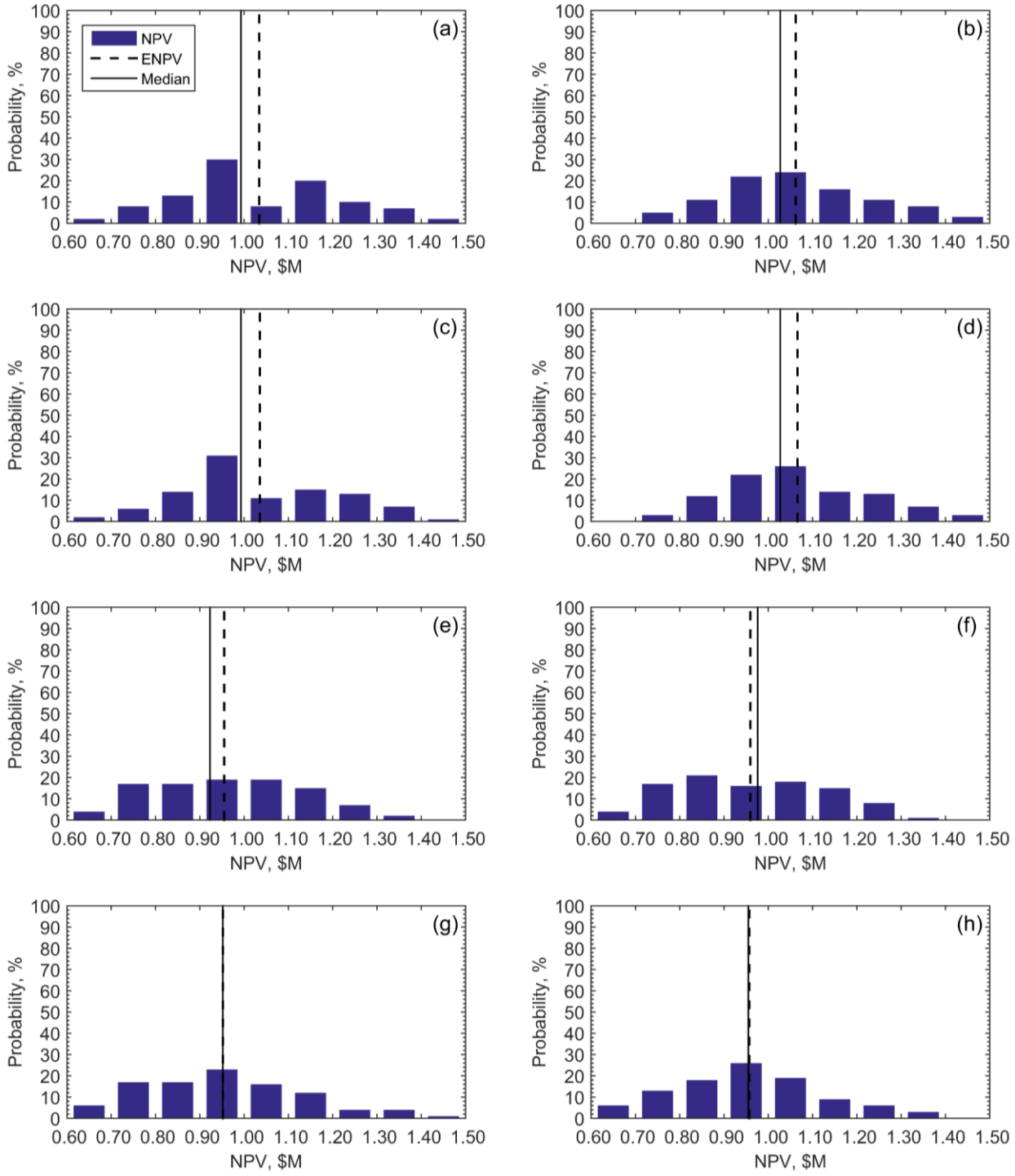

Figure 5.5. Probability distributions of unadjusted NPV total cost excluding penalty cost for Example 2 cases: (a) NoOpt1, (b) NoOpt2, (c) NoOpt3, (d) NoOpt4, (e) Opt1, (f) Opt2, (g) Opt3, and (h) Opt4.

Narrowing our attention to the "current best practice" case (NoOpt1) and the most conservative optimization case (Opt4), we consider the probability of exceeding various adjusted total costs for these cases (Table 5.8). The low ends of the distributions are offset very little with nearly identical minimum costs for both cases. However, the offset between the distributions increases at higher costs with the Opt4 case offset approximately $150,000 below NoOpt1 for NoOpt1 costs above $1,100,000. While the adjusted expected cost for Opt4 is $120,000 less than that for NoOpt1, the maximum adjusted cost is $156,000 less for Opt4. Thus, optimization not only reduced the adjusted expected cost by 11.1%, but reduced the worst-case cost by an even greater amount (14.5%).

Table 5.8 Probability of exceeding failure-adjusted costs for NoOpt1 and Opt4 cases.

Adj. Cost, $	NoOpt1	Opt4
600,000	100%	100%
700,000	98%	94%
800,000	95%	81%
900,000	82%	63%
1,000,000	61%	37%
1,100,000	41%	17%
1,200,000	27%	9%
1,300,000	16%	3%
1,400,000	5%	0%
1,500,000	1%	0%
1,600,000	0%	0%

5.9 Summary

We have presented a simplified model for DNAPL source remediation using ISCO that incorporates the most important physical and chemical processes with a variety of performance monitoring options for making real-time decisions and implementing most cost-effective solutions. Stochastic cost optimization is employed to determine design variables that minimize the expected (probability-weighted average) total cost to achieve defined remediation objectives. Sensitivity analyses indicated that sites with higher groundwater velocities can be expected to reach cleanup objectives sooner, although more oxidant may be required due to larger advective losses. Remediation duration decreased markedly with increases in the second-order NOD rate coefficient at lower velocities, but was much less sensitive at higher velocities due to advective oxidant losses. Remediation duration was predicted to decrease markedly with higher concentrations of injected oxidant due to enhanced DNAPL dissolution. Pore clogging was not found to be significant under the range of conditions studied using a literature value for the pore clogging coefficient S_{rind}. However, since little information is available on the variability of this coefficient, we suggest field data be collected to calibrate the value if pore clogging is of concern.

Simulation results reported here clearly demonstrate the importance of accounting for measurement and model uncertainty in the design process. Cases studied that had <1% probability of failing to meet cleanup criteria showed post-remediation probability-weighted average

groundwater concentrations ranging from 1 to 11 μg/L – far below the cleanup target of 100 μg/L. This implies that if one rigorously designed for average site conditions, the probability of failure would be very high.

A unique feature of the proposed ISCO operational methodology is the introduction of a termination criteria that compares the upper confidence limit of average measured concentration at a specified probability level with the cleanup target to provide a margin of safety to termination decisions. Another component is a strict monitoring protocol for making decisions to reinject oxidant or terminate further treatment for treatment zones (TZ) within the aggregate treatment volume using only groundwater sampling or groundwater and soil sampling. Derived statistical termination criteria allow site-wide and treatment zone termination decisions to be made with equal reliability. In some cases, cleaning up less contaminated TZs to more stringent criteria can allow site-wide average concentration targets to be met earlier and with lower costs. ISCO design variables that may be optimized include:

- Concentration of injected oxidant in each TZ
- Cleanup targets for TZ termination (with fixed site-wide criteria)
- Contaminant concentration above which reinjection will be initiated
- Number of soil and/or groundwater sampling locations in each TZ
- Soil and/or groundwater sampling frequency
- Number of samples per location
- Minimum groundwater sampling events following injection before termination decisions can be made (to allow for rebound)

Non-optimized cases reported here (NoOpt1-NoOpt4) revealed two distinct modes of failure when using the proposed monitoring protocol. The first is measurement error – i.e., limited numbers of samples and measurement "noise" leads us to believe cleanup criteria have been met when they actually have not. The second is rebound lag error – i.e., if we require a minimum of N_{min}^{gw} rounds of groundwater samples after oxidant injection before making a termination decision, but it takes more than N_{min}^{gw} rounds before the concentration rebounds above non-detect, we will erroneously conclude the TZ is clean. The likelihood of the first error can be reduced by specifying a significance level α <0.5 or using a TZ stop criteria for soil or groundwater that is less than the site-wide criteria, i.e., $C_{stop\ TZ}^{gw} < C_{stop\ all}^{gw}$. Considering the complexity of optimized parameter interactions evident in the optimization examples and the fact that α and $C_{stop\ TZ}^{gw}$ (or $C_{stop\ TZ}^{soil}$) cannot be simultaneously optimized, we suggest to use a modest fixed value for α (e.g., 0.2 corresponding to an 80% upper confidence limit) and optimize $C_{stop\ TZ}^{gw}$ values.

Costs for ISCO have been reported to range from $26 to $679 per m^3 with median values between $123 and $163 per m^3 (McDade et al. 2005, Krembs et al. 2010). The extremely wide range in reported volumetric costs likely reflects large variations in contaminant properties, initial concentrations, target cleanup levels, source depth and thickness, geologic complexity, etc. For the Monte Carlo simulations reported here, unit costs ranged from about $115 to $225 per m^3, which is well within the reported range.

For the hypothetical site considered, optimization of TZ oxidant concentrations, treatment zone-level cleanup criteria, reinjection criteria, and performance monitoring variables yielded a failure-

adjusted expected cost about 11% lower than a non-optimized case approximating current best engineering practice. Furthermore, the cost probability distribution for the optimized design eliminated positive skew evident in the "best practice" such that the worst case cost for the optimized design was 14.5% lower than that for the non-optimized design. Since the number of monitoring wells used for the "best practice" case was greater than is often available, and the number assumed fortuitously turned out to be optimal, significantly larger cost savings are likely to be realized in many cases.

Because cost and performance sensitivity are highly dependent on many site-specific factors, we do not want to leave the impression that optimal ISCO operating or performance monitoring variables can be inferred from the specific cases presented here. However, adoption of the stochastic design process in conjunction with proposed real-time performance monitoring and decision-mking protocols promises to yield more robust, reliable and cost-effective applications of ISCO to DNAPL sites with real-world uncertainty taken into account.

ISCO

We have presented a simplified model for DNAPL source remediation using ISCO that incorporates the most important physical and chemical processes with a variety of performance monitoring options for making real-time decisions and implementing most cost-effective solutions. Stochastic cost optimization is employed to determine design variables that minimize the expected (probability-weighted average) total cost to achieve defined remediation objectives. Sensitivity analyses indicated that sites with higher groundwater velocities can be expected to reach cleanup objectives sooner, although more oxidant may be required due to larger advective losses. Remediation duration decreased markedly with increases in the second-order NOD rate coefficient at lower velocities, but was much less sensitive at higher velocities due to advective oxidant losses. Remediation duration was predicted to decrease markedly with higher concentrations of injected oxidant due to enhanced DNAPL dissolution. Pore clogging was not found to be significant under the range of conditions studied using a literature value for the pore clogging coefficient S_{rind}. However, since little information is available on the variability of this coefficient, we suggest field data be collected to calibrate the value if pore clogging is of concern.

Simulation results reported here clearly demonstrate the importance of accounting for measurement and model uncertainty in the design process. Cases studied that had <1% probability of failing to meet cleanup criteria showed post-remediation probability-weighted average groundwater concentrations ranging from 1 to 11 μg/L – far below the cleanup target of 100 μg/L. This implies that if one rigorously designed for average site conditions, the probability of failure would be very high.

A unique feature of the proposed ISCO operational methodology is the introduction of a termination criteria that compares the upper confidence limit of average measured concentration at a specified probability level with the cleanup target to provide a margin of safety to termination decisions. Another component is a strict monitoring protocol for making decisions to reinject oxidant or terminate further treatment for treatment zones (TZ) within the aggregate treatment volume using only groundwater sampling or groundwater and soil sampling. Derived statistical termination criteria allow site-wide and treatment zone termination decisions to be made with equal reliability. In some cases, cleaning up less contaminated TZs to more stringent criteria can allow site-wide average concentration targets to be met earlier and with lower costs. ISCO design variables that may be optimized include:

- Concentration of injected oxidant in each TZ
- Cleanup targets for TZ termination (with fixed site-wide criteria)
- Contaminant concentration above which reinjection will be initiated
- Number of soil and/or groundwater sampling locations in each TZ
- Soil and/or groundwater sampling frequency
- Number of samples per location
- Minimum groundwater sampling events following injection before termination decisions can be made (to allow for rebound)

Non-optimized cases reported here (NoOpt1-NoOpt4) revealed two distinct modes of failure when using the proposed monitoring protocol. The first is measurement error – i.e., limited numbers of samples and measurement "noise" leads us to believe cleanup criteria have been met when they actually have not. The second is rebound lag error – i.e., if we require a minimum of N_{min}^{gw} rounds of groundwater samples after oxidant injection before making a termination decision, but it takes more than N_{min}^{gw} rounds before the concentration rebounds above non-detect, we will erroneously conclude the TZ is clean. The likelihood of the first error can be reduced by specifying a significance level α <0.5 or using a TZ stop criteria for soil or groundwater that is less than the site-wide criteria, i.e., $C_{stop\ TZ}^{gw} < C_{stop\ all}^{gw}$. Considering the complexity of optimized parameter interactions evident in the optimization examples and the fact that α and $C_{stop\ TZ}^{gw}$ (or $C_{stop\ TZ}^{soil}$) cannot be simultaneously optimized, we suggest to use a modest fixed value for α (e.g., 0.2 corresponding to an 80% upper confidence limit) and optimize $C_{stop\ TZ}^{gw}$ values.

Costs for ISCO have been reported to range from \$26 to \$679 per m^3 with median values between \$123 and \$163 per m^3 (McDade et al. 2005, Krembs et al. 2010). The extremely wide range in reported volumetric costs likely reflects large variations in contaminant properties, initial concentrations, target cleanup levels, source depth and thickness, geologic complexity, etc. For the Monte Carlo simulations reported here, unit costs ranged from about \$115 to \$225 per m^3, which is well within the reported range.

For the hypothetical site considered, optimization of TZ oxidant concentrations, treatment zone-level cleanup criteria, reinjection criteria, and performance monitoring variables yielded a failure-adjusted expected cost about 11% lower than a non-optimized case approximating current best engineering practice. Furthermore, the cost probability distribution for the optimized design eliminated positive skew evident in the "best practice" such that the worst case cost for the optimized design was 14.5% lower than that for the non-optimized design. Since the number of monitoring wells used for the "best practice" case was greater than is often available, and the number assumed fortuitously turned out to be optimal, significantly larger cost savings are likely to be realized in many cases.

Because cost and performance sensitivity are highly dependent on many site-specific factors, we do not want to leave the impression that optimal ISCO operating or performance monitoring variables can be inferred from the specific cases presented here. However, adoption of the stochastic design process in conjunction with proposed real-time performance monitoring and decision-mking protocols promises to yield more robust, reliable and cost-effective applications of ISCO to DNAPL sites with real-world uncertainty taken into account.

5.10 References

ASTM (2007) *Standard Test Method for Estimating the Permanganate Natural Oxidant Demand of Soil and Aquifer Solids, Method D7262-07.* ASTM International, West Conshohocken, PA.

Borden, R., K.Y. Cha, T. Simpkin, and M.T. Lieberman (2010) *Development of a Design Tool for Planning Aqueous Amendment Injection Systems Permanganate Design Tool*. Final Report. ESTCP Project ER-200626.

Cardiff, M., X. Liu, P.K. Kitanidis, J. Parker, and U. Kim (2010) Cost Optimization of DNAPL Source and Plume Remediation Under Uncertainty Using a Semi-Analytic Model. *Journal of Contaminant Hydrology* 113(1-4): 25-43. DOI: 10.1016/j.jconhyd.2009.11.004.

Cha, K.Y (2012) *Development of Design Tools for In Situ Remediation Technologies*. Ph.D. dissertation, Civil Engineering, North Carolina State University.

Cha, K.Y. and R.C. Borden (2012) Impact of injection system design on ISCO performance with permanganate - mathematical modeling results. *Journal of Contaminant Hydrology* 128:33-46.

Crimi, M.L. and R.L. Siegrist (2005). Factors affecting effectiveness and efficiency of DNAPL destruction using potassium permanganate and catalyzed hydrogen peroxide. *Journal of Environmental Engineering*, 131(12):1724-1732.

Falta, R.W., P.S. Rao, and N, Basu (2005) Assessing the impacts of partial mass depletion in DNAPL source zones: I. Analytical modeling of source strength functions and plume response. *Journal of Contaminant Hydrology* 78:259–80.

Huling, S.G. and B.E. Pivetz (2006) *In Situ Chemical Oxidation*. EPA Engineering Issue (EPA/600/R-06/072).

Jawitz, J.W., A.D. Fure, G.G. Demmy, S. Berglund, and P.S.C. Rao (2005) Groundwater contaminant flux reduction resulting from nonaqueous phase liquid mass reduction. *Water Resources Research* 41(10): W10408.

Kim, U., J. Parker, P. Kitanidis, M. Cardiff, X. Liu, and J. Gillie (2013) Stochastic Cost Optimization of DNAPL Remediation - Field Application. *Environmental Modeling & Software 46*: 12-20. DOI:10.1016/j.envsoft.2012.05.003.

Krembs, F.J., R.L. Siegrist, M.L. Crimi, R.F. Furrer, and B.G. Petri (2010) ISCO for groundwater remediation: analysis of field applications and performance. *Ground Water Monitoring & Remediation* 30(4): 42-53.

McDade, J.M., T.M. McGuire, and C.J. Newell (2005) Analysis of DNAPL source-depletion costs at 36 field sites. *Remediation* 15(2): 9–18.

McGuire, T.M., J.M. McDade, and C.J. Newell (2006) Performance of DNAPL source depletion technologies at 59 chlorinated solvent-impacted Site. *Ground Water Monitoring & Remediation* 26(1): 73-84.

Park, E. and J.C. Parker (2005) Evaluation of an upscaled model for DNAPL dissolution kinetics in heterogeneous aquifers. *Advances in Water Resources* 28: 1280-1291.

Parker, J.C. and U. Kim (2015) An upscaled approach for transport in media with extended tailing due to back-diffusion using analytical and numerical solutions of the advection dispersion equation. *Journal of Contaminant Hydrology* 182: 157-172. DOI: 10.1016/j.jconhyd.2015.09.008.

Parker, J.C., U. Kim, M. Widdowson, P. Kitanidis, and R. Gentry (2010a) Effects of model formulation and calibration data on uncertainty in predictions of DNAPL source dissolution rate. *Water Resources Research* 46: W12517. DOI: 10.1029/2010WR009361.

Parker, J.C., U. Kim, P. Kitanidis, M. Cardiff, and X. Liu (2010b) Stochastic cost optimization of multi-strategy DNAPL site remediation. *Groundwater Monitoring & Remediation* 30(3): 65-78. DOI: 10.1111/j1745-6592.2010.001287.x.

Parker, J.C. and E. Park (2004) Modeling field-scale DNAPL dissolution kinetics in heterogeneous aquifers. *Water Resources Research* 40: W05109

Parker, J.C. and R.W. Falta (2008) Comparison of alternative upscaled model formulations for simulating DNAPL source dissolution and biodecay. *Advances in Water Resources* 31: 1325–1332

Parker, J.C., U. Kim, A. Fortune, S. Griepke, J. Galligan, A. Bonarrigo (2016) Operational monitoring of thermal treatment systems: methods, data analysis and cost optimization. *Ground Water Monitoring & Remediation*. In revision.

Parker, J.C., U. Kim, P. Kitanidis, M. Cardiff, X. Liu, and J. Lee (2011) *Practical Cost-Optimization of Characterization and Remediation Decisions at DNAPL Sites with Consideration of Prediction Uncertainty*. SERDP Project ER-1611, Final Report.

Rao, P.S.C. and J.W. Jawitz (2003) Comment on "Steady state mass transfer from single component dense nonaqueous phase liquids in uniform flow fields" by T.C. Sale and D.B. McWhorter. *Water Resources Research* 39(3): 1068.

Reitsma, S. and J. Randhawa (2002) Experimental investigation of manganese dioxide plugging of porous media. *Proceedings of the Third International Conference on Remediation of Chlorinated and Recalcitrant Compounds*. May 20-23, 2002, Monterey, California.

Reitsma, S. and Q.L. Dai (2001) Reaction-enhanced mass transfer and transport from non-aqueous phase liquid source zones. *Journal of Contaminant Hydrology* 49: 49-66.

Siegirst, R.L., M. Crimi, J. Munakata-Marr, and T. Illagasakare (2006) *Reaction and Transport Processes Controlling In Situ Chemical Oxidation of DNAPLs*. SERDP CU-1290, Final Report.

Siegrist, R.L, B. Petri, F. Krembs, M. Crimi, S. Ko, T. Simpkin, and T. Palaia (2008) *In Situ Chemical Oxidation for Remediation of Contaminated Groundwater: Summary Proceedings of an ISCO Technology Practices Workshop*. ESTCP Project ER-0623, Workshop Report.

Siegrist, R.L., T. Simpkin, J. Heiderscheidt, T. Illangasekare et al. (2010) *In Situ Chemical Oxidation for Groundwater Remediation - Site Specific Engineering & Technology Application*. ESTCP Project ER-062, Final Report.

Snedecor, G.W. and W.G. Cochran, (1967) *Statistical Methods*. Iowa University Press. Ames Iowa, 593p.

Waldemer, R.H. and P.G. Tratnyek (2006) Kinetics of contaminant degradation by permanganate. *Environmental Science & Technology* 40: 1055–1061.

West, M.R. and B.H. Kueper (2012) Numerical simulation of DNAPL source zone remediation with in situ chemical oxidation (ISCO). *Advances in Water Resources* 44: 126-139.

West, M.R., G.P. Grant, J.I. Gerhard, and B.H. Kueper (2007) The influence of precipitate formation on the chemical oxidation of TCE DNAPL with potassium permanganate. *Advances in Water Resources* 31: 324-338.

Yan, E. and F. Schwartz (2000) Kinetics and mechanisms for TCE oxidation by permanganate. *Environmental Science & Technology* 30: 2535–2541.

Yang, M, M.D. Annable, and J.W. Jawitz (2016) Solute source depletion control of forward and back diffusion through low-permeability zones. *Journal of Contaminant Hydrology* 193: 54-62.

6. Transport Model Calibration and Uncertainty Analysis

6.1 Overview

Before the dissolved plume transport model can be used to evaluate effects of various design variables on the expected performance and cost of remediation strategies of interest, a number of site-specific parameters must be estimated from site characterization data and other sources. Most model parameters will be subject to more or less uncertainty, depending on the quality and quantity of data available. In addition to parametric uncertainty, models are, by definition, simplifications of reality, and thus are subject to intrinsic model formulation errors associated with explicit or implicit simplifying assumptions that have been invoked. Measurements used to estimate model parameters are themselves subject to sampling and analytical errors, which also contribute to prediction uncertainty.

Therefore, the first step that must be undertaken prior to employing a model to evaluate current or proposed remediation strategies is to perform model calibration using all available data and then to quantify parametric, intrinsic and measurement uncertainty. The model can then be used to make forward estimates of performance and cost and to quantify the prediction uncertainty.

6.2 Computational methods

6.2.1 Inverse modeling approach

The purpose of the calibration/uncertainty analysis module is to determine best estimates of key model parameters and to quantify parametric and residual model uncertainty. The SCOToolkit model calibration process utilizes field measurements (which may comprise various types of data, e.g., contaminant concentrations, natural ED concentrations, and contaminant fluxes at various locations and times), and prior information about parameter values and their uncertainty. Assuming Gaussian (or log-Gaussian) measurement errors and prior parameter distributions, we seek to minimize the negative log of the posterior distribution, L, described by

$$L = \frac{1}{2}\mathbf{w}^T\mathbf{w}\left(\mathbf{y}-\mathbf{h}(\mathbf{s})\right)^T \mathbf{R}(\boldsymbol{\theta})^{-1}\left(\mathbf{y}-\mathbf{h}(\mathbf{s})\right)+\frac{1}{2}\left(\mathbf{s}-\mathbf{s}^*\right)^T \mathbf{Q}^{-1}\left(\mathbf{s}-\mathbf{s}^*\right) \tag{6.1}$$

where **y** is a vector of field measurements, **s** is a vector of parameter values, **s*** is a vector of prior parameter estimates, **h**(**s**) is a vector of model predictions corresponding to the field measurements, **R** is a matrix of measurement covariances corresponding to the vector of data types $\boldsymbol{\theta}$ (e.g., measured contaminant concentration, source mass, source mass discharge rate, etc.), **w** is a user-defined weighting matrix, and **Q** is the covariance matrix of prior parameter estimates. Off-diagonal terms are disregarded for **w**, **R** and **Q**.

The last term in (6.1) is often referred to as a "penalty function" because it imposes a penalty on the objective function in proportion to the deviations between calibrated parameter values and their prior estimates normalized by their uncertainty. This functions like an elastic constraint. As parameters stretch further from their prior estimates, the penalty increases to constrain them unless there is a sufficient counteracting force from reduced deviations between measurements and model predictions. This feature makes the inverse solution very robust. By specifying prior best estimates of model parameters and uncertainty in the prior estimates, the inverse solution is much more stable and allows improved estimates of more parameters to be made than would otherwise be

possible. Therefore, it is important to carefully consider all information at your disposal, from direct site data to experience with similar sites or literature correlations, to specify prior estimates of parameters and their uncertainty. In addition to variable constraints on parameters associated with the stipulation of prior parameter uncertainty, absolute upper and lower constraints may also be placed on any parameters.

Each model parameter and each data type may be log-transformed prior to application of eq. (6.1). For parameters or data types that are physically constrained to be non-negative and that are expected to exhibit a coefficient of uncertainty greater than ~20%, log-transformation is advisable. Also, calibration data types that exhibit ranges in the data set that extend over several orders-of-magnitude, log-transformation may be desirable if comparable relative error (as opposed to absolute error) is desired over the measurement range. Otherwise, the regression results will likely be controlled by absolute errors from a small number of large data values.

Field measurements of contaminant concentrations, source mass, etc. that are calibration targets in the objective function may also be log-transformed at the discretion of the analyst. Since these values are invariably physically constrained to be non-negative and exhibit large variability, log-transformation is highly advisable in most cases. It should be recognized that when calibration data are log-transformed, the objective function effectively seeks to minimize the *relative error* in measurements rather than the *absolute error*. This is generally desirable, since a 10 ppm error in a 1000 ppm value is easily acceptable, while a 10 ppm error in a 1 ppm value is much less so. Nevertheless, it should be recognized that log-transformation has the effect of putting greater weight (in absolute terms) on small values than large values, hence on defining the plume perimeter more accurately than the magnitude of "hot spots." To the extent the analyst requires more or less weight on certain values, user-prescribed weights can be assigned to individual data points of groups of data.

A related calibration issue involves the handling of calibration data that are below detection or quantification limits. Since the log of zero is undefined, entering these values as zero is not an option. The inclination to enter such values as small nonzero values, such as 10^{-10}, however, will produce undesirable results. To illustrate, consider a data point that is below the detection limit of say 1 ppb. The model predicts a value of 0.1 ppb. Not too bad, but the ln deviation would be $\ln(0.1) - \ln(10^{-10}) = 20.7$ and the squared deviation would be 429, which would likely dominate the objective function resulting in very poor model calibration. As a practical matter, setting non-detect values equal to around 10% of the detection limit will produce reasonable results.

The magnitude of each data type's uncertainty (i.e., diagonal terms in **R**) is generally not known *a priori*, but posterior estimates can be made using the Restricted Maximum Likelihood (RML) algorithm (Kitanidis, 1987). Note that the final estimate of residual prediction uncertainty **R** for each data type represents the portion of data variability that cannot be accounted for by the model, which may be due to sampling or measurement errors and/or to intrinsic limitations of the model to represent all processes in the field. For simplicity, we will refer to this uncertainty as the "residual" error. A gradient-based nonlinear optimization algorithm is used to find the solution that minimizes (6.1).

6.2.2 Evaluation of model prediction uncertainty

Uncertainty in forward simulations of remediation performance and cost is characterized using a MC modeling approach. Liu et al. (2010) have shown that linearized uncertainty methods compare well with more rigorous and much more computationally intensive than Markov Chain Monte Carlo (MCMC) methods when data is not inordinately noisy and reasonable prior information is available to condition parameter estimates. Thus, we utilize linearized uncertainty propagation methods to generate conditional parameter realizations.

An estimate of the posterior covariance matrix is computed from the final calibration results as

$$\mathrm{cov}(\mathbf{s}) \approx \left(\mathbf{H}^T\mathbf{R}(\boldsymbol{\theta})^{-1}\mathbf{H} + \mathbf{Q}^{-1}\right)^{-1} \tag{6.2}$$

where $H_{ij} = \partial h_i / \partial s_j$ is a sensitivity matrix. As noted above, incorporating prior estimates of parameters and their uncertainty into the regression objective function greatly reduces non-uniqueness problems in the inverse solution and allows many more parameters to be calibrated than would be possible with unconstrained optimization. This not only allows refinement of parameters with relatively low uncertainty that may otherwise be assumed at their prior estimates, but allows interactions among more parameters, through the covariance matrix, to be taken into consideration in the error analysis.

Performance models are used to simulate soil and/or groundwater concentrations in source zones during ISCO or thermal treatment, groundwater concentrations at ED injection gallery monitoring locations, and soil and/or (resident or flux) groundwater concentrations at compliance wells, which are used for making "real-time" operational decisions during simulations (e.g., to turn remediation systems off, terminate monitoring, or incur "penalty costs").

Monet Carlo realizations are computed in two steps:

1. The first step is to generate N_{mc} equiprobable realizations of all uncertain model parameters for the problem under consideration using standard methods for multivariate Gaussian distributions (e.g., Press et al, 2007) based on parameter best estimates and covariances determined from the calibration and user-defined uncertainty for specified non-calibrated variables. If log-transformations of parameters were used during calibration, the same transformations must be used for parameter generation. In addition, uncorrelated normal or log-normal "noise" may be optionally applied to non-calibrated model inputs – including cost model coefficients. Simulations are performed for each parameter set realization.
2. The second step adds log-normal "white noise" to each realization using a user-specified natural-log standard deviation that represents errors associated with sampling and measurement methods and those attributable to deviations from model simplifications. We recommend taking the later as the residual error in the current model calibration (i.e., standard deviation of calibrated and measured ln concentrations.

NPV cost is computed for each MC realization (including penalty costs for noncompliant realizations) and the expected NPV cost across all realizations is determined. This protocol—in conjunction with the "penalty cost" assigned to realizations that fail to meet remediation objectives—ensures that optimized design parameters will be sufficiently conservative to achieve an acceptable probability of meeting compliance criteria.

6.3 Transport model calibration protocol

6.3.1 Overview

Since transport model parameters can, at best, only be roughly estimated a priori, model calibration to measured contaminant concentrations and other data, is critical to realize the maximum possible accuracy. Furthermore, uncertainty in model parameters, and predictions based upon them, can only be determined through inverse modeling methods as discussed above. While a priori estimates of many model parameters have large uncertainty, others exhibit small or moderate uncertainty. Even for parameters with large a prior uncertainty, if the range can be narrowed from 2 to 1 orders-of-magnitude, calibration accuracy, reliability and even feasibility can be significantly improved.

There are two important categories of poor models we will call 'bad' and 'really bad.' Merely bad models exhibit very high uncertainty; however, they are accurate within these wide bounds. That is, reality lies somewhere within the broad confidence limits. This is the realm of "known unknowns." Remediation plans based on such models will lead to very conservative but reliable designs.

Really bad models may have wide or not so wide confidence limits, but reality lies outside the limits. This is the realm of "unknown unknowns," which can lead to very poor decisions. Really bad models are typically the result of erroneous assumptions – most often associated with an inappropriate conceptual model or incorrect boundary conditions. Boundary conditions in the SCOToolkit transport solution are rigorously formulated and the only user requirement is to select an output mode consistent with the sample type (e.g., flux concentrations for monitoring wells). We will consider conceptual model issues later.

Another possible cause of really bad models is non-uniqueness in the inverse solution. The inversion algorithm used by SCOToolkit is very robust and relatively immune to non-uniqueness. However, insufficient or very "noisy" calibration data and/or poor specification of prior parameter values can lead to poorly posed inverse problems. The protocol described below employs all available quantitative and qualitative information to formulate a stable inverse solution and tests for possible non-uniqueness.

6.3.2 Development of site conceptual model

Development of an accurate site conceptual model is a critical task. If it is substantially wrong, nothing else will matter. Important components include characterizing the groundwater flow regime (e.g., aquifer properties, flow velocity and direction) and identifying contaminant sources (e.g., locations, dimensions, contaminants). The aquifer may be unconfined or semi-confined. Groundwater flow is treated as horizontal and planar, although mildly curvilinear horizontal flow paths may be approximated. Vertical groundwater flow is not explicitly considered, although effects of a steady-state vertical hydraulic gradient may be approximated for shallow sources by higher or lower vertical dispersivities for downward and upward gradients, respectively.

The analytical transport solution assumes statistically homogeneous and isotropic aquifer properties – except for decay coefficients, which may be zoned as a function of distance from the source. Of course, no aquifers are strictly homogeneous. Statistical homogeneity means that properties can be upscaled or averaged at a scale sufficient to describe field behavior. For example, if permeability varies in a more-or-less random fashion independent of direction or distance from

a source, the "effective" upscaled permeability will approximate the geometric average of local scale values. If permeability exhibits a high correlation scale in the horizontal direction and a low correlation scale in the vertical direction (i.e., stratified beds), the effective horizontal permeability will correspond to the thickness-weighted arithmetic average. When permeability ratios between adjacent layers are large and lower permeability layers are thick, diffusional mass transfer limitations may arise, which may be upscaled as described in Chapter 2.

Provided upscaled properties do not exhibit substantial spatial trends – i.e., upscaled properties at proximal and distal ends of the plume are similar – the analytical solution will usually be applicable. However, as the degree of local heterogeneity increases, mismatches between the averaging scale of the model and measurement scales will usually increase. For example, if the aquifer consists of alternating 1 m thick high and low permeability layers and monitoring wells are screened over several meters, model and measurement scales would be harmonious. However, if water samples are obtained from multi-level wells with very short screens, model and measurement scales would not be consistent. The later data could still be used for calibration, effectively using the inverse solution to perform upscaling. However, the average deviation between measurements and model simulated values will be much larger than if the measurements were available at a scale consistent with the model. For the example given, this could be achieved by vertically averaging small scale measurements over intervals of 2 m or more. In general, calibration error will decrease as the scale of field measurements increases. Field measurements also exhibit short term fluctuations which may be due to transient hydraulic fluctuations or to variability in sampling and lab analyses. In any case, averaging over time (e.g., annual averaging of quarterly samples) will also reduce calibration error. From an exposure risk standpoint, model accuracy at larger time and space scales is usually more important than at smaller scales.

Keep in mind that a single SCOToolkit source function can represent residual DNAPL or DNAPL lenses or pools, but not both. If both are significant, you should use different sources for residual DNAPL and pools or lenses. Multiple sources may be completely separated, partially overlapping or completely overlapping.

Many DNAPL sites have significant contamination from multiple species, which may occur due to releases of multiple contaminants and/or to in situ biotransformations of an initially released species. For example, PCE can degrade to TCE which degrades in turn to 1,1-DCE and then to VC. Since PCE and TCE have similar toxicological characteristics, when both occur in significant amounts, it may be useful to combine the two as a single "pseudo-species" for purposes of modeling with SCOToolkit, which can only model one nominal species at a time.

Before proceeding further, confirm whether your conceptual model is reasonably within the bounds of SCOToolkit assumptions.

6.3.3 Groundwater flow field

Although the analytical transport model explicitly assumes a uniform planar groundwater flow field, SCOToolkit considers mildly nonlinear flow fields using a coordinate transformation to map nonlinear streamlines described by a cubic polynomial to "equivalent" planar coordinates. Field coordinates are usually specified by survey data in northing and easting values relative to a from a reference location. However, any Cartesian coordinate system may be adopted, provided the units are in meters.

If a planar flow field model is employed, the user must specify field coordinates for the center of a vertical plane at the downgradient edge of the source or ED gallery and the flow direction (in degrees positive counterclockwise or negative clockwise from the field X-axis). If a nonlinear streamline is applicable, in addition to source coordinates (X_o,Y_o), coefficients *a, b* and *c* of the polynomial $Y = Y_o+a(X–X_o)+b(X–X_o)^2+c(X–X_o)^3$ must be specified.

A constraint on the polynomial streamline model is that *X*-axis values of the streamline must increase or decrease monotonically along the streamline. An example of a non-monotonic streamline is illustrated in Figure 6.1a below. Note that from northernmost end of the streamline, flow is initially to the southeast. But this gradually shifts south and then southwest resulting in multiple northing values for single easting values. However, if the coordinates are reversed as illustrated in Figure 6.1b, the function becomes monotonic with respect to the x-axis, now taken as northing.

Unless the streamline is non-monotonic with respect to both the easting and northing, this simple axis swap resolves the problem. All that is required is to fit parameters with the reversed coordinates and to input northing values for all x-axis inputs and easting values for all y-axis inputs in SCOToolkit (e.g., source locations, well locations, gallery locations, etc.). When plotting model results as a map view (e.g., plume contours or posted values), it will simply be necessary to remember to switch the coordinates back for a normal map view (i.e., north up).

The process of fitting linear or polynomial model parameters can be performed easily using the SCOToolkit Excel tool **Streamline calulation.xlsx**, which includes detailed instructions and automatically checks for and performs axis swapping as necessary (Appendix A).

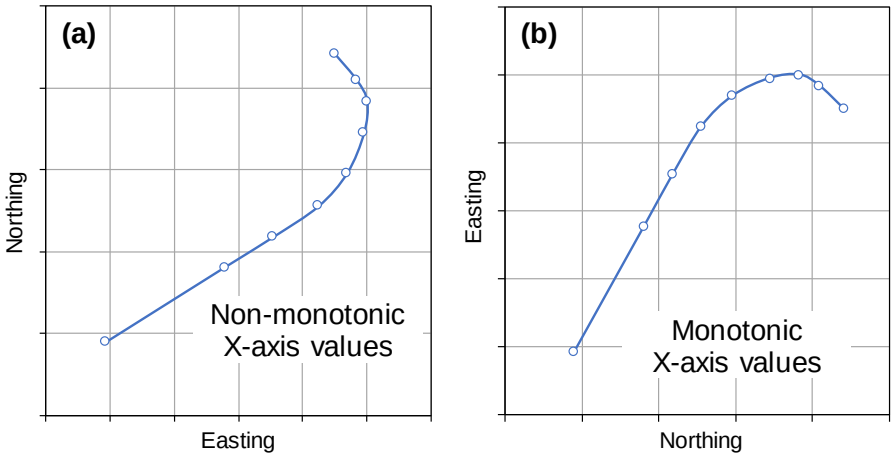

Figure 6.1. Streamline that is (a) non-monotonic with respect to the X-axis (easting), and (b) same data with axes swapped giving a monotonic function versus northing on the X-axis.

6.3.4 Initial estimates of model parameters and their uncertainty

Statistical issues

Make a list of all parameters pertinent to your site conceptual model. You will need to make best estimates of all model parameters considering all site data at your disposal, plus experience with similar sites, published parameter ranges, and reported correlations with other variables. You will also need to quantify the uncertainty in each parameter. We will discuss methods to estimate

various SCOToolkit parameters below. But first, let's consider a few issues regarding the quantification of parameter uncertainty.

SCOToolkit allows users to represent parameter uncertainty using either a normal or log-normal distribution. A normal distribution with a coefficient of variation (ratio of mean to standard deviation) greater than about 0.3 has a significant likelihood of including negative parameter values, which are physically impossible for parameters in SCOToolkit. A few parameters, such as porosity, may have small enough uncertainty that a normal distribution could be used. However, since normal distributions are closely approximated by log-normal curves when the coefficient of variation is small, it is more convenient to use the log-normal distribution for all parameters. Note that the standard deviations of a natural log-transformed parameter (S_{ln}) is a dimensionless measure of relative uncertainty. As discussed in section 6.3.2, most model parameters represent "effective" values averaged over the entire model domain. For physical quantities like porosity, simple arithmetic averaging is applicable if we have measurements from multiple samples. For other parameters, like hydraulic conductivity, the "effective" value depends on the spatial configuration of "point" values. For example, for flow parallel to layers, simple arithmetic averaging is appropriate, for flow perpendicular to layers harmonic averaging is applicable, while for randomly distributed heterogeneity, geometric averaging (i.e., averaging log values) is best.

To the extent that effective field scale property values are determined from multiple local scale measurements, we need to characterize uncertainty in the effective or averaged value ($S_{ln\ avg}$), not that of individual sample measurements ($S_{ln\ smp}$). These quantities are related via

$$S_{\ln} \equiv S_{\ln avg} = \frac{S_{\ln smp}}{N^{1/2}} \tag{6.3}$$

where N is the number of samples in the data set used to compute the average (or "effective") value. For example, if we have data for 9 slug tests with a sample ln standard deviation $S_{ln\ smp}$ of 0.6 (i.e., standard deviation of all ln measurements), then $S_{ln\ avg}$ is $0.6/9^{1/2} = 0.2$. The latter is the uncertainty applicable to SCOToolkit (e.g., for use in computing pore velocity uncertainty which we will discuss later). We use the notation S_{ln} here to designate uncertainty in effective parameter values. If multiple measurements are available from which to compute average or effective values, (1) may be used to calculate S_{ln}.

Another statistical relationship is useful for estimating the uncertainty of a value that is computed from multiple linearly related uncertain variables. If parameter $q = f(p_1, p_2 ... p_n)$, where f is a linear function of uncorrelated variables p_1, p_2, etc., then

$$S_{\ln q} = \left(\sum_{i=1}^{N} S_{\ln p_i} \right)^{1/2} . \tag{6.4}$$

For example, if mean hydraulic conductivity, hydraulic gradient, and porosity are estimated as 25 m/d, 0.01, and 0.3 with S_{ln} values of 0.1, 0.05 and 0.05, respectively, then the mean pore velocity is 25x0.01/0.3 = 0.83 m/d with an S_{ln} of $(0.10^2+0.05^2+0.05^2)^{1/2} = 0.12$.

For some parameters, data will not be available to explicitly compute parameter uncertainty. In such cases, use your experience and/or published results to estimate reasonable upper and lower bounds (P_{max} and P_{min}, respectively) for the parameters. If these bounds are taken to represent p% confidence limits, then $S_{ln} = (\ln P_{max} - \ln P_{min})/t_2(p)$ where t_2 is ~2, 4 or 6 for p = 66, 95 and 99%, respectively.

Prior parameter estimates are used as the starting point for the nonlinear regression algorithm and uncertainty estimates are used to constrain the estimation algorithm by placing a "penalty" on the objective function as estimates stray further from the prior best estimate relative to the parameter uncertainty.

The bane of nonlinear regression problems is non-uniqueness. When data being regressed is "noisy" and there are a lot of uncertain parameters, multiple sets of model parameters can produce nearly indistinguishable fits to the data, which may lead to false parameter estimates. Fewer parameters with smaller uncertainties reduce the likelihood of this. However, if some initial parameter estimates are significantly off and uncertainty has been underestimated, the over-constrained regression may be unable find the "true" solution. So, there is a tradeoff. If parameter uncertainty is overestimated, non-uniqueness may cause problems. However, if it is underestimated, the solution may be over-constrained. In general, it is safer to error on the side of overestimating prior parameter uncertainty. But don't overdo it.

Aquifer parameters

One of the most critical variables in the transport model is the mean contaminant velocity

$$v_{eff} = \frac{q}{\phi R} \tag{6.5a}$$

$$R = 1 + \frac{\rho_b k_d}{\phi} \tag{6.5b}$$

where q is the darcy velocity, ϕ is porosity, ρ_b is bulk density, and k_d is the sorption coefficient. Parameter inputs required by SCOToolkit to compute the mean contaminant velocity are q, ϕ, ρ_b, and k_d. Note that since these parameters are all linearly related, we can only calibrate one of them. Any attempt to calibrate others would result in an infinite number of solutions with identical fits to calibration data.

Darcy velocity is commonly estimated as the product of mean hydraulic gradient estimated from water level data, and hydraulic conductivity based on slug and/or pump tests.

Porosity and bulk density can be measured on core samples. However, since their range is rather small, their values are often assumed based on studies of similar aquifer material. Given an estimate of porosity ϕ, and using a typical particle density ρ_s of 2650 kg/m^3, bulk density ρ_b can be estimated from porosity as

$$\rho_b = \rho_s(1-\phi)\,. \tag{6.6}$$

Sorption coefficients for organic chemicals can be estimated from aquifer organic carbon content f_{oc} as

$$k_d = f_{oc} k_{oc} \tag{6.7}$$

where k_{oc} is a carbon normalized sorption coefficient, values of which are widely tabulated for common organic contaminants. Organic carbon content can be easily measured on samples of aquifer material, but since it can exhibit large spatial heterogeneity in some aquifers, it is advisable

to take several samples. Since only the average value is required for modeling, lab costs can be reduced by compositing the samples.

If multiple species are modeled as a single pseudo-species, a weighted average k_{oc} value will need to be used, which may be computed as

$$k_{oc\ pseudo} = \sum_{i=1}^{N_s} k_{oc\ i}\, f_i \tag{6.8}$$

where $k_{oc\ i}$ is the k_{oc} value for species i and f_i is a ratio of the average concentration of species i within the plume to the average of pseudo-species concentration. Note that differences in k_{oc} for multiple species will result in greater apparent dispersion of the pseudo-species plume compared to individual plumes.

Decay coefficients are difficult to determine directly from individual wells with any accuracy, since nominal attenuation rates observed in wells depend on many factors in addition to chemical or biological transformations (e.g., dispersion, source attenuation). An alternative method for making initial estimates of the decay coefficient is to compute plume-wide ratios f_{ij} of the average concentration of daughter species i to that of parent species j over time and regress the data to compute the decay coefficient λ from

$$\lambda_{ij} = \frac{d \ln f_{ij}}{dt} \tag{6.9}$$

Note that if a pseudo-species is modeled j represents the pseudo-species and i is the net daughter product of the pseudo-species. For example, if the pseudo-species is PCE+TCE, then f_{ij} is the ratio of DCE to PCE+TCE. The decay coefficient for PCE+TCE → DCE will be much smaller than the decay coefficient for PCE → TCE or TCE → DCE. Therefore, uncertainty in the decay coefficient will have much less effect of prediction uncertainty for the pseudo-species model.

Source parameters

As part of the site conceptual model development, estimates of average source length L_x, width L_y, and thickness L_z, and coordinates for the center of the downgradient vertical plane should be made for each source. Note that all source dimensions refer to the source configuration below the water table only. If the source is located completely within the unsaturated zone, width and length refer to the dimensions of the area at the water table impacted by leaching from the source. Source thickness in this case should be specified as a small but non-zero value, e.g., 0.5 m. Vertical dimensions are taken as positive downward with zero at the water table. Thus, a DNAPL pool lying from 4 to 5 m below the water table in a 10 m thick aquifer would have a source thickness of 1 m and a mid-point vertical coordinate of 4.5 m. Estimates of source width and thickness may be refined during calibration within specified lower and upper ranges based on site characterization data.

Additional parameters required for each source include: initial date of contaminant release t_s, final data of contaminant release t_o, source depletion exponent β, total contaminant mass M_{cal} in the source at date t_{cal}, and discharge rate J_{cal} at t_{cal}, where t_{cal} is a specified date prior to any source treatment actions at which data is available to make initial estimates of M_{cal} and J_{cal}. Initial ranges for t_s and t_o can generally be determined based on operational history of the site.

In some cases, estimates of the mass of released contaminant may be estimated from operational records, although inventory records are notoriously uncertain. Nevertheless, such data can sometimes be helpful to establish brackets for reasonable values. Better estimates can generally be made from N_{soil} soil samples collected within the source zone (at time t_{cal}) for which soil concentrations C_{smp}^{soil} [M M^{-1}] are measured for the species or pseudo-species that is to be modeled.

Estimates of M_{cal} and its uncertainty $S_{\ln Mcal}$ can be determined from such data by

$$M_{cal} = \rho V \; avg\left(C_{smp}^{soil}\right) \tag{6.10a}$$

$$S_{\ln Mcal} = \left(\frac{\left(stdev\left(\ln C_{smp}^{soil}\right)\right)^2}{N_{soil}} + \left(S_{\ln \rho}\right)^2 + \left(S_{\ln V}\right)^2 \right)^{1/2} \tag{6.10b}$$

where ρ is the soil dry density with uncertainty $S_{ln\ \rho}$, V is source volume with uncertainty $S_{ln\ V}$, $avg(x)$ is the average of series x and $stdev(x)$ is its standard deviation. $S_{\ln Mcal}$ can be quite high unless the sample size (i.e., soil volume or mass) and/or sample number is large. For the purpose of estimating source mass, compositing samples over the entire boring interval will improve accuracy and reduce lab analysis costs.

Estimates of J_{cal} and its uncertainty $S_{\ln Jcal}$ can be determined from measurements of contaminant concentrations in groundwater C_{smp}^{gw} [M L^{-3}] on a vertical plane representative of the downgradient edge of the source or slightly up- or downgradient. Estimates of J_{cal} and its uncertainty $S_{\ln Jcal}$ can be determined from N_{gw} groundwater samples as

$$J_{cal} = qL_yL_z \; avg\left(C_{smp}^{gw}\right) \tag{6.11a}$$

$$S_{\ln Jcal} = \left(\frac{\left(stdev\left(\ln C_{smp}^{gw}\right)\right)^2}{N_{gw}} + \left(S_{\ln q}\right)^2 + \left(S_{\ln Ly}\right)^2 + \left(S_{\ln Lz}\right)^2 \right)^{1/2} \tag{6.11b}$$

where q is darcy velocity with uncertainty $S_{ln\ q}$, L_y is source width with uncertainty $S_{ln\ Ly}$, and L_z is thickness with uncertainty $S_{ln\ Lz}$

The most difficult to estimate source parameter is β, which controls the shape of the $J(t)$ and $M(t)$ curves. Field observations of source mass and/or discharge rates over time are necessary to calibrate β. As a first step, identify whether the source is predominantly residual DNAPL or DNAPL pools and/or lenses. Values of β for pools or lenses may range from about 0.1 to 1.0. Residual DNAPL values will be greater than 1.0. There is no hard upper bound, but values much above 2 are not common. If you can identify the source as a pool/lens, an initial estimate of β = 0.4 with S_{ln} = 0.3 is reasonable. For residual sources, a value of β = 1.6 with S_{ln} = 0.15 is a good starting point. If you have no idea about the DNAPL "architecture," using a value of β = 0.7 with S_{ln} = 0.45 as a first guess with S_{ln} = 0.3. These values can be used as prior estimates and refined by analyzing field data.

A simple method to estimate β from field can be derived by noting that β is the slope of a log-log plot of discharge rate versus source mass remaining as

$$\beta = \left.\frac{d\ln J(t)}{d\ln M(t)}\right|_{t_1}^{t_2} = \frac{\ln\left(J(t_2)/J(t_1)\right)}{\ln\left(M(t_2)/M(t_1)\right)} \tag{6.12a}$$

where t_1 and t_2 are times when measurements are made. Furthermore,

$$\ln\left(J(t_2)/J(t_1)\right) = \ln\left(C_{avg}^{gw}(t_2)/C_{avg}^{gw}(t_1)\right) \tag{6.12b}$$

$$\ln\left(M(t_2)/M(t_1)\right) = \ln\left(C_{avg}^{soil}(t_2)/C_{avg}^{soil}(t_1)\right) \tag{6.12c}$$

where $C_{avg}^{gw}(t) = avg\left(C_{smp}^{gw}(t)\right)$ and $C_{avg}^{soil}(t) = avg\left(C_{smp}^{soil}(t)\right)$. We may thus substitute (10b) and/or (10c) into (10a) to estimate β from source mass or soil concentration data and source discharge or groundwater concentration data. When limited soil concentration data are available or engineered source mass reduction has occurred, current mass remaining may be computed as

$$M(t_2) = M(t_1) - qL_yL_z\ avg\left(C_{smp}^{gw}(t_1 \ldots t_2)\right) - M_{rem} \tag{6.12d}$$

where $avg\left(C_{smp}^{gw}(t_1 \ldots t_2)\right)$ is the average of all groundwater concentration measurements over the period from t_1 to t_2 and M_{rem} is the quantity of contaminant mass removed by source remediation efforts such as excavation or thermal treatment. The accuracy of β estimates made from various forms of (10) will improve as $t_2 - t_1$ increases, or more specifically as the mass reduction ratio $1 - M(t_2)/M(t_1)$ increases. Ratios greater than 20-30% are more likely to yield reliable β estimates.

A more flexible approach to estimate J_{cal}, M_{cal}, and β simultaneously from soil and/or groundwater data available at multiple dates is to employ the above methods to obtain initial parameter estimates and then employ a nonlinear regression method to further refine parameters. This has been implemented in an Excel program titled ***Source function parameter estimation from field data.xlsm*** which employs measured soil and groundwater concentrations from a source area to estimate source parameters that may be taken as prior estimates for use in eq. (6.1) to refine source parameters concurrently with aquifer and other parameters based on site-wide data (Appendix A).

6.3.5 Decide what parameters to calibrate

Having made prior estimates of all parameters, we now need to decide which parameters will be regarded as "known" and which will be refined by calibration to field data. The more parameters we attempt to calibrate and the less constrained they are (i.e., the greater their prior uncertainty), the more likely we are to have an ill-posed inverse problem, which means there may be multiple parameter sets that fit the data equally well or nearly so. So, we need to be selective about what we calibrate.

Recall that since darcy velocity, porosity, and sorption coefficient are linearly related, only one may be calibrated. The parameter with the greatest uncertainty (S_{ln}) should be selected to calibrate, with others fixed at their best estimates.

Two factors determine the priority ranking as to what other parameters should be calibrated. One factor is the parameter uncertainty (S_{ln}) that we have already discussed. The second factor is the sensitivity of the output of interest to the parameter. The product ε of these two factors represents the uncertainty in model output associated with a unit ln standard deviation from the best estimate. We could evaluate ε by determining the mean square deviation between the model and calibration data (or some other statistic) for a "base case" with all parameters at their best estimates minus the same statistic for each parameter at a value one ln standard deviation above its best estimate. Parameters with the highest ε should be calibrated, while the lowest may be fixed at their best estimate. An alternative but less rigorous method to rank parameters to calibrate is to consider only the parameter uncertainty.

Either way, the cutoff for the number of parameters to calibrate will depend on how well-posed (or ill-posed) the inverse problem is, which depends on the quality of the calibration data. A practical way to decide how many parameters to calibrate is to compare the total model variance $S^2_{\ln tot}$ for calibrations performed using the same regression dataset with different calibrated parameter sets, computed as

$$S^2_{\ln tot} = S^2_{\ln reg} + S^2_{\ln par} \tag{6.13}$$

where $S_{\ln.reg}$ is the log standard deviation of the regression (root mean square deviations between model and measurements), and $S_{\ln.par}$ is log standard deviation associated with parameter uncertainty computed from the parameter covariance matrix and average parameter sensitivities as described in section 6.4.3. Since our goal is to minimize total uncertainty, parameters should only be calibrated if they produce a decrease in $S_{\ln tot}$. As the number of parameters increases, $S_{\ln.reg}$ will decrease monotonically, although the magnitude of reduction will gradually diminish. On the other hand, $S_{\ln.par}$ will generally increase with more parameters as the covariance matrix grows. The optimum parameterization occurs when a increase in $S_{\ln.par}$ overtakes a decrease in $S_{\ln.reg}$. (see Figure 6.6 in section 6.4 of this chapter).

6.3.6 Calibration data averaging and weighting

The calibration data file will include a list of concentration measurements from field samples with their respective survey coordinates, depths below groundwater, and sample dates. Various types of data may be specified including resident concentrations, flux concentrations, soil concentrations, etc. Measurements for water samples taken from monitoring wells or extraction devices are best regarded as flux concentrations.

An important consideration in setting up a calibration problem involves the handling of non-detects. We advise to input non-detect concentrations as values equal to 20% of the detection limit and to set a minimum model concentration equal to 20% lower (i.e., 4% of the non-detect concentration). Any model predicted concentrations less than the prescribed minimum will be set to the minimum value for purposes of computing calibration deviations. This approach reasonably represents non-detects, and prevents simulated concentrations that may be many orders of magnitude smaller than the detection limit from inordinately influencing the calibration.

Although individual measurements may be input for calibration, if multiple samples have been taken annually over a substantial number of years, computational time will be much faster if annual average concentrations are input. Averaging also reduces calibration data "noise," which can help

stabilize the inverse problem. For each data point in the calibration input, the user must specify the number of underlying samples N_{smp} – i.e., 1 for a single sample, 2 for semi-annual averages, 4 for quarterly sample averages, etc.

Also, for each calibration data point, the user must specify a prior estimate of the ln standard deviation between the single measurements and model predictions ($S_{ln\ cal\ prior}$). For a given sampling method, the same $S_{ln\ cal\ prior}$ value is input regardless of the number of samples averaged to obtain the data value. Many factors can affect $S_{ln\ cal\ prior}$ including well or push probe diameter, screen or sample length, purge volume, soil vs. water samples, etc. Note that for a given sampling method, the input value of $S_{ln\ cal\ prior}$ will be the same regardless of the number of samples averaged for the data point.

Finally, for each data point in the calibration file, the user can specify an optional user weight W_{user} to give more or less weight to certain data – e.g., for "key" wells or to put more weight on low concentrations to better delineate the plume perimeter. The net weight applied to each calibration data point is computed internally as

$$W_{net} = \frac{W_{user} N_{smp}^{1/2}}{S_{\ln cal}} \tag{6.14}$$

where $S_{ln\ cal} = S_{ln\ cal\ prior}$ for the first regression iteration. The regression data set is divided into sampling method groups that have the same $S_{ln\ cal\ prior}$ values. After each iteration, posterior estimates of $S_{ln\ cal}$ are computed from the current regression results for each sampling method group. The values are iteratively refined and final values $S_{ln\ cal\ post}$ are reported with the final calibration results.

6.3.7 Calibration verification and refinement

After a calibration run has been performed, a log-log plot of observed versus simulated concentrations should be inspected. Ideally, a regression of the scatter plot should have a slope close to 1 and an intercept close to 0 – i.e., it should center on a 1:1 line with equal scatter above and below independent of concentration. If there is bias in the scatter, additional weight may be applied to data points within specified concentration ranges to help reduce the bias. For example, if concentrations between 100-1000 scatter evenly about the 1:1 line, while values <100 and >1000 are biased above or below the 1:1 line, additional weight may be applied to values <100 and >1000. Weights may be adjusted by trial and error to minimize the sum of squared deviations between the model and data, regression coefficient, or other relevant statistic. Time series plots for "representative" sample locations should also be inspected to verify that time-trends are reasonably captured by the model.

Ideally, a well calibrated model will have a symmetric scatter plot with a majority of data points within about one order-of-magnitude of the 1:1 line and with reasonably consistent time-trends. Models with larger scatter, noisier time trends and minor deviations from the 1:1 line will result in greater prediction uncertainty. Results that show substantial deviations from the 1:1 line are more problematic. In some cases, the problem may be attributable to excessively noisy or insufficient calibration data (e.g., too few or poorly placed observation locations and/or data spanning too short a time-period). Deviations from the 1:1 line or failure to capture general time trends may reflect

deviations from the conceptual model, in which case Step 1 should be reviewed—especially source parameterization and aquifer description, including flow direction and curvature.

To test for non-uniqueness, it is advisable to run inverse solutions starting from different initial values within the prior confidence bands. For example, instead of starting from geometric mean values, randomly select starting values that are within one standard deviation of the prior best estimate. If you get widely different parameter estimates that produce divergent simulation results over time, it may be helpful to reduce the number of parameters being calibrated (i.e., make sure parameters being calibrated produce a lower information criterion as defined by eq. (6.13)). If this fails, additional data may be necessary to improve the model calibration.

6.4 Example application for hypothetical multi-source problem

The objective of this problem is to investigate tradeoffs between DNAPL source model, calibration data, and the accuracy and precision of predicted mass discharge over time. We also address the problem of identifying optimal model formulation and data collection strategies considering prediction uncertainty and cost-benefits of data collection.

6.4.1 Synthetic data sets

A hypothetical problem is considered for a large industrial site involving multiple TCE sources within a roughly 120,000 m^2 area (Figure 6.2) with different location coordinates, areal and vertical extents, release dates, initial masses, and dissolution kinetics (Table 6.1). The depletion coefficient β ranges from 0.6 (pools/lenses) to 1.35 (residual NAPL), representing a range of DNAPL "architectures." Sources 1-3 occur within the upper third of the aquifer ("shallow zone" 0-4 m below water table), Sources 4-6 occur within the "intermediate zone" (4-8 m below water table), and source 7 occurs in the "lower zone" (8-12 m below water table). Source 1, which is the larger source in the shallow zone, may be attributable due to multiple releases at the ground surface, a large buried source, or a waste disposal pond. Source 5 represents vertical DNAPL migration from Source 1. Sources 2 and 3 are less areally extensive releases with smaller total mass than Source 1. Sources 4 and 5 and 6 represent vertical DNAPL migration from Sources 2 and 3, respectively. The shallow and intermediate zones are assumed to be characterized by thin discontinuous fine-grained material interbedded in a permeable matrix with most DNAPL occurring in small pools or lenses (only source 4 in the intermediate zone is dominated by residual DNAPL). Interbedding is assumed to be absent from the lower zone, such that vertical migration from sources 5 and 6 results in predominantly residual DNAPL in source 7.

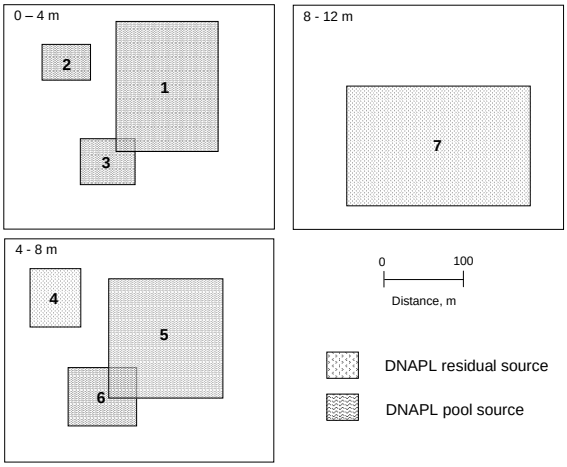

Figure 6.2. Plan view of DNAPL source zones for example problem.

Table 6.1. "True" source parameters for synthetic problem.

	Sources						
	1	2	3	4	5	6	7
Release date, t_{oi} (years)	1966	1962	1960	1965	1969	1960	1971
x coordinate, x_{oi} (m)	10,308	10,111	10,205	10,092	10,322	10,214	10,358
y coordinate, y_{oi} (m)	5,017	5,027	4,865	5,044	4,987	4,863	4,920
Mass flux at toi, J_{oi} (kg/d)	0.153	0.045	0.030	0.073	0.118	0.131	0.069
Source mass on toi, M_{oi} (kg)	1,333	174	242	283	958	409	1,110
Source depletion exponent, β_i	0.60	0.70	0.80	1.10	0.60	0.75	1.35
Source width, L_{yi} (m)	116	32	40	52	108	52	108
Depth (m)	0–4	0–4	0–4	4–8	4–8	4–8	8–12

With 7 parameters per source zone, the combined DNAPL source is described by a total of 49 parameters (not counting aquifer parameters). Thus, although the model formulation is highly idealized, it remains much too complex to calibrate with realistically attainable data without simplification. Synthetic data sets will be used to evaluate the effect of various simplified parametric formulations on prediction uncertainty. TCE concentrations in 22 fully screened monitoring wells were simulated for each year from 1987 to 2009 using the 7-source model assuming v = 0.1 m/d, ϕ = 0.3, R = 1.2, A_L = 120 m, A_T = 16 m, L_Z = 12 m, and x_{12} = 1000 m.

The aquifer is assumed to be aerobic with reductive dechlorination rates of λ_1 = 0.0003 d^{-1} near the source and λ_2 = 0.0001 d^{-1} further downgradient. Log-normally-distributed "noise" in TCE concentrations with a ln-standard deviation (S_{ln}) of 0.8 was assumed to represent conceptual and sampling/measurement error in the synthetic monitoring data. Well locations and "measured" (noisy) concentrations in 2009 are illustrated in Figure 6.3.

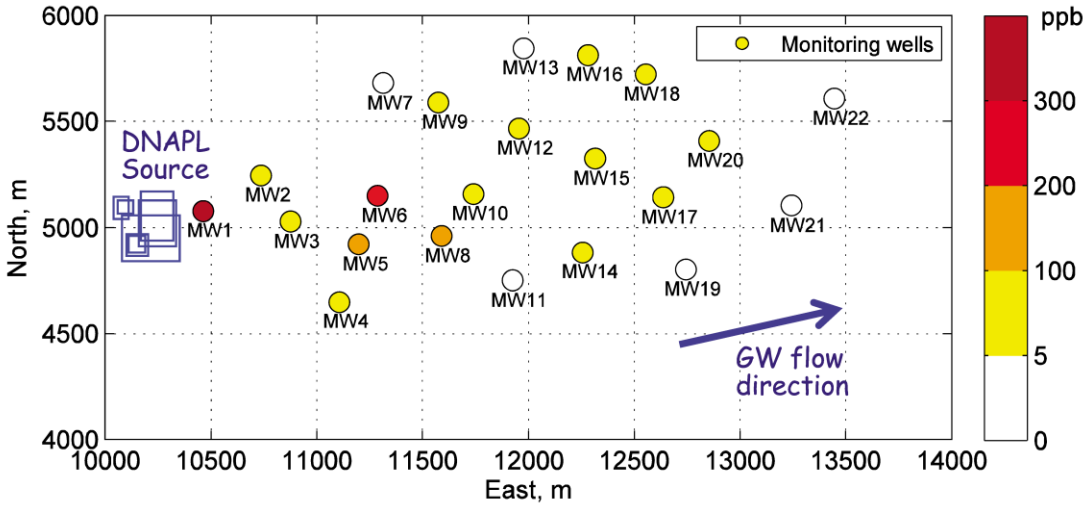

Figure 6.3. Locations of monitoring wells and TCE concentration data in 2009.

In addition to dissolved concentrations from monitoring wells, quarterly measurements of TCE discharge rates from sources were assumed to be obtained from 2005 through 2009 over three depth intervals from a line of multilevel wells across the width of the combined source zones. Data were generated for a depth of 0 to 4 m (representing totals from sources 1-3), 4 to 8 m (representing sources 4-6), and 8 to 12 m (representing source 7 only). High noise mass discharge data were generated with S_{ln} = 0.83 to represent discharge rates estimated from dissolved concentration data and average estimated groundwater velocity. Since actual groundwater velocity at each sampling location will deviate from the estimated average (which is also uncertain), the noise level for these discharge estimates is assumed to be greater than the noise used to generate dissolved concentration "data" from the model. Low noise mass discharge "data" with S_{ln} = 0.24 were generated to represent more accurate direct measurements (Basu et al. 2006, Cho et al. 2007).

6.4.2 Model calibration

The simplest and most straightforward approach to calibrating source model parameters to enable forward estimates of source mass discharge rate versus time is to estimate J_{cal}, M_{cal} and β from field measurements of discharge rate over a period of time for a given source (or combination of sources) to match model predictions. Note that t_{cal} is arbitrary and that in this case the release date, source coordinates and source width cannot be calibrated nor are they needed for forward predictions of mass discharge.

A practical limitation of the foregoing approach is that accurate source flux estimates are rarely available for a very long period if at all, which makes the inverse problem ill-posed, resulting in poor parameter estimates. More seriously, this calibration approach sidesteps the more important problem of predicting future behavior of the dissolved phase plume and disregards information content inherent in monitoring well data, which is more extensive and usually available for a considerably longer time period. These drawbacks can be diminished by simultaneously calibrating source parameters and dissolved plume parameters in the coupled DNAPL source and dissolved transport model (Chapter 2) to fit measured contaminant concentrations and source flux data, if available, using the inverse solution algorithm described by eq. (6.1). We assume that the synthetic data set described in the previous section describes the "real" system.

The "real" system in our hypothetical problem is characterized by a total of 59 parameters (7 for each source plus 10 aquifer parameters). It should be clear that we have little hope of estimating these many unknowns with realistically attainable prior information and calibration data. We must therefore use a simplified model. Of course, reality is infinitely more complicated than our hypothetical problem such that even the most complex model may be a gross simplification. However, as we shall see, our problem will serve its illustrative purpose. In this study, we consider the following different model formulations:

Case 1-3. Single source with 3 parameters – Single source described by J_{cal1}, M_{cal1} and β_1.

Case 1-10. Single source with 10 parameters – Single source described by J_{ca1l}, M_{cal1}, β_1 and t_{o1} plus aquifer parameters q, α, ρk_d, A_L, A_T, and $\lambda_1=\lambda_2$.

Case 2-13. Two sources with 13 parameters – Two source functions described by J_{ca1l}, J_{ca12}, M_{cal1}, M_{cal2}, β_1, β_2 and $t_{o1}=t_{o2}$ plus aquifer parameters q, α, ρk_d, A_L, A_T, and $\lambda_1=\lambda_2$.

Case 3-16. Three sources with 16 parameters – Three source functions described by J_{ca1l}, J_{ca12}, J_{ca13}, M_{cal1}, M_{cal2}, M_{cal3}, β_1, β_2, β_3 and $t_{o1}=t_{o2}=t_{o3}$ plus aquifer parameters q, α, ρk_d, A_L, A_T, and $\lambda_1=\lambda_2$.

Case 3-21. Three sources with 21 parameters – Three source functions described by J_{ca1l}, J_{ca12}, J_{ca13}, M_{cal1}, M_{cal2}, M_{cal3}, β_1, β_2, β_3, $t_{o1}=t_{o2}=t_{o3}$, $x_{o1}=x_{o2}=x_{o3}$, $y_{o1}=y_{o2}=y_{o3}$, and $L_{y1}=L_{y2}=L_{y3}$ plus aquifer parameters q, α, ρk_d, A_L, A_T, λ_1, λ_2 and L_{12}.

Case 3-27. Three sources with 27 parameters – Three source functions described by J_{ca1l}, J_{ca12}, J_{ca13}, M_{cal1}, M_{cal2}, M_{cal3}, β_1, β_2, β_3, t_{o1}, t_{o2}, t_{o3}, x_{o1}, x_{o2}, x_{o3}, y_{o1}, y_{o2}, y_{o3}, L_{y1}, L_{y2} and L_{y3} plus aquifer parameters q, α, ρk_d, A_L, A_T, λ_1, λ_2 and L_{12}.

The single source three-parameter model was calibrated to source flux data only with two variants:

Data set a – high variance source flux data only (J_{hi})

Data set b – low variance source flux data only (J_{lo})

The other models require dissolved plume data to calibrate transport-related parameters, but may also employ source flux data. For Cases 1-10 and higher, the following calibration data sets were employed

Data set c – Monitoring well concentration data only (C)

Data set d – Monitoring well data and high variance source flux data ($C+J_{hi}$)

Data set e – Monitoring well data and low variance source flux data ($C+J_{lo}$).

This results in additional model formulation and data set combinations (e.g., Cases 1-10c, 1-10d). For cases with three source functions, Source 1 is assumed to represent DNAPL from 0 to 4 m below the water table, Source 2 from 4 to 8 m deep, and Source 3 from 8 to 12 m. For cases with two source functions, Source 1 is assumed to represent DNAPL between 0 to 8 m deep – hence flux data for 0 to 4 m and 4 to 8 m are added. For cases in which a single source function is assumed, flux data is summed across all depths. Calibration results for more than three sources are not presented, as the inverse problem was poorly posed due to the large number of unknown parameters.

In addition to the synthetic field data described above that can be used for calibration by comparing with model predictions, we assume that site characterization and literature studies yield prior estimates of model parameters – some with fairly narrow confidence limits and others with large error bounds. For example, porosity can generally be estimated within a narrow range from boring logs with limited core testing, average groundwater velocity can often be estimated with somewhat greater uncertainty via hydraulic tests and water level data, while initial source mass estimates are usually highly uncertain. For each model formulation studied, prior estimates of parameter uncertainty and (biased) initial estimates of parameters themselves were assumed that are deemed to be typical of prior information available at many sites. For the simpler model formulations, prior values of non-calibrated parameters were treated as "known" and remained fixed during calibration. For calibrated parameters, prior estimates serve as initial guesses to be refined by calibrating to the available data subject to the constraint imposed by penalty term in (6.1).

Results from 13 calibration cases will be discussed here. A summary of the model formulations, calibration data employed, prior information assumed, and final parameter estimates is given in Table 6.2. For all cases, t_{cal} = 2009 was assumed.

6.4.3 Accuracy and precision of mass discharge predictions

After performing model calibration, combined total TCE mass discharge from the source zones was computed through year 2100 using the calibrated parameters. Prediction precision was quantified by

$$S^2_{\ln tot_k} = S^2_{\ln reg_k} + S^2_{\ln par_k} \tag{6.15}$$

where $S_{\ln tot_k}$ is the total ln uncertainty is source discharge on date $t=t_k$, $S_{\ln par_k}$ is the error due to parameter uncertainty, and $S_{\ln reg_k}$ is the residual regression error. The regression variance for prediction k with independent variables (x_k, y_k, t_k) is computed as

$$S^2_{\ln reg_k} = MSE\left(1+\frac{1}{N_o}+\frac{(x_k-\bar{x})^2}{\sum_{i=1}^{N_o}(x_i-\bar{x})^2}+\frac{(y_k-\bar{y})^2}{\sum_{i=1}^{N_o}(y_i-\bar{y})^2}+\frac{(t_k-\bar{t})^2}{\sum_{i=1}^{N_o}(t_i-\bar{t})^2}\right) \tag{6.16}$$

where i =1 to N_o refers to observations used for calibration, overbars signify averages over the calibration data set, and MSE is the mean square error in concentrations used for calibration, computed as

$$MSE = \frac{\sum_{i=1}^{N_o}(\ln C_{obs\ i} - \ln C_{pred\ i})^2}{N_o - N_p}. \tag{6.17}$$

where N_p is the number of calibrated parameters. Error due to parameter uncertainty is estimated using a first-order error propagation method (e.g., Unlu et al., 1995), given in matrix notation as

$$\mathbf{S}^2_{P\ \ln C} = \mathbf{J^T Cov\ J} \tag{6.18}$$

where the LHS is a vector of variances due to parameter uncertainty for all predictions of interest, **J** is a Jacobian matrix, and **Cov** is the parameter covariance matrix. Terms in the Jacobian are

$$J_{ij} = \frac{\partial \ln C_i}{\partial P_j} \tag{6.19}$$

where C_i is the ith prediction and P_j denotes the jth uncertain parameter, which as previously noted is either the actual parameter value or its natural logarithm depending on the variable. The covariance matrix is estimated as

$$\mathbf{Cov} = MSE\left(\mathbf{J^T J}\right)^{-1}. \tag{6.20}$$

One-sigma error bars on model predictions prior to, during and after the calibration period are shown for selected calibration cases in Figure 6.4 along with the "true" behavior, which is known for our hypothetical problem. Average values of $S_{T\ln J_k}$ for post-calibration dates between t_k = 2010 to 2100 (i.e., "out-of-sample" predictions) are tabulated for all cases in Table 6.2.

The true discharge curves (Figure 6.4) exhibit a distinct change in slope on the semi-log scale after 2025, reflecting the increasing dominance of fluxes from low β pools in Source 7 as the shallower lower β sources become nearly depleted. Not surprisingly, the single source function models are not able to capture this trend change. The 3-parameter single source models calibrated to J data only (Cases 1-3a and 1-3b) perform particularly poorly, predicting discharge rates <1 g/d by 2060,

whereas the true discharge does not reach this level for another 130 years in 2190 (not shown in figures). Using lower variance *J* data (Case 1-3b) improved prediction precision somewhat (i.e., lower prediction uncertainty), but did not improve accuracy.

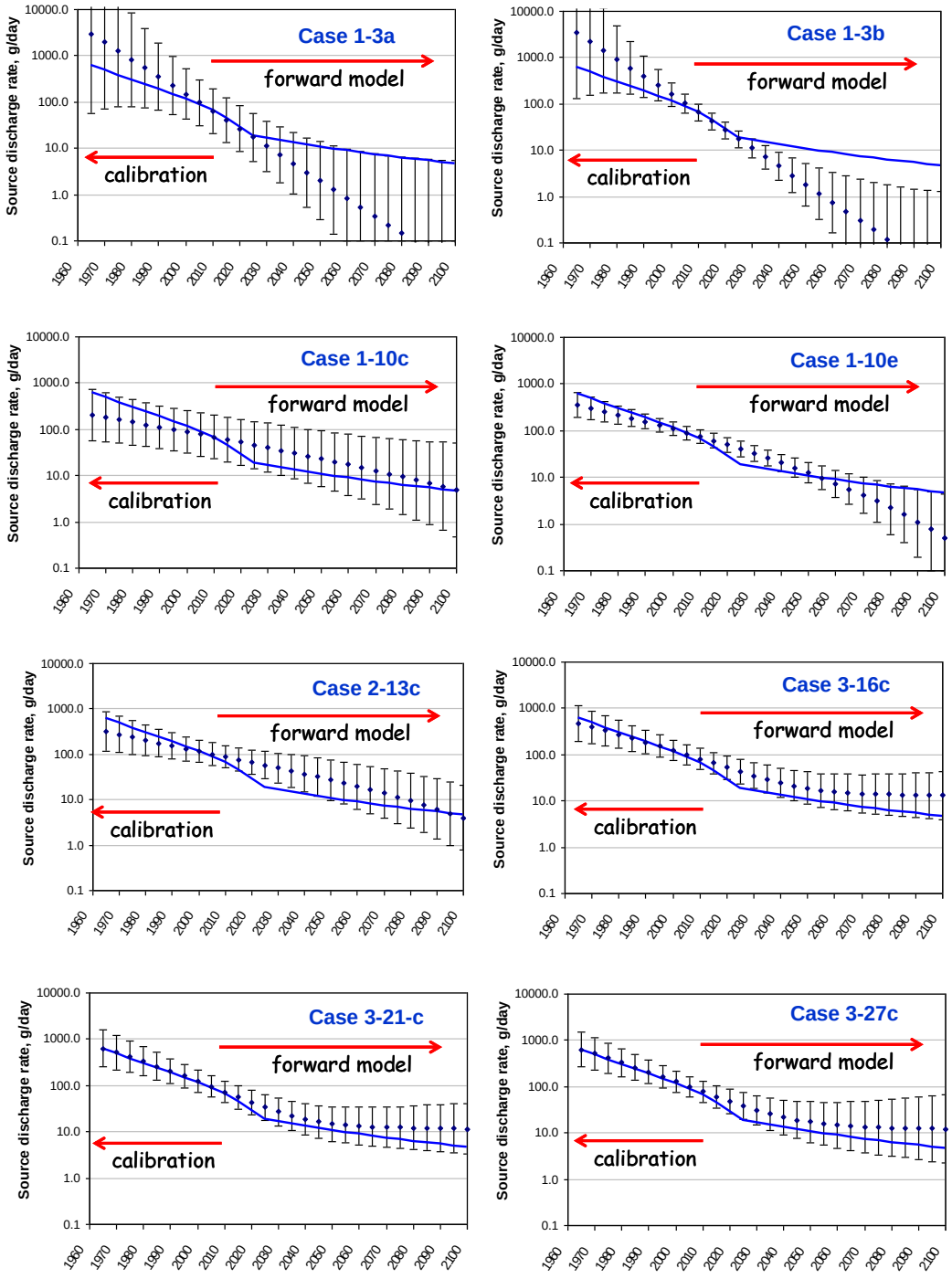

Figure 6.4. One-sigma error bars for predicted total TCE discharge from source zone vs. time for selected calibration cases. Solid points are best estimates for the calibrated model and smooth blue lines are "true" discharge for the exact multi-source functions.

Table 6.2. Summary of calibration analysis results.

	Case 1–3a		Case 1–3b		Case 1–10c		Case 1–10d		Case 1–10e		Case 2–13c		Case 2–13e		Case 3–16c		Case 3–16e		Case 3–21c		Case 3–21e		Case 3–27c		Case 3–27e	
Data	high var J		low var J		C only		C + high var J		C + low var J		C only		C + low var J		C only		C + low var J		C only		C + low var J		C only		C + low var J	
Sources	1		1		1		1		1		2		2		3		3		3		3		3		3	
Parameters	3		3		10		10		10		13		13		16		16		21		21		27		27	
Final avg $S_{\ln J}$	2.57		1.65		1.58		1.55		0.83		1.09		0.64		0.86		0.46		0.89		0.45		1.08		0.67	
	Case 1–3a		Case 1–3b		Case 1–10c		Case 1–10d		Case 1–10e		Case 2–13c		Case 2–13e		Case 3–16c		Case 3–16e		Case 3–21c		Case 3–21e		Case 3–27c		Case 3–27e	
Parameters	Prior[a]	Final	Prior[a]	Final	Prior[a]	Final	Prior[a]	Final	Prior[a]	Final	Prior[a]	Final	Prior[a]	Final	Prior[a]	Final	Prior[a]	Final	Prior[a]	Final	Prior[a]	Final	Prior[a]	Final	Prior[a]	Final
J_{cal1} (kg/d)	0.132	0.070	0.132	0.072	0.132	0.07	0.132	0.072	0.132	0.077	0.068	0.043	0.068	0.044	0.068	0.045	0.068	0.027	0.068	0.041	0.068	0.027	0.068	0.042	0.068	0.027
M_{cal1} (kg)	270	902	270	296	270	902	270	964	270	634	65	547	65	166	65	268	65	120	65	187	65	110	65	257	65	116
b_1 (−)	1.00	0.90	1.00	1.00	1.00	0.90	1.01	0.91	1.01	0.87	0.90	0.73	0.90	0.80	0.90	0.83	0.90	0.86	0.90	0.84	0.90	0.83	0.90	0.83	0.90	0.86
t_{o1} (yr)	NA		NA		1965	1965	1965	1965	1965	1968	1965	1968	1965	1972	1965	1970	1965	1973	1965	1963	1965	1965	1965	1964	1965	1964
X_{o1} (m)	NA		NA		= 10226		= 10226		= 10226		= 10226		= 10226		= 10226		= 10226		10226	10231	10226	10229	10226	10230	10226	10231
Y_{o1} (m)	NA		NA		= 5021		= 5021		= 5021		= 5021		= 5021		= 5021		= 5021		5021	4996	5021	4991	5021	5005	5021	4963
L_{y1} (m)	NA		NA		= 500		= 500		= 500		= 500		= 500		= 500		= 500		500	260.78	500	240.6	500	347.56	500	301.7
J_{cal2} (kg/d)	NA		NA		NA		NA		NA		0.039	0.048	0.039	0.026	0.034	0.023	0.034	0.018	0.034	0.021	0.034	0.018	0.034	0.024	0.034	0.018
M_{cal2} (kg)	NA		NA		NA		NA		NA		105	523	105	290	30	124	30	43	30	108	30	41	30	90	30	42
b_2 (−)	NA		NA		NA		NA		NA		1.10	1.01	1.10	1.08	0.90	0.84	0.90	0.81	0.90	0.86	0.90	0.79	0.90	0.84	0.90	0.81
t_{o2} (yr)	NA		NA		NA		NA		NA		= t_{o1}		= t_{o1}		= t_{o1}		= t_{o1}		= t_{o1}		= t_{o1}		= t_{o1}		= t_{o1}	
X_{o2} (m)	NA		NA		NA		NA		NA		= X_{o1}		= X_{o1}		= X_{o1}		= X_{o1}		= X_{o1}		= X_{o1}		10226	10227	10226	10147
Y_{o2} (m)	NA		NA		NA		NA		NA		= Y_{o1}		= Y_{o1}		= Y_{o1}		= Y_{o1}		= Y_{o1}		= Y_{o1}		5021	5011	5021	5011
L_{y2} (m)	NA		NA		NA		NA		NA		= L_{o1}		= L_{o1}		= L_{o1}		= L_{o1}		= L_{o1}		= L_{o1}		500	350	500	379
J_{cal3} (kg/d)	NA		NA		NA		NA		NA		NA		NA		0.039	0.017	0.039	0.0260	0.039	0.015	0.039	0.0268	0.039	0.016	0.039	0.026
M_{cal3} (kg)	NA		NA		NA		NA		NA		NA		NA		105	2225	105	294	105	2027	105	2290	105	1937	105	291
b_3 (−)	NA		NA		NA		NA		NA		NA		NA		1.10	1.00	1.10	1.00	1.10	1.00	1.10	1.00	1.10	1.00	1.10	1.00
t_{o3} (yr)	NA		NA		NA		NA		NA		NA		NA		= t_{o1}		= t_{o1}		= t_{o1}		= t_{o1}		= t_{o1}		= tol	
X_{o3} (m)	NA		NA		NA		NA		NA		NA		NA		= X_{o1}		= X_{o1}		= X_{o1}		= X_{o1}		10226	10227	10226	10199
Y_{o3} (m)	NA		NA		NA		NA		NA		NA		NA		= Y_{o1}		= Y_{o1}		= Y_{o1}		= Y_{o1}		5021	5013	5021	5014
L_{y3}	NA		NA		NA		NA		NA		NA		NA		= L_{o1}		= L_{o1}		= L_{o1}		= L_{o1}		500	398	500	413
q (m/d)	NA		NA		0.035	0.041	0.035	0.041	0.035	0.052	0.035	0.053	0.035	0.055	0.035	0.055	0.035	0.057	0.035	0.033	0.035	0.031	0.035	0.032	0.035	0.032
a (deg)	NA		NA		−8.8	−7.8	−8.8	−7.8	−8.8	−7.7	−8.8	−7.7	−8.8	−7.8	−8.8	−7.7	−8.8	−7.8	−8.8	−8.5	−8.8	−8.6	−8.8	−8.1	−8.8	−8.3
L_z (m)	NA		NA		= 12		= 12		= 12		= 12		= 12		= 12		= 12		= 12		= 12		= 12		= 12	
f (−)	NA		NA		= 0.33		= 0.33		= 0.33		= 0.33		= 0.33		= 0.33		= 0.33		= 0.33		= 0.33		= 0.33		= 0.33	
r k_d (−)	NA		NA		0.10	0.09	0.10	0.09	0.10	0.09	0.10	0.09	0.10	0.09	0.10	0.09	0.10	0.09	0.10	0.09	0.10	0.09	0.10	0.09	0.10	0.09
A_L (m)	NA		NA		50	160.4	50	162.6	50	143	50	137.8	50	160	50	149.9	50	173	50	151.4	50	165.4	50	156	50	144.4
A_T (m)	NA		NA		10	8	10	8.1	10	7.3	10	7.3	10	7.6	10	7.5	10	7.9	10	16.2	10	18.1	10	14.5	10	13.4
g_1 (1/d)	NA		NA		0.0001	0.00014	0.0001	0.00014	0.0001	0.00018	0.0001	0.00017	0.0001	0.00022	0.0001	0.00020	0.0001	0.00025	0.0001	0.00027	0.0001	0.0003	0.0001	0.00027	0.0001	0.00031
g_2 (1/d)	NA		NA		= g_{T1}		= g_{T1}		= g_{T1}		= g_{T1}		= g_{T1}		= g_{T1}		= g_{T1}		0.0001	0.00013	0.0001	0.00014	0.0001	0.00012	0.0001	0.00013
L_{12} (m)	NA		NA		NA		NA		NA		NA		NA		NA		NA		500	1070	500	1071	500	1069	500	1149

[a]Prior values preceded by an equal sign denote values that were fixed at the prior estimate during calibration; NA indicates parameters that are not relevant for a specific case.

Calibrating the single source model with plume *C* data only (Case 1-10c) substantially improved long-term accuracy compared to the 3-parameter models calibrated with near-source *J* data only (Cases 1-3). Using low quality (high noise) source zone discharge measurements in addition to plume *C* data (Case 1-10d) yielded an insignificant reduction in prediction uncertainty compared with plume *C* data only (Case 1-10c), indicating that the low-quality source discharge measurements conveyed little additional information for calibration. However, high-quality source discharge measurements in conjunction with plume data (Case 1-10e) reduced prediction uncertainty approximately in half.

Adding second and third source functions (Cases 2-13c and 3-16c) resulted in progressive reductions in uncertainty as well as improved prediction accuracy. Increasing the number of parameters in the three-source model to 21 (Case 3-21c) resulted in little change in precision or accuracy. Further parameter additions (Case 3-27c) also yielded little change in accuracy, but yielding a notable increase in prediction uncertainty.

The foregoing results demonstrate that the quality and quantity of data available for model calibration has a strong effect on the accuracy and precision of out-of-sample predictions. This is clearly illustrated by comparing the average S_{TlnJ} for TCE discharge predictions (post-calibration) for the five single-source model formulations (Cases 1-3a, 1-3b, 1-10c, 1-10d, and 1-10e), which incrementally employ more and/or higher quality data (Figure 6.5). The results reveal monotonically diminishing out-of-sample prediction uncertainty as the quantity and quality of data increase while using the same source model formulation.

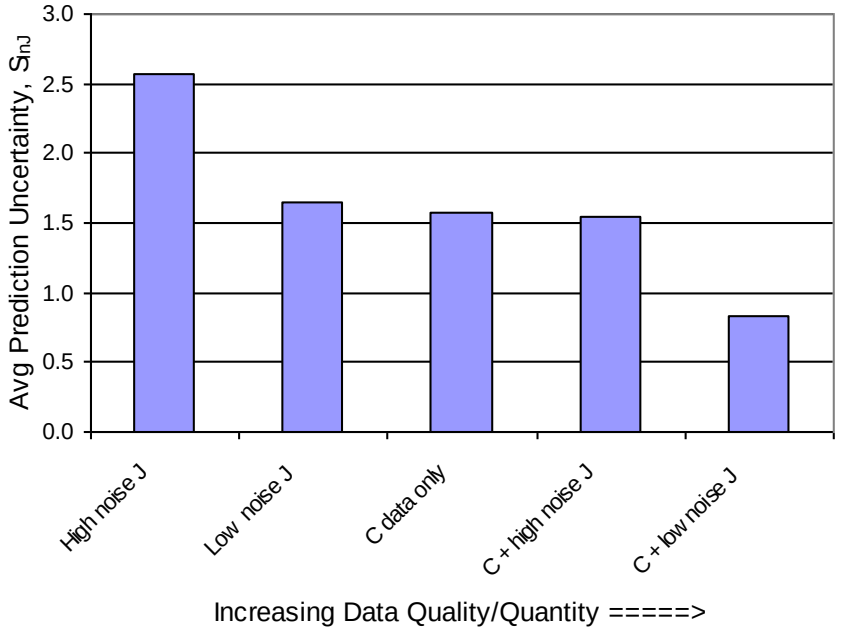

Figure 6.5. Effect of increasing data quality/quantity on average prediction uncertainty for single source models (Cases 1-3a, 1-3b, 1-10c, 1-10d, 1-10e from left to right).

6.4.4 What is the optimal conceptual model formulation?

Now, let us turn to the somewhat philosophical question of defining the "best" model formulation. Scientific purists may contend that the "best" model is the one that describes all processes of interest with the greatest rigor known to science, and hence that presents the truest possible depiction of reality. From this perspective, the notion of an "optimal" model may seem like statistically inspired heresy. However, it is beneficial to reflect that all mathematical models are by definition simplifications of reality that attempt to predict a limited number of dependent variables in response to a limited number of independent variables within limited time and space scales. From a practical perspective, mathematical models serve as tools to predict system responses to certain variables to facilitate real-world decision-making.

For the moment, let us define "best" as the model that gives the lowest uncertainty in predictions of interest for a given set of data that is available for calibrating uncertain model coefficients. For the case addressed in this paper, let us assume that future source mass discharge is the output that we are interested in predicting. Figure 6.6 plots average out-of-sample prediction uncertainty (S_{TlnJ}) for models with a range of complexity, as represented by the number of calibrated parameters. Using monitoring well concentration data only, Cases 1-10c, 2-13c, 3-16c, 3-21c, and 3-27c exhibit a minimum prediction uncertainty with 16 calibrated parameters. Prediction uncertainty increases sharply for simpler models and more gradually for models with more parameters, but it is clear that too much as well as too little complexity can adversely affect model precision.

Using concentration data plus low variance source flux measurements for calibration, Cases 1-10e, 2-13e, 3-16e, 3-21e, and 3-27e exhibit similar behavior to the C-data only, except that the optimum model shifts to 21 parameters with a minimum prediction uncertainty that is about 40% less than when only concentration data is available (Figure 6.6). The results suggest that an optimal model complexity exists that will minimize total prediction uncertainty for a given set of calibration data. Adding further complexity to the model beyond this optimum not only does not improve model predictions, but actually induces *greater* uncertainty. The only way to reduce prediction uncertainty further is to obtain more and/or better data to support calibration of a more rigorous model.

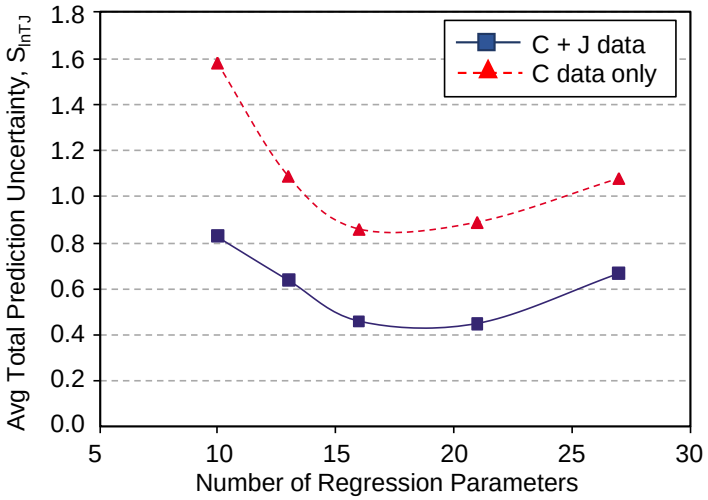

Figure 6.6. Prediction uncertainty vs. number of fitted parameters for 1, 2 and 3 source models using C data only (triangle) or C data plus low noise J data (square).

Extrapolation of the above results suggests that perfect predictions may be possible if unlimited, error-free data were available to calibrate a model that rigorously represents reality. Unfortunately, real data is subject to error and costs time, effort and money to collect and process. Therefore, the optimal model complexity will ultimately depend on tradeoffs between the cost of collecting specific additional data versus the value of the data in terms of the benefits resulting from improvements in prediction precision and accuracy. Since the value of model improvements clearly depend on the models' application and purpose, the "best" model must be viewed an elastic concept that depends on the specific objectives of the model.

To investigate the effect of problem specific objectives on model selection and the value of additional data, let us return to our example problem and consider the use of our source zone model to guide remediation decisions. For this purpose, assume that natural processes at the site have been determined to be capable of attenuating source zone discharge of up to 1 g/d. We wish to evaluate costs for the following remediation options and illustrative cost functions:

Permeable Reactive Barrier (PRB). A reactive barrier is installed and operated downgradient of the source until the source discharge is <1 g/d. The cost is $200k fixed cost + $100k/yr.

Partial Source Reduction (PSR). Source zone thermal treatment is performed to reduce contaminant discharge to <1 g/d. The cost is $2,400k fixed cost + $50k/yr.

Total net present value (NPV) costs are computed with operating costs discounted at 3% per year. Expected (probability-weighted average) cost and 99% upper confidence limit (UCL) cost are tabulated for Cases 3-16c and 3-21e for the two remedial options in Table 6.3. The NPV cost for PRB is higher than for PSR; however, there is very little difference between the expected cost and the UCL despite the sensitivity of PRB duration to uncertainty in source mass. Low sensitivity of NPV cost to source mass uncertainty is due to time discounting. A lower discount rate would sharply increase the UCL as well as the expected cost (due to positive skew in cleanup time). This is a good example of the sensitivity of decision problems on even seemingly minor details of the objective function formulation.

If expected NPV cost is taken as the "best" (unbiased) statistical measure of cost performance, PSR would be selected as the best remedial option regardless of model formulation. Although the estimated PSR *expected* cost is lower for Case 3-16c than for Case 3-21e, the *actual* cost will be the same regardless of the model used because both formulations yield the same decision (i.e., PSR cost < PRB cost for both parameterizations. In this sense, the additional data employed for Case 3-21e (low variance source flux measurements) has no value in terms of the decision outcome or actual cost savings.

However, a risk-averse party may prefer to make decisions that minimize an UCL of cost. Based on the 99% UCL, Case 3-16c indicates the PRB system is slightly preferable to PSR. However, since this decision would be contrary to the choice based on expected cost and also contrary to selecting the lowest UCL PSR cost for Case 3-16c, such a decision looks foolhardy. With regard to the value of collecting data to calibrate Case 3-21e, if one takes into consideration the need to hold cash reserves sufficient to cover the UCL cost, then the value of the low variance flux data for Case 3-21e may be estimated as the difference between the UCL cost for Cases 3-16c and 3-21e times the foregone investment return over the holding period.

So, for this practical example, we find that although Case 3-21e offers significantly lower uncertainty in source mass discharge predictions, the value of this improvement may not warrant

the cost of the additional data needed to support the more complex model. Given different remediation objectives, technologies, unit costs or discount rates that lead to greater decision sensitivity to prediction uncertainty, a higher value of additional information may arise that justifies a more rigorous model.

Table 6.3. Total net present value costs for simplified decision analysis problem.

Model Formulation	PRB Expected Cost	PRB 99% UCL Cost	PSR Expected Cost	PSR 99% UCL Cost
Case 3-16c	$3,390,000	$3,460,000	$2,785,000	$3,556,000
Case 3-21e	$3,415,000	$3,460,000	$2,476,000	$2,629,000

6.5 Summary

The ability to estimate DNAPL source mass discharge versus time from contaminated sites is important to facilitate effective and efficient remediation technology selection and design. Unfortunately, the extreme complexity of source zone "architecture" makes rigorous characterization impractical and mandates adoption of simplified empirical models. The practitioner is faced with a number of difficult questions: How much simplification or complexity is optimal given the remediation objectives, data available and time/cost constraints? What is the uncertainty in predicted performance and how does this affect the decision process? What data should be collected?

The results of this study indicate that source functions calibrated to measured source discharge time-series of relatively short duration have the poorer accuracy and precision than functions calibrated jointly with transport parameters using longer time-series dissolved concentration data from wells over the entire dissolved plume. Accuracy and precision generally improved further when both dissolved concentration data and low variance source discharge measurements were used for calibration. High variance source discharge measurements (e.g., computed from dissolved concentration data and estimated mean groundwater velocity) did not improve predictions. Although we did not directly address the problem of identifying what additional data may be beneficial, the proposed methodology can easily be employed to evaluate the effect of specific additional types of data and sampling locations, frequency, and duration may be most beneficial in terms of reducing prediction uncertainty. Of course, this approach cannot be implemented until some minimum amount of data is available to perform a preliminary calibration. In practice, an iterative approach involving incremental calibration, assessment of data needs, and collection of additional data would likely be most cost effective.

For a given data set available for calibration, an optimal model complexity – as represented by the number of calibrated parameters - was found that minimized forward prediction uncertainty. More complex models (e.g., multiple source functions, spatially variable decay, estimated source coordinates, release dates, etc.) generally reduced prediction uncertainty up to a point beyond which added complexity proved to be a liability unless additional or more accurate data can be obtained. Thus, the "no free lunch" principle exerts its influence when model complexity surpasses the information content of calibration data.

Defining the optimal model formulation and optimal data collection program for a given specific field application requires quantification of the benefit of improved model precision and the cost of additional data. As illustrated by a simple cost analysis problem, the optimal model formulation and data collection depends not only on the site and model characteristics but on remediation objectives, characteristics of specific technologies under consideration, and cost functions. Due to high costs for field data collection, quantification of the monetary value of specific data within the context of model-informed decision analysis deserves more attention. While detailed analyses to determine optimal model formulation may not be justified in many cases, the use of error propagation methods to circumscribe prediction uncertainty holds the potential to greatly improve more-based decisions.

It should be evident that the "best" model cannot be selected based merely on minimization of residual calibration error. The addition of a sufficiently large number of adjustable parameters can always produce vanishingly small residual error. Unfortunately, small calibration error provides no assurance of neither forward prediction accuracy nor precision. Since we do not know the future (and if we did we would have no need for a model), forward accuracy cannot be assessed until after the future arrives. However, we can evaluate forward prediction uncertainty from calibration results, which provides the best means available to assess the utility of a model for forecasting the future. This approach is not foolproof since limited or erroneous data, fundamentally flawed conceptual models (e.g., unidentified sources, misunderstood processes), or just plain bad luck (low probability events outside the confidence bands can occur) can intervene to lead models astray, but we can stack the odds in our favor.

6.6 References

Basu, N. N., P.S.C. Rao, I.C. Poyer, M.D. Annable, and K. Hatfield, 2006, Flux-based assessment of a manufacturing site with trichloroethylene, J. Contam. Hydrol., 86, 105-127.

Basu, N.B, P.S.C. Rao, R.W. Falta, M. D. Annable, J. W. Jawitz, K. Hatfield, 2007, Temporal evolution of DNAPL source and contaminant flux distribution: Impacts of source mass depletion, J Contam Hydrol., 95, 93-109.

Basu, N.B., P.S.C. Rao, I.C. Poyer, S. Nandy, M. Mallavarapu, R. Naidu, G.B. Davis, B.M. Patterson, M.D. Annable and K. Hatfield, 2009, Integration of traditional and innovative characterization techniques for flux-based assessment of dense non-aqueous phase liquid (DNAPL) sites, J. Contam. Hydrol., 105, 161-172.

Brooks, M. C., A. L. Wood, M. D. Annable, K. Hatfield, J. Cho, C. Holbert, P. S. C. Rao, C. G. Enfield, K. Lynch, and R. E. Smith (2008), Changes in contaminant mass discharge from DNAPL source mass depletion: Evaluation at two field sites, J. Contam. Hydrol., 102, 140–153.

Cardiff, M., X. Liu, P. K. Kitanidis, J. Parker, and U. Kim, 2010, Cost optimization of DNAPL source and plume remediation under uncertainty using a semi-analytic model, J. Contam. Hydrol., in press.

Christ, J. A., C. A. Ramsburg, K. D. Pennell, and L. M. Abriola, 2006, Estimating mass discharge from dense nonaqueous phase liquid source zones using upscaled mass transfer coefficients: An evaluation using multiphase numerical simulations, Water Resour. Res., 42, W11420, doi:10.1029/2006WR004886.

Christ, J. A., A. Ramsburg, K. D. Pennell, and L.M. Abriola, 2010, Predicting DNAPL mass discharge from pool-dominated source zones, J. Contam. Hydrol., in press.

Cho, J., M.D. Annable, J.W. Jawitz, and K. Hatfield, 2007, Passive flux meter measurement of water and nutrient flux in porous media, J. Environ. Quality, 36, 1266-1272.

Falta, R. W., P. S. Rao, and N. Basu, 2005a, Assessing the impacts of partial mass depletion in DNAPL source zones: I. Analytical modeling of source strength functions and plume response, J. Contam. Hydrol., 78, 259-280.

Falta, R. W., P. S. Rao, and N. Basu, 2005b, Assessing the impacts of partial mass depletion in DNAPL source zones: II. Coupling source strength functions to plume evolution, J. Contam. Hydrol., 79, 45-66.

Fure, A.D., J. W. Jawitz, and M. D. Annable, 2006, DNAPL source depletion: Linking architecture and flux response, J Contam Hydrol, 85, 118-140.

Jawitz, J. W., A. D. Fure, G. G. Demmy, S. Berglund, and P. S. C. Rao, 2005, Groundwater contaminant flux reduction resulting from nonaqueous phase liquid mass reduction, Water Resour. Res., 41, W10408, doi:10.1029/2004WR003825.

Kool, J. B., J. C. Parker and M. Th. van Genuchten, Parameter estimation for unsaturated flow and transport models: A review, J. Hydrol., 91, 255-293, 1987.

Mishra, S. and J. C. Parker, Parameter estimation for coupled flow and transport, Water Resour. Res., 25, 385-396, 1989.

Park, E. and J. C. Parker, 2005, Evaluation of an upscaled model for DNAPL dissolution kinetics in heterogeneous aquifers, Adv. in Water Resources., 28, 1280-1291.

Parker, J. C. and E. Park, 2004, Field-scale DNAPL dissolution kinetics in heterogeneous aquifers, Water Resources Research, vol 40, W05109, doi:10.1029/2003WR002807.

Park, E. and J. C. Parker, Effects of mass reduction, 2008, flow reduction and enhanced biodecay of DNAPL source zones, Transport in Porous Media, 73, 95-108.

Parker, J. C., E. Park, and G. Tang, 2008, Dissolved plume attenuation with DNAPL source remediation, aqueous decay and volatilization – Analytical solution, model calibration, and prediction uncertainty. Journal of Contaminant Hydrology 102, 61-71.

Parker, J. C., U. Kim, P. K. Kitanidis, M. Cardiff, and X. Liu, Stochastic cost optimization of multi-strategy DNAPL site remediation, Ground Water Monitoring & Remediation, 3, 65-78, 2010.

Parker, J. C., U. Kim, M. Widdowson, P. Kitanidis, and R. Gentry, 2010a, Effects of model formulation and calibration data on uncertainty in DNAPL source dissolution predictions, Water Resour. Res., 46, W12517.

Rao, P.S.C., J.W. Jawitz, C.G Enfield, R. Falta, M.D. Annable, A.L. Wood, 2001, Technology integration for contaminanted site remediation" Cleanup goals and performance metrics, Ground Water Quality, Sheffield UK, p. 410-412.

Rao, P. S. C., and J. W. Jawitz, 2003, Comment on ''Steady-state mass transfer from single-component dense non-aqueous phase liquids in uniform flow fields'' by T.C. Sale and D. B. McWhorter, Water Resour. Res., 39, 1068, doi:10.1029/2001WR000599.

Saenton, S. and I. Illangasekare, 2007, Upscaling of mass transfer rate coefficient for the numerical simulation of dense nonaqueous phase liquid dissolution in heterogeneous aquifers. Water Resour. Res., 43, doi: 10.1029/2005WR004274.

Sale, T. C., and D. B. McWhorter, 2001, Steady state mass transfer from single-component dense nonaqueous phase liquids in uniform flow fields, Water Resour. Res., 37(2), 393– 404.

Soga, K., J. W. E. Page, and T. H. Illangasekare, 2004, A review of NAPL source zone remediation efficiency and the mass flux approach, J. Hazardous Mat., 110, 13-27.

Tang, G., M. A. Mayes, J. C. Parker, and P. M. Jardine, CXTFIT/Excel – A modular adaptable approach for parameter estimation and uncertainty/sensitivity analysis, Computers and Geosciences, 36, 1200-1209, 2010.

Unlu, K., J. C. Parker, and P. K. Chong, 1995, A comparison of three uncertainty analysis methods to assess groundwater impacts from land-disposed waste, Hydrogeology Journal, 3(2).

Zhu, J. and J.F. Sykes, 2004, Simple screening models of NAPL dissolution in the subsurface, J. Contam. Hydrol., 72, 245-258.

7. Remediation Design, Assessment and Optimization

7.1 Overview

Predictions of remediation performance, no matter how sophisticated the performance model that is employed, are always subject to considerable uncertainty. Quantification of performance uncertainty is critical for remediation design, so that sufficient safety factors can be built into the design to avoid failure to meet system objectives, while avoiding unnecessarily high costs incurred by excessive overdesign. Remediation design (and engineering design in general) is an exercise in identifying optimal tradeoffs between risk of failure and cost of overdesigning.

SCOToolkit addresses this problem by using an optimization algorithm to find design parameter values that minimize the expected NPV cost of achieving specified objectives. Expected NPV cost is computed as the average NPV cost over a number of equally probable Monte Carlo simulations.

7.2 Compliance rules

7.2.1 Statistical criteria

The overall goal of groundwater remediation is taken to be the reduction of contaminant concentrations in designated compliance locations to less than specified values within a certain timeframe at the least possible cost. For a given remediation design, one of three possible outcomes is assumed to apply for a given remedial action at the actual site and hence for each simulated MC model realization:

No Further Action (NFA). If compliance well monitoring data meet specified NFA criteria before the maximum simulation date, t_{max}, and after a date t_{end} when all active remediation systems have ceased operation, then that MC realization simulation terminates and no further operating costs are accrued (i.e., all remediation and monitoring activities are terminated).

Non-Compliance (NC). If contaminant concentrations for one or more compliance wells exceed certain noncompliance criteria after a specified "penalty date", $t_{penalty}$, or if NFA has not been achieved prior to t_{max}, then a specified fixed present value "penalty cost" will be added to the cost function. Simulation of the MC realization is terminated. The realization is deemed a "failure." Note that if $t_{penalty} > t_{max}$ then no penalty cost can be incurred.

Conditional Containment (PT). If contaminant concentrations at a designated PT trigger well exceed certain criteria after a specified PT trigger date t_{PT}, then pump-and-treat or another type of containment system is assumed to be implemented upgradient of the trigger location. Discounted capital and annual operating costs for the containment system are accrued until NFA or NC conditions occur. Other remedial actions and their costs continue until the individual actions meet their specified termination criteria or t_{max} is reached. The PT system is not explicitly simulated, but is assumed to contain the plume. Model-predicted concentrations at compliance wells (which must be upgradient of the PT system) are computed as though unaffected by the containment system – i.e., attainment of NFA is conservatively assumed to be unaffected by the containment system. No PT costs are considered if $t_{PT} > t_{max}$. If NFA is not reached before t_{max}, the case is regarded as NC and a penalty cost may be applied if applicable. We assume site-wide monitoring of contaminant concentrations at a frequency of f_{samp}^{SW} per year at each designated compliance location. Since

concentration measurements at a given well can exhibit considerable temporal variability, compliance rules must be carefully defined to filter out measurement "noise" so that the likelihood of a false NFA determination is small.

Two compliance rule options to filter measurement noise are considered. The first option employs annual averaging of concentrations from f_{samp}^{SW} compliance well samples per year and requires all annual averages within a lookback period of $N_{lookback}$ years to be below a specified target concentration C_{nfa} to attain NFA. This approach is very conservative, and noisy data may inordinately extend the remediation duration. The second option, which has been suggested by the USEPA (Levine, 2010), involves a regression of concentration data from f_{samp}^{SW} samples per year versus time within a lookback period $\Delta t_{lookback}$. If the one-sided α-probability upper confidence limit of the regression value at the end of the lookback period is less than C_{nfa} for each compliance well and the current date is after t_{end} then NFA is indicated. This approach accounts for data noise in the decision process, but is less sensitive to outliers. A summary of the compliance rules is given in Table 7.1.

Table 7.1. Compliance rule protocol options.

	Extreme Value (EXV) Rule	Regression Confidence Limit (RCL) Rule
NFA	If annual averages of contaminant concentration measurements for all compliance wells are less than C_{nfa} for each of the last $\Delta t_{lookback}$ years ending on or after t_{end} then site monitoring activities are terminated. If rebound does not exceed $C_{nfa,}$ NFA is met, otherwise a penalty cost is added to the cost function.	If the upper confidence limit of the current value of a regression of annually averaged contaminant concentration measurements vs. time over the last $\Delta t_{lookback}$ years ending on or after t_{noact} is less than C_{nfa} for all compliance wells, then site monitoring activities are terminated. If rebound does not exceed $C_{nfa,}$ NFA is met, otherwise a penalty cost is added to the cost function.
NC	If annual averages of contaminant concentration measurements exceed C_{nfa} in any of the last $\Delta t_{lookback}$ years ending on or after $t_{penalty\ i}$ for compliance well i or if NFA has not been achieved prior to t_{max} for any compliance well, then a penalty cost is added to the cost function and the simulation is terminated.	If the upper confidence limit of the current regression value at compliance location *i* over the last $\Delta t_{lookback}$ years ending on or after $t_{penalty\ i}$ exceeds C_{nfa} for any compliance well or if NFA has not been achieved prior to t_{max}, then a present value penalty cost is added to the cost function and the simulation is terminated.
PT	If the annual average of contaminant concentration measurements in a designated PT trigger well exceed C_{PT} for all of the last $\Delta t_{lookback}$ years ending on or after t_{PT}, then discounted capital and operating costs for pump-and-treat or other plume containment system are accrued. The simulation continues until NFA or NC criteria are met.	If the lower confidence limit of the current regression value over the last $\Delta t_{lookback}$ years ending on or after t_{PT} exceeds C_{PT} for a designated PT trigger well, then discounted capital and operating costs for pump-and-treat or other plume containment system are accrued. The simulation continues until NFA or NC criteria are met.

When the remediation strategy includes ED injection galleries, there is a possibility of rebound downgradient of ED injection galleries after injection ceases. This can lead to exceedance of C_{nfa} if downradient compliance wells are not stipulated for optional ED performance monitoring and C_{EDstop} values for upgradient performance monitoring wells are greater than C_{nfa} (see Chapter 3). When the latter conditions apply for simulations meeting NFA criteria at t_{end}, "true" (i.e., no noise) concentrations at compliance well locations at $t_{rebound} = t_{end} + \Delta t_{rebound}$ are computed to evaluate rebound. If the computed rebound concentrations C_{rbd} are less C_{nfa}, then NFA status is confirmed. Otherwise, a penalty cost $\$_{penalty}$ is added to the cost function and the MC realization is regarded as noncompliant (NC).

Annual average concentrations are treated as geometric averages. Measured or simulated concentrations less than detection limits should be set to a stipulated fixed value (e.g., 10% of the detection limit). Log-normal measurement "noise" is applied to annual averages in MC realizations with a standard error equal to the ln *C* standard deviation from model calibration ("residual error)" divided by $f_{samp}^{SW\ 1/2}$. Note that increasing sampling frequency decreases the noise in annual averages, which allows earlier NFA attainment. The optimal sampling frequency will depend on a tradeoff between cost reductions due to earlier termination versus additional sampling and analytical costs.

The computational effort required for stochastic cost optimization increases in direct proportion to the number of simulated compliance well locations. For this reason, we recommend selecting a single worst-case compliance location at least for initial optimization runs. If desired, additional well locations may be added after the design has been refined. Compliance monitoring costs per sampling event can be specified to include all required monitoring locations.

The "penalty cost" may be a real cost (e.g., for a last-ditch containment measure) or a fictitious cost applied merely to incentivize the optimization algorithm to reduce the failure probability. Penalty cost is specified in NPV dollars (i.e., no discount is applied internally). Care should be taken not to specify a penalty date ($t_{penalty}$) that cannot be realistically achieved with current site conditions and proposed remedial technologies lest compliance will be nearly impossible to meet and the optimization problem will be ill-defined. Likewise, if t_{max} is too early to achieve a low failure probability and high NFA probability, low remediation costs may be misleading. An exception may be if long-term containment with institutional controls is under consideration, t_{max} may be set to reach a pseudo-steady state condition, fixed and penalty costs set to zero, and design variables optimized to minimize operating costs. If optimization results produce an unacceptably high failure probability, increasing the penalty cost may produce a better outcome. If this does not improve the results, the problem is likely that you are proposing something that cannot be reasonably achieved. You will need to figure out why and either develop a plan to circumvent the problem, or if nothing reasonable works, you should have a good case for "technical infeasibility."

Note that pump-and-treat, if considered, is not explicitly simulated. Pump-and-treat is assumed to contain the plume, but model-predicted concentrations at compliance wells are treated as though unaffected by the PT system. Therefore, compliance well locations downgradient of the PT system should not be stipulated.

Real-time implementation of RCL rule would involve performing regressions of the last $N = \Delta t_{lookback} f_{samp}^{SW}$ ln-concentration values after each sampling round versus Julian date, *T*, to fit a log-linear trend model

$$\ln C = a + bT \tag{7.1}$$

where *a* and *b* are regression coefficients. The regression error is

$$S_{\ln C}^2 = \frac{SSE}{N-2} \tag{7.2}$$

where SSE is the sum of squared ln *C* regression residuals. To reduce computational effort in MC simulations, we generate a single (geometric) average concentration value for each year in each realization with noise $S_{\overline{\ln C}} = S_{lnC} / f_{samp}^{SW\ 1/2}$ rather than generating f_{samp}^{SW} sample values per year with noise $S_{lnC.}$. One-sided upper or lower confidence limits of annual average concentrations at probability level α are computed by

$$\begin{aligned} LCL_\alpha &= \exp\left(a + bT_{end} - t(\alpha, f_{samp}^{SW}) S_{\overline{\ln C}} \right) \\ UCL_\alpha &= \exp\left(a + bT_{end} + t(\alpha, f_{samp}^{SW}) S_{\overline{\ln C}} \right) \end{aligned} \tag{7.3}$$

where T_{end} is the date at the end of the regression period and $t(\alpha, df)$ is the one-sided Student-*t* value for probability α with *df* degrees of freedom. The regressions are performed during simulations on time series with $N = N_{lookback}$ concentration values, which yields $S_{\overline{\ln C}}$ directly. Note that in real-time, regressions would be performed on $N = f_{samp}^{SW} N_{lookback}$ concentration values to determine when NFA is met.

7.2.2 Determining $t_{penalty}$, t_{max} and $t_{rebound}$

Correct specification of $t_{penalty}$, t_{max} and $t_{rebound}$ are important constraints on the optimization solution, but must be set with consideration of physical limitations that can make it difficult or impossible to find a feasible solution.

The duration of time allowed before cleanup criteria are required to be met will have a significant effect on remediation design and cost. Specifically, if $t_{penalty}$ or t_{PT} are decreased or the magnitudes of contingent containment or penalty costs are increased, then earlier, more aggressive and more costly remediation will be favored. In the case of no contingent penalty or containment costs (or $t_{penalty} > t_{max}$ and $t_{PT} > t_{max}$) with a positive discount rate, the cost optimal solution will be to simply monitor until t_{max} or NFA is reached, regardless of the probability of achieving NFA. Some cost consequence of "failure" must be stipulated to induce active remediation.

The penalty date represents the time at which concentrations at compliance well locations are required to meet the specified RCL or EXV conditions. For example, it may be required to contain the leading edge of the plume with an ED gallery as quickly as possible, while recognizing that it will take much longer to remediate the source and entire dissolved plume. In that case, $t_{penalty}$ can be used to enforce the short-term requirement. In doing so, the value of $t_{penalty}$ and the capability of the proposed remediation strategy for conditions at the site must be consistent. For example, if an ED gallery 50 m upgradient of the compliance location is under consideration and the retarded velocity is estimated to be about 10 m/yr, then the advective travel time Δt_{travel} is 5 years. If the lookback period $\Delta t_{tlookback}$ is 3 years and the ED start date is 2020, then $t_{penalty}$ should be at least $t_{EDstart} + \Delta t_{travel} + \Delta t_{tlookback} = 2028$. A more conservative approach would be to use a multiple of

the travel time, e.g., $t_{EDstart} + 2\Delta t_{travel} + \Delta t_{tlookback} = 2033$. If there is not short-term requirement, but it is desired to return the site to normal use by a certain date, then this value may be set as the penalty date, recognizing that if the proposed remediation technology is not capable of meeting this requirement, the program will return a high failure probability.

The maximum simulation date t_{max} is primarily a computational failsafe to prevent your computer from running forever in an attempt to solve an intractably posed optimization problem. From a practical standpoint, it can be regarded as the maximum date you are willing to accept as a possible outcome. Like the penalty date, consideration should be given to the site conditions when specifying this value – in particular, the length and velocity of the plume, how long it may take to reduce the source mass to a sufficiently small value (naturally or otherwise), and the number of ED galleries, if any.

If optional downgradient ED performance monitoring at compliance locations is elected and C_{EDstop} for the upgradient performance monitoring well is less than C_{nfa}, then $\Delta t_{rbd} = 0$ and rebound is disregarded. Otherwise, rebound is computed a date

$$t_{rebound} = \max_i \left(t_{EDstop(i)} \right) + \max_j \left(\max_i \left(t_{EDstart(i)} + \Delta t_{travel(i,j)} - t_{EDstop(i)} \right) \right) \qquad (7.4)$$

where $t_{EDstart(i)}$ and $t_{EDstop(i)}$ are the dates ED injection starts and stops, respectively, for ED gallery i, $\Delta t_{travel\ ij}$ is the user-specified travel time to compliance well j from upgradient ED gallery i, and $t_{EDstop\ i}$ is the termination date for gallery i. Note that that $\max_i$ argument is evaluated only for ED galleries that are upgradient of compliance location j but <u>not</u> upgradient of any other compliance locations.

Typically, it is desired to achieve plume containment within a limited timeframe while recognizing that subsequent long-term measures may be required before achieving "no further action" status. The variable $t_{penalty}$ is a user-specified date by which short-term controls are desired to be fully implemented such that compliance wells meet the criteria for being "clean."

If there is no short-term requirement mandate, $t_{penalty}$ may be specified equal to or slightly less than the maximum simulation duration, t_{max}. If short-term cleanup requirements do apply, care needs to be exercised in specifying $t_{penalty}$ to ensure that it is realistically attainable with the technology options under consideration. Specifying a value that is too short to be realistically achieved will produce a high failure probability. Too long a value will increase exposure risk unnecessarily.

If any remediation or plume control measures are considered for deployment upgradient of compliance points, t_{NFA} values specify the waiting time, if any, following termination of all system components (e.g., ED injection galleries) before compliance monitoring is terminated to allow rebound in monitoring data and prevent false "clean" determinations (hence, potentially large failure probabilities).

7.3 Site-wide and total costs

The net present value (NPV) cost for site-wide monitoring, reporting and maintenance are computed as follows

$$\begin{aligned} C_{NPV}^{SW} &= C_{NPV}^{SWcap} + C_{NPV}^{SWop} \\ C_{NPV}^{SWcap} &= \left(C_{well}^{SWcap} N_{well}^{SW} + C_{other}^{SWcap} \right) (1-d)^{t_{start} - t_{ref}} \\ C_{NPV}^{SWop} &= \sum_{t=t_{start}}^{t_{comp}} \left(C_{samp}^{SWop} f_{samp}^{SW} N_{well}^{SW} + C_{other}^{SWop} \right) (1-d)^{t-t_{ref}} \end{aligned} \tag{7.5}$$

and the total NPV cost for all site remediation activities and penalty costs, which is the objective function to be minimized by the stochastic optimization algorithm, is

$$C_{NPV}^{all} = C_{NPV}^{SW} + C_{NPV}^{ED} + C_{NPV}^{TR} + C_{NPV}^{OX} + C_{NPV}^{PT} + I_{pen} C_{NPV}^{plty} \tag{7.6}$$

where

C_{NPV}^{all} is the total NPV remediation and penalty cost ($k),

C_{NPV}^{SW} is the total NPV site-wide cost ($k),

C_{NPV}^{ED} is the total NPV ED injection system cost ($k),

C_{NPV}^{TR} is the total NPV thermal remediation cost ($k),

C_{NPV}^{OX} is the total NPV ISCO remediation cost ($k),

C_{NPV}^{PT} is the total NPV PT cost ($k),

C_{NPV}^{plty} is the NPV penalty cost ($k),

C_{NPV}^{SWcap} is the total NPV site-wide fixed cost ($k),

C_{well}^{SWcap} is the fixed cost for monitoring well construction ($k/well),

C_{other}^{SWcap} is any other site-wide fixed costs ($k),

C_{total}^{SWop} is the total NPV operating cost for site-wide monitoring and reporting ($k),

C_{samp}^{SWop} is the cost per sample for site-wide monitoring ($k/sample),

C_{other}^{SWop} is other annual site-wide operating costs ($k/yr),

f_{samp}^{SW} is the number of samples per well per year taken for site-wide monitoring,

I_{pen} is 1 if a penalty cost is triggered, else 0,

I_{PT} is 1 if PT implementation is triggered, else 0,

N_{well}^{SW} is the number of site-wide monitoring wells (including compliance wells),

t_{PT} is the year that PT is triggered (yr),

t_{nfa} is the year compliance is achieved or the max simulation date for NC (yr),

t_{start} is the first year capital costs are incurred (yr),

t_{ref} is the basis date for NPV adjustment (yr), and

d is the annual discount rate (fraction).

If the time discount factor, *d*, is decreased, future costs are less sharply discounted, thus favoring earlier and more aggressive action. In this regard, it should be noted that the discount rate useful to a rational decision maker would be the real discount rate, i.e., the nominal "risk free" rate of return minus the inflation rate. In the long term in "normal" times, the real discount rate is typically 2-3%. At the present time, it is near zero or negative, depending on how you compute inflation. Federal Reserve chairs and hedge fund managers can't predict this key economic variable a few months out, never mind a few decades. So, consider putting hubris aside, use a zero discount rate and push fewer problems onto our grandchildren.

7.4 Iterative assessment and design optimization

Following initial calibration of source and dissolved plume parameters using all currently available data, one or more potential remedial action strategies may be identified to meet the site objectives. These may involve multiple technologies applied concurrently or serially. Stochastic cost optimization can then be undertaken to select the best approach going forward given the information at hand. After the strategy is implemented, new data regular site-wide monitoring as well as monitoring specific to individual technologies will accrue over time. Periodically, this new data may be incorporated into the calibration data set and the calibration updated. Monte Carlo simulations may then be run forward in time with updated parameters and covariances to evaluate whether the existing system is performing satisfactorily. Reoptimization can be performed to refine monitoring and other operational design variables or, if necessary, to evaluate alternative technologies. This process can be repeated periodically to identify and correct problems before the costs grow and the completion date slips further into the future. A flowchart for the iterative assessment and optimization protocol is given in Figure 7.1.

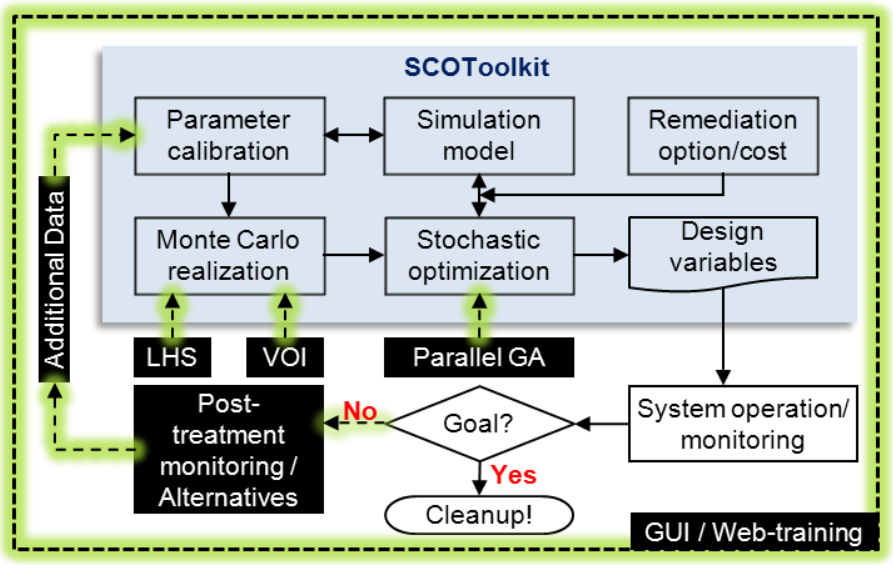

Figure 7.1. Flowchart for iterative assessment and optimization protocol.

7.5 Hypothetical example problem

7.5.1 Problem description

A hypothetical problem is considered involving trichloroethene (TCE) contamination in a 30 m thick unconfined aquifer. The water table occurs at a depth of 5 m bgs and a continuous clay layer occurs at a depth of 35 m bgs. The aquifer consists of sand interstratified with discontinuous 0.5 – 2 m thick silty clay layers. The underlying clay layer is at least 5 m thick. The clay lenses represent about 28 percent of the aquifer volume. The average darcy velocity across the aquifer thickness is 0.09 m/d. DNAPL releases were assumed to occur between 1950 and 1987 resulting in two DNAPL sources (Figure 7.2). Soil characterization borings performed on a grid pattern initially identified the one larger source, but missed the smaller second source. Assumed true values of source parameters (Table 7.2) and aquifer parameters (Table 7.3) were used to generate groundwater monitoring data for a network of 26 well clusters (Figure 7.3).

Lognormally distributed "noise" with a ln-standard deviation (S_{ln}) of 1.4 for each observation (0.7 for annual averages of quarterly data) was added to simulated concentrations to represent spatial and temporal variability and measurement uncertainty. Each well cluster sampled groundwater from 8-12 m, 18-22 m and 28-32 m bgs (3-7, 13-17 and 23-27 m below the water table) starting in 1980. A surface water body occurs at the far-right boundary of Figure 7.3. Also shown in Figure 7.3 is a key compliance well located immediately upgradient of the surface water and two potential locations of ED injection galleries including gallery ED2 upgradient of the stream and ED1 midway between the source and the stream. DNAPL in the source area is removed by a thermal source reduction (TSR) method described in Chapter 4.

The objective of this example problem is to evaluate the iterative calibration-assessment-optimization capability of SCOToolkit v3. The remediation objectives are to bring concentrations entering surface water below 5 μg/L as quickly as possible with ED injection at ED2 and to permanently decrease concentrations below 5 μg/L throughout the aquifer using one additional ED gallery (ED1) by 2050. In this example, $t_{penalty}$ and t_{max} are set to Dec 2015 and Dec 2050 respectively. To avoid the computational expense of simulating a large number of compliance wells, we will use a single downgradient compliance well with a lag time of 15 years that the single compliance well must remain clean after shutting off ED1, 5 years after ED2, and 30 years after TSR.

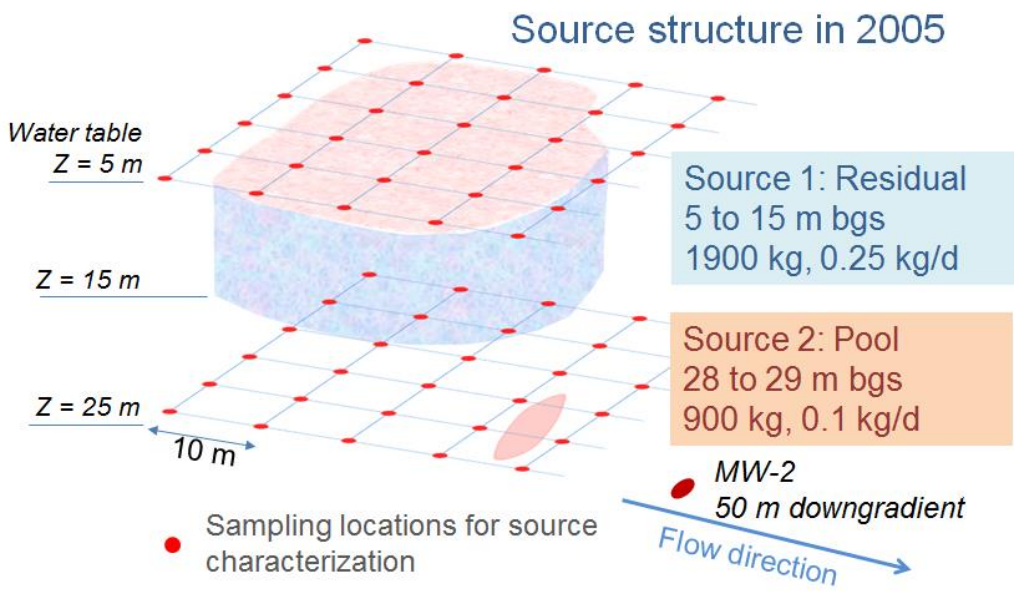

Figure 7.2. DNAPL source configuration for hypothetical site. Red dots on grid are boring locations for source characterization (depths are below ground surface, water table is 5 m deep). Note that Source 2 is not found until 2009 at which additional source characterization is performed.

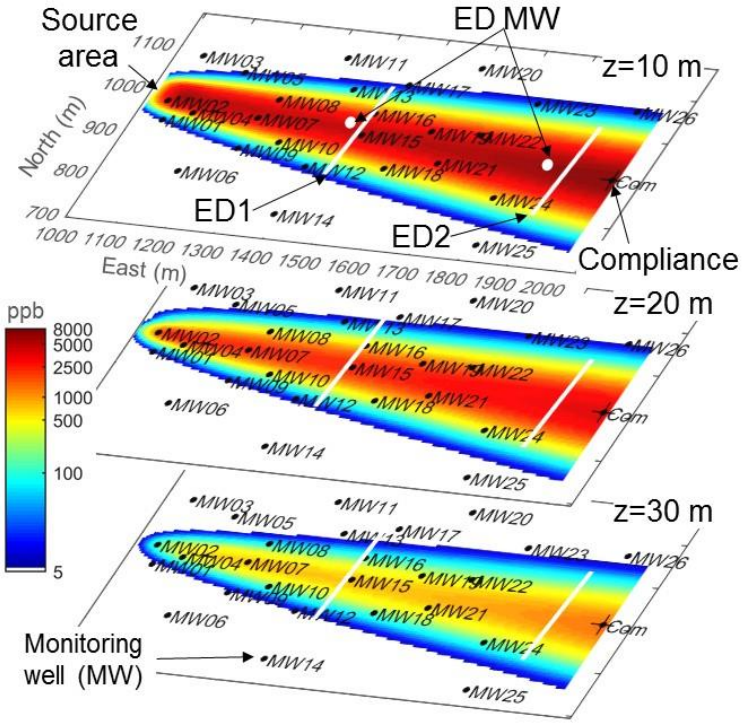

Figure 7.3. TCE concentrations in monitoring wells in 2005 and locations of the DNAPL sources, compliance well, ED injection galleries, and wells for monitoring upgradient of ED galleries.

We will employ a 5-year assessment cycle with a timeline as follows.

Stage 1

- Make initial prior estimates for model parameters and perform model calibration using monitoring wells data from Jan 1980 – Dec 2005 (Source 2 is not included in this stage)
- Optimize remediation design considering possible TSR of Source 1 and one or more ED injection galleries.
- Monitor TSR performance of Source 1 quarterly at multi-depth in MW2 that is immediately downgradient of the source area.
- Operate the Stage 1 remediation plan from Jan 2007 – Dec 2010.

Stage 2

- Failure of thermal treatment to meet flux reduction expectations triggers additional source characterization and identification of Source 2. Recalibrate the model using monitoring well data from Jan 1980 – Dec 2009, mass recovery data from thermal treatment (266 days from Jan 1, 2007) and additional source characterization data from MW2. Use Stage 1 calibrated parameters as new prior estimates.
- Reoptimize remediation design based on new model calibration considering additional source thermal treatment and modification of existing ED gallery operating parameters.
- Implement Stage 2 remediation plan modifications Jan 2011 and operate through Dec 2014.

Stage 3

- Recalibrate the model using monitoring well data from Jan 1980 – Dec 2014 and mass recovery data from additional thermal treatment. Use Stage 2 calibrated parameters as new prior estimates.
- Reoptimize remediation design based on new model calibration considering modifications of ED gallery operating parameters and possible ISCO if source needs "polishing."
- Implement Stage 3 remediation plan modifications Jan 2015 and operate through Dec 2021.

Stage 4 etc

- Continue as above until NFA achieved

7.5.2 Results and discussions

We had completed these simulations in late 2015, but in the meantime developed a more flexible and rigorous means of dealing with uncertainty in termination decisions for thermal and ISCO systems that promises to enable significant cost savings to be realized with these technologies. We have implemented these modifications in the SCOToolkit v3 code. The example problem for iterative reoptimization was rerun with the revised code. Time and total cost to achieve NFA for the actual system (i.e., using "true" parameters) for one-stage vs. multiple-stage optimization is presented as follows.

Stage 1
Calibration

Stage 1 calibration includes only Source 1 while it was calibrated to concentrations dissolved from combined source (Source 1 and 2). Although the calibration efficiency (r, linear correlation coefficient) was 0.80, Stage 1 calibration overestimated mass flux and mass for Source 1 about 2.5 and 2.4 times higher than true values (which are unknown in reality), respectively (Table 7.3 and Figure 7.4). Log uncertainty of both parameters was substantially reduced after Stage 1 calibration compared to the prior value of 0.5. It is notable that although a prediction uncertainty (SlnC) decreased to 1.05 from its prior value 1.4, it is still 50% higher than true uncertainty of 0.7. This observation implies that some MWs showed high bias between measurement and prediction due to uncounted Source 2 dissolution.

Calibrated aquifer parameters are presented in Table 7.4. The darcy velocity and longitudinal dispersivity were overestimated compared to their true values. It may be the same issue in Source 1 calibration that caused by the absence of Source 2 in calibration.

The 100 Monte Carlo realizations of calibration parameters were generated for stochastic cost optimization after Stage 1 calibration using their covariance matrix and Jacobian (Chapter 6).

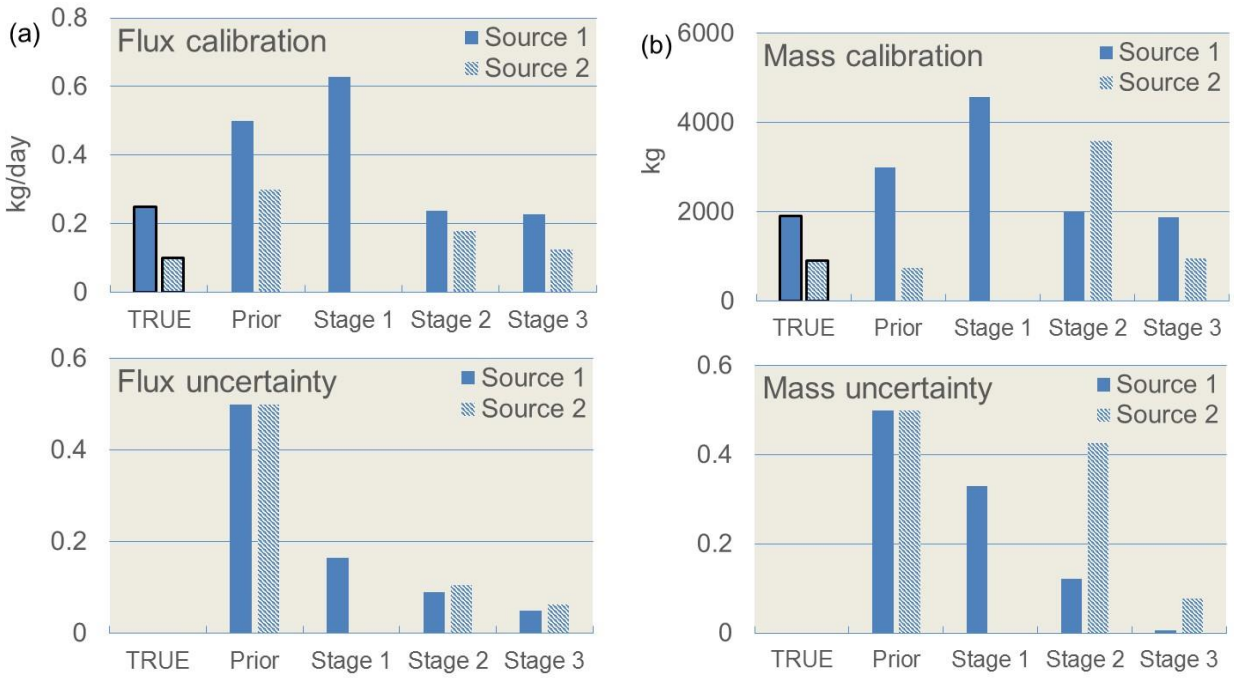

Figure 7.4. Calibration results of (a) mass flux and (b) mass remaining for Stage 1, 2, and 3.

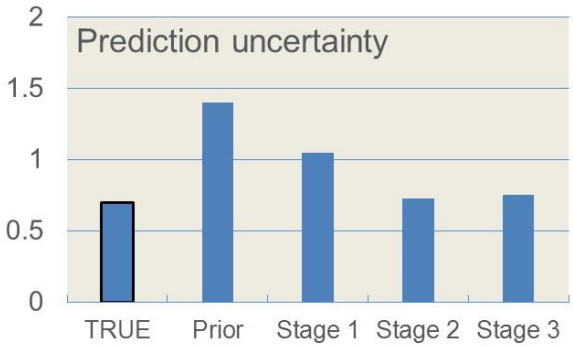

Figure 7.5. Changes in prediction uncertainty for Stage 1, 2, and 3.

Table 7.2. True source parameters and prior/posterior estimates for Stage 1, 2, 3 calibrations.

Parameter	PDF[1]	True Value	Stage 1 Prior Values	Stage 1 Prior Std[3]	Stage 2 Prior Values	Stage 2 Prior Std[3]	Stage 3 Prior Values	Stage 3 Prior Std[3]	Stage 3 Posterior Values	Stage 3 Posterior Std[3]
Source 1 start date (t_s), yr	N	1950	1965	7	**1964.03**	**2.23**	**1964.93**	**1.43**	1964.65	0.01
Source 1 end date (t_o), yr	N	1987	1985	0	**1987.00**	**0.00**	**1987.00**	**0.00**	1987.00	0.00
Source 1 mass on t_{cal}[2], kg	LN	0.25	3500	0.50	**0.63**	**0.17**	**0.24**	**0.09**	0.23	0.05
Source 1 rate on t_{cal}[2], kg/d	LN	1900	0.50	0.50	**4568**	**0.33**	**2012**	**0.12**	1885	0.01
Source 1 depletion exponent, -	N	1.55	1.3	0.25	**1.09**	**0.16**	**1.48**	**0.15**	1.39	0.07
Source 1 width, m		45	45	0						
Source 1 horiz. area, m^2		1100	1000	0						
Source 1 depth to top, m		0*	0	0						
Source 1 depth to bottom, m		10	10	0						
Source 2 start date (t_s), yr	N	1960			1965	7	**1966.62**	**1.13**	1966.36	1.05
Source 2 end date (t_o), yr	N	1985			1985	0	**1985.00**	**0.00**	1985.00	0.00
Source 2 mass on t_{cal}[2], kg	LN	0.1			0.3	0.50	**0.18**	**0.10**	0.13	0.06
Source 2 rate on t_{cal}[2], kg/d	LN	900	If blank, it was not identified before Stage 1.		750	0.50	**3593**	**0.43**	963	0.08
Source 2 depletion exponent, -	N	0.65			0.5	0.25	**0.51**	**0.13**	0.50	0.12
Source 2 width, m		15			15	0				
Source 2 horiz. area, m^2		350			400	0				
Source 2 depth to top, m		18			18	0				
Source 2 depth to bottom, m		19			19	0				

* Note depths are measured from ground surface. Water table is a 5 m depth.

Bold: posterior values from previous stage calibration

[1] Assumed probability distributions: N = normal, LN = lognormal.

[2] Source mass and discharge rates on t_{cal} = Jan. 2005.

[3] Standard deviations (Std) of LN variables are log-transformed (dimensionless); all other values are in specified units.

Table 7.3. True aquifer parameters and prior/posterior estimates for Stage 1, 2, 3 calibrations.

Parameter	PDF[1]	True value	Stage 1 Prior Values	Stage 1 Prior Std[2]	Stage 2 Prior Values	Stage 2 Prior Std[2]	Stage 3 Prior Values	Stage 3 Prior Std[2]	Stage 3 Posterior Values	Stage 3 Posterior Std[2]
Avg aquifer darcy velocity, m/d	LN	0.09	0.08	0.20	**0.10**	**0.10**	**0.10**	**0.08**	0.09	0.06
Mobile volume fraction (f_m)[3]		1	1							
Mobile zone porosity, -		0.32	0.3							
Mobile zone TCE (k_d)[4], m^3/kg	LN	1.30E-4	1.60E-4	0.20	**1.34E-4**	**0.19**	**1.04E-1**	**0.08**	1.21E-4	0.14
Mobile zone density, kg/m^3		1860	1890							
Immobile zone porosity, -										
Immobile zone TCE k_d, m^3/kg										
Immobile zone density, kg/m^3										
Immobile zone TCE diff coef, m^2/d										
Max diffusion path length (L_{im}^{max}), m										
Longitudinal dispersivity, m		10	15	1	**14.03**	**0.11**	**11.10**	**0.07**	11.33	0.05
Ay/Ax	LN	0.08	0.1	1	**0.05**	**0.12**	**0.07**	**0.08**	0.07	0.06
Az/Ax	LN	0.005	0.01	1	**0.01**	**0.13**	**0.003**	**0.09**	0.003	0.08
Flow direction, degrees		5	4.5							
Aquifer thickness, m		30	30							
Effective decay coef w/out ED, 1/d		2E-4	1E-4	1	**4.1E-4**	**0.16**	**1.6E-4**	**0.21**	1.3E-4	0.20
ED reaction rate coef (α_{ED}), 1/d		0.005	0.01							
Mobile ED (k_d)[4], m^3/kg	LN	2.00E-4	3.00E-4							
Immobile ED (k_d), m^3/kg										
Immobile zone ED diff coef, m^2/d										
ED decay coef, 1/d		0	0							
H-equiv EA concentration, g/m^3		2.75	2.39							
H-equiv O_2 concentration, g/m^3		0.57	0.49							
H-equiv ED ratio, -		0.26	0.26							
H-equiv CH ratio, -		0.061	0.05							
Serial decay fraction, -		0.32	0.5							

Bold: posterior values from previous stage calibration

[1] Assumed probability distributions: N = normal, LN = lognormal.

[2] Standard deviations of LN variables are log-transformed (dimensionless); all other values are in specified units.

[3] Mobile and immobile zone pore fractions include 5 m thick underlying clay

[4] k_d mobile and immobile for TCE are assumed to be same and are calibrated (same to ED)

Optimization

As it is the best knowledge obtained from Stage 1 calibration, design optimization for Stage 1 is based on this. Design optimization includes TSR for Source 1 and ED1 (middle) and ED2 (downstream). All remediation activities begin in Jan 1, 2007 except ED1 in which its optimal commencing date and duration are determined according to other remediation performance during optimization.

TSR design variables are 1) local soil concentration to terminate heating a monitoring zone (MZ) in a treatment zone (TZ) (1 TZ for Source 1), 2) number of MZs in a TZ, and 3) number of soil sample locations and samples per bore hole. Time to peak mass recovery rate (t_{peak}) is assumed as 64 days. ED1 design variables are its starting date, TCE concentration upgradient of ED1 to terminate ED1, and number of groundwater monitoring samples per year. ED2 is, however, immediately active on Jan 1, 2007 to maintain the TCE concentration below MCL 5 ppb while being operated same as ED1.

Results from Stage 1 optimization show that mass was recovered about 4000 kg in Dec 2017, which is much higher than true mass and impossible. Figure 7.6 summarizes the total projected cost-to-complete (CTC that is ENPV to reach NFA). CTC by Stage 1 optimization is about \$11,000k with t_{nfa} = 2038, while the true cost simulated by these optimized design variables is about \$19,200k with t_{nfa} = 2079, where Source 2 is included in simulation. This indicates that Stage 1 optimization based on Source 1 will not perform correctly in the real site (i.e., two sources).

Therefore, we collected quarterly multi-depth TCE concentration at MW2 for two years (2007-2008) as part of post-remediation monitoring that contribute to additional source zone characterization. This additional data is included in Stage 2 calibration in addition to regularly monitoring data in other MWs data from 2006 to 2009.

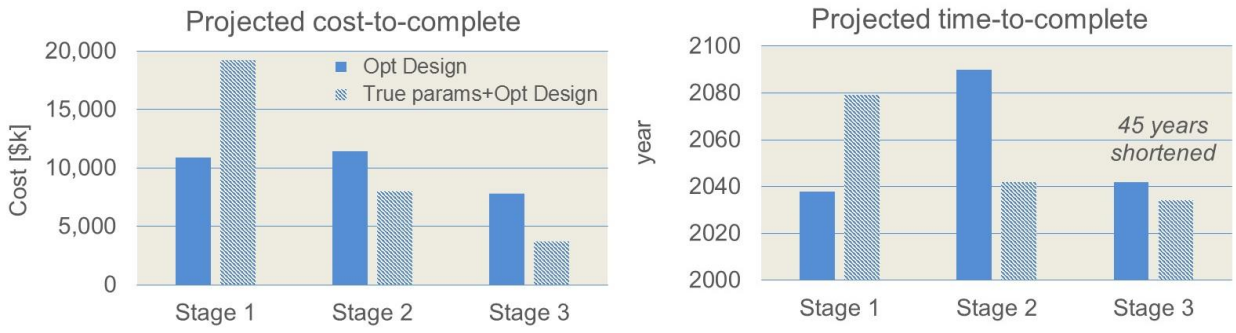

Figure 7.6. Projected cost-to-complete and time-to-complete.

The actual cost incurred until t_{nfa} is summarized in Figure 7.7, which was computed for true parameters using true TSR optimization result (Source 1 in 2007 and Source 2 in 2011) and optimized ED variables in each stage. Those variables are summarized in Tables 7.5 and 7.6, respectively.

Stage 2

Calibration

The optimized variables form Stage 1 were implemented during 2007 to 2010. TCE concentration in MW2 was monitored at 10, 20, and 30 bgs during and after TSR1. Figure 7.8 describes the TCE concentration of MW2 at 20 m bgs for true parameters and Stage 1 calibration using Stage 1 optimization that includes only Source 1. In Dec 2008 after 2 years of TSR1, Stage 1 optimization substantially mislead TCE concentration about 100 ppb at Z = 20 m bgs (where Source 2 is located at Z = 23 m bgs), while quarterly measurements (noisy data based on 'True+TSR1' with SlnC = 1.4) still show 1000~8000 ppb. This finding initiated site recharacterization resulting Source 2 identified. Therefore, Stage 2 calibration includes both Source 1 (treated) and Source 2 (untreated) (see Table 7.3).

Past remediation activities included in Stage 2 calibration are 1) mass recovery data from TSR1 and 2) injection rate for both EDs and start date of ED1 optimized in Stage 1. The calibration efficiency (r) was 0.82 slightly higher than Stage 1. However, Stage 2 calibration improved the estimates of mass flux and mass for Source 1, which are close to true values (Table 7.3 and Figure 7.4). Although the log uncertainty of both parameters for Source 1 was substantially reduced compared to Stage 1 calibration, Source 2 mass is still uncertain (Figure 7.4b) because Source 2 characterization data is only for 2 years (2007-2008). The overall prediction uncertainty (SlnC) decreased from 1.05 to 0.73 that is close to assumed uncertainty 0.7 for annual average. Dispersivity related parameters were particularly improved compared to Stage 1 (Table 7.4).

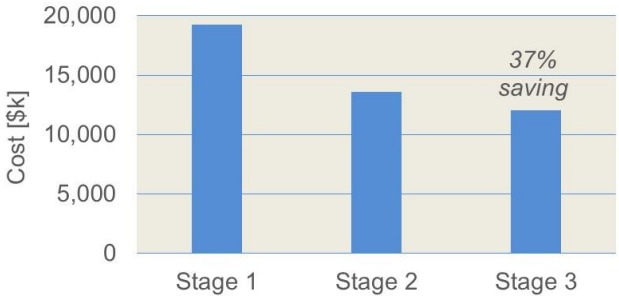

Figure 7.7. Actual cost incurred until t_{nfa}.

Table 7.4. True TSR optimization results for each source.

Variables	TSR 1	TSR 2
Start year	2007	2011
Duration (days)	266	350
C_{stop_local} (μg/kg)	**105**	**114**
N_{MZ}/TZ	**11**	**1**
N_{GP}/MZ	**1**	**3**
N_{smp}/GP	**3**	**3**
True mass recovery (kg)	1712	693

Note) **Bold**: optimized values based on true source parameters.

Table 7.5. ED design variables for each stage.

Variables	Stage	ED1	ED2
Injection rate (kg/d)	1	**2.1**	**8.0**
	2	**8.5**	**7.6**
	3	**6.3**	**4.8**
Start date	1	**2009.5**	2007.0
	2	2011.0	2011.0
	3	2015.0	2015.0
C_{EDstop} (μg/L)	1	**89.8**	**12.8**
	2	**3.1**	**2.0**
	3	**1.6**	**27.5**
Termination year*	1	2020.5	2061.0
	2	2031.0	2023.0
	3	2023.0	2023.0
N_{smp} (/yr)	1	**3**	**3**
	2	**1**	**1**
	3	**1**	**1**

Note) **Bold**: optimized values based on the calibration in Stage
* Termination year was post-simulated for true parameters using optimize ED variables.

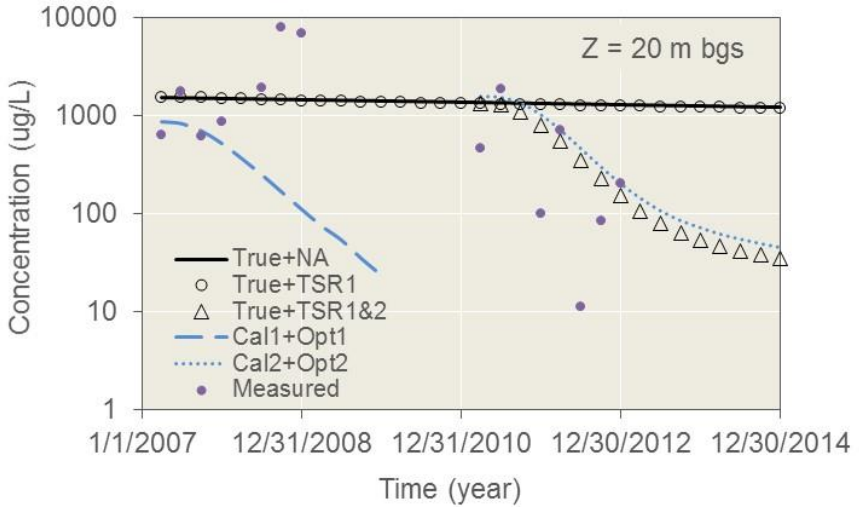

Figure 7.8. TCE concentration of MW2 based on true parameters + recovery data, and calibration + optimization in Stages 1 and 2.

Optimization

Measured mass recovery data for Source 1 and the design variables of ED1 and ED2 from Stage 2 optimization were implemented continuously up to the beginning date of Stage 2 optimization Jan 2011. Stage 2 optimization determines 1) optimal mass recovery and sampling strategy for Source 2 (TSR2) and 2) optimal injection rate, termination date, and sampling frequency of both EDs. Compared to Stage 1, the injection rate of ED1 (middle) increased due to Source 2 identification and ED2 (downstream) maintained its injection rate similar to Stage 1. It is notable that the termination criteria for both EDs are substantially decreased compared to Stage 1 (Table 7.6). This observation needs careful attention because the reduced (stricter) termination criteria did not extend injection duration because Stage 2 calibration provided more accurate parameters leading to less uncertain decision-making than Stage 1.

As presented in Figure 7.6, the projected CTC computed by Stage 2 optimization is similar to Stage 1 in which optimization was ideal only to Stage 1 calibration without Source 2. The projected CTC computed for the true parameters using Stage 2 optimization results are 40% less than the Stage 2 ENPV. Stage 2 optimization showed about 50 years longer NFA date than Stage 1 optimization but just 10 years longer than the Stage 1 true NFA date. As uncertain Source 2 is included in Stage 2 optimization, it is closer to the true behavior. By forward simulating Stage 2 optimization results with true parameters, the true t_{nfa} is shortened 40 years compared to that by Stage 1 optimization (Figure 7.6).

The actual cost toward t_{nfa} based on Stage 2 optimization is about \$13,600k that is much lower than the actual cost by Stage 1, \$19,200k. Note that actual cost includes the previously paid actual cost (Figure 7.7). As a part of post TSR monitoring, TCE concentration was quarterly measured at MW2 for multiple depths to improve Stage 3 calibration and optimization. Additional data for Stage 3 calibration include 1) TCE concentration data in all MWs up to 2015 and 2) TSR2 mass recovery data. Note that deterministic optimization was performed for Source 2 to estimate true mass recovery data.

Stage 3

Calibration

The optimized variables form Stage 1 and Stage 2 were implemented during the period of Jan 2007 to Dec 2010 and Jan 2011 to Dec 2015, respectively. TCE concentration in MW2 was monitored at 10, 20, and 30 bgs during and after TSR2 (2011~2012). Recall that Figure 7.8 describes the TCE concentration of MW2 at 20 m bgs for true parameters and Stage 1~2 calibration. Stage 2 calibration and optimization better describes the true TCE curve than Stage 1. This observation strongly supports that post-remediation monitoring is essential in decision-making for further progress. The measured concentrations in MW2 after TSR2 show significant reduction after TSR2 yet still highly uncertain due to noise.

TCE mass of Source 1 and Source 2 was more consolidated by adding MW2 data from 2007 to 2012. Calibrated values for mass flux and mass in Stage 3 are close to true values as shown in Figure 7.4, which is supported by posterior uncertainties for those parameters less than 0.1. Prediction uncertainty was also maintained similar to Stage 2 (Figure 7.5). Overall calibration efficiency (r) was 0.82, which is same as Stage 2 implying further calibration does not improve the prediction performance by adding extra data. As a result, final parameter values after Stage 3 calibration in Table 7.3 are close to their true values.

Optimization

Stage 3 optimization determines only ED1 and ED2 operation strategy. Because Stage 3 calibration with mass recovery data of Source 1 and 2 was credible, Stage 3 optimization can be a final stage to determine the design variables for the remaining period until met NFA. ED termination criteria ($C_{ED\ stop}$) are finally optimized as 1.6 and 27.5 ppb for ED 1 and ED2, respectively. Those are representative values that should be less than 95% UCL of previous 5-year measurements with $Sl_{nC}=S_{lnCpost}/N_{smp}^{1/2}$., where $S_{lnCpost}$ is the posterior SlnC from previous calibration. As $C_{ED\ stop}$ is stochastically optimized across 100 MC simulations, longer measurement series is recommended to estimate reliable UCL in fields.

Figure 7.6 indicates that t_{nfa} = 2042 determined by Stage 3 optimization is close to t_{nfa} = 2034 by true parameters simulated using Stage 3 optimization results. We expect those two values will be closer after Stage 4 calibration and optimization. Finally, the total accumulated actual cost to be incurred by t_{nfa} = 2034 is 37% lower than Stage 1 if implemented until t_{nfa} = 2079 (Figure 7.8)

7.6 References

Levine, H. (2010) EPA perspective on site closure: how clean is clean? US Department of Defense SERDP/ESTCP Partners in Environmental Technology Technical Symposium and Workshop, Washington DC, Nov 30-Dec 2.

8. Application to Joint Base Lewis-McChord EGDY site

8.1 Site Description

The East Gate Disposal Yard (EGDY) is a source of groundwater contamination at the Logistics Center National Priority List Site located on Joint Base Lewis-McChord (JBLM) in Fort Lewis, Washington (Figure 8.1). EGDY was used between 1946 and the mid-1970s as a waste disposal site for solvents from cleaning and degreasing operations. Material was transported to the disposal yard in barrels and vats from various areas. About seven barrels of liquid waste per month were disposed during peak operation. A TCE plume in the shallow aquifer evolved from the disposal site with concentrations in the range of hundreds μg/L in the source area and concentrations exceeding 5 μg/L over 4 km downgradient (Dinicola, 2005; USACE, 2008).

The climate of Fort Lewis is characterized by warm dry summers and cool wet winters with a mean annual temperature of about 13 °C and mean annual precipitation of about 1000 mm. Fort Lewis is underlain by a complex and heterogeneous sequence of glacial and non-glacial deposits including a shallow aquifer (Vashon) and a deep aquifer (Sea Level Aquifer, SLA). The Vashon aquifer is unconfined and continuous throughout the Fort Lewis area. It ranges in thickness between about 30 to 60 meters. The Vashon and SLA aquifers are separated by a mostly continuous low permeability aquiclude. However, a "window" occurs about 2 km downgradient of the disposal area that allows water and contaminants from the shallow Vashon aquifer to migrate to the deep SLA aquifer.

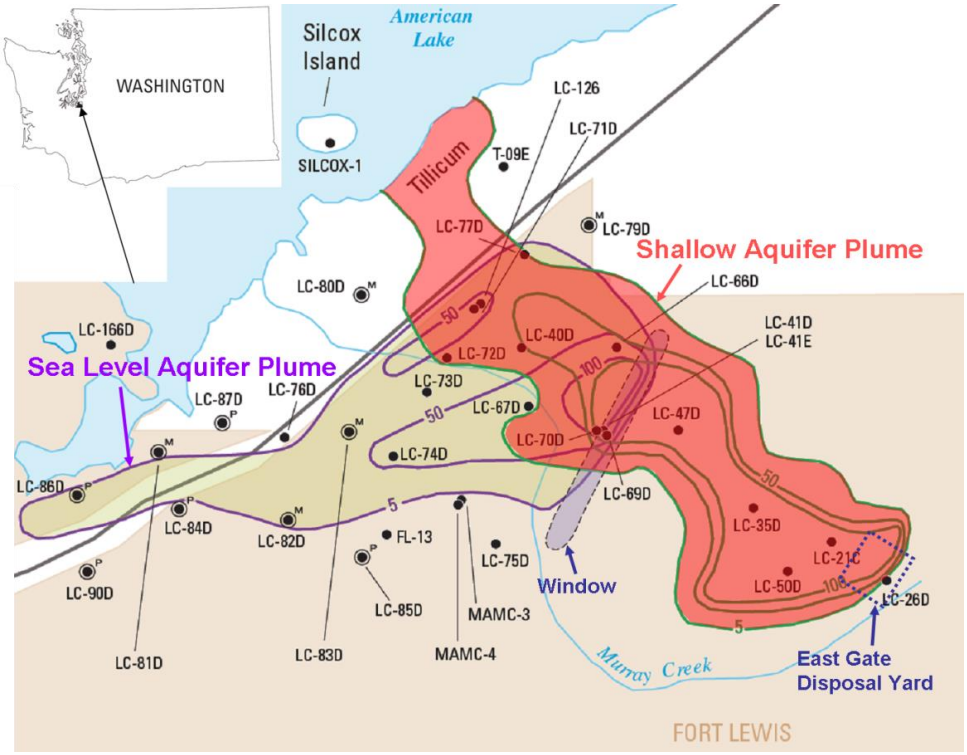

Figure 8.1. Location of EGDY site and TCE plumes as of 2004 (Dinicola, 2005).

Groundwater at Fort Lewis generally flows to northwest in the Vashon aquifer and west-southwest in the SLA aquifer. A simplified geologic cross section of the Fort Lewis site is shown in Figure 8.2. More details on the site geology are found in Dinicola (2005), Truex et al. (2006), and USACE (2008).

Several remediation actions have been performed at the EGDY site to contain the existing contaminant plume or reduce DNAPL mass in the source zone. Disposal trenches were excavated in 2000 to remove contaminated waste buried above the water table. About 1260 drums of contaminant were removed. To reduce DNAPL mass below the water table, Thermal source treatment (TSR) using electrical resistance heating was implemented for three source zones between late 2003 and early 2007. Tables 8.1 and 8.2 summarize the activities.

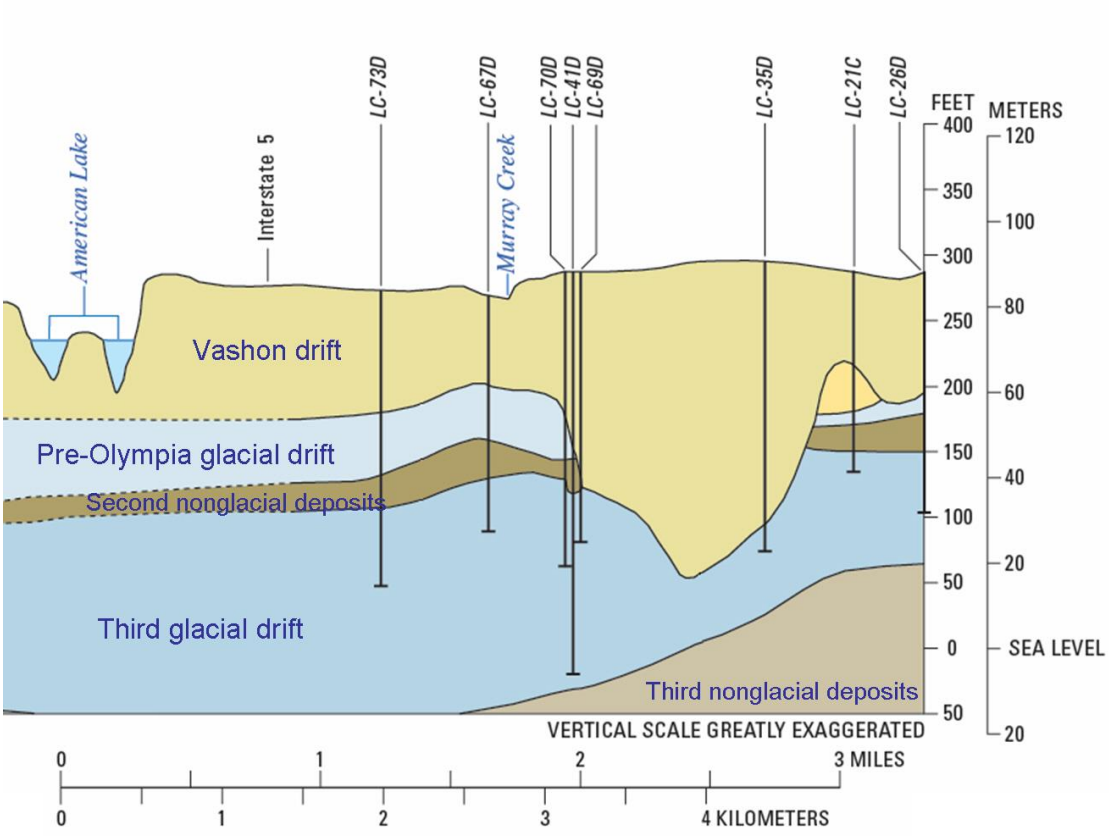

Figure 8.2. Hydrogeologic cross section of Fort Lewis site (Dinicola, 2005).

Table 8.1. EGDY site remediation history (USACE, 2008)

Date	Activity	Location
1995 - 2005	Pump-and-treat systems installed in Vashon Aquifer	One near EGDY second near highway I-5
2003 - 2005	Integrated pump test in Areas 1 and 3 in Nov 2003 and Sep 2005, respectively	EGDY
2003 - 2005	Source flux measurements in Areas 1 and 3 in Nov 2003 and Sep 2005, respectively	EGDY
2003 - 2006	TSR and monitoring in Areas 1, 2 and 3 in Dec 2003 - Aug 2004, Feb 2005 - Aug 2005, and Oct 2006 - Jan 2007, respectively	EGDY
2005-2006	Whey injection pilot tests	EGDY
2005 - 2007	Post-TSR monitoring in Areas 1,2 and 3 in May 2005, Sep. 2005, and Feb 2007, respectively	EGDY
2006 - 2008	Post-treatment soil coring in Areas 1,2 and 3 in Apr 2006, Apr 2006, and Mar 2008, respectively	EGDY
2009	Pump-and-treat system installed in SLA	Near hospital
2010	SLA P&T system in operation	

Table 8.2. Summary of TSR operations at EGDY site (USACE, 2008)

Variable	Area 1	Area 2	Area 3
TSR treatment area (m^2)	2360	2080	1691
TSR max depth below ground surface (m)	10	16	9
TSR treatment volume (m^3)	23625	135953	15368
Energy on date	12/17/2003	02/14/2005	10/11/2006
Energy off date	08/04/2004	08/05/2005	01/26/2007
Duration (days)	231	172	107
Mass removal, TCE + DCE (kg)	2990	1340	1120

8.2 Model Calibration

8.2.1 Characterization of groundwater flow field

The EGDY site was analyzed by Kim et al. (2013) as a part of ER-1611 using version 1 of SCOToolkit that used a semi-analytical vertically-averaged 2-D transport solution. The present analysis employs SCOTolkit version 3 that is capable of simulating 3-D transport for both contaminant and electron donor and uses a more rigorous model for thermal treatment. Therefore, as a first step to set-up a revised site characterization model for calibration, all previous monitoring data were converted to a 3-D format using the mid-screen elevation as the model depth.

Improved functionalities of SCOToolkit enable iterative recalibration and reoptimization to refine remediation and monitoring strategies over time. The analysis considers multiple zones in the aquifer with different first-order decay coefficients to simulate distance-dependent natural attenuation and losses from the shallow Vashon aquifer to the deeper SLA through a "window" between the two units (Figure 8.1)

Groundwater flow at the EGDY site was characterized by USACE (2008). The model used in this project simulates groundwater flow and transport with curvilinear streamlines as described in Chapter 2. Streamlines commence from each DNAPL source and actual or planned ED injection galleries. Groundwater streamlines were digitized and fitted to third-order polynomial equations of the form $y = ax+bx^2+cx^3$ (see Chapter 2). The model computes travel distances from sources to the wells of interest along streamlines. Transport in the SLA is not simulated since the contaminant plume in SLA has been contained by P&T since 2010. Instead, this analysis models vertical mass losses through the "window" between the two aquifers using a first-order reaction coefficient to simulate advective losses proportional to the Vashon aquifer concentration and the vertical hydraulic flux.

Coefficients of individual streamline equations are presented in Figure 8.3. ED galleries 1 to 3 upgradient of each source are not simulated in this analysis, which focuses on the effects of TSR and possible additional source zones. An electron donor gallery immediately upgradient of an inferred but unknown source zone (Source 4 hereafter) will be considered for potential mass transfer enhancement and downstream plume remediation. ED gallery streamlines follow the same functions as the associated sources.

8.2.2 Calibration using pre- and post-TSR data

Chlorinated solvent concentrations in groundwater reported by Truex et al. (2006) were utilized to construct time-series for each monitoring well. Measured concentrations of TCE and DCE were converted to "TCE-equivalent" total concentrations such that the H-demand is equal to that for complete reduction of TCE and DCE to ethane (vinyl chloride levels are not significant). Note that calibration to total solvent concentration rather than to TCE alone means that the effective decay coefficient represents the product of individual species decay coefficients. Since the latter are typically much less than 10^{-2} $days^{-1}$, the effective decay for the total concentration will be very small and hence will contribute little to model uncertainty. Locations of monitoring wells in the Vashon aquifer used for model calibration are shown in Figure 8.3. Pre-TSR data include dissolved concentration measurements from 17 wells from Sep 1990 to Aug 2003.

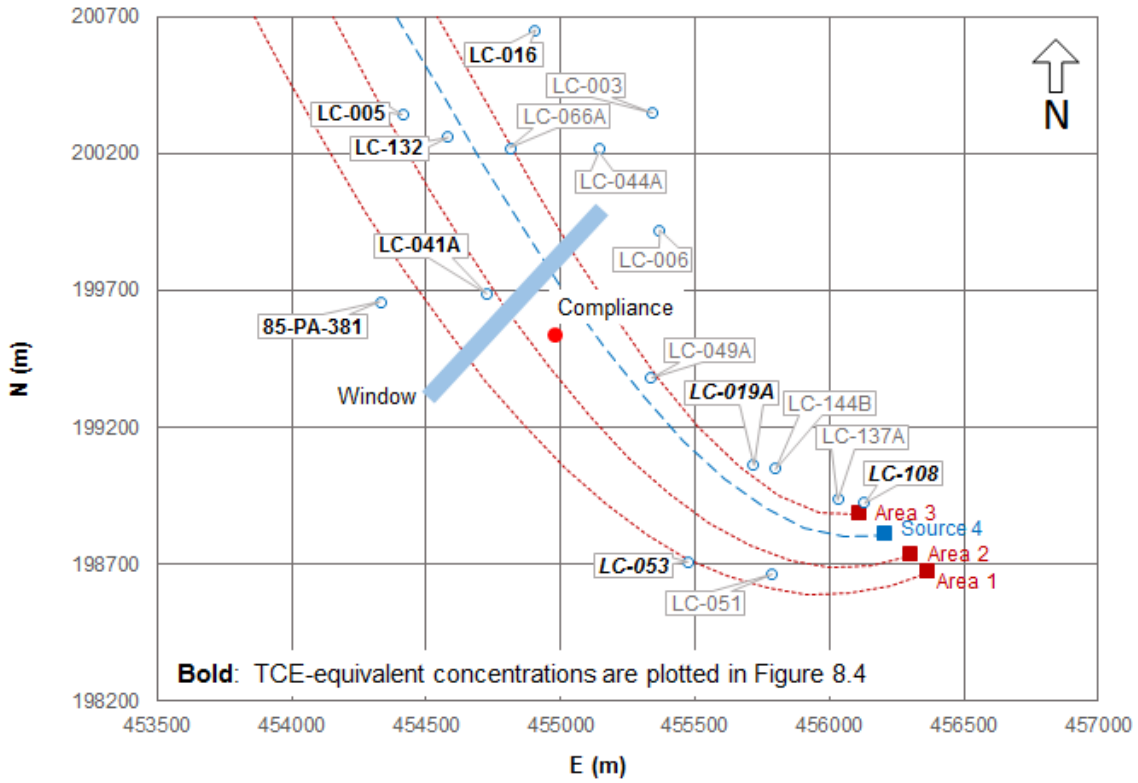

Origin	a	b	c
Area 1 (Source 1)	4.275E-01	5.615E-04	2.756E-08
Area 2 (Source 2)	3.500E-01	7.257E-04	6.437E-08
Area 3 (Source 3)	1.129E-01	1.244E-03	2.758E-07
Source 4 (unknown)	2.213E-01	4.172E-04	-9.595E-08

Figure 8.3. Streamlines and MWs used to model groundwater flow at the EGDY site. The blue zone represents the "window" connecting the Vashon and SLA units.

We assume that contamination in the SLA is transported from the Vashon aquifer through a window between the two aquifers (Fig. 8.3). The Vashon aquifer is divided into three zones with different decay coefficients. Zone 1 extends from the DNAPL sources to the window; Zone 2 encompasses the window itself; and Zone 3 is the region downgradient of the window. The model uses 0.0001 d^{-1} as a prior estimate of biodecay coefficients of for Zones 1 and 3 and 0.002 d^{-1} for Zone 2.

Mass flux was estimated to be 0.754 kg/d from Area 1, and 0.323 kg/d from Area 2 in November 2003, and 0.420 kg/d from Area 3 in April 2006. To model source zone mass dissolution and transport downstream, initial estimates of source and aquifer parameters were estimated from information in various reports (Dinicola, 2005; Truex et al., 2006; USACE, 2008) summarized in Table 8.3. Model parameters were calibrated to site data using 2000 as the reference year (t_{cal}) for source mass and source flux. Post-TSR data included longer time-series for pre-TSR wells through Mar 2015, plus measurements of source mass flux (Nov 2003 ~ Apr 2006) and mass removed by TSR (Dec 2003 ~ Oct 2006).

Figure 8.4 shows the time-series of available quarterly monitoring well (MW) data. Data was obtained from the JBLB and other USACE (2008). Calibration was performed using annually-averaged concentration data. Depending on the number of samples taken per year, this may involve averages of 2, 3 or 4 quarterly measurements or in some cases only a single measurement. Since calibration data variability will diminish with the number of samples averaged, measurement uncertainty is classified according to the number of samples averaged per year.

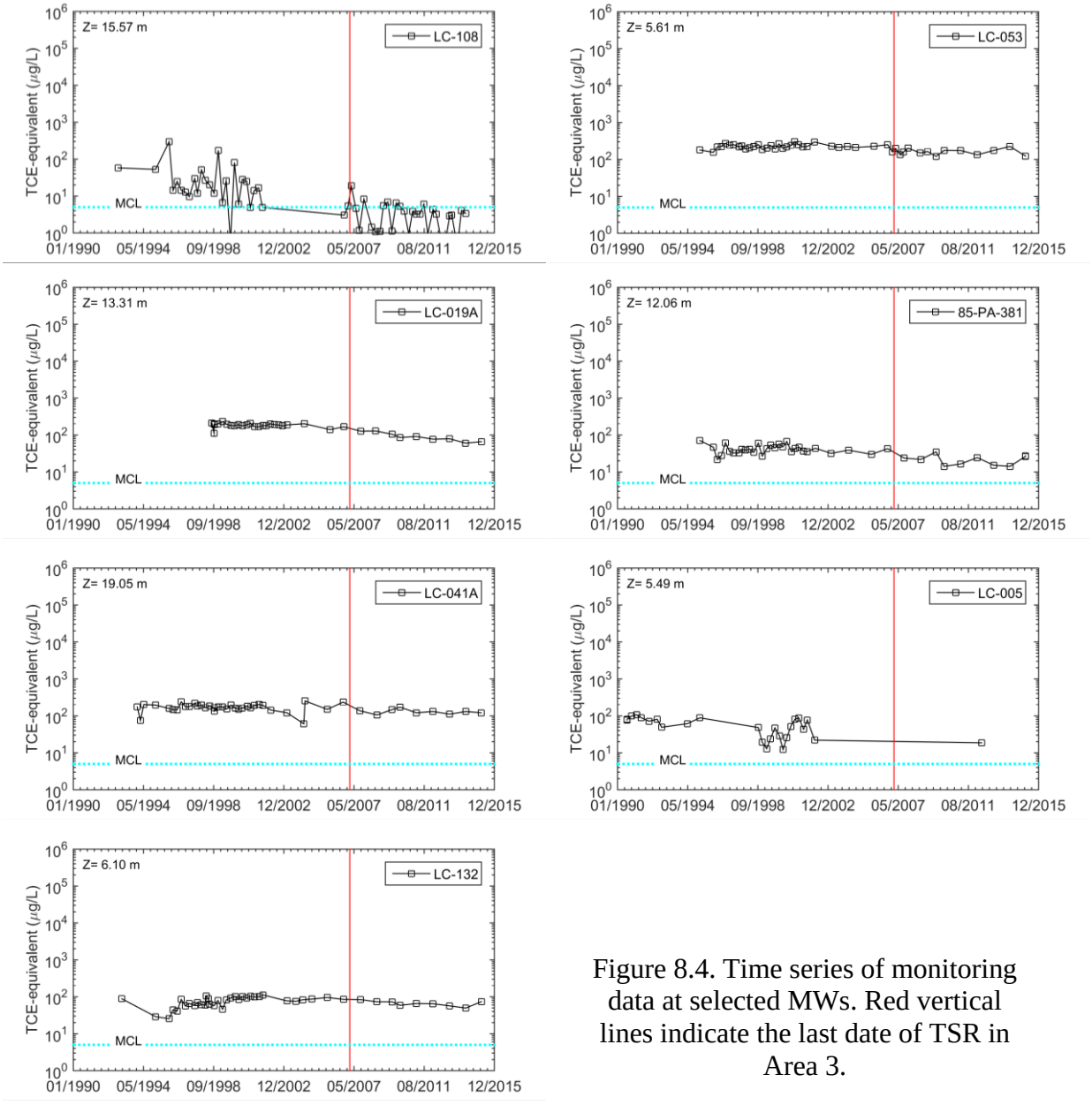

Figure 8.4. Time series of monitoring data at selected MWs. Red vertical lines indicate the last date of TSR in Area 3.

We performed calibration for three cases to incrementally improve parameter estimates:

1. Pre-TSR/S3/2003: calibrate 3-source model to MW data from Sep 1990 to Aug 2003 using prior estimates of source mass from pre-TSR data based on USACE (2008)
2. Post-TSR/S3/2007: calibrate 3-source model to MW data from Sep 1990 to Dec 2007 with actual TSR data based on USACE 2008 (with 3 standard deviation limits for M_{cal}).
3. Post-TSR/S4/2007: same as post-TSR/S3/2007 except (a) fixed M_{cal} for 3 known sources based on measured TSR recovery, and (b) calibrate parameters for a fourth unidentified source (S4).
4. Post-TSR/S4/2015: same as post-TSR/S4/2007 except include additional MW data through 2015

Table 8.3. Fort Lewis site characterization data.

Area	Parameters	Prior Value[1]	STD[2]	Reference
Area 1	Mass at 12/16/2003 (kg)	8600	0.27	USACE, 2008
	Flux at 12/16/2003 (kg/d)	0.75	1.00	USACE, 2008
	Release date	1970	5.00	USACE, 2008
	Width (m)	47		USACE, 2008
	Thickness (m)	9		USACE, 2008
Area 2	Mass at 02/13/2005 (kg)	7500	0.25	USACE, 2008
	Flux at 02/13/2005 (kg/d)	0.32	1.00	USACE, 2008
	Release date	1970	5.00	USACE, 2008
	Width (m)	42		USACE, 2008
	Thickness (m)	13		USACE, 2008
Area 3	Mass at 10/10/2006 (kg)	9500	0.27	USACE, 2008
	Flux at 10/10/2006 (kg/d)	0.42	1.00	USACE, 2008
	Release date	1973	5.00	USACE, 2008
	Width (m)	34		USACE, 2008
	Thickness (m)	8		USACE, 2008
Vashon	q (m/d)	0.4	0.25	Truex et al., 2006; Dinicola, 2005
	Porosity	0.29	-	Truex et al., 2006; Dinicola, 2005
	K_d (m^3/kg)	3.1E-5	0.25	Truex et al., 2006
	AL (m)	80	1.00	Assumed 10% of plume length
	AT/AL	0.1	1.00	Typical value
	AV/AL	0.01	1.00	Typical value
	λ for Zones 1 and 3 (/d)	1.0E-4	0.50	Initial value
	λ for Zones 2 (/d)	2.0E-4	0.50	Initial value
	Saturated depth (m)	30	0.20	Truex et al., 2006
	ED average (H-eq ppb)	48	0.15	Dinicola, 2005
	Saturated depth (m)	30	0.20	Truex et al., 2006

[1] Prior estimates represent arithmetic mean for release date, geometric mean for other parameters.

[2] Standard deviations of prior estimates are dimensionless statistics for ln-transformed values for all parameters except release dates, which are in actual units.

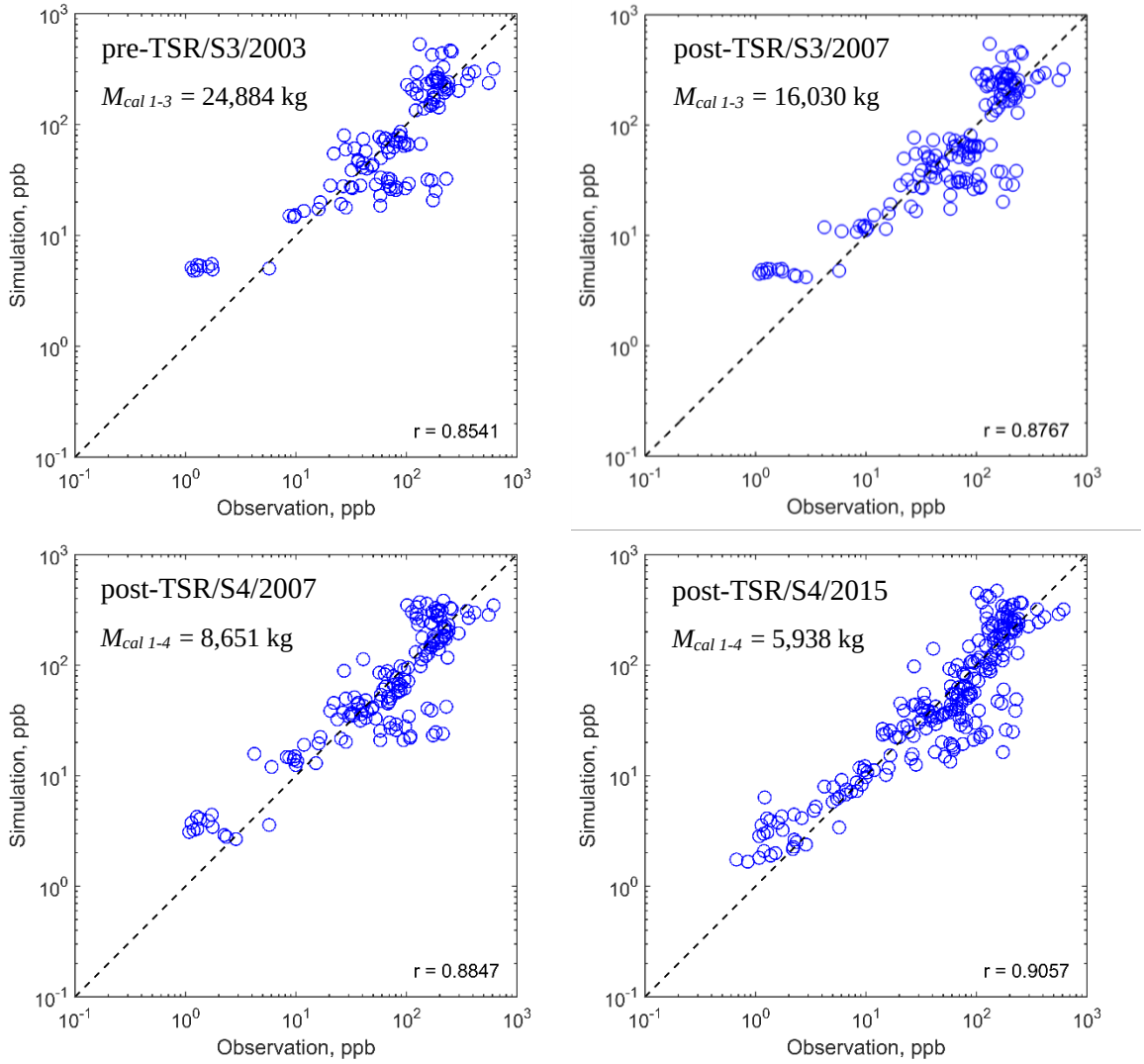

Figure 8.5. Observed vs. simulated concentrations for different model calibrations. $M_{cal\ 1\text{-}3}$ is the total calibrated mass in sources 1-3 in 2003; $M_{cal\ 1\text{-}4}$ is the mass in sources 1-4.

Figure 8.5 shows scatter plots and correlations for observed versus predicted concentrations for each calibration. Correlation coefficients improve slightly for each progressive calibration from 0.85 for pre-TSR/S3/2003 to 0.91 for post-TSR/S4/2015. However, estimated parameter values differ significantly. In particular, the total M_{cal} for the three identified sources ($M_{cal1\text{-}3}$) is 24,884 kg for the pre-TSR/S3/2003 calibration and 16,030 for the post-TSR/S3/2007 calibration in 2003 (t_{cal}), which are 4.6 and 2.9 times the actual mass recovery during TSR indicating thermal recoveries of only 22% and 34% for the respective calibrations (Table 8.4).

These unreasonably low recovery ratios led us to infer that a fourth unidentified source is likely. Upon initially reaching this conclusion, we performed a modified post-TSR/S3/2007 calibration with upper bounds for M_{cal} of the three known sources specified assuming 99% recovery by thermal. The results (not shown) yielded very poor results with a correlation of only 0.28, indicating the three-source model is not consistent with observed thermal recovery.

No empirical data is available to identify the location or dimensions of a fourth source. However, preliminary sensitivity analyses indicated a location on a streamline between TSR areas 2 and 3 produced the greatest regression improvement. No attempt was made to rigorously calibrate the source location and geometry. In our experience, calibrating source locations is very difficult in the absence of a very dense monitoring network. In particular, a source located roughly along the identified streamline but substantially up or downgradient could produce very similar results. Additional field investigations would be necessary to locate the unidentified source if this is deemed necessary.

Post-TSR/S4/2007 and post-TSR/S4/2015 calibrations in Table 8.4 fixed M_{cal} for the three known sources at 5,506 kg assuming 99% recovery by thermal treatment yielding estimates for a fourth unidentified source of 3,145 kg and 432 kg, respectively, based on the assumed source location.

Table 8.4. Calibration summary for EGDY site.

	Pre-TSR/ S3/2003		Post-TSR/ S3/2007		Post-TSR/ S4/2007		Post-TSR/ S4/2015		
Parameters	*Best*	S_{ln}	*Best*	S_{ln}	*Best*	S_{ln}	*Best*	S_{ln}	Notes
M_{cal1}	8473	0.27	7702	0.32	3020	*	3020	*	2990 kg removed by Aug'04
M_{cal2}	7150	0.24	3598	0.38	1354	*	1354	*	1340 kg removed by Aug'05
M_{cal3}	9262	0.27	4730	0.47	1132	*	1132	*	1120 kg removed by Jan'07
M_{cal4}	-	-	-	-	3145	0.78	432	0.50	unidentified
$M_{cal\ sum}$	24884	-	16030	-	8651	-	5938	-	5450 kg removed by Jan'07
J_{cal1}	0.16	0.77	0.09	0.68	0.27	0.28	0.20	0.21	0.75 kg/g in Nov'03
J_{cal2}	0.77	0.30	0.34	0.27	0.12	0.64	0.10	0.47	0.32 kg/d in Nov'03
J_{cal3}	0.34	0.31	0.19	0.25	0.12	0.37	0.10	0.26	0.42 kg/d in Apr'06
J_{cal4}	-	-	-	-	0.25	0.31	0.08	0.20	
$J_{cal\ sum}$	1.26	-	0.62	-	0.76	-	0.48	-	
β_1	1.00	0.50	1.00	0.50	0.98	0.40	1.07	0.37	
β_2	1.00	0.35	1.29	0.28	1.03	0.48	1.12	0.46	
β_3	1.00	0.48	1.14	0.45	1.10	0.36	1.07	0.33	
β_4	-	-	-	-	1.09	0.44	1.03	0.24	
λ_1	9.4E-5	0.45	6.7E-5	0.42	8.7E-5	0.43	5.8E-5	0.43	
λ_2	9.7E-4	0.42	1.0E-3	0.30	9.9E-4	0.40	9.2E-4	0.31	
λ_3	5.8E-4	0.30	4.7E-4	0.21	7.8E-4	0.26	7.9E-4	0.15	
q_w	0.18	0.20	0.10	0.15	0.15	0.19	0.10	0.08	
A_L	89	0.54	119	0.47	33	0.55	41	0.46	
A_T/A_L	0.20	0.53	0.15	0.45	0.37	0.57	0.27	0.48	
A_V/A_L	0.03	0.81	0.02	0.82	0.03	0.79	0.02	0.76	

Notes: Calibration reference date (t_{cal}) is 2003.

Best values denote calibrated best estimates.

S_{ln} values are posterior estimates of ln-transformed parameter standard deviations.

Units are kg for M_{cal}, kg/d for J_{cal}, d^{-1} for λ, m/d for q_w, and m for A_L

*indicates indeterminant S_{ln} because parameters are fixed based on actual TSR recovery data.

The pre-TSR/S3/2003 calibration represents our best *initial* estimate of model parameters with data available through 2003, while the post-TSR/S4/2015 calibration represents best *final* estimate with thermal recovery data and 12 additional years of monitoring data (Table 8.4). The largest differences occur in source parameters, with an estimated total mass in all sources of 24,884 kg in 2003 for the initial calibration, but only 5,938 kg for the final calibration of which 432 kg is in the unidentified fourth source.

The mass discharge from all sources in 2003 was estimated to be 1.26 kg/d for the initial calibration, but only 0.48 kg/d for the final calibration. Source depletion exponents (β) are essentially the same for all calibrations, although sensitivity to this parameter appears to be low. Effects of lower estimates of source mass and discharge rate for the final calibration (which tend to decrease predicted concentrations) appear to be offset by a zone 1 decay coefficient (λ_1 closest to the sources) that is 38% smaller and a transverse dispersivity (A_T) that is 39% smaller for the final calibration relative to initial calibration values (which tend to increase simulated concentrations in the core of the plume).

8.3 Remedial design evaluation and optimization

8.3.1 Long-term simulations with no further remediation action

Non-optimized MC simulations were performed to assess the long-term effectiveness of thermal treatment at the site based on the initial pre-TSR/S3/2003 and final pre- and post-remediation parameter estimates. Simulations of TSR were made such that the contaminant mass removed from each source was equal to the measured removal. The following simulations were performed:

- NoOpt1a - No TSR or subsequent remedial action for pre-TSR/S3/2003 calibration
- NoOpt1b - Actual TSR with no other remedial action for pre-TSR/S3/2003 calibration
- NoOpt2a - No TSR or subsequent remedial action for post-TSR/S3/2007 calibration
- NoOpt2b - Actual TSR with no other remedial action for post-TSR/S3/2007 calibration
- NoOpt3a - No TSR or subsequent remedial actions for post-TSR/S4/2007 calibration
- NoOpt3b - Actual TSR with no further remediation for post-TSR/S4/2007 calibration
- NoOpt4a - No TSR or subsequent remedial actions for post-TSR/S4/2015 calibration
- NoOpt4b - Actual TSR with no further remediation for post-TSR/S4/2015 calibration.

Simulations for the above cases were performed to simulate probability distributions for TCE-equivalent concentration at a compliance well (Figure 8.3) screened over the upper 10 m of the Vashon aquifer. Median estimates and two-sided 95 and 99% probability confidence limits were computed for each case (Figure 8.6).

NoOpt1 results, based on the pre-TSR/S3/2003 calibration, indicate a 50% probability that the TCE-equivalent concentration will be less than 5 μg/L in the year 2205 without thermal treatment (95% confidence limits from 2095 to 2303) and in 2150 with the actual thermal treatment (95% confidence limits from 2080 to 2294).

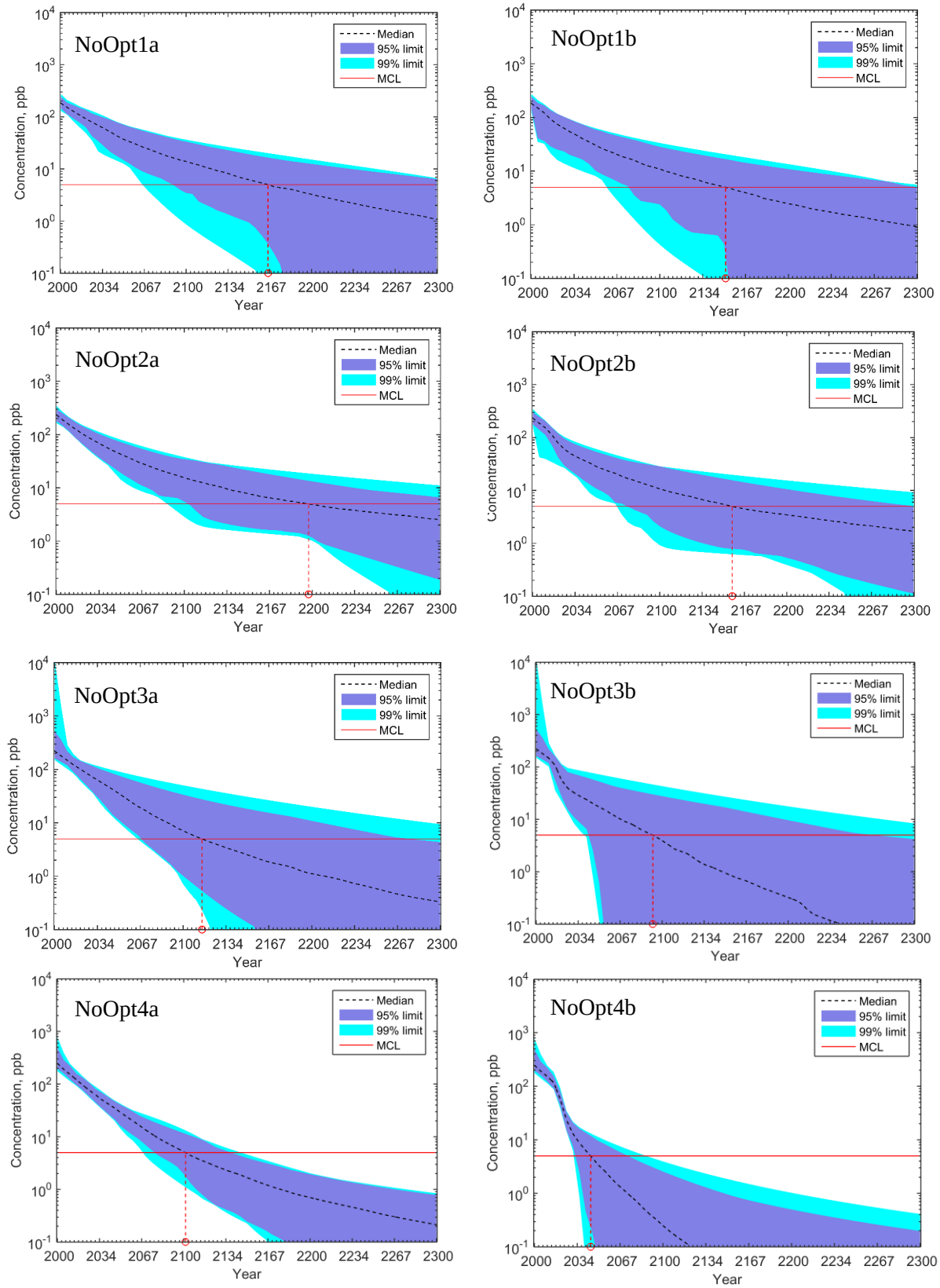

Figure 8.6. TCE-equivalent concentration at the compliance well without source treatment (left) and with actual source treatment (right) based on different calibrations (rows). Solid red lines represent the MCL for TCE. Dashed red lines denote 50% probability time to reach MCL.

Results for NoOpt2, based on the post-TSR/S3/2007 calibration, do not differ substantially from NoOPt1 results. The results indicate there is a 50% probability that the TCE-equivalent concentration will be less than 5 µg/L in 2200 without thermal treatment (95% confidence limits from 2123 to 2334) and in 2160 with the actual thermal treatment (95% confidence limits from 2074 to 2288).

NoOpt3, based on the post-TSR/S4/2007 calibration, yields a 50% probability that the TCE-equivalent concentration will be less than 5 µg/L in 2115 without thermal treatment (95% confidence limits of 2067 to 2275) and in 2095 with the actual thermal treatment (95% confidence limits of 2053 to 2239). The median dates are significantly earlier that for NoOpt1 and NoOpt2.

NoOpt4, based on the pre-TSR/S4/2015 calibration, indicates a 50% probability that the TCE-equivalent concentration will be less than 5 µg/L in 2100 without thermal treatment (95% confidence limits of 2078 to 2132) and in 2040 with thermal treatment (95% confidence limits of 2027 to 2069).

While the spread between upper and lower 95% confidence limits decreases little from NoOpt1 to NoOpt3, averaging about 200 years, the spread decreases to about 50 years for NoOpt4, indicating the last 8 years of monitoring data has significantly improved model precision. Specifically, NoOpt4b indicates that without any additional active remediation, compliance is expected by 2040 with 50% confidence and by 2069 with 95% confidence. In the meantime, pump-and-treat systems in the Vashon and Sea Level aquifers would need to continue operation to control plume migration.

Figure 8.7 summarizes the predicted upper and lower 99% confidence limits and median dates at which concentrations are predicted to fall below 5 µg/L based on initial and final calibrations with no remedial actions (NoOpt1a and NoOpt4a) and with actual thermal treatment of known sources (NoOpt1b and NoOpt4b). While confidence bands for simulations of no remedial action based on initial and final calibrations mostly overlap at the 99% level, confidence bands for simulations with remedial actions only partially overlap and the median NoOpt4b date lies below the lower 99% confidence limit of the analogous NoOpt4b simulation. This indicates that error bounds based on the early calibration are not accurate, which we attribute, at least partially, to errors in the conceptual site model (i.e., missing source).

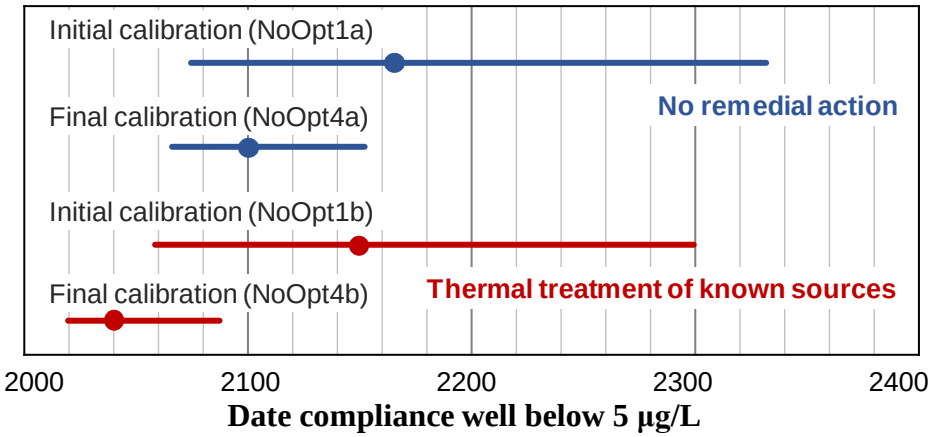

Figure 8.7. Confidence bands (two-tailed 99%) for date to reach 5 ppb concentration at the compliance well with no remedial action (blue lines) or with actual thermal treatment of the three known sources only (red lines) based on initial or final calibrations. Circles are median dates.

8.3.2 Progressive calibration-optimization analysis

Data from the EGDY site was used to perform a two-stage progressive calibration-optimization analysis as follows:

1. Perform initial calibration (pre-TSR/S3/2003),
2. Optimize thermal system for S1-S3 using pre-TSR/S3/2003 parameters (Opt1),
3. Implement optimized design and monitor site through 2007,
4. Recalibrate with additional data (post-TSR/S4/2007) which identifies a likely S4 source,
5. Optimize thermal remediation system for S4 using post-TSR/S4/2007parameters (Opt2).

The first optimization (Opt1) addresses thermal system design for the three known sources as of 2003. Each source is regarded as a single thermal "treatment zone" (TZ), which is divided into 4 "monitoring zones (MZ). All heating units within a given TZ are turned off when the upper confidence limit of the measured TZ soil concentration is below $C_{stop\ global}$. Heating units within individual MZs may be terminated prior to reaching the TZ level criteria if the upper confidence limits of measured MZ soil concentration is below $C_{stop\ local}$ Values for $C_{stop\ local}$ and $C_{stop\ global}$ were optimized subject to the condition that $C_{stop\ local} \leq C_{stop\ global}$. Vapor monitoring of each TZ and MZ was assumed for making thermal system termination decisions (Chapter 4). Compliance is based on the RCL rule (Chapter 7) with 95% confidence using a 5-year lookback period with quarterly groundwater sampling. A cost penalty (Chapter 7) was applied if compliance well concentrations do not meet compliance levels by a penalty date $t_{penalty}$ (2035) or if site-wide cleanup criteria are not met by t_{max} (2050). Cost variables used for both optimizations are summarized in Table 8.5.

Table 8.5. Cost variables used in design optimization.

Description	Variable	Value	Unit
Thermal treatment costs [a]			
Total fixed cost for thermal treatment excluding monitoring	$cap	937, 559, 334, 748	$k
Operating cost per day excluding heating unit operating cost	$SiteOp/day	12.00, 11.95, 15.50, 11.97	$k/day
Operating cost per day for TZ*i* with all heating units on	$TZop/day	6.18, 6.15, 7.98, 6.17	$k/day
Treatment cost per unit recovered	$mass	0.01	$k/kg
Cost per MZ for equipment to monitor mass recovery	$MZcap	0	$k
Cost per day per MZ to monitor cumulative mass recovery	$MZ/day	0	$k/day
Cost per soil boring	$boring	9.00, 6.44, 9.31, 7.72	$k
Cost per soil sample taken from a given boring	$soil smp	0.5	$k
Other costs			
Cost per compliance sampling event	$C_{samp}^{SWop} N_{well}^{SW}$	2.5	$k/event
PT operating costs and other site-wide costs [b]	C_{total}^{PTop}	87.5	$k/year
Penalty cost for non-compliance	C_{NPV}^{pen}	50,000	$k
Reference year for cost discounting	t_{ref}	2005	year
Discount rate	d	0	$year^{-1}$

[a] Estimated based on Table 6.6-5 of USACE (2008). Note: values do not include source characterization costs, post-remediation flux measurements or groundwater pumping at source. Four cost values are for each source.

[b] J. Gillie, CTR US USA IMCOM, personal communication (2010).

Optimized TSR design variables and costs for Opt1 are given in Table 8.6. The expected (probability-averaged) total cost for Opt1 was $15.828 million for operation from 2003 until site-wide NFA was attained with a failure probability of less than 1%. Opt1 results indicate a 99% probability of achieving NFA by 2029. (Figure 8.8a). Following completion of S1-S3 thermal treatment, the post-TSR/S3/2007 and post-TSR/S4/2007 calibrations revealed a likely fourth source (S4). As of late 2007, NoOpt3b, which is based on the post-TSR/S4/2007 calibration (Figure 8.6), provides the best forecast of performance following thermal treatment of S1-S3 with no additional active remediation. Contrary to the rosy projections of Opt1 (Figure 8.8a), which are predicated on only three sources and data through 2003, the four-source NoOpt3b simulation indicates that it is likely to take 100 years and may take 300 years or more to achieve NFA without additional remedial actions.

Accordingly, a second optimization (Opt2) was performed using post-TSR/S4/2007 calibration parameters to design an S4 thermal system to potentially commence operation in early 2008. Opt2 assumes S1-S3 treatment based on Opt1 design variables. Predicted remediation performance over time for Opt2 (Figure 8.8b) is very similar to that predicted for Opt1, which is not surprising since both assume all DNAPL sources to be treated to comparably small residual source levels. The expected total cost from 2003 to NFA attainment for Opt2 was computed from the expected cost for S4 treatment and site-wide operations from 2008 to NFA plus expected costs from 2003 through 2008 from Opt1, yielding a total of $21.922 million. This is significantly higher than that for the 2003 calibration-based optimization (Opt1). However, the low Opt1 cost is largely attributable to the inaccurate site conceptual model underlying the 2003 calibration (i.e., missing S4 source).

Table 8.6. Progressive optimization results for thermal remediation for EGDY site: Opt1 for sources 1-3 based on Pre-TSR/S3/2003 calibration. Opt2 for source 4 based on Post-TSR/S4/2007 calibration. Costs are not discounted.

Opt1 results	ENPV ($k)	Design Variables	
Source		$C_{stop\ global}$ (mg/kg)	$C_{stop\ local}$ (mg/kg)
TSR for S1	5,694	13.52	1.05
TSR for S2	4,730	2.40	0.46
TSR for S3	2,869	4.78	0.27
Expected other costs 2003-2007	2,535		
Expected total cost 2003-NFA	15,828		
Expected NFA date	2026		
Opt2 results		Design Variables	
Source	ENPV ($k)	$C_{stop\ global}$ (mg/kg)	$C_{stop\ local}$ (mg/kg)
TSR for S4	5,831	0.54	0.46
Realized 2003-2007 costs	12,958		
Expected other costs 2007-NFA	3,133		
Expected total cost 2003-NFA*	21,922		
Expected NFA date	2024		

* includes $500k for S4 characterization

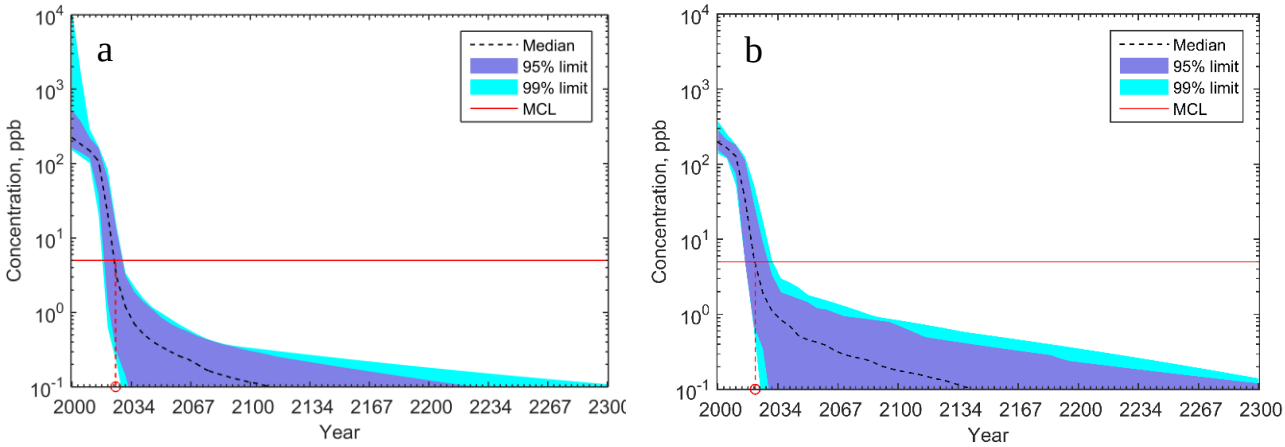

Figure 8.8. Confidence limits of TCE-equivalent concentration at the compliance location for (a) Opt1 based on pre-TSR/S3/2003 calibration, and (b) Opt2 based on post-TSR/S4/2007 calibration. Solid red line is MCL and dashed line is 50% probability date to reach MCL.

While the 2007 calibration exposes Opt1 results as unreliable, it is still pertinent to ask whether the Opt2 strategy for thermal treatment of S4 is cost advantageous relative to continuing to monitor and operate the existing pump-and-treat systems with no S4 treatment. We can evaluate this by comparing the Opt2 cost from 2008 to NFA attainment with the cost of monitoring and pump-and-treat from 2008 to the expected NFA date with prior remediation of S1-S3 but without S4 remediation. The latter result may be obtained from the previously discussed NoOpt3b simulation, which is based on the same calibration as Opt2 (post-TSR/S4/2007). A comparison is presented in Table 8.6 for undiscounted costs as well as for costs discounted at 3% per year. The results indicate that thermal treatment of S4 is preferable if costs are not discounted, while discounted costs favor not undertaking thermal treatment of S4.

Given uncertainty regarding the location of S4, steadily decreasing observed and simulated dissolved phase concentrations, and effective pump-and-treat systems in place for plume containment, a decision was taken to defer field investigations of the apparent fourth source.

The most recent calibration update based on monitoring data through 2015 provides an opportunity to evaluate remediation progress and reassess the need for further investigation and treatment of the S4 source. The NoOpt4b Monte Carlo simulation (Figure 8.6), which simulates dissolved contaminant concentrations over time at the compliance location based on the post-TSR/S4/2015 calibration with actual thermal treatment of S1-S3, provides a basis for this assessment.

NoOpt4b predicts a much earlier expected NFA date of 2050 versus 2110 for the 2007 calibration-based NoOpt3b simulation (Table 8.7). An analysis of expected costs based on the 2015 calibrated NoOpt4b simulation indicates that no treatment of the S4 source was more favorable than treating the source for both discounted and undiscounted expected costs, which validates the earlier decision to defer treatment of S4.

Table 8.7. Expected NFA date and cost from 2008 to NFA for 2007 and 2015 calibrations at two discount rates. Bold values indicate minimum cost remediation option for each calibration and discount rate.

Calibration	No S4 treatment			S4 thermal treatment		
	NFA date	Cost, $k (d=0%)	Cost, $k (d=3%)	NFA date	Cost, $k (d=0%)	Cost, $k (d=3%)
Post-TSR/S4/2007	2110	11.07	**3.43**	2035	**8.84**	7.89
Post-TSR/S4/2015	2050	**4.62**	**2.61**	2033	8.62	7.79

The 2007 calibration predicts that thermal treatment of S4 would decrease the NFA date from 2110 to 2035 with a slightly lower undiscounted total cost, but a substantially higher discounted cost (Table 8.7). The decision to treat or not treat S4 based on cost is sensitive to the discount rate due to a tradeoff between the large present cost for thermal treatment (~$6 million) versus long-term pump-and-treat costs (~$100k/year). In such cases, it is more conservative to use a lower discount rate, which suggests deferring treatment of S4 at least until the analysis is less ambiguous.

With additional data through 2015, long-term prediction uncertainty decreased resulting in a much earlier expected NFA date and lower discounted and undiscounted costs without S4 treatment, confirming the decision to defer treatment.

The decision not to pursue thermal treatment of S4 resulted in a 46% undiscounted cost savings and a 67% discounted cost savings based on the 2016 calibration.

8.4 References

Dinicola, R. S. (2005) Hydrogeology and trichloroethene contamination in the sea-level aquifer beneath the Logistics Center, Fort Lewis, Washington: U.S. Geological Survey Scientific Investigations Report 2005-5035, 50 p.

Kim, U., J. Parker, P. Kitanidis, M. Cardiff, X. Liu, and J. Gillie (2013) Stochastic Cost Optimization of DNAPL Remediation - Field Application. Environmental Modeling & Software 46: 12-20.

Macbeth, T. W. and K. S. Sorenson, Jr. (2008) Final Report: In Situ Bioremediation of Chlorinated Solvent Source Areas with Enhanced Mass Transfer. ESTCP Project ER-0218.

Truex, M. J., C. D. Johnson, and C. R. Cole (2006) Numerical Flow and Transport Model for the Fort Lewis Logistics Center, Fort Lewis, Washington. DSERTS NO. FTLE-33. Pacific Northwest National Laboratory, Richland, Washington, 121 p.

US Army Corps of Engineers (2008) East Gate Disposal Yard Thermal Remediation Performance Assessment After Action Report. 248 p.

9. Application to Dover AFB Area 5

9.1 Site Description

Dover Air Force Base (AFB) is located in Kent County, Delaware, and has been in operation since 1942. Base operations have generated numerous wastes, including solvents and hydrocarbons, which were historically buried in drums or disposed in the storm drainage system. Wastes were disposed in various on-base locations, which have resulted in several NAPL sources with comingled contaminant plumes. Our focus in this study is a merged groundwater plume associated with several sources within the West Management Unit (WMU) designated as Area 5 (ORNL, 2008).

Dover AFB is underlain by unconsolidated sediments of the Atlantic Coastal Plain (USGS, 2000). The units of interest are the Columbia Formation and the underlying Calvert Formation. The Columbia Formation is mainly composed of sands, silts and gravels. A clayey silt unit separates it from the Frederica aquifer in the upper Calvert Formation. The water table configuration at Dover AFB is generally controlled by surface water bodies including Little River, St. Jones River, and Delaware Bay (USGS, 2000) and recharge from precipitation. The average darcy velocity in Area 5 is estimated to be about 0.02 m/d (USGS, 2000).

Five contaminant sources in Area 5 have been identified, including three oil-water separator sites (OT51, OT50, OT44), a location with underground fuel storage tanks (SS20), and a waste collection drain site (OT41). Locations of the sources and time-series of TCE-equivalent concentrations at selected monitoring wells (MW) are shown in Figure 9.1. Chlorinated ethenes, ranging from VC to PCE and soluble fuel hydrocarbons (BTEX) have been monitored semi-annually since 1988 (Table 9.1).

A number of remedial actions have been undertaken to address chlorinated solvent contamination in Area 5, which are summarized in Table 9.2. Emulsified vegetable oil (EVO) and lactate solution have been injected as electron donors (ED) since 2006 to enhance microbial reductive dechlorination of chlorinated ethenes. The process, referred to as Accelerated Anaerobic Bioremediation (AAB), involves intermittent ED injection in 12 galleries known as Permanent Injection Circulation Transects (PICT).

Table 9.1. Contaminant source locations (ORNL, 2008).

Contaminant	OT51	Source E	OT50	SS20	OT44*	OT41*
Benzene	X			X	X	X
Toluene	X			X		X
cis-1,2-DCE	X	X	X	X		X
PCE	X	X	X	X		X
TCE	X	X	X	X	X	X
cis-1,2-DCE	X	X	X	X		X
VC	X	X	X			

Notes: X indicates contaminant is present at this source;
* indicates sources not considered in the present study (see text for discussion)

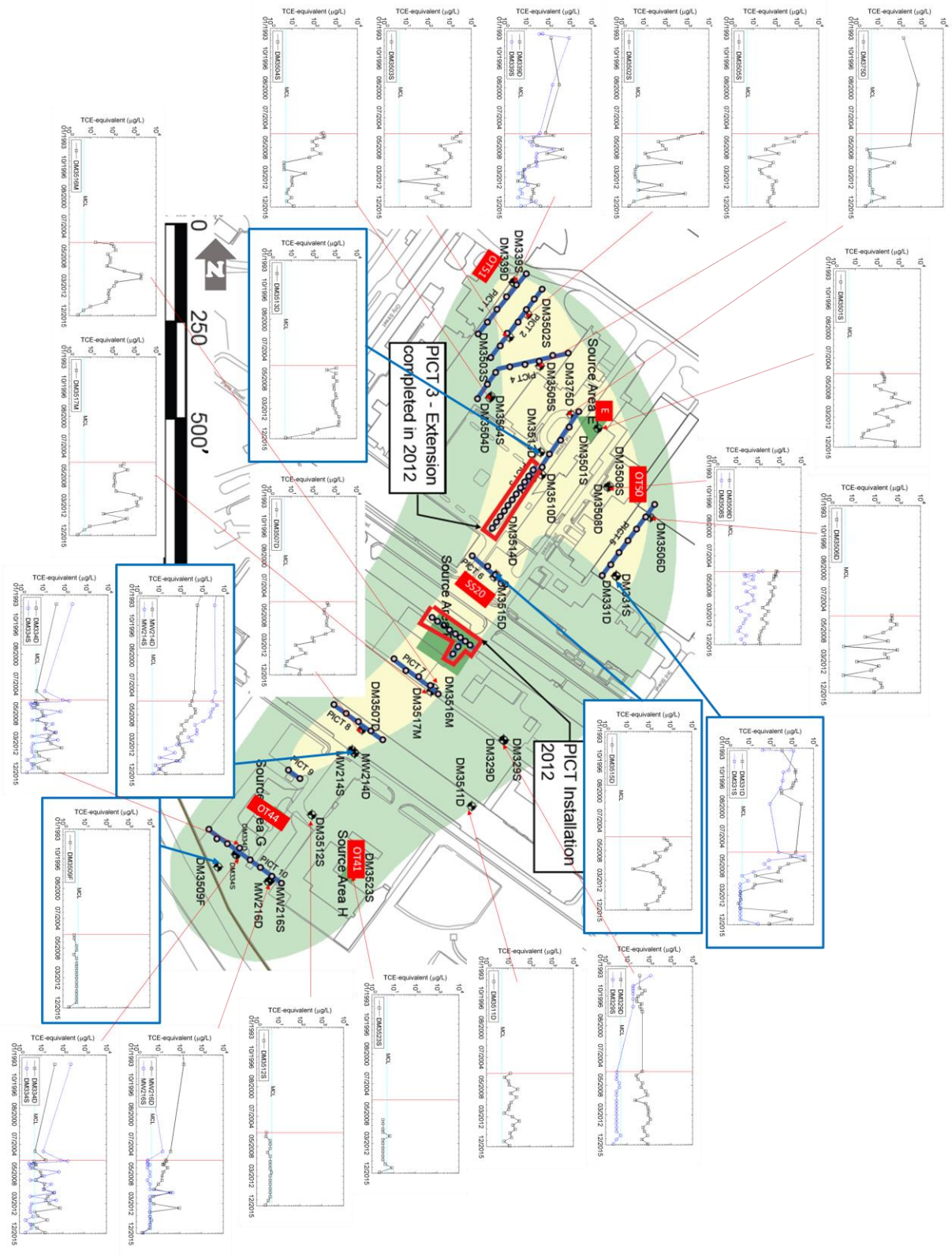

Figure 9.1. Contaminant plume as of 2005 with 5 and 500 ppb boundaries, locations of sources and MWs, and EVO injection galleries at Dover AFB Area 5. Red vertical line in plot: first injection of ED. Plot with thick border: compliance MWs.

Table 9.2. Chronology of events in Dover AFB (ORNL, 2008).

Date	Event
April 2006	Record of decision (ROD) prepared for OT51, OT50, SS20, O T44, OT41/Motor Pool, and Area 5 (WMU)
May 2006	Finalized Area 5 remedial action work plan (RAWP)
May 8 – 24, 2006	Collected membrane interface probe data delineate Source Ar eas D and E prior to treatment injections
May 16 – June 9, 2006	AAB direct injection performed at Source Areas E, F, G, and H
May – July 2006	Installation of AAB and monitoring wells
May – October 2006	First round of AAB PICT injections
Week of June 12, 2006	Baseline groundwater sampling conducted in upgradient porti on of Area 5 (OT51/OT50)
June 2006 – on going	AAB groundwater monitoring
July 2006	Natural Attenuation (NA) monitoring conducted for Area 5
January/February 2007	NA monitoring conducted for Area 5
July 2007 – November 2007	Second round of AAB PICT injections; stopped before compl etion because of cold weather
Apr 2012~ Oct 2012	Installed PICT3 extension and Source Area F (SAF)-PICT

Table 9.3. Classification of MWs in Area 5 (ORNL, 2008).

Well ID	AAB	NA	Well ID	AAB	NA	Well ID	AAB	NA
DM3501S	X		DM3511D		X	DM335S		X
DM3502S	X		DM3512S		X	DM335D		X
DM3503S	X		DM3513D*	X		DM339S	X	
DM3504S	X	X	DM3514D	X	X	DM339D	X	
DM3504D	X	X	DM3515D*	X		DM375D		X
DM3505S	X		DM3516M	X	X	DM378F		X
DM4507D	X		DM3517M	X		MW078S		X
DM4506D	X		DM329S		X	MW078D		X
DM3507D	X		DM329D		X	MW214S		X
DM3508S	X	X	DM331S*		X	MW214D*	X	X
DM3508D	X	X	DM331D		X	MW216S	X	X
DM3509F*		X	DM334S	X	X	MW216D	X	X
DM3510D	X		DM334D	X	X			

Note: S = shallow, M = middle, D = deep, * = selected compliance locations.

9.2 Model Calibration

Groundwater streamlines originating at each contaminant source were estimated from water table contours and the contaminant plume and described by cubic polynomial regressions (Figure 9.2). Streamline functions starting from each EVO injection gallery were also determined. To obtain streamline functions that increase monotonically in the x-direction, streamline regressions were performed with northing as the x-coordinate and easting as the y-coordinate as discussed in Chapter 3.

The Area 5 model simulates DNAPL source dissolution and transport for each source as well as transport of injected ED from each injection gallery (i.e., PICTs in Figure 9.2). Since the model does not explicitly simulate incomplete dechlorination, we model total chlorinated ethenes as a pseudo-species. We sum the concentrations of all chlorinated ethene species after converting to their stoichiometric equivalent quantity of TCE as described in Chapter 3. Model calibration was performed initially using chlorinated solvent data collected from 1988 to 2005 before ED injection started, followed by a series of post-remediation calibrations by using MW data up to 2015.

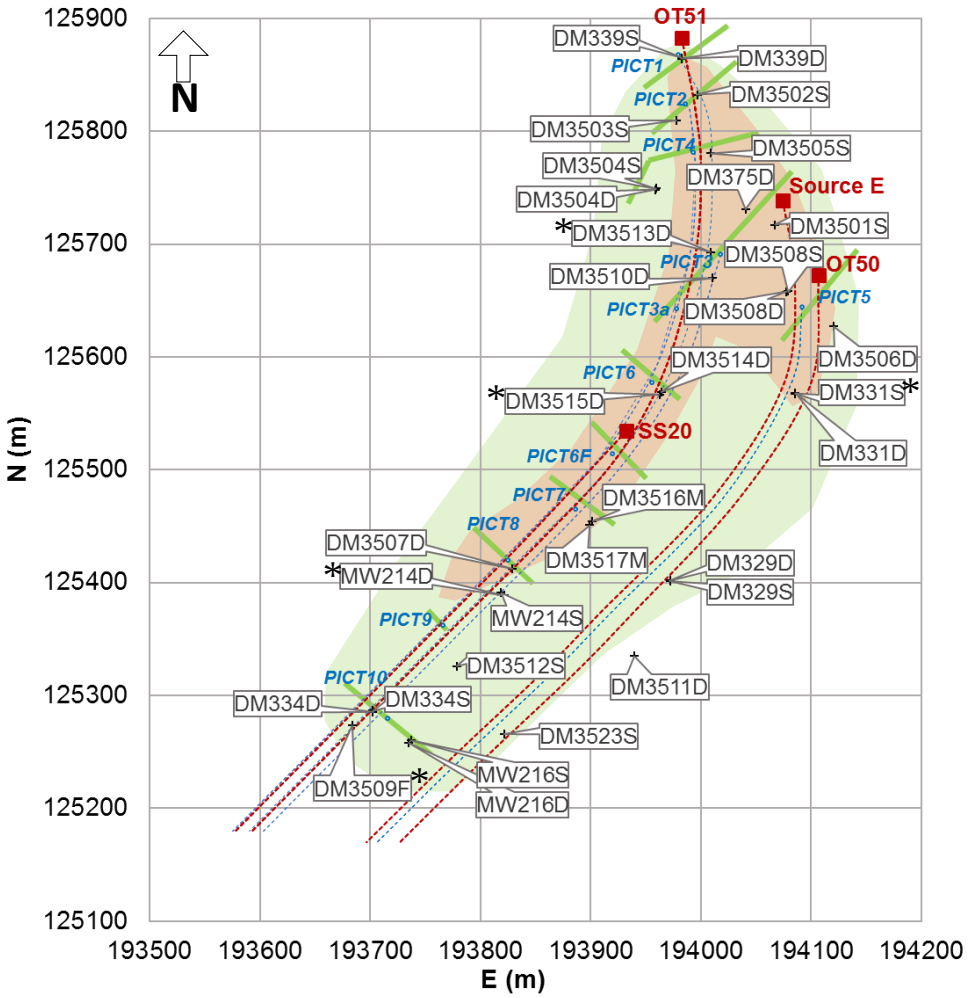

Figure 9.2. Streamlines for sources and ED injection galleries (PICTs). Compliance MWs are marked with *.

While Lee et al. (2012) used depth-averaged data in a 2-D model, the present analysis used data from various depths to calibrate a three-dimensional model. Non-detect measurements that represent 22% of entire MW data were omitted to avoid biased calibration on a log-scale, which can be sensitive to the numerical value that must be assigned to non-detects to enable calibration. A sufficiently large number of low concentration measurements remained in the calibration data to constrain the plume perimeter. Most measurements (87%) are less than 500 ppb. Based on preliminary calibrations, high concentrations were not well calibrated using equal weights on log-concentrations. Therefore, a weighting factor classification method was used to give greater weight to high log-concentrations. Final weighting factors were determined as 1 for <500 ppb, $2^{1/2}$ for 500-1000 ppb, 2^{1} for 1000-5000 ppb, and $2^{1.5}$ for 5000-10000 ppb.

Unlike Lee et al (2012), sources OT41 and OT44 were omitted from the model in this study, because preliminary calibrations indicated they had negligible contribution to observed chlorinated solvent concentrations. PICT gallery widths, start and stop dates for injection each year, and quantities of ED injected were obtained from AAB operational data.

Each contaminant source was characterized by its width, initial release date, contaminant mass M_{cal}) in Jan 2006 (t_{cal}), source discharge rate (J_{cal}) in Jan 2006, and mass depletion exponent (β). Initial estimates of parameters for each source are given in Table 9.4. Values of J_{cal}, M_{cal}, and β were calibrated for each source. To reduce the number of parameters, all sources were assumed to have the same source release year calibrated with minimum and maximum dates of 1960 and 1980, respectively. Reported estimates of source width were regarded as sufficiently accurate and were not calibrated.

Since the effective (retarded) contaminant pore velocity is a linear function of darcy velocity, porosity, and retardation factor, only one of these parameters may be calibrated. Since darcy velocity is the most uncertain, we calibrate it and use best estimates of porosity (0.3) and contaminant retardation factor (1.2). Additional aquifer parameters that were assumed known are the aquifer saturated thickness (10 m), natural background ED concentration (1200 H-eq ppb), and natural background electron acceptor (EA) concentration (2400 H-eq ppb). We assume the natural background concentrations of ED and EA are stochastic with their log uncertainty of 0.1 during Monte Carlo simulations. Other aquifer parameters that were calibrated are longitudinal dispersivity, transverse-to-longitudinal dispersivity ratio, vertical-to-longitudinal dispersivity ratio, first-order decay coefficients for contaminant and ED, and ED retardation factor.

Two additional calibrated parameters that control the efficiency of the ABB system are the H-equivalents per mass of ED (f'_{ED}) and the fraction of reductive dechlorination that follows a serial pathway (F_{serial}) as described in Chapter 3. All parameters are characterized by lognormal probability distributions. For lognormally distributed parameters, prior best estimates represent the geometric mean of the variable and the standard deviation is the statistic for natural logarithm of the variable (S_{ln}). The 99% confidence limits for log-normally distributed variables range from approximately $\exp(-3S_{ln})$ to $\exp(3S_{ln})$ times the geometric mean. For example, the prior estimate of Source 1 contaminant flux in 2006 has a geometric mean of 0.01 kg/d with a ln standard deviation of 1 indicating a 99% confidence range from 0.0005 to 0.2 kg/d. Prior best estimates of all parameters and their ln standard deviations are given in Table 9.4.

Table 9.4. Parameter prior estimates and their uncertainty for Area 5.

	Parameters	Prior value[1]	STD[2]	Reference
Site OT51	Mass in 2005 (kg)	2000	3.0	ORNL, 2008
(Source 1)	Source flux in 2005 (kg/d)	0.01	1.0	ORNL, 2008
	Release date (y)	1980	-	ORNL, 2008
	Width (m)	45	-	ORNL, 2008
	Depletion exponent (-)	1.50	0.5	
Source E	Mass in 2005 (kg)	1000	3.0	ORNL, 2008
(Source 2)	Source flux in 2005 (kg/d)	0.005	1.0	ORNL, 2008
	Release Date (y)	1980	-	ORNL, 2008
	Width (m)	45	-	ORNL, 2008
	Depletion exponent (-)	1.50	0.5	
Site OT50	Mass in 2005 (kg)	1000	3.0	ORNL, 2008
(Source 3)	Source flux in 2005 (kg/d)	0.01	1.0	ORNL, 2008
	Release date (y)	1980	-	ORNL, 2008
	Width (m)	45	-	ORNL, 2008
	Depletion exponent (-)	1.50	0.5	
Site SS20	Mass in 2005 (kg)	3000	3.0	ORNL, 2008
(Source 4)	Source flux in 2005 (kg/d)	0.005	1.0	ORNL, 2008
	Release date (y)	1980	-	ORNL, 2008
	Width (m)	45	-	ORNL, 2008
	Depletion exponent (-)	1.50	0.5	
Aquifer	Darcy velocity (m/d)	0.02	0.5	USGS, 2000
& AAB	Porosity (-)	0.3	-	USGS, 2000
system	Contaminant retardation (-)	1.20	-	Estimate from literature
	ED retardation (-)	1.20	0.5	Estimate from literature
	A_L (m)	30	0.5	Estimate from literature
	A_T/A_L (-)	0.1	0.5	Estimate from literature
	A_V/A_L (-)	0.01	0.5	Estimate from literature
	TCE Decay (d^{-1}), λ_{TCE}	0.0001	0.5	Estimate from literature
	ED Decay (d^{-1}), λ_{ED}	0.00001	1.0	Estimate from literature
	F_{serial}[3]	0.5	0.5	Assumed
	f'_{ED} (kg/kg)[3]	0.16	0.1	Chapter 3
	Saturated thickness (m)	10	-	USGS, 2000

[1] Prior values are initial best estimates representing the geometric mean for all variables

[2] Standard deviations are for natural logarithms

[3] Post-ED calibrations only

Three different datasets were used to assess the effects of incremental model refinement using additional data available over time (Table 9.5):

- Cal-1 uses data available through 2005 before commencing ED injection.
- Cal-2 adds additional monitoring well data and actual ED-injection data through 2009.
- Cal-3 adds additional monitoring well data and actual ED-injection data through 2016.

Initially, a "progressive" calibration approach was used in which Cal-2 was executed using Cal-1 posterior parameter estimates and uncertainties as Cal-2 priors, and Cal-3 was performed using Cal-2 posteriors as Cal-3 priors on the grounds that each calibration would progressively improve parameter estimates and narrow uncertainty. For reasons discussed below, this assumption proved doubtful and an additional set of calibrations was performed in which Cal-2 and Cal-3 used the same priors as Cal-1.

Table 9.5. Data sets collected in Area 5 for model calibration.

Calibration	MW data period	# data points	AAB status.
Cal-1	1988 - 2005	46	not operating
Cal-2	1988 - 2010	339	operating
Cal-3	1988 - 2016	559	operating.

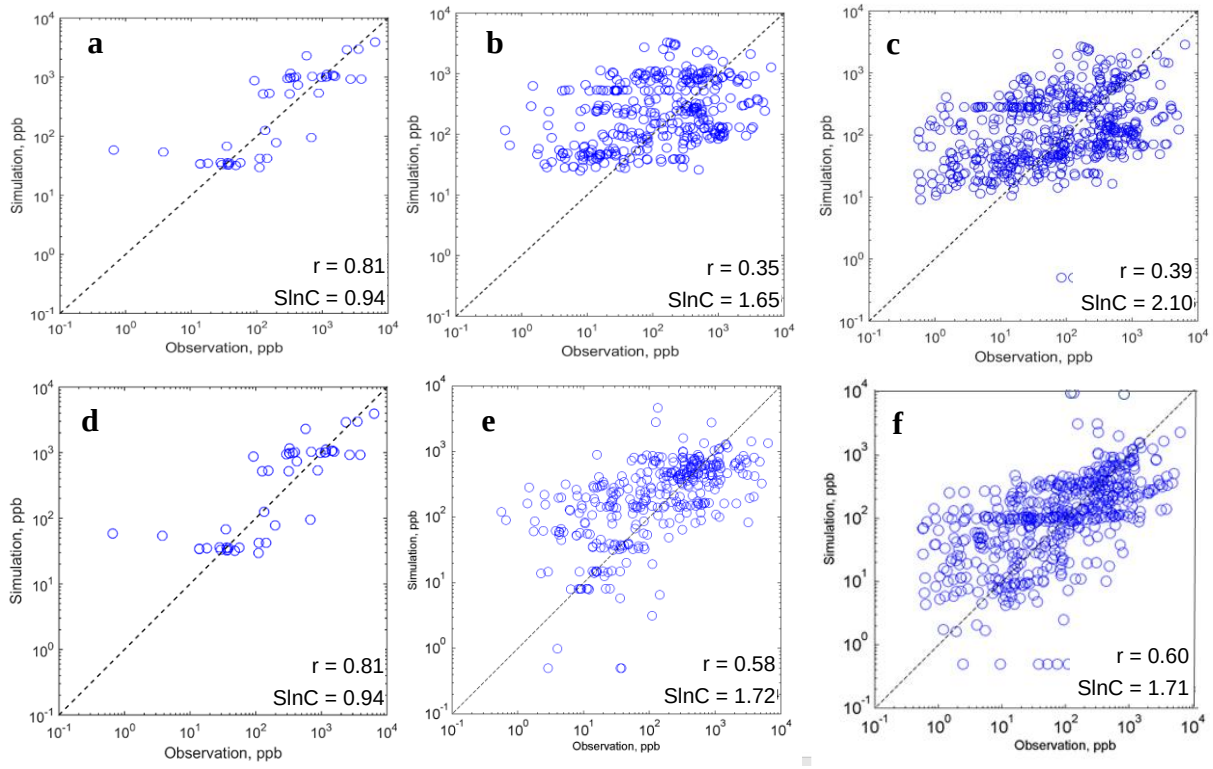

Figure 9.3. Observed versus calibrated contaminant concentrations for: (a) Cal-1, (b) Cal-2 progressive, (c) Cal-3 progressive, (d) Cal-1, (e) Cal-2 fixed priors, and (f) Cal-3 fixed priors.

Scatter plots of observed versus predicted concentrations, along with correlation coefficients and residual regression uncertainty for calibrations using progressively updated and fixed priors are shown in Figure 9.3. Relatively low scatter for Cal-1 results (Figure 9.3a) suggests Cal-1 parameters are reasonably accurate. However, limited deviations between observed and predicted values for Cal-1 may be misleading because the number of calibration data points (46) is only 2.7 times the number of calibrated parameters (17). Ratios of 5 or more are generally desirable for nonlinear regressions. Model deviations increase significantly as the number of data points increases to 339 for Cal-2 and 559 for Cal-3. In part, this may simply reflect an increase in outliers due to the much larger sample size. However, it may also reflect greater variability in measurements induced by ED injection in 12 injection galleries at rates that vary spatially and temporally.

With progressive refinement of priors, the Cal-3 regression pegged the estimate for Source 1 (OT51) β at its upper confidence limit (prior best estimate minus $3S_{ln}$), indicating prior estimates and/or S_{ln} values are not accurate. This does not occur when initial prior estimates are used for all calibrations. Furthermore, the correlation coefficient for Cal-2 increases from 0.35 for progressively updated priors to 0.58 with fixed priors, and Cal-3 correlations increase from 0.39 to 0.60. Therefore, we conclude that calibration results with fixed prior estimates are more reliable than those using progressive refinements for this data set. Parameter estimates and their uncertainty for calibrations with fixed priors are summarized in Table 9.6.

Table 9.6. Summary of Area 5 calibration results using fixed prior estimates. "Best" values are calibration estimates and STD is the concentration ln standard error for the regression.

Parameters	Cal-1		Cal-2		Cal-3	
	Best	STD	Best	STD	Best	STD
M_{cal1} (kg)	2151	1.00	7	0.13	2	0.27
M_{cal2} (kg)	497	0.88	509	1.00	453	1.00
M_{cal3} (kg)	436	0.98	22	0.75	27	0.55
M_{cal4} (kg)	209	0.87	111	0.76	28	0.75
J_{cal1} (kg/d)	1.93E-03	0.44	1.57E-03	0.27	2.25E-03	0.30
J_{cal2} (kg/d)	6.93E-02	0.48	2.16E-03	0.33	2.35E-03	0.23
J_{cal3} (kg/d)	1.67E-02	0.69	5.83E-03	0.34	7.52E-03	0.25
J_{cal4} (kg/d)	6.83E-02	0.61	2.39E-02	0.33	1.08E-02	0.39
β_1	1.66	0.50	1.47	0.11	0.99	0.03
β_2	1.00	0.46	1.38	0.50	1.51	0.50
β_3	1.48	0.50	1.02	0.33	1.13	0.23
β_4	1.00	0.32	1.00	0.35	1.00	0.21
λ_{TCE} (1/d)	7.72E-04	0.21	5.25E-04	0.13	7.61E-04	0.07
λ_{ED} (1/d)	-	-	9.36E-06	1.00	9.75E-06	1.00
qw (m/d)	0.006	0.26	0.0077	0.0878	0.0103	0.0907
A_L (m)	41	0.39	17	0.28	19	0.26
A_T/A_L	0.254	0.22	0.099	0.31	0.062	0.29
A_V/A_L	0.005	0.47	0.003	0.41	0.002	0.39
F_{serial}	-	-	0.252	0.44	0.186	0.45
f'_{ED}	-	-	0.171	0.10	0.146	0.07

9.3 Remediation performance assessment and optimization

There are 12 ED injection galleries (i.e., PICTs) in Area 5 located as shown in Figures 9.1 and 9.2. The remediation objective is to reduce dissolved plume concentrations below 500 μg/L per regulatory agreement. For purposes of optimization, we designate five monitoring wells (DM3513, DM3515, MW214, DM3509, DM3315) distributed over the dissolved plume as compliance monitoring locations. Since there is large uncertainty in the contaminant mass remaining in the DNAPL sources, the duration that ED will need to be injected is uncertain. Therefore, we use an adaptive method based on real-time field data to make termination decisions for individual galleries. As discussed in Chapter 3, we assume each injection gallery and associated performance monitoring location immediately upgradient, and in some cases also downgradient. When the measured performance well contaminant concentrations are less than a specified value, C_{EDstop}, further injection is terminated. This protocol allows each PICT to be terminated independently.

In practice, ED injection will be intermittent to minimize pore clogging, e.g., injection may occur a limited number of hours per day or be cycled on and off for months at a time. Such operations will cause fluctuations in ED concentrations near the ED gallery, which will attenuate with distance depending on the cycle duration and groundwater velocity. With the low groundwater velocity in Area 5, such fluctuations will be minor, so we opt to model ED injection as a continuous process. Therefore, ED injection rates are regarded as time-averaged values taking into consideration cycling on and off. Specifically, we assume each PICT will operate one month per year, so modeled average ED injection rates are $1/12^{th}$ of the rate during actual operation.

All 12 PICTs are assumed to have performance monitoring wells immediately upgradient (in practice, one or more of the actual injection wells can be monitored several months after the last injection period). For PICTs immediately upgradient of compliance monitoring wells, the downgradient compliance well is also regarded as a performance monitoring well.

The specific criteria used to achieve site-wide "no further action" (NFA) status are (Chapter 3):

1. The 95% upper confidence limits of current contaminant concentration for each compliance well, determined from a regression of measured concentration vs time over a 5-year lookback period, must be less than the cleanup level (C_{nfa} = 500 μg/L), and
2. ED injection needs to have terminated for all galleries.

During optimization, to achieve concentrations below 500 μg/L at all compliance wells as soon as possible, we impose a "penalty cost" (Table 9.7) to any Monte Carlo realization for which condition 1 is not met after a penalty date $t_{penalty}$ of 2021 (computed based on the max travel time from injection galleries to the nearest downgradient compliance well). The penalty cost is also applied if NFA criteria are not met by a maximum date taken as 2300.

Individual galleries are allowed to terminate when

1. The current contaminant concentration in a performance monitoring well immediately upgradient of the gallery is less than a specified value ($C_{EDstop} < C_{nfa,}$),
2. All galleries upgradient of the one in question have previously terminated injection, and
3. For galleries that are the closest upgradient to a compliance well, the respective compliance well concentration must be less than C_{nfa}.

All simulations used an ED stochiometric coefficient (f'_{ED}) of 0.156, estimated from Table 3.1 as the average of lactate and EVO, and a stochiometric coefficient for TCE (f'_{TCE}) of 0.051, also from Table 3.1. Unit operating costs are summarized in Table 9.7. Total costs were computed using a discount rate of zero.

Table 9.7. Summary of cost variables used in optimization.

Cost	Description	Value
ED capital cost	Construction cost per width	\$500/m
ED operating costs	Cost per gallery width	\$75/m/year
	Other op costs	\$120,000/year
Site-wide op cost	Monitoring and reporting	\$150,000/year
Penalty cost	"Cost" for non-compliance	$\$10^9$

9.3.1 Simulations based on actual ED injection rates

For comparison with optimized design results, performance of the actual system at the site was simulated using actual ED injection rates employed at the site from 2006 to 2016. Injection in all galleries was modeled with a constant injection rate corresponding to the time-average of actual rates over the period of record (Table 9.8). Unoptimized Monte Carlo simulations were performed using actual average injection rates with site parameters for each of the three model calibrations:

- NoOpt-actual-1: actual injection rates with Cal-1 model parameters
- NoOpt-actual-2: actual injection rates with Cal-2 model parameters
- NoOpt-actual-3: actual injection rates with Cal-3 model parameters.

Table 9.8. ED injection rates (J_{ED}) and injection gallery termination criteria (C_{EDstop}) for non-optimized and optimized cases. Opt-2 values apply after 2010 and Opt-3 values after 2016.

	Actual		NoOpt		Opt1		Opt2		Opt3	
	J_{ED}	C_{EDstop}	J_{ED}	C_{EDstop}	J_{ED}	C_{EDstop}	J_{ED}	C_{EDstop}	J_{ED}	C_{EDstop}
Gallery	kg/yr	µg/L	kg/yr	µg/L	kg/yr	µg/L	kg/yr	µg/L	kg/yr	µg/L
PICT01	4.0	500	7.7	500	-	-	-	-	-	-
PICT02	6.9	500	77.0	500	-	-	-	-	-	-
PICT03	7.3	500	46.0	500	-	-	-	-	-	-
PICT03a	1.8	500	23.0	500	-	-	-	-	-	-
PICT04	8.8	500	46.0	500	208.4	291	9.5	4	9.5	4
PICT05	9.1	500	30.7	500	67.2	500	7.3	4	6.2	4
PICT06	2.2	500	15.3	500	47.8	36	50.0	8	2.9	8
PICT06f	8.0	500	15.3	500	-	-	-	-	-	-
PICT07	3.7	500	30.7	500	-	-	-	-	-	-
PICT08	5.8	500	15.3	500	20.1	177	13.1	16	3.7	12
PICT09	4.7	500	61.7	500	-	-	-	-	-	-
PICT10	8.4	500	2.9	500	0.7	225	1.1	20	1.1	16
Total	71		372		344		81		23	

9.3.2 Simulations based on contaminant flux-derived ED injection rates

Again, for comparison with optimized design results, performance was evaluated for a system using ED injection rates estimated from a reaction mass balance as

$$J_{ED} = qAC_{\max}^{CH} f_{TCE}^{'} / f_{ED}^{'} \quad (9.1)$$

where J_{ED} is the average darcy velocity, A is the vertical cross-section area of the plume estimated to be 689 m^2, $C_{\max}^{CH}$ is the maximum measured total chlorinated solvent concentration near the ED gallery prior to initiating ED injection, and f'_{ED} and f'_{TCE} are as discussed above. Calculated J_{ED} values are summarized in Table 9.8. Unoptimized Monte Carlo simulations were performed using flux-based injection rates with parameters for each of the three model calibrations:

- NoOpt-flux-1: flux-based injection rates with Cal-1 model parameters.
- NoOpt-flux-2: flux-based injection rates with Cal-2 model parameters.
- NoOpt-flux-3: flux-based injection rates with Cal-3 model parameters.

All PICTs are assumed to operate in the same manner described for simulations using actual average injection rate.

9.3.3 Optimized design simulations

Optimization was performed to refine design variables with the objective of meeting remediation criteria with minimum expected (probability-weighted average) total cost. Design variables to be optimized were ED injection rates (J_{ED}) for each ED gallery and the termination criteria ($C_{ED\ stop}$) for each gallery at upgradient performance monitoring well locations subject to the constraint that $C_{ED\ stop}$ cannot exceed the site cleanup requirement (500 μg/L). $C_{ED\ stop}$ values for PICTs with downgradient performance monitoring wells (corresponding to site-wide compliance wells) were fixed at 500 μg/L (not optimized) to ensure that site-wide cleanup criteria were met. Any gallery with an optimized injection rate less than 0.36 kg/yr was assumed to be inactive, the rate set internally to zero, and no operating costs applied for that gallery.

Three optimization simulations were performed corresponding to the three calibration analyses:

- Opt-1 optimized J_{ED} and $C_{ED\ stop}$ values for all PICTs using Cal-1 model parameter estimates and their uncertainty based on field data through 2005 for remediation to be initiated January 2006 and to operate until remediation criteria were met or $t_{penalty}$ exceeded.
- Opt-2 used Cal-2 model parameters and their uncertainty estimated using data through 2009 and assumes the Opt-1 design was implemented January 2006 and operated through 2009. New operating parameters were optimized for remediation to be initiated January 2010 and to operate until remediation criteria were met or $t_{penalty}$ exceeded.
- Opt-3 used Cal-3 model parameters and their uncertainty estimated using data through 2016 and assumes the Opt-1 design was implemented January 2006 and operated through 2009, followed by the Opt-2 design from 2010 through 2016. New operating parameters were optimized for remediation to be initiated January 2016 and to operate until remediation criteria were met or $t_{penalty}$ exceeded.

9.3.4 Results

Expected (mean) cost-to-complete and date-to-complete with 5% and 95% cumulative probability values are shown in Table 9.9 and Figure 9.4 for each unoptimized and optimized remedial design and each set of calibrated parameters. For a given design, uncertainty in costs and completion dates decreased sharply with longer calibration data sets from Cal-1 to Cal-3. Expected costs and completion dates also decreased with longer calibration data sets for a given design. This emphasizes the importance of periodic recalibration, assessment and optimization to update performance estimates and evaluate the need for design adjustments.

Although ED injection rates for the NoOpt-flux case averaged about five times higher than those for NoOpt-actual, the estimated cost-to-complete was only 1% lower and remediation duration only 2 years earlier based on the final calibration (Cal-3), which produced simulations with low uncertainty. Stochastic optimization, in contrast, predicted large performance improvements. **Stepwise optimization yielded a 30% expected cost reduction and a 19-year shorter remediation duration compared to the actual site design. Most of this improvement was obtained with the first-stage optimization (Opt-1 design). However, Opt-2 and Opt-3 design adjustments added 3% to Opt-1 cost savings and decreased the expected remediation duration additional 6 years** (Opt-1 with Cal-3 vs. Opt-3 with Cal-3).

Optimization performance improvements were achieved by deploying only 5 of the 12 potential injection galleries, injecting at high rates initially, decreasing rates at later times, and shutting individual galleries off early when performance monitoring wells for the gallery met defined criteria (Table 9.8).

Table 9.9. Expected cost-to-complete and date-to-complete with 5 and 95% cumulative probability confidence limits for each remedial design and set of calibrated parameters. Bold values are best design performance estimates for optimized and unoptimized cases.

		Cost-to-complete, $million			Completion date		
Design	Calibration	5% LCL	Mean	95% UCL	5% LCL	Mean	95% UCL
NoOpt-actual	Cal-1	59.8	85.2	168.5	2047	2089	2232
NoOpt-actual	Cal-2	62.8	68.3	89.2	2055	2070	2131
NoOpt-actual	**Cal-3**	**62.8**	**63.4**	**66.5**	**2055**	**2057**	**2066**
NoOpt-flux	Cal-1*	58.4	83.0	166.9	2047	2087	2232
NoOpt-flux	Cal-2	62.8	63.2	65.0	2055	2056	2058
NoOpt-flux	**Cal-3**	**62.8**	**62.8**	**63.0**	**2055**	**2055**	**2055**
Opt-1	Cal-1*	51.7	59.1	75.8	2027	2040	2054
Opt-1	Cal-2*	50.4	51.5	52.3	2032	2036	2039
Opt-1	Cal-3*	49.7	50.4	51.1	2030	2032	2034
Opt-2	Cal-2	51.0	52.0	55.3	2037	2040	2052
Opt-2	Cal-3	51.0	51.2	52.2	2037	2037	2042
Opt-3	**Cal-3**	**48.9**	**48.9**	**49.0**	**2038**	**2038**	**2038**

* PICT3a and PICT6f are not included (constructed after 2006)

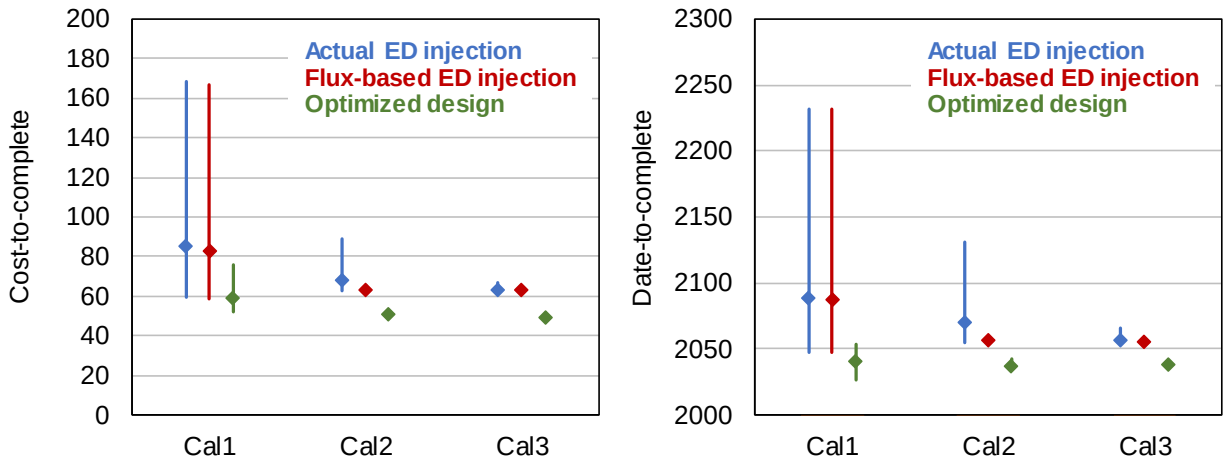

Figure 9.4. Cost- and date-to-complete expected value and range for each remedial design and set of calibrated parameters.

9.4 References

Lee, J., X. Liu, P.K. Kitanidis, U. Kim, J. Parker, A. Bloom, and R. Lyon (2012) Cost Optimization of DNAPL Remediation at Dover Air Force Base Site. Ground Water Monitoring & Remediation 32(2): 48-56.

Oak Ridge National Laboratory (2008) Area 5 monitoring report (through January 2008), Dover Air Force Base, Delaware, June 2008.

U.S. Geological Survey (2000) Hydrogeology and Simulation of Ground-Water Flow at Dover Air Force Base, Delaware. Water-Resources Investigations Report 99-4224.

10. Application to Atlas Missile Site 11

10.1 Overview

Atlas 11 is a former Atlas E missile site in northeastern Colorado that was operated by the Air Force from 1960-1965 and was decommissioned in 1966 when ownership was transferred to Colorado Engineering Experiment Station, Inc. (USACE 2014). Operations at Atlas 11 involved use of TCE to clean up residual rocket fuel. Waste solvent was drained to a sump, which discharged to the ground surface. A site investigation in 1998 identified TCE to be the primary contaminant of concern (COC) contamination with concentrations up to 1000 µg/L in a perched aquifer approximately 50-60 ft below grade in southern and southeastern portions of the facility and adjacent off-site property (Figure 10.1). No evidence of DNAPL was reported.

Due to variations in the elevation of the underlying low permeability layer, the perched water thickness varies from 0-22 ft with flow generally towards the southeast at a velocity of about 40 ft/yr. Contamination extends off site to the south and east of the property. Remediation investigations and feasibility studies have been conducted at the site resulting in selection of ISCO using sodium permanganate with pairs of injection and extraction wells. Additional characterization was undertaken to design and implement the ISCO system, including further soil and groundwater sampling, an aquifer pump test, and a bench-scale treatability study. A field pilot study was conducted in 2012 and expanded in 2013 with full-scale operations commencing in 2014 (Arrowhead 2015a,b,c; USACE 2015).

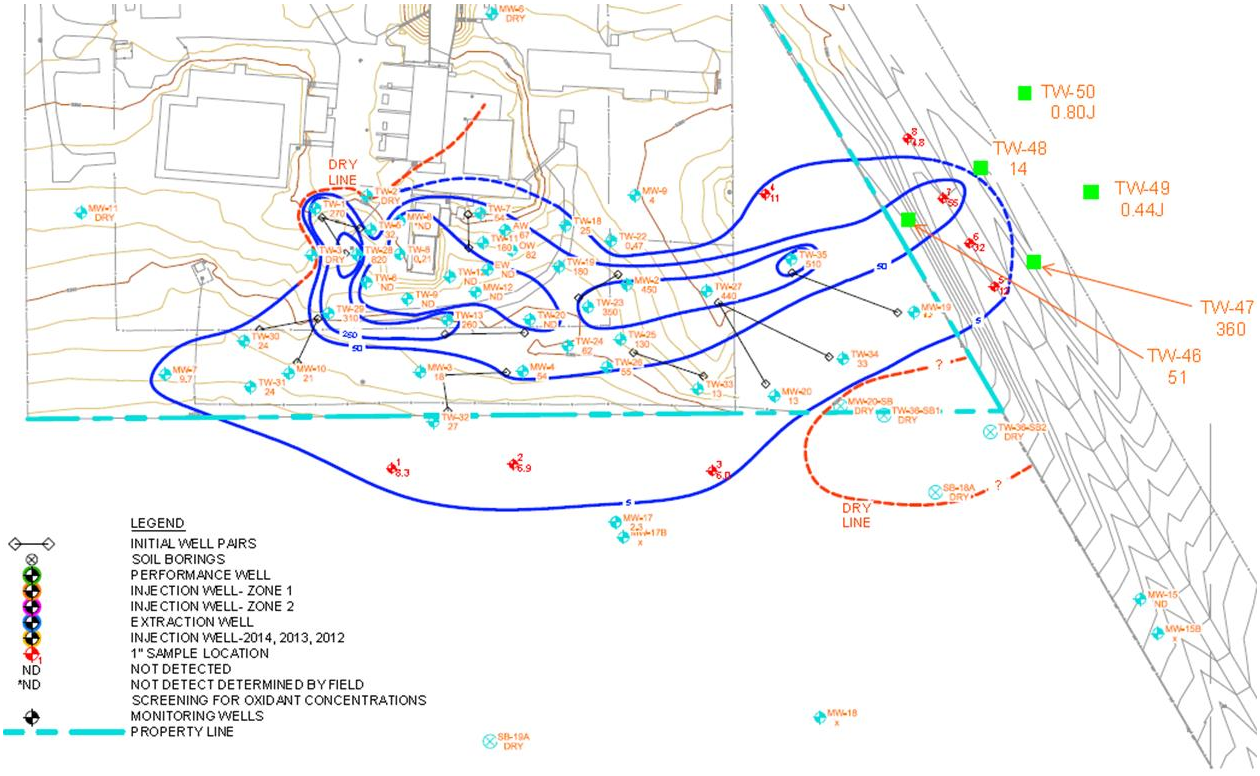

Figure 10.1. Distribution of TCE in perched aquifer at Atlas 11 site and well locations.

Average perched zone hydraulic conductivity was estimated to be 16.4 ft/d. With a natural gradient of 0.004 and an effective porosity of 0.2, the unretarded pore velocity under natural conditions is estimated to be about 0.33 ft/d. Planned oxidant injection rates were 2.0 - 2.5 gpm. The gradient between injection and extraction wells separated by 25-50 ft is estimated to be about 0.067, yielding an unretarded pore velocity of 5.5 ft/d during injection. Unretarded travel times over a 50 ft distance are accordingly about 150 days under natural gradient conditions and 9 days during oxidant injection.

Bench tests with various amounts of $NaMnO_4$ added to soil samples from the site indicated the total oxidation potential to be less than 2000 mg $NaMnO_4$ per kg soil, which may be fully oxidized by addition of one pore volume of 5000 mg/L $NaMnO_4$ solution. NOD measurements do not appear to have been made, but total organic carbon in soil samples was determined to be 0.34%. The plan is to inject oxidant in an injection well at a concentration of about 5000 mg/L and to maintain recirculation until the system is shut down for winter, then restart as necessary in the spring.

Oxidant injection has been undertaken with several well pairs in the most highly contaminated areas, which pushed aqueous concentrations below the MCL. However, some monitoring wells have rebounded by 100 to 300 μg/L. This may reflect small isolated amounts DNAPL, or more likely aqueous or adsorbed contaminant in low permeability pockets.

The Atlas site was identified in late 2015 as a potential demo site for the Stochastic Cost Optimization Toolkit (SCOToolkit). Objectives of the demo site exercise were two-fold: (1) to evaluate historical and projected performance of remedial actions at the site and provide suggestions to improve performance and/or reduce costs, and (2) to field test SCOToolkit to evaluate its practical application for ISCO design optimization.

10.2 Historical ISCO Operations

A pilot test conducted in 2012 involved sodium permanganate ($NaMnO_4$) injection in application wells (AW) with concurrent groundwater extraction in downgradient extraction wells (EW). Effluent from EW was reinjected in AW with additional oxidant. Oxidant injection/recirculation was performed for about 2.5 months in late summer 2012 with quarterly monitoring under natural gradient conditions through the following summer.

Oxidant was introduced in the original pilot test wells again in summer 2013 along with three additional injection-extraction well pairs (Table 10.1). Five new well pairs were operated in 2014, with no further injection in previous treatment zones. In 2015, two of the 2014 well pairs plus 13 new well pairs were operated. Six previous well pairs and five new pairs were operated in 2016. The duration of summer injection-recirculation periods averaged about 3 months. A summary of injection-extraction well operating dates, fluid volumes, and oxidant mass are given in Table 10.1.

To assess the magnitude of dissolved TCE attenuation at the site over the period from 2012 through 2016, quarterly TCE concentration measurements from individual wells were fit to a simple first-order (exponential) depletion function. For wells employed as ISCO injection or extraction locations, the function was fit to concentration data for dates after initiation of ISCO operations for the considered location. For wells not employed for ISCO, measurements for all sampled dates were used. Regression functions for individual wells are shown in Figure 10.2 for ISCO wells and Figure 10.3 for non-ISCO wells. The average correlation coefficient was 0.57 for ISCO well regressions and 0.60 for non-ISCO wells.

Table 10.1. Treatment zone information for ISCO operations at Atlas site through 2016. In cases where more than one injection well is associated with an extraction well or vice versa, fluid and oxidant quantities have been adjusted to avoid double counting. TZ 28-30 are suggested additional locations for ISCO operation.

TZ	Well Pair		Start date	End date	Injection duration	Initial TZ concentration	2016 TZ concentration	TZ length	TZ sat thickness	TZ pore volume	Total fluid extracted	Total fluid Injected	Total pore volumes injected	Total $NaMnO_4$ injected	Avg $NaMnO_4$ conc injected
	Injection	Extraction			days	ug/L	ug/L	ft	ft	gal	gal	gal		kg	mg/L
1	AW	EW	07/01/12	09/19/12	80	343	5	48.8	10.2	35,386	26,400	26,400	0.75	1,766	17,655
1	AW	EW	05/16/13	08/01/13	77	-	-	48.8	10.2	35,386	9,415	9,415	0.27	313	8,768
2	MW-08	TW-08	05/16/13	08/01/13	77	650	1	37.1	4.4	11,596	8,672	8,672	0.75	288	8,768
3	MW-12	TW-19	05/16/13	07/19/13	64	590	10	98.6	12.7	89,020	11,355	11,355	0.13	377	8,768
4	TW-19	MW-02	07/19/13	08/01/13	13	510	129	79.5	12.8	72,552	2,259	2,259	0.03	75	8,768
5	TW-12	TW-19	07/14/14	09/12/14	60	640	10	123.8	10.8	95,766	25,328	25,328	0.26	678	7,062
6	TW-06	TW-12	09/12/14	11/10/14	59	860	1	94.0	6.6	44,222	20,749	20,749	0.47	555	7,062
6	TW-06	TW-12	07/20/15	10/14/15	86	-	-	94.0	6.6	44,222	26,287	26,287	0.59	575	5,778
7	MW-03	MW-04	07/14/14	11/10/14	119	145	83	115.8	19.7	162,388	16,826	16,826	0.10	450	7,062
7	MW-03	MW-04	04/23/15	11/04/15	195	-	-	115.8	19.7	162,388	36,839	36,839	0.23	806	5,778
7	MW-03	MW-04	05/16/16	08/01/16	77	-	-	115.8	19.7	162,388	41,519	8,805	0.05	387	11,609
8	TW-08	TW-11	07/14/14	11/10/14	119	550	7	95.0	6.6	44,693	26,749	26,749	0.60	716	7,062
9	TW-20	TW-23	07/14/14	11/10/14	119	217	11	141.0	11.2	112,264	2,190	2,190	0.02	59	7,062
10	TW-01	TW-28	04/23/15	07/20/15	88	502	1	70.5	2.7	13,626	36,620	36,620	2.69	802	5,778
11	TW-07	TW-11	04/23/15	07/20/15	88	141	18	33.7	7.4	17,760	39,606	39,606	2.23	867	5,778
11	TW-07	TW-11	05/16/16	08/01/16	77	-	-	33.7	7.4	17,760	48,208	22,040	1.24	969	11,609
12	TW-13	TW-20	04/23/15	07/23/15	91	222	11	93.2	14.8	98,188	22,596	22,596	0.23	495	5,778
13	TW-29	TW-12	04/30/15	07/23/15	84	760	172	167.9	7.3	87,616	25,038	25,038	0.29	548	5,778
14	MW-07	MW-10	07/20/15	11/04/15	107	31	15	139.0	6.1	60,488	42,954	42,954	0.71	940	5,778
14	MW-07	MW-10	05/16/16	08/01/16	77	-	-	139.0	6.1	60,488	33,647	21,693	0.36	954	11,615
15	TW-08	OW	08/05/15	10/19/15	75	565	45	126.8	9.0	81,189	32,797	32,797	0.40	718	5,778
16	TW-32	MW-04	08/05/15	10/19/15	75	84	28	118.0	22.6	190,258	66,645	66,645	0.35	1,459	5,778
17	OW	TW-19	08/05/15	11/04/15	91	200	54	56.8	13.0	52,744	9,082	9,082	0.17	199	5,778
18	TW-35	TW-46	08/05/15	11/04/15	91	378	56	152.3	17.5	189,492	18,900	18,900	0.10	414	5,778
19	TW-26	TW-25	08/05/15	11/04/15	91	448	116	34.9	18.4	45,747	1,147	1,147	0.03	25	5,778
20	TW-23	MW-02	08/05/15	09/30/15	56	595	119	50.0	14.5	51,535	18,212	18,212	0.35	399	5,778
20	TW-23	MW-02	05/16/16	08/01/16	77	-	-	50.0	14.5	51,535	5,521	6,696	0.13	294	11,610
21	MW-20	TW-34	08/15/15	11/04/15	81	67	1	88.2	9.0	56,255	17,029	17,029	0.30	373	5,778
21	MW-20	TW-34	05/16/16	08/01/16	77	-	-	88.2	9.0	56,255	4,897	4,897	0.09	215	11,609
22	TW-27	TW-34	08/24/15	11/04/15	72	237	1	172.3	9.8	120,577	29,287	15,694	0.13	413	6,940
22	TW-27	TW-34	05/16/16	08/01/16	77	-	-	172.3	9.8	120,577	29,287	15,694	0.13	690	11,609
23	TW-29	MW-12	05/16/16	08/01/16	77	215	161	167.9	7.3	87,616	28,930	27,222	0.31	1,197	11,609
24	TW-35	MW-19	05/16/16	08/01/16	77	337	31	150.7	16.5	177,288	718	17,343	0.10	763	11,609
25	TW-23	TW-25	05/16/16	08/01/16	77	300	116	51.7	17.1	62,788	9,090	10,045	0.16	442	11,609
26	TW-24	TW-33	05/16/16	08/01/16	77	39	17	154.7	17.6	194,025	21,343	13,134	0.07	578	11,609
27	TW-44	TW-46	05/16/16	08/01/16	77	95	54	142.0	17.2	173,791	25,702	13,753	0.08	605	11,609
28	TW-37	TW-47	5/15/17	8/15/17	92	755	715	151	6.5	69,961	-	-	-	-	-
29	TW-54	TW-49	5/15/17	8/15/17	92	275	275	118	6.5	54,251	-	-	-	-	-
30	TW-38	TW-39	5/15/17	8/15/17	92	50	50	75	6.8	36,353	-	-	-	-	-

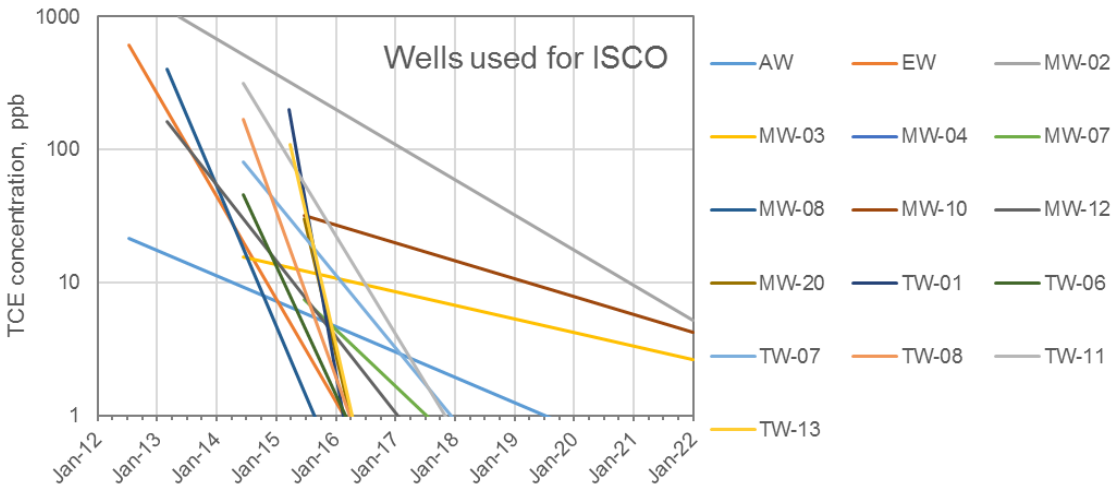

Figure 10.2. First-order TCE attenuation functions fit to data from wells used for ISCO.

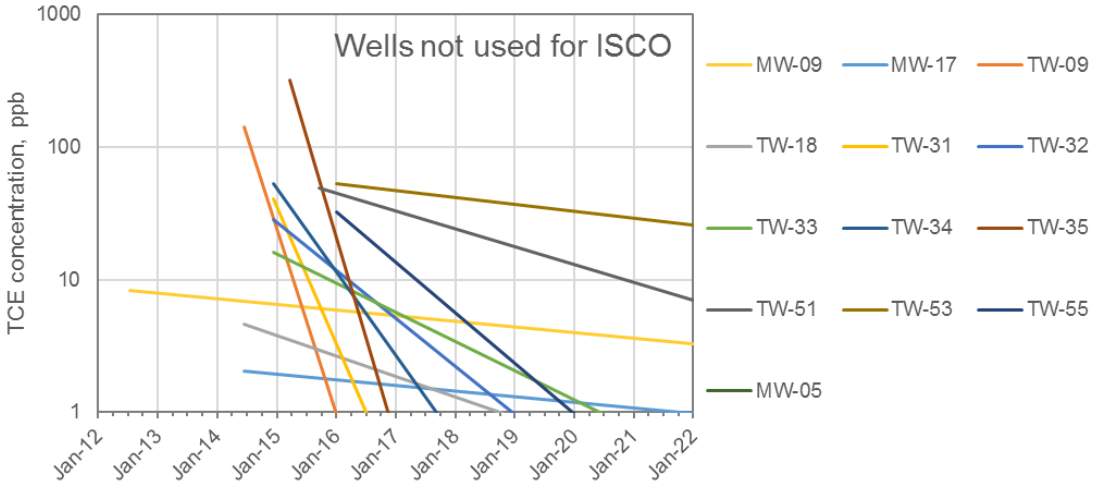

Figure 10.3. First-order TCE attenuation functions fit to data from wells not used for ISCO.

Slopes of the depletion functions represent the fractional rate of change in TCE concentration ("depletion rates") observed for each well over the period analyzed. Minimum and maximum depletion rates, average depletion rates for each quartile, overall averages and median values for ISCO and non-ISCO wells are summarized in Table 10.2. The variability of inferred depletion rates is higher for non-ISCO (monitored natural attenuation, MNA) wells than for ISCO wells (max/min ratio is 3 times greater for MNA wells) and the ratio of ISCO to non-ISCO average depletion rates ranges from 4.4 for the lowest quartile to 1.7 for the highest quartile, with a ratio of 2.1 for overall averages and 2.5 for median values. Since the rate distribution is positively skewed, median values (which have an equal likelihood of being exceeded or not) is a more conservative value for use in making performance estimates.

Table 10.2. Average depletion rates by quartile and for all values for ISCO wells and non-ISCO wells.

Statistics	Attenuation coefficients (d^{-1})		ISCO vs. non-ISCO Ratio
	ISCO wells	Non-ISCO wells	
Lowest value	0.00064	0.00014	4.7
Avg 1st quartile	0.00109	0.00025	4.4
Avg 2nd quartile	0.00315	0.00088	3.6
Median value	0.00413	0.00167	2.5
Avg 3rd quartile	0.00557	0.00265	2.1
Avg 4th quartile	0.01207	0.00722	1.7
Highest value	0.01594	0.00957	1.7
Overall average	0.00547	0.00265	2.1

While the foregoing results confirm our expectation that ISCO accelerates remediation compared to MNA, the relatively small difference in ISCO and MNA attenuation rates is somewhat surprising. The time to reach a TCE concentration of 5 μg/L from various initial concentrations with and without ISCO was estimated using median depletion rates from the Atlas site data. The results indicate that ISCO is likely to reduce time-to-completion from about 8.5 to 3.5 years with an initial concentration of 1000 μg/L (approximate maximum observed at the Atlas site), from 4.8 to 2.0 years with an initial concentration of 100 μg/L, and from 1.1 to 0.5 years starting from 10 μg/L (Table 10.3). The time reduction for ISCO relative to MNA may not justify its cost for treatment zones having initial concentrations less than 10 μg/L or perhaps higher unless critical receptors are present.

Table 10.3. Estimated time to reach MCL based on median depletion rates for ISCO and non-ISCO wells and time reduction achieved by ISCO for different initial TCE concentrations.

Initial TCE (μg/L)	Years to reach 5 μg/L		MNA–ISCO years
	ISCO	MNA	
1000	3.5	8.5	5.0
500	3.1	7.4	4.3
250	2.6	6.3	3.7
100	2.0	4.8	2.8
50	1.5	3.7	2.2
25	1.1	2.6	1.5
10	0.5	1.1	0.7

10.3 Phase 1 SCOToolkit analyses

10.3.1 Model formulation and calibration

The SCOToolkit ISCO model is formulated to consider one or more DNAPL source zones, which may be subdivided into multiple "treatment zones" (TZ) with different quantities of contaminant. TZs may be terminated independently when "local" cleanup criteria are met or simultaneously when "global" criteria are met. Oxidant may be injected over short periods followed by a longer duration in which oxidant migrates under natural gradient conditions and reacts with natural oxidant demand (NOD) and dissolved contaminant. After oxidant is depleted by reactions or by advective movement out of the treatment zone, aqueous contaminant concentrations gradually rebound in response to DNAPL dissolution and/or mass transfer from lower permeability zones. A second ISCO operation mode may be simulated that involves continuous oxidant introduction in injection wells and withdrawal from extraction wells. Some or all effluent may be recirculated with additional oxidant added. For continuous recirculation, contaminant concentrations will be depressed by reactions and will not reflect equilibrium conditions. Termination decisions during continuous injection can only be reliably made based on soil sampling, unless injection is periodically terminated long enough to allow groundwater concentrations to rebound.

ISCO operation at the Atlas site is a hybrid of the foregoing two operating modes, with injection and recirculation for approximately 3 months alternating with natural gradient conditions for 9 months. The current model version includes an option to simulate this hybrid method. Another aspect of the Atlas site is that DNAPL does not appear to be present. However, we assume that part of the contaminant mass at the site and in individual treatment zones occurs in lower permeability zones, which interact with higher permeability zones by diffusive mass transport. This "mobile-immobile" mass transfer process is modeled using the same mathematical formulation employed to simulate DNAPL dissolution. Specifically, the net rate of contaminant mass entering the mobile aqueous phase within each treatment zone is described by

$$J_i(t) = F_{mt}(t) F_k(t) J_{oi} \left(\frac{M_i(t)}{M_{oi}} \right)^{\beta} \tag{10.1}$$

where $J_i(t)$ is the mass transfer rate in TZ_i at time t [MT^{-1}], J_{oi} is the rate prior to ISCO (Jan 2012) [MT^{-1}], $M_i(t)$ is the mass at time t [M], M_{oi} is the mass in Jan 2012 [M], F_{mt} is a dimensionless mass transfer enhancement factor, and F_k is a mass transfer inhibition factor, and β is an empirical depletion exponent. For DNAPL sources, β is governed by the DNAPL "geometry" (e.g., $\beta < 1$ for pools or $\beta > 1$ for residual). For the present case involving diffusive mass transfer with no DNAPL, we assume β=1.

When permanganate is used as the oxidant, mass transfer inhibition due to pore clogging by MnO_2 precipitation is modeled following West et al. (2007) and West and Keuper (2012) as

$$F_k(t) = 1 - S_{rind}\ C_{MnO_2}(t) \tag{10.2}$$

where $C_{MnO_2}(t)$ is the mass of precipitated MnO_2 per treatment zone pore volume [ML^{-3}] as a function of time, and S_{rind} = 4.6 x 10^{-6} L/mg. When a DNAPL is considered, mass transfer enhancement is estimated based on Reitsma and Dai (2001) as

$$F_{mt}(t) = 1 + f_{mt} \frac{C_{ox}(t) W_{CH}}{S_{CH} W_{ox}} \tag{10.3a}$$

$$f_{mt} = \frac{D_{ox}}{n_{ox/CH} D_{CH}} \tag{10.3b}$$

where $C_{ox}(t)$ is the current aqueous oxidant concentration [ML^{-3}], S_{CH} is the effective solubility of DNAPL phase contaminant [ML^{-3}], W_{ox} is the molecular weight of oxidant [M mol^{-1}], W_{CH} is the molecular weight of contaminant [M mol^{-1}], D_{OX} is the aqueous diffusion coefficient of oxidant [L^2T^{-1}], D_{CH} is the contaminant aqueous diffusion coefficient [L^2T^{-1}], and $n_{ox/CH}$ is the stoichiometric ratio of oxidant to contaminant for the redox reaction. For the diffusion-limited aqueous phase contaminant source considered at the Atlas site, we retain the form of eq. (10.3), simplified as follows

$$F_{mt} = 1 + f_{mt}^{aq} C_{ox} \tag{10.4}$$

with f_{mt}^{aq} for the Atlas site estimated from previously discussed depletion rates. An initial estimate of f_{mt}^{aq} was estimated taking F_{mt} as the ratio of median ISCO versus MNA depletion rates (2.5 from Table 10.2) and C_{ox} as the average injected oxidant concentration (8,433 mg/L), yielding f_{mt}^{aq} = 1.78x10^{-4} L/mg. Since the quantity of oxidant available for reaction with contaminant is reduced by reactions with NOD, the effective value of f_{mt}^{aq} is expected to be larger. We therefore calibrated the final f_{mt}^{aq} value to obtain a simulated ratio of ISCO versus MNA depletion rates of 2.5. This yielded a final value for f_{mt}^{aq} of 2.8x10^{-4} L/mg.

Total initial contaminant mass across all TZs, M_o, and the corresponding site-wide mass transfer rate, J_o, are related to the individual TZ values, M_{oi} and J_{oi} respectively, as follows

$$M_o = \sum_{i=1}^{N_{TZ}} M_{oi} \tag{10.5a}$$

$$M_{oi} = \phi R V_i C_{oi} \tag{10.5b}$$

$$J_o = \sum_{i=1}^{N_{TZ}} J_{oi} \tag{10.5c}$$

$$J_{oi} = J_o \frac{M_{oi}}{M_o} \tag{10.5d}$$

where V_i is the bulk volume of TZ *i*, C_{oi} is the initial mobile dissolved contaminant concentration in TZ *i* taken as the average of injection and extraction well measurements prior to commencing ISCO, ϕ is aquifer porosity, and R is a dimensionless ratio of total to mobile phase TCE mass. Values for V_i and C_{oi} are tabulated in Table 10.1. Treatment zone widths for all TZs were taken as 50 ft per USACE (2014) estimates. The porosity is assumed to be 0.2. Values of M_o and J_o, and R were calibrated to field data.

Contaminant mass and aqueous concentration versus time in each TZ is computed by solving mass balance equations that consider the current mass transfer rate from eq. (1) and oxidant-contaminant

and oxidant-NOD reactions. Total NOD mass at the site (NOD_{tot}) is assumed to be distributed among TZs proportional to TZ bulk volume, V_i (Table1). Total NOD mass in each TZ ($NOD_{tot\ i}$) is divided into "fast" NOD, which is assumed to react instantaneously with oxidant, and "slow" NOD, which follows second-order reaction kinetics. The site-wide total NOD is allocated to individual TZs in proportion to TZ bulk volume. Since bench tests for aquifer material from the Atlas site indicate relatively low NOD levels, results are not expected to be sensitive to NOD parameters. We assume a typical ratio of "fast" NOD to total NOD of 0.12 and calibrated the total NOD content (NOD_{tot}, g/kg), and the "slow" NOD rate coefficient (γ, L mmol $NaMnO_4^{-1}$ day^{-1}).

Note that contaminant reactions with oxidant will generally result in rapid decreases in aqueous contaminant concentrations, which will slowly rebound after oxidant injection ceases as the mass transfer rate described by eq. (10.1) gradually reestablishes a steady state. The last quarterly measurement before commencing a new round of injection is assumed to be close to full rebound. Treatment zones are assumed to meet termination requirements when the maximum of injection and extraction well rebound concentrations for the TZ are less than a specified termination criteria (C_{stop}). Each injection-extraction well pair at the Atlas site is regarded as a treatment zone.

Model calibration was performed using a nonlinear regression method to minimize deviations between measured TCE concentrations in the spring following injection to simulated concentrations for a period starting in 2012 and extending through 2016. A total of 27 injection-extraction well pairs, regarded as TZs, were treated with permanganate. Of these, 21 were treated for a single year only, five were treated two years, and one was injected for three years. Inspection of all monitoring well data indicated several additional locations with significant TCE concentrations. In order to treat these areas, we defined three additional TZs denoted 28, 29, and 30 with wells and TCE concentrations in 2016. Measured fluid volume and oxidant mass injected and initial contaminant concentrations for each TZ as given in Table 10.1 were input to the model and measured contaminant concentrations versus time were employed for calibration. The resulting parameter estimates obtained were M_o = 8.9 kg and J_o = 0.014 kg/d in January 2012, R = 3.40, f_{mt}^{aq} = 2.8x10^{-4} L/mg, NOD_{tot} = 0.74 g/kg, and γ = 0.073 L mmol $NaMnO_4^{-1}$ day^{-1}.

10.3.2 Monte Carlo methods

Since unit cost data was not available, in lieu of performing stochastic cost optimization simulations, we performed forward Monte Carlo simulations for a range of key operational parameters.

All simulations are assumed to commence oxidant injection with recirculation May 2017 for 3 months followed by 9 months under natural gradient conditions. Simulated monitoring data for each TZ at the end of the 9-month period are used to determine if the TZ meets the termination criteria. This process is repeated annually until stop criteria are met for all TZs, at which point the simulation terminates.

Considering our earlier observation that TCE concentrations may attenuate significantly in a few years with MNA, we consider the effect of terminating oxidant injection at a stop criterion above 5 μg/L TCE assuming that MNA would continue after ISCO until the regulatory limit was met.

We also consider the effect of the concentration of injected oxidant and the total volume of fluid injected per ISCO event. The average oxidant concentration injected historically at the Atlas site

is about 8000 mg/L and the average quantity of fluid injected annually per TZ represents about 0.4 pore volumes (PV) of the TZ. Cases include all combinations of (a) maximum TCE concentration for ISCO termination (C_{stop}) values of 5 and 25 μg/L, (b) injected oxidant concentration (C_{ox}) values of 4000, 8000, and 16000 mg/L, and (c) injected fluid volumes per TZ per year (V_{inj}) of 0.4, 1.0 and 2.5 PV.

Initial TCE concentrations for each TZ were set equal the average of measured concentrations in injection and extraction wells within each TZ in late 2016 (last data available). Field data show that six TZs (1, 2, 6, 10, 21, 22) were equal or less than 5 μg/L in late 2016 and an additional eight TZs (3, 5, 8, 9, 11, 12, 14, 26) were below 25 μg/L. These TZs were eliminated from forward simulations for ISCO termination criteria corresponding to the respective levels. For each case considered, uncertainty in simulation results was evaluated by generating 100 Monte Carlo realizations with model parameters that exhibit joint statistical distributions of model parameters determined from the inverse solution as well as "noise" in simulated monitoring data used for termination decisions assuming a ln-standard deviation of 0.25.

10.3.3 Monte Carlo results

Results for Monte Carlo simulations are presented in Tables 10.4 and 10.5 as a percentage of the total TZs (30) that have reached the ISCO termination criterion of 5 or 25 μg/L, respectively, versus time starting in 2017. Note that six TZs meet the 5 μg/L criteria before commencing treatment in 2017 (20% of 30 TZs) and 14 meet the 25 μg/L criteria (47%). In addition to the expected value (i.e., probability-weighted average) of percent completion shown as circles and a black line, dashed red lines indicate 95% upper and 5% lower confidence limits (central 90% confidence bands). Visual inspection indicates that remediation is accelerated by increasing the injected solution volume and oxidant concentration. And, of course, ISCO treatment duration is decreased significantly by increasing the termination criteria from 5 to 25 μg/L, although the associated cost savings will be somewhat offset by continuing MNA costs. A relative measure of cumulative operating cost differences for each simulation case may be obtained by integrating the area under the percent completion curves versus time as

$$N_{inj} = \sum_{t=1}^{t_{\max}} \sum_{i=1}^{N_{TZ}} H_{i,t} \tag{10.6}$$

where $H_{i,t}$ is an indicator for TZ i at time t that is 1 if the treatment zone concentration is above the termination level and 0 if it is less. If time is discretized in months, eq. (10.6) yields the total TZ-months of oxidant injection to reach the site-wide termination criteria. N_{inj} can be used to estimate total ISCO operating costs $\$_{tot\text{-}op}$ as

$$\$_{tot\text{-}op} = \$_{inj} N_{inj} \tag{10.7}$$

where $\$_{inj}$ the ISCO operating cost per month per active TZ. Expected values and reasonable worst case (95% upper confidence limit) of N_{inj} are given in Table 10.4 for all simulation cases.

For reference, the case with C_{stop} = 5 μg/L, C_{ox} = 8,000 mg/L and 0.4 PV of fluid injection per TZ for each injection event (bold values in Table 10.4) approximates average historical operating conditions at the Atlas site. We designate this the "base case." With C_{stop} = 5 μg/L, N_{inj} (hence total operating cost) is predicted to decrease with increasing oxidant concentration and injection volume. Both of the later variables result in an increase in total oxidant mass injected. However, increasing C_{ox} produced a slightly greater operating cost decrease per unit oxidant mass than increasing injection volume. Normalizing the results to percent N_{inj} reduction per doubling of oxidant mass relative to the base case, we obtain results for the C_{stop} = 5 μg/L simulations summarized in Table 10.5, which indicates that the largest cost reduction per unit oxidant mass is obtained with C_{ox} = 16,000 mg/L and one PV injection. A slightly smaller reduction per mass was obtained with C_{ox} = 16,000 mg/L and 0.4 PV. While increasing injection volume from 1 to 2.5 PV produced the lowest N_{inj} values, the efficiency in terms of cost reduction per unit oxidant mass injected was poorer than the lower PV cases.

Table 10.4. Expected values and 95% upper confidence limits of cumulative TZ-months oxidant injection for all cases. Bold values denote approximate average historical operating conditions.

		Cumulative TZ-months of oxidant injection (N_{inj})		
PVs injected	C_{stop} (μg/L)	C_{ox} = 4,000 mg/L	**C_{ox} = 8,000 mg/L**	C_{ox} = 16,000 mg/L
		Expected values (most probable)		
0.4	**5**	124	**116**	98
1.0	5	116	95	68
2.5	5	100	78	51
0.4	25	29	28	23
1.0	25	27	23	17
2.5	25	24	18	12
		95% upper confidence limits (reasonable worst case)		
0.4	**5**	161	**150**	131
1.0	5	148	127	101
2.5	5	136	114	85
0.4	25	39	39	35
1.0	25	39	32	25
2.5	25	32	25	22

Simulations with C_{stop} = 25 μg/L were considered to evaluate the consequences of terminating ISCO at a value above the site cleanup target of 5 μg/L to be followed by MNA until the cleanup target is reached. As noted previously, the higher termination criteria reduced the number of treatment zones at the 2017 start date from 24 that exceeded 5 μg/L to only 16 in excess of 25 μg/L (Figures 10.4 and 10.5, respectively). As expected, the duration of ISCO treatment decreased relative to corresponding cases with C_{stop} = 5 μg/L. Somewhat less obvious, however, is the markedly different shape of the recovery curves with much steeper initial slopes for the C_{stop} = 25 μg/L curves. This causes a disproportionately greater reduction in cumulative ISCO operating cost (N_{inj}) relative to the reduction in remediation duration. N_{inj} values for the C_{stop} = 25 μg/L cases are about 25% of the respective C_{stop} = 5 μg/L case values (Table 10.5). This observation reflects decreasing ISCO efficiency as contaminant concentration decreases, which occurs because diffusion-limited contaminant mass transfer rates decrease with concentration and limit oxidation rates.

Table 10.5. Expected values of percent operating cost reduction per doubling of oxidant mass injected for selected cases relative to the base case.

C_{stop} (μg/L)	C_{ox} (mg/L)	Pore volumes	%N_{inj} decrease per doubling oxidant mass
5	8,000	1.0	14.8
5	8,000	2.5	10.6
5	16,000	0.4	15.7
5	16,000	1.0	16.7
5	16,000	2.5	9.0
25	8,000	1.0	13.0
25	8,000	2.5	10.8
25	16,000	0.4	15.2
25	16,000	1.0	16.1
25	16,000	2.5	9.0

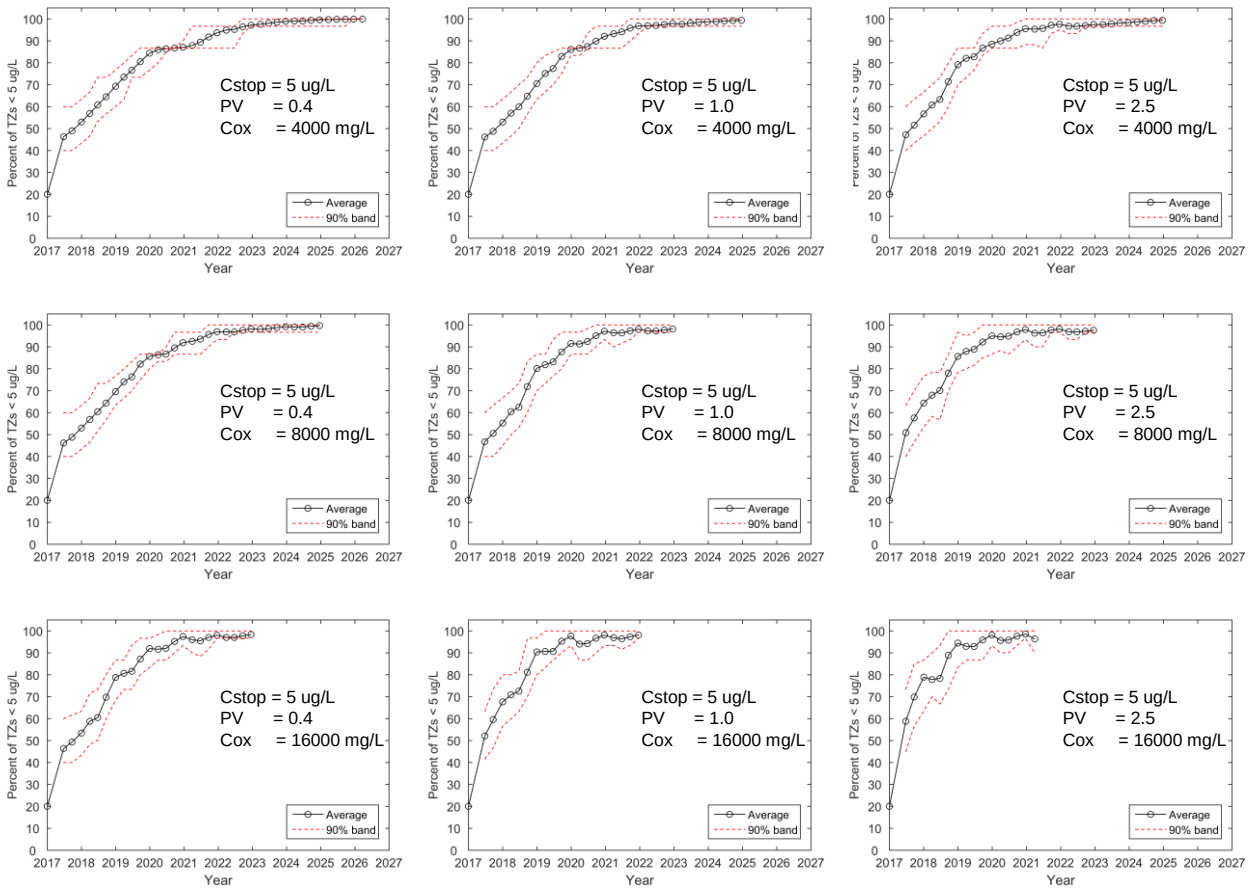

Figure 10.4. Monte Carlo simulations of ISCO from 2017 forward with a termination criterion of 5 µg/L. Symbols with dark line represent the probability-weighted average outcome. Red lines are lower 5% and upper 95% confidence limits.

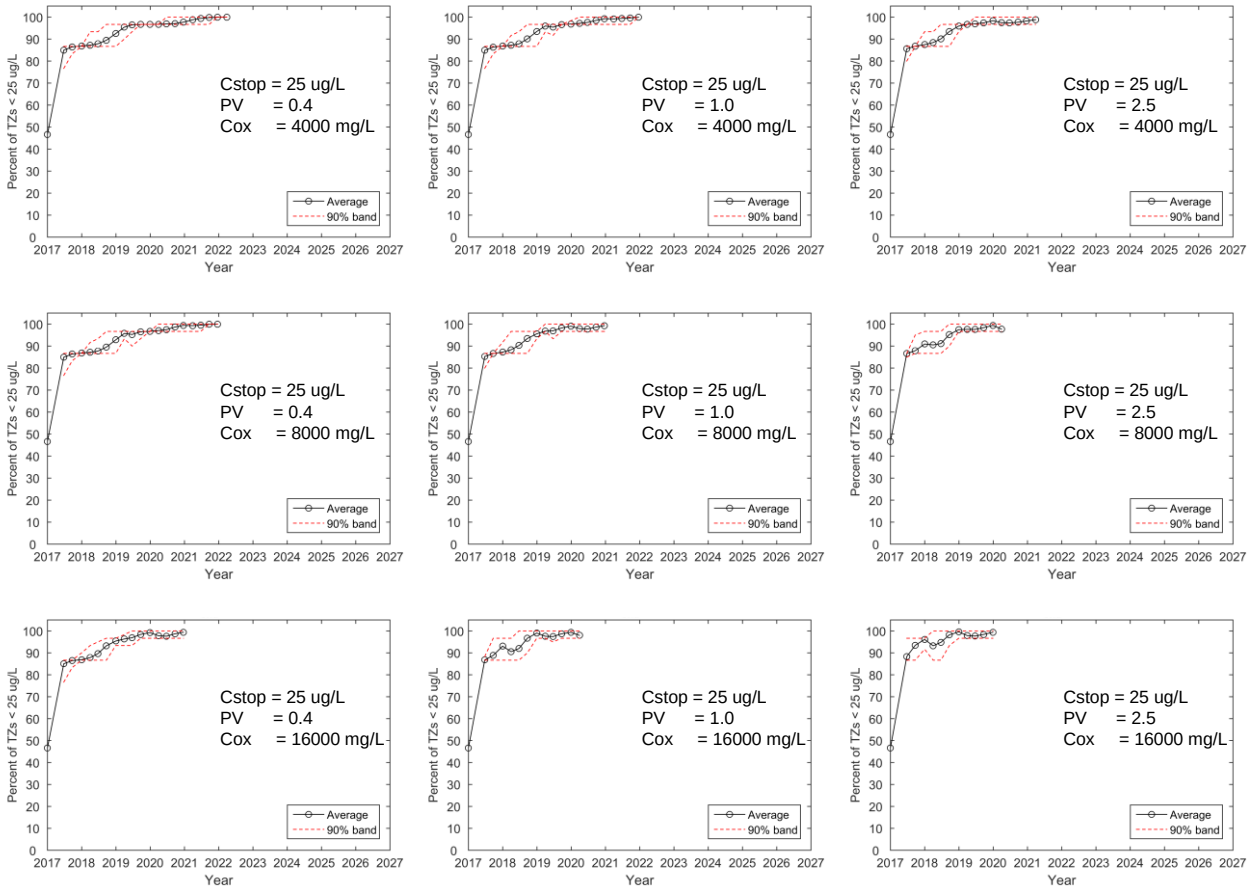

Figure 10.5. Monte Carlo ISCO simulations from 2017 forward with a termination criterion of 25 µg/L. Symbols with dark line represent the probability-weighted average outcome. Red lines are lower 5% and upper 95% confidence limits.

10.3.4 Phase 1 conclusions

From the foregoing analyses, we draw the following conclusions.

1. Recently added monitoring wells have identified off-site areas with TCE concentrations up to about 1,000 µg/L. Additional ISCO treatment zones are needed to remediate these areas. We have identified three injection-extraction well pairs (TW37/TW47, TW54/TW49, TW38/TW39) that may be considered for this purpose.
2. First-order attenuation rates at the site were estimated for untreated and ISCO treated wells. Median rates were 0.0041 d^{-1} for treated wells and 0.0017 d^{-1} for untreated wells. The median ISCO rate is only 2.5 times larger than that for natural attenuation. Spatial variations in attenuation rates are significant for both treated and untreated locations, with slightly higher variability for untreated wells, which exhibit a minimum rate equal to 8% of their median value compared to 16% for ISCO wells.

3. Considering the relatively small differences between ISCO and natural attenuation rates, we performed Monte Carlo simulations using the SCOToolkit program to compare relative performance and cost of (a) ISCO injection with recirculation for 3 months followed by natural gradient conditions for 9 months, repeating until groundwater TCE concentration is less than 5 μg/L, or (b) treating with ISCO until TCE is less than 25 μg/L followed by MNA until TCE <5 μg/L. The results indicate that total ISCO operating costs for early ISCO termination cases (25 μg/L) were less than 25% of the costs for terminating at 5 μg/L. This cost reduction will be offset only slightly by MNA costs.

4. The median time for TCE to naturally attenuate from 25 to 5 μg/L following ISCO termination is 2.6 years (50% probability of exceedance) while the 95% upper confidence limit is about 16 years based on rates computed for untreated wells at the site. To ameliorate this uncertainty, if the annual rate of TCE decrease for a well pair is less than about 50% (approximate median MNA rate), then ISCO injection should be employed. This would allow about half of the ISCO cost savings to be realized without increasing the remediation time more than 3 years.

5. For each of the simulation cases mentioned in Point 2 above, we also evaluated effects of ISCO operations for a range of oxidant concentrations (4,000 to 16,000 mg/L) and injected fluid volumes (0.4 to 2.5 pore volumes per TZ per year). The results indicate that the cumulative count of TZ injection events (N_{inj}) required to meet site-wide termination criteria decreases with increasing pore volume of fluid injected and concentration of oxidant. The greatest reduction in N_{inj} per mass of oxidant was obtained with an oxidant concentration of 16,000 mg/L and fluid injection volume of 1 pore volume per TZ per year, followed closely by the same oxidant concentration with 0.4 pore volumes of fluid. If practicable, we recommend using these values for future ISCO operations.

6. A more nuanced optimization of oxidant concentration and fluid injection volume may be performed by first estimating operating costs per TZ-month ($\$_{inj}$) for different combinations of oxidant concentration and fluid volume. Total ISCO operating cost ($\$_{tot\text{-}op}$) can then be computed from eq. (10.7) and N_{inj} values for the relevant case from Table 10.4. If applicable, MNA and other costs may be added to $\$_{tot\text{-}op}$ and the minimum total cost option identified for field implementation.

10.4 Phase 2 analyses

10.4.1 Background

A conference call with USACE personnel responsible for the site following Phase 1 completion raised the following issues.

1. The current remediation contract specifies remediation at the site should be completed by the end of 2021. This is interpreted to mean completion of active remediation with a likely follow-on monitoring contract to confirm that remediation criteria have been met. A remediation strategy suggested in our May report was to inject oxidant in treatment zones (TZ) until the dissolved concentration was less than 25 μg/L followed by monitored natural attenuation (MNA) until concentrations dropped below 5 μg/L, with additional oxidant injection for well pairs with low MNA attenuation rates. Although this strategy promised to decrease total operating costs by about 75%, it had to be set aside due to the short time constraint.
2. Simulations in Phase 1 assumed oxidant injection for only 3 months per year, based on historical operations. During the discussion with USACE, it was noted that modifications to the system were in progress that would enable oxidant to be injected for longer durations up to continuous injection throughout the year.
3. Phase 1 simulations investigated effects of increasing the mass of injected oxidant per year by increasing the oxidant concentration and/or oxidant fluid injection rates. It was noted in the discussion, however, that as the current system utilizes passive gravity-fed oxidant delivery, higher oxidant injection rates would require injection under positive pressure. Although modifications for this purpose are possible, they would involve significant additional cost.
4. Increasing the duration of oxidant injection, as discussed in Point 2, offers an alternative way to increase oxidant mass injected per year without system modification.

Additional Monte Carlo simulations were performed subject to operational constraints noted above for comparison with a Base Case corresponding approximately to current operating practice at the site, and the previous best case subject to the noted operational constraints (denoted as Case 1), three additional cases were investigated with longer on-cycle durations of 6, 9 and 12 months. Since site data suggests that 6 months is needed between injection events to assess rebound, a minimum off-cycle duration of 6 months was employed. For all cases, an injection rate of 0.133 pore volumes per month was assumed, corresponding to average gravity-fed field conditions. During periods without injection, oxidation reactions were simulated under natural groundwater gradient conditions.

Total operating costs for oxidant injection were estimated assuming $5.5 per kg of oxidant, $20 per m^3 of fluid injected, plus $300 per day for other operating costs (Kim et al. 2018). The results were normalized to the base case defined to be 100.

10.4.2 Phase 2 results and conclusions

A summary of the Phase 2 results is given in Table 10.6. The Base Case is predicted to reach the 95% upper confidence NFA date in January 2025 with 150 TZ-months of injection. Relative total operating cost for the Base Case is taken to be 100. **Increasing the injection concentration from**

8,000 to 16,000 mg/L with the on/off cycle at 3/9 (Case 1) was predicted to reduce the operating cost relative to the Base Case from 100 to 76, for a 24% savings with a 2.7 year earlier 95% NFA date (April 2022 vs. Jan 2025). There is a 10 to 15% probability that Case 1 will not achieve the target cleanup level of 5 μg/L by the end of 2021.

Cases 2 through 4, with increasing on-time durations of 6, 9 and 12 months, respectively, are predicted to reach the cleanup criteria 44 to 47 months earlier than the Base Case (12 to 16 months earlier than Case 1), but with 44 to 71% higher cost than the Base Case (55 to 84% higher than Case 1). Therefore, Case 1 appears to be the best option to meet the cleanup level by late 2021.

Nevertheless, it is worthwhile to note that Case 1a, which follows the same design as Case 1 but with a oxidant injection termination level 25 μg/L, shows a high probability of reaching the interim cleanup level by early 2021 with a cost that is 80% less than the Base Case and 75% less than Case 1. Given the high median natural decay rate at the site, MNA should bring most TZs below 5 mg/L within 3 more years, and selective use of ISCO in TZs with lower decay rates could avoid a protracted MNA period to reach 5 μg/L.

Considering the possible effects of spatial variability on performance uncertainty, it may be advisable to inject oxidant continuously in TZs within the lowest quartile of first-order attenuation rates as well as off-site well pairs with high concentrations through 2021 or until all other TZs have met termination criteria. This will decrease the possibility of missing the 2021 target completion date. TZs that meet the suggested criteria for continuous injection are 7, 14, 16, 17, 19, 21, and 26 (Table 10.1).

Table 10.6. Results for Phase 2 cases.

Case	Cstop μg/L	Cox mg/L	Months on/off	NFA Date 95% UCL	Relative operating cost
Base	5	8,000	3/9	Jan 2025	100
Case 1	5	16,000	3/9	Apr 2022	76
Case 2	5	16,000	6/6	Apr 2021	118
Case 3	5	16,000	9/6	Jan 2021	140
Case 4	5	16,000	12/6	Jan 2021	128
Case 1a	25	16,000	3/9	Jan 2021	20

An additional point that should be noted is that the above simulations assume oxidant to be injected at the site-wide average rate of about 0.133 pore volumes per month in all injection wells. However, measured rates at the site vary widely from well to well from about 0.008 to 0.8 pore volumes per month. One would expect this to significantly affect ISCO performance for different TZs. Surprisingly, the correlation between oxidant injection rate and observed first-order contaminant attenuation rate for ISCO wells is essentially zero ($r = -0.03$). This suggests that factors other than oxidation reactions, which have not been identified, are significantly influencing ISCO effectiveness at the site. As such, uncertainty in remediation times may be greater than that estimated from the Monte Carlo simulations.

10.5 References

Arrowhead Contracting and Weston Solutions (2015a) Final Remedial Design Plan In Situ Chemical Oxidation Injection – Full Scale Design and Implementation Warren AFB Former Atlas E Missile Site 11, Nunn Colorado, USACE, January 2015.

Arrowhead Contracting and Weston Solutions (2015b) Final Characterization Report for Bench Scale and Pilot-Scale Studies Warren AFB Former Atlas E Missile Site 11, Nunn Colorado, USACE, June 2015.

Arrowhead Contracting and Weston Solutions (2015c) Draft Final Remedial Construction Report Warren AFB Former Atlas E Missile Site 11, Nunn Colorado, USACE August 2015.

Kim, U., J.C. Parker, and R.C. Borden (2018) Stochastic Cost-optimization and Risk Assessment of In-situ Chemical Oxidation for Dense Nonaqueous Phase Liquid (DNAPL) Source Remediation. Stochastic Environmental Research and Risk Assessment. In revision.

Reitsma, S. and Q.L. Dai (2001) Reaction-enhanced mass transfer and transport from non-aqueous phase liquid source zones. Journal of Contaminant Hydrology 49: 49-66.

USACE (2014) Proposed Plan In Situ Chemical Oxidation Using Sodium Permanganate for Groundwater Remediation Former Atlas E Missile Site 11 Weld County Colorado, April 2014.

West, M.R. and B.H. Kueper (2012) Numerical simulation of DNAPL source zone remediation with in situ chemical oxidation (ISCO). Advances in Water Resources 44: 126-139.

West, M.R., G.P. Grant, J.I. Gerhard, and B.H. Kueper (2007) The influence of precipitate formation on the chemical oxidation of TCE DNAPL with potassium permanganate. Advances in Water Resources 31: 324-338.

11. Conclusions and Implications

11.1 Summary and Conclusions

11.1.1 Overview of modeling approach

Complex field sites with multiple groundwater contaminant sources, DNAPLs, back-diffusion, etc. invariably exhibit large prediction uncertainty, which often results in poorer than expected remediation performance and, typically, greater time-to-completion and cost-to-completion than planned or expected. Even relatively "simple" field sites can be prone to larger than expected prediction uncertainty, depending to a large degree on the quality and quantity of data available for calibration.

The overarching objective of this project was to develop a practical methodology and associated computational tools to optimize remediation strategies that may involve multiple technologies applied serially or concurrently with relevant performance monitoring protocols for real-time decision making to minimize the expected (probability-weighted) cost to meet site cleanup objectives with explicit consideration given to uncertainty in future performance. Furthermore, the process should be applied iteratively over time to assess and refine the remediation strategy as necessary.

The computational strategy proposed to solve this problem is as follows:

1. Use all available quantitative and qualitative site data to develop a conceptual site model and quantify initial estimates of model parameters and their uncertainty.
2. Refine model parameter estimates and their covariances using robust inverse modeling techniques.
3. Use stochastic optimization methods to identify design strategies that minimize the probability-weighted cost while meeting remediation criteria with acceptable reliability.
4. Iterate steps 1 to 3 periodically as additional monitoring and operational data become available.

Step 1 is a deterministic optimization problem that requires on the order of $2N_P N_{iter}$ direct solutions of the site model, where N_P is the number of calibrated parameters and N_{iter} is the number of iterations required. For a problem with 5 to 10 parameters and 25 to 100 iterations, this yields 250 to 2,000 direct simulations. This is a substantial, but not overwhelming, computational cost for a numerical model.

The computational cost for step 3 is roughly $2N_{opt}N_{mc}N_{iter}$, where N_{opt} is the number of optimized design variables, N_{mc} is the number of Monte Carlo realizations, and N_{iter} is the number of solution iterations. A stochastic remediation design problem with 5 to 10 design variables, 100 Monte Carlo realizations, and 25 to 100 iterations would total 25,000 to 200,000 direct simulations. The latter number of runs of a numerical model would be impractical for environmental consultants with a fast multiprocessor workstation. Faced with the foregoing arithmetic, most engineers and hydrologists opt for deterministic analyses using a numerical model perhaps with a few manual sensitivity analyses and very rarely using formal optimization.

The approach used in this project is founded on the recognition that uncertainty in performance predictions will always be large, regardless of how sophisticated a model is used or how much site data is available. In fact, since more sophisticated models almost always require more parameters, greater prediction uncertainty will occur if it is calibrated to data of less than optimal quality and/or

quantity. Regardless, any model predictions based solely on "best estimates" of model parameters will augur optimistic (often grossly optimistic) performance. Precision gained from more sophisticated models can be more than off-set if prediction uncertainty is disregarded.

The stochastic optimization toolkit (SCOToolkit) was developed on the principle that it is better to use simpler, more computationally efficient models that account for dominant physical processes coupled with explicit consideration of prediction uncertainty over more sophisticated but computationally expensive deterministic models. SCOToolkit employs an efficient 3-D semi-analytical transport model to simulate dissolved phase transport of contaminants and injected electron donor species in steady-state, planar or mildly nonlinear flow fields with multiple contaminant sources (Parker et al. 2010).

Contaminant discharge rate from each source is modeled as a power function of source mass remaining. The discharge rate can be enhanced by injection of electron donors or chemical oxidants within or upgradient of the source (Reitsma and Dai 2001). Forward- and back-diffusion between permeable and low permeability zones in an aquifer are modeled using a computationally efficient upscaled dispersion approach that distinguishes between resident and flux concentration solutions (Parker and Valocchi 1986, Parker and Kim 2015).

The transport model is coupled with performance and cost models for DNAPL source remediation using electric resistance heating (ERH), thermal conduction heating (TCH), steam enhanced extraction (SEE), source zone electron donor (ED) injection, or in situ chemical oxidation (ISCO) with recirculation, and dissolved plume remediation or control using ISCO pulsed injection, dissolved plume ED injection, other reactive barriers, or groundwater extraction, as well as MNA. All methods may be performed concurrently or serially.

Each remediation system or subsystem (e.g., individual ED injection galleries) may be terminated independently based on real-time performance monitoring data with rules specific to each type of remediation system. Furthermore, subregions within source zone treatment systems may be terminated early using spatially adjusted statistical criteria, which can produce significant operating cost savings.

After all performance rules have been met (i.e., all active systems terminated), site-wide no-further-action decisions are made based on compliance monitoring data and rules designed to prevent measurement "noise" from rendering erroneous decisions. Compliance rules include a target maximum concentration, a date by which all compliance wells should be under the target level, a maximum date by which compliance targets have been met and all active remediation systems have been terminated long enough to ensure no rebound above the target, as well as various means of dealing with noisy measurements.

Compliance rules are assumed to be set by negotiation with regulatory personnel, while performance rules are treated as optimizable. This capability to optimize performance monitoring protocols is important, because it allows SCOToolkit to significantly reduce expected cost and because it removes subjectivity from decisions that must be made from inevitably noisy data enabling more reliable decisions to be made.

Stochastic design optimization is performed using a robust optimization algorithm with Monte Carlo (MC) realizations to quantify uncertainty. Cost-to-complete for each realization is computed from unit capital and operating costs for each remediation technology and for site-wide monitoring. Penalty costs are added to realizations that fail to meet remediation criteria. The

average cost (including penalties) across all realizations is taken as the “expected” cost, which we seek to minimize.

The handling of noisy data is a troublesome issue for compliance monitoring. Levine (2010) with the US EPA proposed to compute confidence limits on an N-year simple moving average (SMA) of measured concentrations to smooth noise. If the upper one-sided SMA confidence limit for a specified probability level (e.g., 95%) is less than the compliance concentration for each compliance well, regulatory closure criteria are deemed met. We have found that stochastic simulation-optimization analyses using Levine's and other "noise management" approaches improves performance reliability.

Results show that *increasing or decreasing* monitoring frequency relative to an optimum value can increase the expected cost-to-complete. Fewer samples lead to wider confidence limits, which increase the duration of long-term monitoring, and hence operating costs for the longer duration, more than the savings from reduced frequency. Effectively, more conservative operation is required to compensate for greater measurement uncertainty associated with fewer samples. We have found that cost savings are generally achieved by simultaneously optimizing the moving average lookback period and monitoring frequency along with remedial system design variables. While typical long-term monitoring statistical methods may be useful for optimizing the number and location of monitoring wells, optimization of sampling frequency should be performed in the context of a more comprehensive stochastic optimization approach that considers cost tradeoffs. Furthermore, methods for handling measurement noise vis á vis compliance rules should be optimized to minimize cost to complete.

A final factor that contributes to uncertainty in predicted performance, and hence to higher expected total remediation cost, is intrinsic uncertainty in the model used to make predictions. After we calibrate a model to field measurements, residual deviations remain that are attributable to a combination of sampling/measurement error and intrinsic model error. These cannot be practically distinguished, although model error will usually dominate. Intrinsic error can be reduced by refining the model to account for more details of the real system. However, to the extent that the "refined" model requires more parameters that are imperfectly known, the reduction in intrinsic error may be offset by an increase in parameter uncertainty when calibrated to the same data. The optimum model to minimize prediction uncertainty is ultimately limited by the data available for calibration.

Estimates of site properties based on more data, collected over longer time periods, are generally more accurate and less uncertain. Thus, it is important to periodically evaluate and adjust the remediation plan. SCOToolkit is designed to do this by facilitating periodic recalibration of site properties as new data becomes available, reassessing projected system performance, and reoptimizing remediation system design and operation as needed to meet objectives with minimum cost. This protocol enables timely adjustments of operational variables for existing remediation systems, or adoption of alternative technologies, if necessary, to meet objectives in a timely manner with the least ongoing cost-to-complete.

11.1.2 Enhanced reductive dechlorination model

Enhanced biodecay of chlorinated hydrocarbons by injection of electron donor (ED) species, such as lactate or emulsified vegetable oil, in one or more ED injection galleries is modeled using a

superposition method based on extensions of the method described by Borden and Bedient (1986). The method employed involves (1) simulation of baseline contaminant transport without ED injection, (2) simulation of nonreactive ED transport using the same modeling approach used for contaminants, (3) adjustment of ED concentrations for reactions with natural electron acceptor (EA) species in groundwater assuming serial and/or parallel reactions with EA of different redox potential, (4) adjustment of net ED concentrations for reaction kinetics based on mean travel time to a given location and date and for reaction stoichiometry, and (5) superposition of the solutions from 1 and 4 to obtain post-reaction contamination concentrations.

For ED galleries placed upgradient of DNAPL sources, enhanced dissolution of the DNAPL source is modeled using an empirical mass transfer enhancement coefficient, which can be calibrated from bench- or pilot-scale tests. Performance monitoring for galleries upgradient of DNAPL uses measurements of contaminants and all decay products (total concentration) downgradient of the source. Termination of injection is based on the total concentration to avoid rebound. Performance monitoring for other ED galleries utilize contaminant concentrations a short distance upgradient of the injection gallery for injection termination decisions. When multiple ED galleries are employed along a streamline, ED galleries are not allowed to terminate until all upgradient galleries terminate.

While DNAPL source remediation technologies (thermal treatment and upgradient ISCO or ED injection) can reduce the duration of a DNAPL source, downgradient ED injection is most useful to meet compliance targets within specified times. Earlier meet-by dates may require multiple galleries to reduce the maximum ED travel time along the plume length.

11.1.3 Thermal treatment model

A thermal treatment model that assumes a lognormal recovery rate as a function of time was developed and field-verified. In addition to serving as a practical tool for simulating thermal treatment within the design optimization framework, the method provides a practical means of interpreting real-time performance monitoring data.

Thermal system termination decisions are commonly made by comparing the average concentration computed from a round of soil samples directly with a cleanup target. However, averages from soil data are subject to large uncertainty even when the number of soil samples is large. An alternative method, which estimates average soil concentration from mass recovery measurements during thermal treatment using the lognormal recovery model, was found to exhibit less uncertainty and lower cost than soil sampling.

To explicitly account for uncertainty in average soil concentrations estimated from soil and/or mass recovery data, the multi-level termination strategy stops treatment when an upper confidence limit of estimated mean concentration at a specified probability is below the target concentration. We employ a statistical methodology for computing confidence limits at site-wide, treatment zone and monitoring zone levels that allows termination decisions to be made at all scales with equal reliability.

We allow target soil concentrations for regions smaller than the full site (local stop criteria) to be specified at a value less than the site-wide stop criterion. Cleaning up *less* recalcitrant regions to a lower average concentration enables *more* recalcitrant regions to be terminated at a higher average concentration to achieve the same site-wide average (or total mass). This offers the possibility of

reducing overall treatment duration and total operating cost. The multi-level monitoring and termination strategy allows for site-wide termination as well as early termination of subregions, resulting in decreased operating costs.

Results for example problems indicated that the practice of using computed average soil concentration (as opposed to an upper confidence limit) cannot achieve a high probability of meeting the target average soil concentration. Optimizing the confidence limit probability, local scale cleanup level, number of monitoring zones per treatment zone, soil borings per monitoring zone for each sampling event, sample depths per boring, date for first sampling event, and time interval between sampling events for a site treated as a single treatment zone using only soil sampling data achieved cleanup objectives with a higher probability of success than a more conventional approach.

Dividing the site into multiple treatment zones with different soil concentration ranges and optimizing the same variables reduced total cost by 6%. Optimizing the confidence limit probability, local-scale cleanup level, and number of monitoring zones per treatment zone with three treatment zones, using mass recovery data instead of soil data, achieved an additional 10% cost reduction. If confirmation of mass recovery-based results with soil sample data is desired or required, delaying each local termination decision until confirmed by soil sampling will increase cost. Therefore, if confirmatory soil sampling is required, we recommend waiting until all heating units have been stopped based on mass recovery data before performing site-wide soil sampling.

In addition to computing the probability-weighted average cost for optimized designs, the method gives cost probability distributions that reflect uncertainty in measurements and calculations. An optimized example problem using only mass recovery data to make termination decisions had a 16% lower expected total cost than a case that approximates typical industry practice, while the 95% upper confidence limit of total cost for the former was 28% lower. Thus, the proposed methodology not only yields "expected" cost savings, but also sharply reduces the magnitude of potential cost overruns.

11.1.4 In situ chemical oxidation model

An efficient model for DNAPL source remediation using ISCO was developed that accounts for the important physical and chemical processes. A unique feature of the proposed ISCO operational methodology is the introduction of termination criteria that compare upper confidence limits of average measured concentrations at a specified probability level with the cleanup target to provide a margin of safety to termination decisions. Statistical termination criteria allow site-wide and treatment zone termination decisions to be made with equal reliability. In some cases, cleaning up less contaminated treatment zones (TZs) to more stringent criteria can allow site-wide average concentration targets to be met earlier and with lower costs.

Optimization of TZ oxidant concentrations, treatment zone-level cleanup criteria, reinjection criteria, and performance monitoring variables yielded a failure-adjusted expected cost for an example problem about 11% lower than a non-optimized case approximating best engineering practice. Furthermore, the cost probability distribution for the optimized design eliminated positive skew evident in the "best practice" such that the worst case cost for the optimized design was 14% lower than that for the non-optimized design. Since the number of monitoring wells used for the best practice case was greater than is often available, and the number assumed fortuitously turned

out to be optimal, significantly larger cost savings are likely to be realized in many cases. Adoption of the proposed stochastic design method in conjunction with proposed real-time performance monitoring and decision-making protocols promises to yield more robust, reliable and cost-effective ISCO applications to DNAPL sites with real-world uncertainty taken into account.

11.1.5 Field applications

Joint Base Lewis-McChord

The East Gate Disposal Yard (EGDY) at JBLM was used as a waste disposal site for solvents between 1946 and the mid-1970s. A TCE plume extends over 4 km downgradient. Pump-and-treat systems were installed to control contaminant migration. Three DNAPL source areas were identified and thermal treatment of the sources was undertaken between 2003 and 2007. A step-wide calibration-assessment-optimization was applied to the site.

Model parameters were initially calibrated to data through 2003 before thermal treatment commenced. Re-calibration of the three-source model with actual mass recovery data and monitoring data through 2007 indicated a large amount of DNAPL remained, suggesting a probable fourth unidentified source. Date and cost to reach no-further-action (NFA) with and without treatment of the inferred fourth source treatment were determined using the final (most reliable) 2015 calibration with and without cost discounting. The 2007 calibration predicted that thermal treatment of the fourth source would decrease the NFA date from 2110 to 2035 with a slightly lower undiscounted total cost, but a substantially higher discounted cost. The decision to treat or not treat the fourth source based on cost is sensitive to the discount rate due to a tradeoff between the large present cost for thermal treatment (~$6 million) versus long-term pump-and-treat costs (~$100k/year). In such cases, it is more conservative to use a lower discount rate, which suggests deferring treatment of the fourth source until the analysis is less ambiguous.

With additional data through 2015, long-term prediction uncertainty decreased, resulting in a much earlier expected NFA date as well as discounted and undiscounted costs without thermal treatment of the fourth source, confirming the decision to defer treatment. The decision not to pursue thermal treatment of the fourth source resulted in a 46% undiscounted cost savings and a 67% discounted cost savings based on the 2015 calibration.

Dover Air Force Base Area 5

Several sources of chlorinated ethenes were present within the Dover AFB Area 5 in Dover, Delaware. From the northern part of the site, groundwater flowed south-southeasterly before gradually turning southwest. Twelve injection galleries for electron donor (EVO and lactate) began operating in 2006 to enhance reductive dechlorination. SCOToolkit was initially calibrated to site data from 1988 through 2005 prior to commencement of actual ED injection (Cal-1), and subsequently recalibrated with data through 2010 (Cal-2), and 2016 (Cal-3).

Monte Carlo simulations were performed for three design scenarios:

Case 1. Actual average injection rates employed from 2006 to 2016
Case 2. Best practice injection rates based on estimates of field contaminant fluxes
Case 3. Optimized injection rates and monitoring parameters with incremental updating

Final best estimates of cost-to-complete for each of the three design approaches based on the final (most reliable) calibration parameters were $63.0, $62.8, and $48.7 million for the actual, best practice, and incrementally optimized designs, respectively. The actual design cost was very close to the estimated "best practice" cost, while the incremental stochastic optimization protocol yielded an expected cost savings of 29% and decreased the expected time-to-complete by 18–20 years.

These time and cost reductions were achieved by using only 5 of the 12 injection galleries, injecting at high rates initially, decreasing rates at later times, and shutting off individual galleries early when performance monitoring wells for each gallery met defined criteria.

Stochastic optimization also sharply reduced cost uncertainty, especially for results based on the initial and most uncertain (Cal-1) parameter estimates (Figure 9.4). This is an important benefit of stochastic cost optimization, but it is not unexpected, since stochastic cost optimization explicitly seeks to reduce the likelihood of positive cost excursions, which mandate a more conservative (and costly) design.

Atlas Missile Site 11

Atlas 11 is a former Atlas E missile site in northeastern Colorado that was decommissioned in 1966. Operations at Atlas 11 involved use of TCE to clean up residual rocket fuel. Waste solvent drained to a sump, which discharged to the ground surface. Dissolved phase TCE was detected on- and off-site in a shallow perched water table. No evidence of DNAPL was found at the site.

Remediation investigations and feasibility studies resulted in a decision to employ ISCO using sodium permanganate in paired injection and extraction wells. A field pilot study was conducted in 2012 and expanded in 2013 with full-scale operations commencing in 2014. Oxidant injection and extraction was performed in coupled wells for about 3 months in the summer with natural gradient conditions otherwise. Through 2017, twenty-seven well pairs received oxidant injections, 18 of which were injected only once, 7 were injected twice, and 2 were injected three times.

Analyses with SCOToolkit were undertaken to optimize ongoing operations to meet the NFA target for TCE of 5 μg/L by a target date of January 2021. All simulations assumed that each previously operated well pair plus three additional pairs with high off-site concentrations were injected with oxidant annually until the well pair met remediation criteria.

Preliminary simulations indicated that increasing the mass of oxidant injected annually into each well pair by a factor of 2 (by increasing the oxidant concentration and/or the oxidant volume injected) would reduce the cost to reach the cleanup objective by about 13%.

Monte Carlo simulations were performed for comparison with a base case corresponding to current operating practice at the site (3-month injection period with 8,000 mg/L oxidant concentration). Other cases assumed an oxidant concentration of 16,000 mg/L with on-cycle durations of 3, 6, 9 and 12 months. All cases assumed an injection rate of 0.133 pore volumes per month, corresponding to average gravity-fed field conditions. During periods without injection, oxidation reactions were simulated under natural groundwater gradient conditions.

Total operating costs for oxidant injection were estimated assuming $5.5 per kg of oxidant, $20 per m^3 of fluid injected, plus $300 per day for other operating costs (Kim et al. 2018).

The base case was predicted to have a 95% upper confidence NFA date of January 2025 with a low probability of meeting the January 2021 NFA date. Increasing the oxidant concentration to 16,000 mg/L with the on-cycle duration of 3-months was predicted to reduce the expected operating cost by 24% with a 90% probability of meeting the NFA date. Increasing on-cycle duration to 6 months nudged the probability of meeting the NFA date to 95%, but pushed the cost to 18% above the base case. Increasing the on-cycle duration to 9 months pushed the probability of meeting the NFA date close to 100% at a cost 40% above the base case. However, it is questionable whether a 6-month off-cycle time is adequate to obtain full rebound, which would make termination decisions difficult. Considering the large cost to increase the probability of meeting the NFA from 90% to 95%, Case 1 appears to be the most cost-effective option with a 24% cost savings of the base case.

11.1.6 Other Tools

A comprehensive User Guide was developed for SCOToolkit, which includes detailed instructions for the preparation of input files, program execution and interpretation of model results. A dedicated web site was also developed that includes download links for the SCOToolkit program, example data files, and related tools, including the Excel worksheets described below.

The following Excel worksheets were developed to assist users in preparing input files for SCOToolkit and to track real-time field performance data for ISCO and thermal treatment that implement the multiscale statistical remediation termination protocols developed in this project and employed by SCOToolkit.

ISCO treatment termination decisions using real time data

This workbook implements real time termination decisions for ISCO source treatment using soil and/or groundwater sample data for multiple monitoring zones (MZ) within multiple treatment zones (TZ) using a rigorous statistical approach based on soil and/or groundwater sample data in a manner that provides consistent decision reliability at scales ranging from individual monitoring zones, to groups of monitoring zones (aka, treatment zones) to site-wide.

ISCO unit cost calcs for continuous injection

This worksheet computes unit cost parameters for the continuous injection ISCO source treatment model from cost sensitivity analysis results.

ISCO unit cost calcs for pulsed injection

This worksheet computes unit cost parameters for the pulsed injection ISCO source treatment model from cost sensitivity analysis results.

Source function parameter estimation from field data

The purpose of this workbook is to calculate prior estimates of source parameters M_{cal}, J_{cal}, and β from measured source zone groundwater concentration data and soil data for input into the SCOToolkit calibration tool. These values and uncertainty estimates can be used as prior estimates for transport model calibration to monitoring well data over time.

Streamline calculations

This worksheet fits linear or polynomial streamline functions to digitized streamline data for contaminant source locations, ED injection galleries, or reactive barriers.

Thermal treatment model calibration

This workbook calibrates thermal model parameters to measured mass recovery data for single or multiple recovery functions.

Thermal treatment termination decisions using real time data

This workbook enables real-time termination decisions to be made for thermal source treatment that allows for multiple monitoring zones (MZ) using a rigorous statistical approach based on soil and/or mass recovery measurements to provide consistent decision reliability at multiple scales. The worksheet also can be used to calibrate thermal model parameters to measured recovery data.

Thermal treatment unit cost calcs

This worksheet computes unit cost parameters for the source zone thermal treatment model from cost sensitivity analyses.

11.2 Implications for Future Research and Implementation

The current version of SCOToolkit has been thoroughly tested on several hypothetical problems and three field sites by ER-2310 personnel as well as on "virtual sites" generated with a high-resolution numerical model by ER-2313 personnel as beta testers. The results of these studies have shown SCOToolkit to be very robust, despite the complexity of the problems that have been addressed involving incremental calibration, assessment and optimization over time with a wide range of remediation strategies involving multiple contaminant sources, multiple technologies (including source treatment with thermal, ISCO or enhanced DNAPL dissolution, and dissolved plume treatment with enhanced bioremediation, ISCO, or pump-and-treat) operated concurrently or serially.

In addition to the large number of design variables associated with the range of remedial technologies, we have introduced a number of additional optimizable variables associated with compliance and performance monitoring protocols. Cost savings from optimization of monitoring variables can be as significant as those from design variables per se. Generalized guidelines for selecting variables to optimize and initial values and ranges would be helpful to users, but need further testing for a variety of conditions.

Application of SCOToolkit to substantially more demo sites with most of the work being performed by personnel affiliated with the sites and SCOToolkit developers serving as advisors would have a number of benefits. It would increase the SCOToolkit user base enabling savings to be realized for DoD sites. It would also serve as a training ground for the trainers to develop videos or interactive tools to enable more users to be trained efficiently. Furthermore, if results from these studies were presented at stochastic cost optimization sessions at SERDP annual meetings, further waves of users would be encouraged to apply SCOToolkit to sites with attendant cost savings to DoD.

Currently, the Navy, Air Force and Army are conducting portfolio optimization evaluations with cost estimation as a technical component. If each of these identified a number of sites interested in using SCOToolkit, an initial training session could be held for all personnel with periodic conference calls and email as needed to provide individualized advice. Most of the cost would therefore be borne by the individual sites.

A variety of enhancements to SCOToolkit are possible. Some that have been suggested include:

- Consider the existence of co-contaminant with fuel hydrocarbons, which are common at many sites and can serve as electron donors for reductive dechlorination. Reactions could be modeled by superposition in the same manner as the current ED injection model.
- Another common contaminant at many sites is 1,4-dioxane. A parallel solution could be implemented for this species. Modifications would be required in thermal, ISCO and enhanced bio modules to allocate reaction rates for two species.
- Currently only one contaminant species is modeled. Daughter products of the primary chlorinated solvent are commonly present. We typically sidestep this problem by modeling the sum of primary and daughter products (e.g., PCE, TCE, DCE) as a pseudo-species. However, a modification of the SCOToolkit analytical solution is possible to model the serial decay chain.
- The current ISCO model includes stoichiometric and other variables that can be specified for different oxidant species. However, the model has only been tested for permanganate. Applications involving other oxidants may require modifications to quantify mass transfer enhancement and/or suppression. Further research may be needed.
- Improvements in the user interface or web site.

Before undertaking any of the above, input from users or potential users would be desirable to prioritize limited resources.

Appendix A.

Stochastic Cost Optimization Toolkit (SCOToolkit)

User Guide

by
Ungtae Kim[1] and Jack Parker[2]

[1]Civil and Environmental Engineering Department
Cleveland State University

[2] Civil and Environmental Engineering Department
University of Tennessee at Knoxville

developed for
Strategic Environmental Research and Development Program
Project ER-2310

Feb 2018

Table of Contents

List of Figures

List of Tables

SCOToolkit Disclaimer and Terms of Use

The program SCOToolkit, including various accessory Excel worksheets is provided the User "as is" without warranty, implied or otherwise on the following terms and conditions:

1. The University of Tennessee, Cleveland State University, Stanford University, and the U.S. Department of Defense (hereafter, the "Developers") make no warranty of any kind, express or implied, with respect to the subject software products, and specifically make no warranty that said products shall be fit for any particular application. Furthermore, any description of said products shall not be deemed to create an express warranty that such products shall conform to the description.

2. The User assumes all risk and liability for loss, damage, claims or expense resulting from use, possession or resale of any of software products delivered subject to this agreement.

3. The User agrees to indemnify, defend and hold harmless the Developers and their agents and employees from and against any and all claims, liability, loss, damage or expense, including reasonable attorney's fees, arising from or by reason of receiver's use, possession or resale with respect to any of the software products furnished by the Developers pursuant to this agreement and such obligation shall survive acceptance of said products therefore by receiver.

4. This agreement constitutes the complete and final agreement of the parties hereto.

Preface

This user guide provides documentation for operation of the Stochastic Cost Optimization Toolkit (SCOToolkit) v.3 developed as a part of the Strategic Environmental Research and Development Program (SERDP) project ER-2310, "Practical Cost-Optimization of Characterization and Remediation Decisions at DNAPL Sites with Consideration of Prediction Uncertainty."

The program enables periodic assessment and optimization of remediation-in-progress (RIP) sites to minimize expected total net present value (NPV) cost considering failure probability and measurement and prediction uncertainty and to facilitate early identification and correction of problems associated with remediation technologies and/or goals. Remediation technologies that may be considered with concurrent and/or sequential operation include:

1. Electric resistance heating (ERH) DNAPL source remediation
2. Thermal conduction heating (TCH) DNAPL source remediation
3. Steam enhanced extraction (SEE) DNAPL source remediation
4. DNAPL source excavation
5. In situ chemical oxidation (ISCO) with recirculation for DNAPL source remediation
6. ISCO with pulsed injection for DNAPL source remediation
7. Electron donor (ED) injection for enhanced DNAPL source remediation
8. Electron donor (ED) injection for enhanced dissolved plume remediation
9. Reactive barriers (RB) or groundwater extraction for dissolved plume control

Aqueous phase transport associated with multiple DNAPL sources is modeled using an efficient semi-analytical 3-D solution that can account for mass transfer limitations associated with diffusion into and out of low permeability zones (aka, "back diffusion"). The solution leads to differences between volume-averaged soil concentrations and flux-averaged monitoring well concentrations, either or both of which may be used for model calibration.

Stochastic cost optimization is a computationally intensive iterative process that requires hundreds of evaluations of expected cost for different design and operation variables. Furthermore, each expected cost evaluation requires multiple simulations (typically 100) to represent uncertainty in model predictions and measurements. As a result, tens of thousands of individual forward model simulations over a multi-decade time period are commonly required to solve a single optimization problem. Our overall objective has been to develop a practical tool to meet remediation objectives with the least possible cost. Due to uncertainty in future performance, this objective involves tradeoffs between the probability of successfully meeting remediation goals within a certain timeframe and the aggressiveness of the remediation strategy. Performance uncertainty arises from three sources. First, for a given model formulation, uncertainties in model parameters and boundary conditions over time produce prediction uncertainty. Second, field and lab measurements are subject to sampling and measurement uncertainty. And finally, there are inherent accuracy limitations associated with assumptions and simplifications – even for the most sophisticated models. SCOToolkit explicitly addresses errors from the first source. The last two sources or uncertainty are lumped together in the treatment of residual calibration error.

The foregoing considerations require a performance simulation model that is very robust and computationally efficient. This requires giving up some degree of model complexity to enable practical application with typically available computer hardware. Our experience indicates that

the level of sophistication in the SCOToolkit performance models is adequate for most sites considering the magnitude of uncertainty from other sources.

In the inverse modeling mode, historical site data is used to calibrate the simulation model and to estimate parameter covariances and residual prediction error. Forward predictions of remediation performance and cost are performed for defined remediation strategies, operating rules and remediation criteria. A Monte Carlo (MC) method is used to quantify uncertainty in performance and cost attributable considering uncertainty in model parameters, measurements employed for real-time decisions, and cost function variables.

Design optimization is performed to determine values of design variables that minimize the expected value (average over MC realizations) of NPV, which may include "penalty costs" for failure to achieve defined remediation objectives within a specified time-period.

This document describes the input structure and procedures for setting up and operating the program.

The SCOToolkit web site can be found at http://scotoolkit.csuohio.edu/.

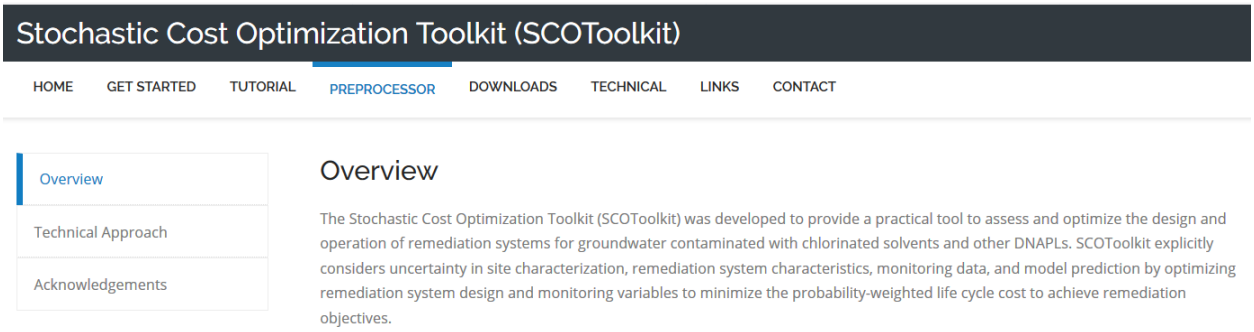

The website provides an overview of the program, detailed technical information, tutorials, an interactive pre-processor, downloadable source code, executable files, example input files, and various Excel-based utilities to facilitate input file preparation, plus various other information and useful links.

A1. Model Parameters and Design Variables

A main input file [*.inp] of SCOToolkit is an ASCII text file that defines the features of a project, site characteristics (e.g., DNAPL sources and aquifers), and the associated file names to be included the defined project. The input file consists of two parts, project definition (A1.1) and parameters (or variables) (A1.2~1.8). All variables (both numbers and strings) are separated by spaces (tabs). Multiple spaces or tabs are just treated as one delimitator.

A1.1 Project Definition

Table A1-1 lists the variables of a project to define line by line, followed by an example block. Note that the number inside ( ) used in the Explanation column is a sequential number.

Table A1-1. Project definition in an input file [*.inp]

Line	Variable	Explanation	Comment
1	run_mode	(1) 1 = Parameter calibration, 2 = Design optimization using ENPV with a user-specified penalty value for failure, -2 = Design optimization using failure-adjusted ENPV, 3 = Forward simulation for given parameters, (2) Number of cores available for parallel computing (3) Dimension (2D or 3D) of transport solution. If two digits, first digit is for contaminant transport and second digit is for ED transport (2, 3, 23, or 32). (4) Minimum model concentration to truncate when calibrating	Integer Integer Integer Real
2	num_sources	Number of DNAPL sources	Integer
3	num_complnc	Number of compliance locations	Integer
4	num_pt	Number of Pump and Treat system (P&T) locations	Integer
5	num_EDs	Number of ED galleries including RBs	Integer
6	ED_types	List all ED_types as many as ‘num_EDs’	Integers
7	isSZR	List the types of source removal (-1, 0, 1, 2) as many as 'num_sources'	Integers
8	isCost	(1) 1 = compute costs, 0 = do not compute costs If isCost(1) = 1, define the following. (2) 1 = consider uncertainty, 0 = fixed costs (3:4) Reference year to discount and discount rate	Integer Integer Real, Real
9	SlnGW	(1) a prior or best estimate of log standard deviation of groundwater samples	Real
10	randset	Random number seeding	Integer
11	param_MC	(1) Number of MC sets to evaluate (max = 1000) (2) File name containing parameter realizations (3) Flag for creating each MC output file	Integer String Y or N
12	file_CON	(1) Flag for use of dissolved concentration data (2) Flag for generating a concentration curve for each well (3) File name containing concentration data	Y or N Y or N String
13	file_FLX	(1) Flag for use of source flux data (2) File name containing source flux data	Y or N String
14	file_MAS	(1) Flag for use of source mass removal data (2) File name containing mass removal data	Y or N String
15	Name Prior STD Log Tune isSync LB UB		String

The model reads a [*.inp] file based on a space- or tab-separated format. Instruction to write each line is provided as follows. Note that Lines 1-18 are mandatory even though some of them may not be used during simulation.

Line 1: Example of 'run_mode' is '3␣1␣3' (1=forward simulation, 1=number of computer cores, 3=dimension of transport solution). Note that parallel computing is only implemented when Matlab source codes are run directly in a Matlab command window and hyper-threading is not considered. The minimum concentration simulated by SCOToolkit can be added as 'run_mode(4) if calibration is performed, i.e., 'run_mode(1)=1'. If not defined, 0.05 is assigned internally for the calibration mode. A value 2^{-52} (a numerically zero value inside Matlab) is internally used for other simulation modes.

Line 2: num_sources (default = 1). Note that although there is no limitation of maximum number of sources, the maximum is recommended as 5 in calibration and optimization for time-efficient computing.

Line 3: num_complnc (default = 0) can be defined up to 5 locations.

Line 4: num_PT (default = 0) can be defined up to 5 locations.

Line 5: num_EDs (default = 0) can be defined as many as needed. Note that when 'num_EDs' = 0, then Line 6 'ED_type' will be read but ignored internally.

Line 6: List the types of ED injection defined as 'num_EDs'. EDs should be ordered from upstream to downstream. For example, 'ED_types' can be '3 ␣3 ␣3 ␣3' when 'num_EDs' = 4, indicating 4 ED galleries with Type 3. 'ED_types' is defined as follows.
1 = aqueous phase ED injection via wells (Type 1): assigned to RB currently
2 = non-aqueous phase ED injection via wells (Type 2): not used currently
3 = aqueous phase ED injection via galleries (Type 3): most common
4 = non-aqueous phase ED injection via galleries (Type 4): not used currently

Line 7: List the types of source removal methods defined as 'num_sources'. The methods used in this program is as follows.
-1 = no removal (i.e., natural depletion)
0 = instant or progressive source zone removal, SZR
1 = thermal source removal (TSR) or electrical resistant heating (ERH)
2 = In-situ chemical oxidation (ISCO)

Line 8: Example of 'isCost' is '1␣0 ␣2014␣0.05'. If 'isCost(1)' = 1 and cost uncertainty is considered (i.e., 'isCost(2)' = 1), use should provide uncertainty range in a related cost file that is defined in SCOToolkit remedial practices. To consider discount rate (e.g., 0.05 which is 5%), a reference year for discount 'isCost(3)' should be specified. Note that any cost incurred in the model before the reference year is disregarded (i.e., zero). Note that 'Y', 'T', and '1' are treated as 'True' internally.

Line 9: Log uncertainty of groundwater measurement (SlnGW). 'SlnGW' listed in this line is used as the default uncertainty in individual GW sample measurements.

Line 10: 'randset' (default = 1) can be an integer from 1 to 5.

Line 11: If param_MC(1) >0, user should provide a set of parameter realizations generated from calibration in a previous step. Note that the realized parameters should be corresponding to the parameters marked as 'Tune = 1' in the column of 'Tune?'. If param_MC(1) = 0, the remaining of Line 11 is skipped. It is should be noted that a [*.rlz] file is automatically generated from previous calibration using covariance matrix and Jacobian, where * is the input file name taken from [*.inp] used in calibration.

Line 12: If ‘file_CON(1)’ = Y, user should determine whether to generate a plot for concentration vs. time for each well by entering ‘file_CON(2)’ = Y or N. If ‘file_CON(1)’ = Y, user should also provide the file name with ‘file_CON(3)’ that contains monitoring locations and other required information (see the format of concentration file in Table A2.3)

Line 13: If ‘file_FLX(1)’ = Y, user should provide the file name with ‘file_FLX(2)’ that contains source identifications and other required information (see the format of flux file in Table A2.4)

Line 14: If ‘file_MAS(1)’ = Y, user should provide the file name with ‘file_MAS(2)’ that contains source identifications and other required information (see the format of mass file in Table A2.5)

Line 15: One line of eight column heading definitions should be inserted as a placeholder (i.e., Line 15 is read but ignored internally). The suggested heading names are:

‘Name Prior STD Log? Tune? SyncID LB UB’

Format of each column in Line 15 is as follows.

(1) Name: a string to name a parameter or variable (user can name any length of a word without space)
(2) Prior: a real number (without transformation) to define a prior value (mean or best estimate) of the parameter
(3) STD: a real number to define a standard deviation of ‘Prior’ (ln-standard deviation should be entered when the ‘Log’ column is 1 for that parameter)
(4) Log? (0 or 1): 0 for normal distribution and 1 for log-normal distribution
(5) Tune? (0, 1, 2, or 3): 0 for the fixed value without any calibration or optimization, 1 for parameter calibration, 2 for variable optimization, and 3 for random generation. The parameters indexed as 1 in ‘Tune?’ are realized after calibration, and those parameters are used in Monte Carlo (MC) simulation when ‘run_mode(1)’ = 2 or 3. Therefore, the parameters to consider for MC simulation in these two options should have the same ‘Tune?’=1 for those parameters that have been realized in a previous calibration step. Note that the parameters indexed as ‘Tune’ =3 in ‘run_mode(1)’ = 2 or 3 will be randomly generated based on user-specified values for the columns in ‘Prior’, ‘STD’, ‘Log?’, ‘LB’, and ‘UB’.
(6) SyncID (integer): 0 for no synchronization. A group number can be assigned for the parameters or design variables to be synchronized during calibration or optimization. The first parameter or variable in the same group should have a non-zero value (1, 2, or 3) in the ‘Tune?’ column.
(7) LB: a real number (without a transformation) to define a lower bound (LB) of a parameter or variable
(8) UB: a real number (without a transformation) to define an upper bound (UB) of a parameter or variable

The Input file demonstrated in this user guide is based on the following source structure and downstream plume. Note that the groundwater is at the top of Source 1.

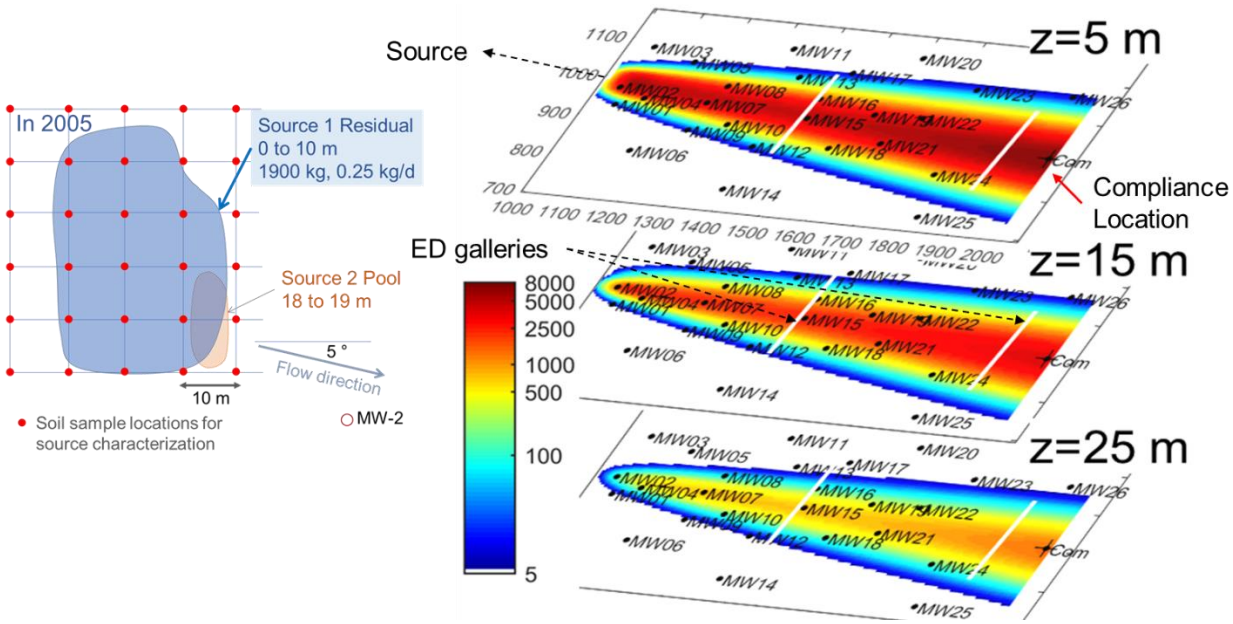

An example of project definition (Lines 1 to 15) is as follows (File name: XXX.inp).

```
1_run_mode       2 28 3 % 2=optimization, 28 cores, 3D transport
2_num_sources    2    % 2 DNAPL sources
3_num_complnc    1    % 1 compliance points
4_num_PT         0    % no Pump & Treat
5_num_EDs        2    % 2 ED locations
6_ED_type        3  3  % 2 aqueous ED injection galleries (type 3)
7_isTSR          1  1  % 2 TSR operation in two defined sources
8_iscost       Y  N  2012 0 % compute cost: Y, uncertainty: N, y_ref=2012, r=0
9_Sln          0.5  % GW monitoring uncertainty for system moni
10_randset     1    % random number seeding
11_param_MC    100  Cal1st.rlzh    N % 100 Monte Carlo sets from Cal1st.rlzh
12_CONC        Y  N  conc_test.dat % Compute conc. for MWs in conc_test.dat
13_FLUX        N  % flux is not computed as output
14_MASS        N % mass is not computed as output
15_name   prior     prior_sd  log?   tune?  synch?    LB      UB  % header
```

Note that the file extensions used in this document are listed as follows for demonstration purpose. User can define any file extension.

(1) [*.inp]: Main input file
(2) [*.rlz]: Parameter realizations based on a parameter covariance matrix.
(3) [*.gen]: Non-correlated parameter generation (i.e., random generation) based on mean, std, and pdf.
(4) [*.dat]: Measurements of contaminant concentrations (μg/L), source mass flux (kg/d), and source mass removal (kg) to be used for calibration or forward simulations.

After defining the project information and required files described above, a set of parameters and variables are immediately listed as follows in order. It should be noted that the 'variable' names in a parameter matrix used in this document are for demonstration only. User may define any meaningful 'variable' name when creating an input file because it does not have any value.

A1.2 Domain Coordinates and Groundwater Flow Field Specification

Although the analytical transport model explicitly assumes a uniform planar groundwater flow field, SCOToolkit considers mildly nonlinear flow fields using a coordinate transformation to map nonlinear streamlines described by a 3rd order polynomial to "equivalent" planar coordinates. Field coordinates are usually specified by survey data in Northing and Easting values relative to a from a reference location. However, any Cartesian coordinate system may be adopted, provided the units are in meters.

If a planar flow field model is employed, the user must specify field coordinates for the center of a vertical plane at the downgradient edge of the source or ED gallery and the flow direction (in degrees positive counterclockwise or negative clockwise from the field X-axis). If the nonlinear model is adopted, in addition to source coordinates (X_o,Y_o), coefficients *a*, *b* and *c* of the polynomial $Y = Y_o+a(X–X_o)+b(X–X_o)^2+c(X–X_o)^3$ must be specified.

An important constraint on the polynomial streamline model is that X-axis values of the streamline must increase or decrease monotonically along the streamline. An example of a non-monotonic streamline is illustrated in Figure A1.1a below. Note that from northernmost end of the streamline the flow is initially to the southeast. But this gradually shifts south and then southwest resulting in multiple Northing values for single Easting values. However, if the coordinates are simply reversed as illustrated in Figure A1.1b, the function becomes monotonic with respect to the X-axis, now taken as Northing.

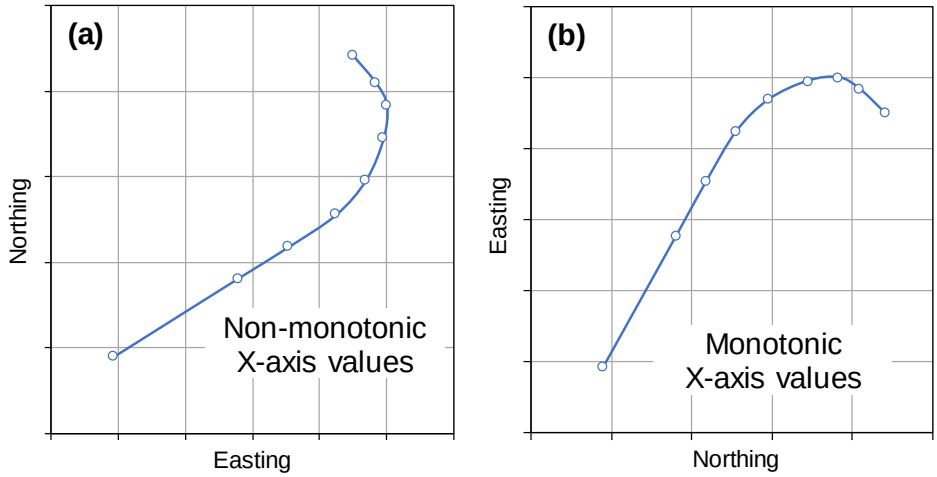

Figure A1.1. Streamline that is (a) non-monotonic with respect to the X-axis (easting), and (b) same data with axes swapped giving a monotonic function versus northing on the X-axis.

Unless the streamline is non-monotonic with respect to both the Easting and Northing, this simple axis swap resolves the problem. All that is required is to fit parameters with the reversed coordinates and to input Northing values for all X-axis inputs and Easting values for all Y-axis inputs in SCOToolkit (e.g, well locations, etc.). When plotting model results on a map view (e.g., plume contours or posted values), it will simply require remembering to switch the coordinates back for a normal map view (i.e., north up).

The process of fitting linear or polynomial model parameters can be performed easily using the SCOToolkit Excel tool **Streamline calulations.xlsx**, which includes detailed instructions and automatically checks for and performs axis swapping as necessary (Appendix A4).

A1.3 DNAPL Source Parameters

The '**paramSource**' matrix stores the characteristics of sources. The matrix dimension is [num_sources, 9] where 'num_sources' is the number of DNAPL sources to analyze (Table A1.2). Multi-biodecay zone and source geometry is described in Figure A1.2 for example.

Table A1.2. Parameters for Source Definition

Variable	Matrix	Definition	Unit
ts_i	paramSource(i,1)	Initial deposition date (decimal year) for source i	year
t0_i	paramSource(i,2)	Final deposition date (decimal year) for source i	year
tcal_i	paramSource(i,3)	Calibration date for Jcal and Mcal (decimal years) of source i	year
Jcal_i	paramSource(i,4)	Mass discharge rate from source i at specified tcal (internally converted to J0, flux at t0, if needed)	kg/d
Mcal_i	paramSource(i,5)	DNAPL mass in source i at the time of calibration (internally converted to M0, mass at t0, if needed)	kg
beta_i	paramSource(i,6)	Depletion exponent for source i	-
L1_i	paramSource (i,7)	Distance from source i to the downstream boundary of Zone 1 (enter a big number like 1E+6 if one decay zone). If either L1 or L2 <=0, it is one decay zone.	m
L2_i	paramSource(i,8)	Distance from source i to the downstream boundary of Zone 2 (enter a big number like 1E+6 if one decay zone). If either L1 or L2 <=0, it is one decay zone.	m
AL_i	paramSource(i,9)	Longitudinal dispersivity specified for source i. If AL_i is negative, a global AL value computed in **paramAquifer** will be used (see Table A1-4).	m

Note that 'tcal' may be set as an arbitrarily year at the user's discretion, which is logically later than 't0' and earlier than the date when the remaining mass is zero. However, if source mass removal data is available for a date later than 'tcal', the user should set a lower boundary of 'Mcal' accordingly, i.e., 'Mcal' > M_removed. To calculate prior estimates of source parameters M_{cal}, J_{cal}, β and t_{cal} from measured source zone groundwater concentration data and soil data, the SCOToolkit Excel tool **Source function parameter estimation from field data** can be used (Appendix A4).

An example of source parameters is as follows (File name: XXX.inp).

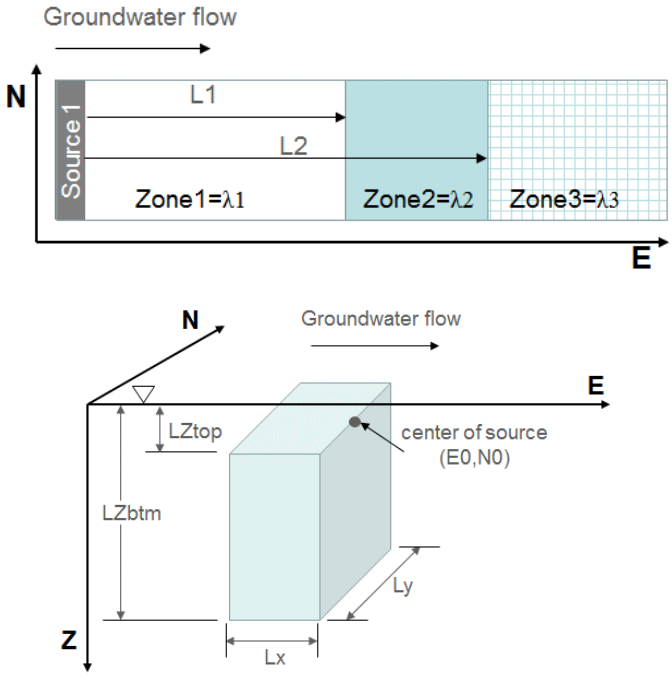

Figure A1.2. Multi-biodecay zones (top) and DNAPL source geometry (bottom).

```
Lines 1~14
15_name   prior     prior_sd  log?   tune?   synch?    LB      UB   % header
paramSource1
ts1       1965      7         0      1       0         1950    1984.9
t01       1985      7         0      0       0         1980    2004.9
tcal1     2005      0         0      0       0         0.00    0.00
Jcal1     0.5       0.5       1      1       0         0.11    2.24
Mcal1     3000      0.5       1      1       0         700     13000
beta1      1.3      0.25      0      1       0         1.01    2.05
L1(m)   10000       0         0      0       0         0.00    0.00
L2(m)   10000       0         0      0       0         0.00    0.00
AL1     -999        0         0      0       0         0.00    0.00
paramSource2
ts1       1965      7         0      1       0         1950    1984.9
t01       1985      0         0      0       0         1980    2004.9
tcal2     2005      0         0      0       0         0.00    0.00
Jcal2      0.3      0.5       1      1       0         0.06    1.3
Mcal2     750       0.5       1      1       0         200     3000
beta2      0.5      0.25      0      1       0         0.2     0.95
L1      10000       0         0      0       0         0.00    0.00
L2      10000       0         0      0       0         0.00    0.00
AL2     -9999       0         0      0       0         3       300
 ~
```

Note: When 'run_mode(1)'=2 or 3, the indicator '1' in the 'tune?' column means this parameter was calibrated in the previous step and generated as a stochastic variable based on covariance. Generated parameters (showing 'tune?' =1) were saved in 'Cal1st.rlz' in a previous calibration step for example.

The '**paramSourceGeom**' matrix defines the geometry of sources and has the dimension of [num_sources, 10] as shown in Table A1.3.

Table A1.3. Parameters for Source Geometry.

Variable	Matrix	Definition	Unit
Lx_i	paramSourceGeom(i,1)	Source i length parallel to the flow direction	m
Ly_i	paramSourceGeom(i,2)	Source i width perpendicular to the flow direction	m
X0_i	paramSourceGeom(i,3)	Model X-axis coordinate at center of downgradient face of source i	m
Y0_i	paramSourceGeom(i,4)	Model Y-axis coordinate at center of downgradient face of source i	m
a_i	paramSourceGeom(i,5)	1st order coefficient of the streamline from source i	
b_i	paramSourceGeom(i,6)	2nd order coefficient of the streamline from source i	
c_i	paramSourceGeom(i,7)	3rd order coefficient of the streamline from source i	
alpha_i	paramSourceGeom(i,8)	Angle measured to tangent of the streamline toward the flow direct at Source i (negative to clockwise).	deg
Lztop_i	paramSourceGeom(i,9)	Depth to the top of source i measured from a water table	m
Lzbtm_i	paramSourceGeom(i,10)	Depth to the bottom of source i measured from a water table	m

An example of source geometry parameters is as follows (File name: XXX.inp).

```
Lines 1~14
15_name   prior     prior_sd  log?   tune?  synch?    LB      UB   % header
paramSource1
 ~
paramSource2
 ~

paramSourceGeom1
Lx      24.44       0         0      0      0         0       0
Ly      45          0         0      0      0         0       0
E0      995         0         0      0      0         0       0
N0      994         0         0      0      0         0       0
a       -0.0787     0         0      0      0         0       0
b       0           0         0      0      0         0       0
c       0           0         0      0      0         0       0
alp     -4.5        0         0      0      0         0       0
Lztop   0           0         0      0      0         0       0
Lzbtm   10          0         0      0      0         0       0
paramSourceGeom2
Lx      19.52       0         0      0      0         0       0
Ly      17.93       0         0      0      0         0       0
E0      997         0         0      0      0         0       0
N0      985         0         0      0      0         0       0
a       -0.0787     0         0      0      0         0       0
b       0           0         0      0      0         0       0
c       0           0         0      0      0         0       0
alp     -4.5        0         0      0      0         0       0
Lztop   18          0         0      0      0         0       0
Lzbtm   19          0         0      0      0         0       0
 ~
```

Note) the streamline equation from each source (local coordinate = (0,0)) is $-0.0787X+0*X^2+0*X^3$. This equation represents groundwater flow toward SE with an angle of 4.5 degree ('alpha' = -4.5).

A1.4 Aquifer Parameters

The '**paramAquifer**' matrix defines the aquifer properties and has the dimension of [num_layers, 18] as shown in Table A1.4. The retardation factor for a contaminant, 'R', is internally computed based on a soil bulk density, d_m or d_im, (kg/m^3) and distribution coefficient, k_m or k_im, (aka K_d) (m^3/kg) of the contaminant to analyze.

Table A1.4. Parameters for Aquifer

Variable	Matrix	Definition	Unit
qw	paramAquifer(i,1)	Groundwater darcy velocity. If mobile-immobile transport is modeled, this is the average across mobile and immobile regions – i.e., qw = Fm*qm, where qm is mobile zone velocity and Fm is mobile volume fraction.	m/d
Fm	paramAquifer(i,2)	Mobile zone fraction to the total aquifer volume	-
geom	paramAquifer(i,3)	Geometry factor for porous media (15=spherical, 5=planar)	-
phi_m	paramAquifer(i,4)	Aquifer porosity for the mobile zone	-
d_m	paramAquifer(i,5)	Dry bulk density for the mobile zone	kg/m^3
k_m	paramAquifer(i,6)	Absorption coefficient for the mobile zone	m^3/kg
phi_im	paramAquifer(i,7)	Aquifer porosity for the immobile zone	-
d_im	paramAquifer(i,8)	Dry bulk density for the immobile zone	kg/m^3
k_im	paramAquifer(i,9)	Absorption coefficient for the immobile zone	m^3/kg
L_im	paramAquifer(i,10)	Effective diffusion path length (average thickness of the low permeability layers). See Eq. 19 of Parker and Kim (2015)	m
Dim	paramAquifer(i,11)	Molecular diffusion coefficient for immobile zones	m^2/d
AL_m	paramAquifer(i,12)	Longitudinal dispersivity for a mobile zone or a whole zone. If Fm=1, AL_m is used for a whole aquifer. If Fm<1, effective AL is internally computed for mob-immob zone. See Eq. 19 of Parker and Kim (2015).	m
AT	paramAquifer(i,13)	Transverse dispersivity ratio to AL (=AT/AL)	
AV	paramAquifer(i,14)	Vertical dispersivity ratio to AL (=AV/AL)	
Laq	paramAquifer(i,15)	Saturated aquifer thickness	m
lambda1	paramAquifer(i,16)	First-order decay coefficient for Zone 1 for a contaminant	day^{-1}
lambda2	paramAquifer(i,17)	First-order decay coefficient for Zone 2 for a contaminant (enter 0 if not used)	day^{-1}
lambda3	paramAquifer(i,18)	First-order decay coefficient for Zone 2 for a contaminant (enter 0 if not used)	day^{-1}

An example of aquifer parameters is as follows (File name: XXX.inp).

```
Lines 1~14
15_name   prior     prior_sd  log?   tune?  synch?    LB      UB  % header
omitted: paramSource1, paramSource2, paramSourceGeom1, paramSourceGeom2

paramAquifer
qw        0.08        0.2    1      1      0    0.04    0.15
Fm        1           0      0      0      0       0       0
geom      5           0      0      0      0       0       0
phi_m     0.30        0      0      0      0       0       0
d_m       1890        0      0      0      0       0       0
k_m       1.6E-4      0.2    1      1      0    8.78E-5   2.92E-4
phi_im    0.40        0      0      0      0       0       0
d_im      1620        0      0      0      0       0       0
k_im      1.6E-4      0      0      0      0       0       0
L_im      5           0      0      0      0       0       0
D0        3.9E-5      0.3    1      0      0    1.6E-5    9.6E-5
AL        15          1      1      1      0       1       300
AT/AL     0.1         1      1      1      0    0.005      1
AZ/AL     0.01        1      1      1      0    0.0005     0.2
Laq       30          0      0      0      0       0       0
lambda1   1E-4        1      1      1      0      5E-6    2E-3
lambda2   0           0      0      0      0       0       0
lambda3   0           0      0      0      0       0       0
 ~
```

Note: ‘lambda1’, ‘lambda2’, and ‘lambda3’ are defined for Zone1, Zone2, and Zone3, respectively (see ‘paramSource’ in Table A1.2).

A1.5 Basic Information for Electron Donors and Acceptors

The '**paramED0**' matrix with dimension [11, 1] defines one set of basic information of ED injection well galleries as summarized in Table A1.5. 'alp_ED', which represent a rate coefficient for ED reaction with EA, may be estimated by calibrating to pilot test data or set to a value determined from prior experience. 'Fmt_max' is an upper limit for a mass transfer enhancement factor, Fmt(t), which can be an experimental or user-specified maximum value (e.g., 10) to avoid an unrealistically high Fmt(t) value during simulation. Fmt(t) is internally computed from ED concentrations for galleries upgradient of a DNAPL source as designated by the variable 'CED_locs' in Table A1.11. More details on enhancing mass dissolution rate by ED injection are found in Chapter 3 of the ER-2310 final report. Note that the 3rd and 4th parameters are only relevant for ED injection upgradient of a DNAPL source (i.e., source bio-enhancement).

Table A1.5 and Table A1.6 are mandatory input parameters even though there is no ED injection. User may enter all zero values for holding places or real analytical value for natural background ED and EA when they substantially affect plume degradation.

Table A1.5. Parameters for ED injection

Variable	Matrix	Definition	Unit
f_c	paramED0(1)	H-equivalent (kg) required per mass (kg) of NAPL degraded	-
alp_ED	paramED0(2)	Rate coefficient for ED reaction with EA.	day^{-1}
Fmt_max	paramED0(3)	Maximum of Fmt(t), a factor describing the degree to which DNAPL dissolution rate is enhanced by ED injection.	-
fmt	paramED0(4)	DNAPL mass transfer enhancement coefficient	-
lambda_ED	paramED0(5)	Decay coefficient for ED	/d
km_ED	paramED0(6)	Adsorption coefficient for ED in the mobile zone	m^3/kg
kim_ED	paramED0(7)	Adsorption coefficient for ED in the immobile zone	m^3/kg
Dim_ED	paramED0(8)	Molecular diffusion of ED in the immobile zone	m^2/kg
AL_ED	paramED0(9)	Longitudinal dispersivity of ED for a mobile zone • If negative, same as AL used for contaminant. • If Fm = 1 and AL_ED>0, AL_ED is used. • If Fm <1, effective (i.e., upscaled) AL_ED is internally computed for mob-immob zone. See Eq. 19 in Parker and Kim (2015).	m
W_ED	paramED0(10)	Molecular weight of ED injected to a DNAPL source	kg/mol
S_CH/W_CH	paramED0(11)	Maximum molar concentration of DNAPL (Solubility/ Molecular weight)	mol/m^3

Note) See Chapter 3 of the ER-2310 final report.

The '**paramEDEA**' matrix of dimension [num_layers, 4] as shown in Table A1.6 defines natural ED and EA background concentrations, which are used in the serial, parallel, or combined reaction pathways (see Chapter 3 of the ER-2310 final report). Even if there are no ED injection galleries, 'paramED0' and should be defined for each aquifer layer. Unless ED injection is implemented in the upgradient of a DNAPL source, the values of 'Fmt_max', 'fmt', 'W_ED', and 'S_CH/W_CH' do not affect simulation results (i.e., entered values are simply "placeholders"). It should be noted that background ED/EA will react with contaminant and

other injected ED species only when a user defines at least one ED gallery described in Table A.11. Therefore, if natural attenuation should be modelled, a user can set up an ED gallery with zero injection rate.

Uncertainty in parameters in Tables A1.6 can be considered using random numbers (normal or log-normal) in Monte Carlo simulations by specifying 'PriorSD', 'Log', and 'IsSync'. In this case, zero correlation with other parameters will be assumed.

Table A1.6. Definition of background ED/EA concentration and biodecay pathway.

Variable	Matrix	Definition	Unit
natEA	paramEDEA(i,1)	H-equivalent natural EA concentration in aquifer i, a weighted sum of all EAs. See Chapter 3 of the ER-2310 final report for stoichiometirc coefficients.	H-eq μg/L
natED	paramEDEA(i,2)	H-equivalent natural ED concentration in aquifer i	H-eq μg/L
fo2Co2	paramEDEA(i,3)	Bio-available H-equivalent O_2 concentration in the aquifer (f_{O2}*O_2 concentration in μg/L)	H-eq μg/L
Fs	paramEDEA(i,4)	Serial fraction (1 for 100% serial and 0 for 100% parallel, 0.5 for equally combined reaction)	

An example of basic ED/EA parameters is as follows (File name: XXX.inp).

```
Lines 1~14
15_name   prior     prior_sd  log?   tune?  synch?    LB      UB  % header
omitted: paramSource1, paramSource2, paramSourceGeom1, paramSourceGeom2,
paramAquifer
 ~
paramED0 % This block can be entered zeros if there is no ED injection.
fc          0.05        0       0       0       0       0       0
alp_ED      0.01        0       0       0       0       0       0
Fmt_max     100         0       0       0       0       0       0
fmt         5.5E-6      0       0       0       0       0       0
lamb_ED     0           0       0       0       0       0       0
kdm_ED      3E-4        0       0       0       0       0       0
kdim_ED     5E-4        0       0       0       0       0       0
D0_ED       3.5E-5      0       0       0       0       0       0
AL_ED     -9999         0       0       0       0       0       0
W_ED        0           0       0       0       0       0       0
S_CH/W_CH   0           0       0       0       0       0       0

paramEDEA1 % This is to define natural background EA and EA if significant.
C_natEA   2390          0       0       0       0       0       0
C_natED   0             0       0       0       0       0       0
fo2Co2    490           0       0       0       0       0       0
Fs        0.5           0       0       0       0       0       0
 ~
```

A1.6 Source Zone Reduction

In addition to DNAPL source mass depletion computed from the power function mass transfer function described in Chapter 2 of the ER-2310 final report, source mass reduction can be specified by one or more of three methods in SCOToolkit: (1) user-specified mass removal versus time, (2) application of the thermal treatment model, and/or (3) application of the in-situ chemical oxidation (ISCO) model. Note that one source can have only one type source zone reduction.

A1.6.1 Source zone mass removal

The '**paramSZR**' defines the variables for source mass reduction implemented by any source mass removal technology. Note that 'paramSZR' should be defined for the sources that has 'isSZR'=0 in Line 7. Users may utilize this option to model measured historical mass removal via excavation or any other method (e.g., for calibration runs). A set of variables listed in Table A1-7 needs to be defined for each DNAPL source *i*.

Table A1.7. Variables for Source Zone Reduction

Variable	Matrix	Definition	Unit
SZRbeg	paramSZR(i,1)	SZR beginning date for source mass removal (mm/dd/yyyy)	
SZRend	paramSZR(i,2)	SZR ending date for source mass removal (mm/dd/yyyy or a negative number for internal computing) • If 'SZRend' = 'SZRbeg', the model assumes this case as instant source removal and user should define 'Mrmv' in the following line. • If 'SZRend' is not same as 'SZRbeg', in next three lines user should define the number of steps, elapsed days, and cumulative mass removed at each step. SZRend will be internally computed using the cumulative days.	
Mrmv or Nsteps	paramSZR(i,3)	When 'SZRend' = 'SZRbeg', it is 'Mrmv' indicating the DNAPL mass removed from a source zone instantly, or it is 'Nsteps' that is the number of time steps at which cumulative mass removal (recovery) was measured.	kg or -
Days	varSZR(i,Nsteps)	If 'Nsteps' is used, list the cumulative days at which mass recovery data is measured. Define this as many as 'Nsteps'.	days
Mrmv	varSZR(i,Nsteps)	If 'Nsteps' is used, list the cumulative mass recovered at the defined time steps.	kg
CostSZR	path\file name	When 'isCost(1)'=1, a cost file should be defined. If the cost file is in the same directory, the path can be omitted (see the example cost file)	

For clarity, two examples for 'paramSZR' are presented as follows. If 'isCost(1)' = 1 (i.e., TRUE), a line to define cost variables should be followed.

Example (1) - SZR input to consider instant source removal when isCost(1)=1.

```
~
paramSZR      This line is skipped internally.
SZRbeg    2005
SZRend    2005
Mrmv(kg)  100
CostSZR   F:\DNAPL\cost_szr.dat ← This line is skipped when isCost(1)=0.
~
```

Example (2) - SZR input to consider progressive source removal when isCost(1)=1.

```
~
paramSZR         This line is skipped internally.
SZRbeg    2005
SZRend    -999 % SZRend is computed internally (i.e., 2005+200/365 = 2005.55)
Nsteps    5
Days      50   85   120  150  200
Mrmv_acc  10   70   100  120  130
CostSZR   F:\DNAPL\cost_szr.dat ← This line is skipped when isCost(1)=0.
~
```

A cost file for SZR, [cost_szr.dat] in 'F:\DNAPL\', may be written as follows.

```
Item        Cost($K)  Unc. Comment       ← This line is skipped internally.
Capital     500       0    % capital cost
Monitoring  100       0    % monitoring cost
Penalty     1E6       0    % penalty cost
```

Note: All 'Comments' after the 'Unc.' column will be skipped. Therefore, it can be used to record user notes.

A1.6.2 Thermal Source Reduction (TSR)

TSR may include all type of heating methods such as electrical resistant heating (ERH), thermal conduction heating (TCH), or stream enhanced extraction (SEE), etc. Table A1.8 defines the parameters, variables, and costs for most general TSR practice. A set of parameters and variables listed in Table A1.8 should be defined as many as the sources indicated as "isSZR' = 1.

Table A1.8. Variables for TSR

Variable	Matrix	Definition	Unit
TSRbeg	paramTSR(i,1)	TSR beginning date (numeric year such as 2005.7)	year
TSRend	paramTSR(i,2)	TSR ending date (numeric year) • If unknown, enter a negative number (like -999) to be computed internally. If 'TSRend' is specified, TSR will be forced to terminate at 'TSRend'.	year
Wsoil	paramTSR(i,3)	Weighting factor for soil concentration (0~1) only when monitoring both soil concentration and mass recovery data. If negative, it is determined internally.	-
Ntz	paramTSR(i,4)	Number of treatment zones divided into the source to treat (see Chapter 4 of the ER-2310 final report)	-
dtmon1	paramTSR(i,5)	Vapor monitoring interval or the first soil concentration monitoring time counted since commencing TSR (therefore, it is always required even if vapor is not monitored)	days
dtmon2	paramTSR(i,6)	Soil monitoring interval after waiting 'dtmon1'. If both vapor and soil are monitored, first soil sample will be taken when vapor monitoring indicates Csoil $\leq$ Cstop_TZ with a 'dtmon2' interval after that.	days
Fmiss	paramTSR(i,7)	Fraction of missing mass of the source not captured by TSR (0~1)	-
alpha	paramTSR(i,8)	Significant level of t-distribution (0<alpha $\leq$ 0.5), e.g., t(1-alpha, dof), to define a upper confidence limit (UCL) of measured concentrations at a level of (1-alpha) and a degree of freedom (dof). Note it is one-sided.	-
Cgw_all	paramTSR(i,9)	Criterion of groundwater concentration averaged for the entire TZs (e.g., the entire treatment zone) to terminate TSR (if negative, it is computed from 'Csoil_all')	µg/L
Csoil_all	paramTSR(i,10)	Criterion soil concentration averaged for the entire TZs to terminate TSR (if negative, it is computed from 'Cgw_all').	µg/kg
Cgw_TZ	paramTSR(i,11)	Criterion of groundwater concentration to terminate heating a monitoring zone (MZ) in a TZ.	µg/L
Csoil_TZ	paramTSR(i,12)	Criterion of soil concentration to terminate heating a MZ in a TZ ('Csoil_TZ' is not allowed to be higher than 'Csoil_all'. 'Csoil_TZ' = min['Csoil_TZ','Csoil_all'] internally)	µg/kg

Table A1.8 continued

TZ_vars_j	Repeat the block below with this head line 'TZ_vars' as many as 'Ntz' in 'paramTSR'		
tpeak	TSR-TZ(j,1)	Time to reach the peak of recovery rate while heating	days
Nmz	TSR-TZ(j,2)	Number of MZs to be divined in the TZ	ea
Ngp	TSR-TZ(j,3)	Number of geoprobe locations (or bore holes) in a MZ	ea
Nsmp	TSR-TZ(j,4)	Number of samples per geoprobe location	ea

Z_const	Treatment zone constants (define 'Ntz' columns followed by this comment line)		
Area	VarTSR(1,1~Ntz)	Horizontal area of the TZ	m^2
Thickness	VarTSR(2,1~Ntz)	Treatment thickness of the TZ	m
Width	VarTSR(3,1~Ntz)	Width of the TZ for computing flux	m
SL_avg	VarTSR(4,1~Ntz)	Average soil centration of the TZ	µg/kg
SL_min	VarTSR(5,1~Ntz)	Minimum soil concentration of the TZ	µg/kg
SL_max	VarTSR(6,1~Ntz)	Maximum soil concentration of the TZ	µg/kg
Nhw*	VarTSR(7,1~Ntz)	Number of heating wells in the TZ (not used)	-
Nvw**	VarTSR(8,1~Ntz)	Maximum number of vapor monitoring wells in the TZ (not used)	-
MONtype	VarTSR(9,1~Ntz)	Monitoring type of the TZ (0 = vapor only, 1 = soil only, 2 = Both)	-
SlnVW	VarTSR(10,1~Ntz)	Log standard deviation of vapor data (0.01~0.05)	-
SlnGP	VarTSR(11,1~Ntz)	Log standard deviation of geoprobe data (0.5~5) If less than or equal to zero, it is computed internally using soil concentration data (i.e., SL_min and SL_max).	-
SlnM0	VarTSR(12,1~Ntz)	Log uncertainty of DNAPL mass estimation (~0.7) If less than or equal to zero, it is computed internally using soil concentration data (i.e., SL_min and SL_max).	-
dura_max	VarTSR(13,1~Ntz)	Maximum allowed time duration of TZs	days
CostTSR	path\file name	When isCost(1)=1, a cost file should be defined. If the cost file is in the same directory, the path can be omitted (see the example cost file)	

Note: * Nvw is not current used in the model but assigned as a placeholder for future use.
** Nhw does not affect optimizing expected cost but is used to compute a global energy usage factor after simulation (i.e., post-processing).

An example of TSR parameters and variables is as follows (File name: XXX.inp). It is recommended to utilize the SCOToolkit Excel tool **Thermal treatment model calibration.xlsx** in calibrating thermal model parameters to the actual mass recovery data. To implement real time termination decisions that allow for multiple monitoring zones using a rigorous statistical approach, the SCOToolkit Excel tool **Thermal treatment termination decisions using real time data.xlsx** can be used.

```
Lines 1~14
15_name   prior     prior_sd  log?   tune?  synch?    LB      UB   % header
omitted: paramSource1 ~ paramEDEA1
 ~
paramSZR for Source 1: this line is a place holder and skipped.
1t_beg    2007
2t_end    -999
3Nsteps   8
4days     1    40      80        120       160       200       240       266
```

```
5Mrmv     0.03 310.86 1142.06   1505.37   1629.40   1680.26   1703.66   1712.1
costSZR   costSZR.dat

paramTSR for Source 2 with Ntz=1: this line is a place holder and skipped.
1t_beg    2011   0       0    0    0    0    0
2t_end    -9999  0       0    0    0    0    0
3Wsoil    -999   0       0    0    0    0    1
4Ntz      1      0       0    0    0    0    0
5dtmon1*  2      0       0    0    0    68   180
6dtmon2*  14     0       0    0    0    6.9  29
7Fmiss    0      0       0    0    0    0    0
8SigPer*  0.5    0       0    0    0    0.01 0.5
9Cavg_gw  50     0       0    0    0    0    0
10Cavg_sl 1000   0       0    0    0    5    5000
11Ctz_gw  50     0       0    0    0    0    0
12Ctz_sl  750    0       1    2    0    100    1000
%TZ_1 (1=A, 2=B.., Nvw=Nmz), 7 param for each TZ
1tpeak    65     0       0    0    0    50   200
2Nmz/tz*  3      0       0    2    0    1    9
3Ngp/mz*  4      0       0    2    0    1    8
4Nsmp/gp* 2      0       0    2    0    1    4
% Zone    TA1       TZ2 (if Ntz=2): This line is a place holder and skipped.
1Area     350
2Thick    10
3Width    15
4SL_avg   1.13E6
5SL_min   2.53E5
6SL_max   5.08E6
7Nhw      33
8Nvw      9
9montype  2
10Slnvw   0.4
11SlnGP   2.0
12SlnM0   0.7
13duramax 730
costTSR1  costTSR1.dat
```

If a cost data file is in the same path as main input file, the path name can be omitted. An example cost data file (e.g., 'costTSR3TZ.dat') for TSR with 3 treatment zones (TZ) is presented as follows. To estimate unit cost parameters for the source zone thermal treatment model, the SCOToolkit Excel tool **Thermal treatment unit cost calcs.xlsx** can be used (Appendix A4).

```
Cost_name TZ1    TZ2    TZ3    Unc. Comment % this line is skipped internally
Ccap=     116.0  262.5  262.5  0    paramCost(1)   all unit=$K
Cenergy=  2.77   6.27   6.27   0    paramCost(2)
Cother=   0.995  2.252  2.252  0    paramCost(3)
Cmzcap=   0.024  0.053  0.053  0    paramCost(4)
Cmzday=   0.008  0.008  0.008  0    paramCost(5)
Cgp=      2.18   2.18   2.18   0    paramCost(6)
Cgpsmp=   0.28   0.28   0.28   0    paramCost(7)
Cmass=    0.1    0.1    0.1    0    paramCost(8)
Cpen=     1E6    1E6    1E6    0    paramCost(9) It applies once
```

Note: The column head line ('Cost name TZ1 TZ2… Unc. Comments') is skipped while loading the cost file. All comment after the 'Unc' column will be skipped. Therefore, it can be used as user's note.

A1.6.3 In Situ Chemical Oxidation (ISCO)

ISCO is a popular source mass reduction practice. Two types of oxidant injection methods were identified; 1) intermittent (aka, pulse) injection and 2) continuous injection, defined in Table A1.10a and Table A1.10b, respectively. The current version of SCOToolkit includes both methods. Either method should be indicated in the first two lines before defining their parameters and variables (see the example file listed next). Historical injection events can be also simulated for various purposes (parameter calibration, design reoptimization, etc.). Table A1.9a, Table A1.9b, or Table A1.9c (historical injection events) should be defined as many as the number of 'isSZR = 2' listed in Line 7 in Table A1.1.

1) Pulse ISCO injection

ISCO systems can be terminated by stop criterion based on groundwater concentrations (gw), soil concentrations (soil), or both. Users must define 'Cgw_all' and/or 'Csoil_all' for global decision (i.e., terminate ISCO when average concentration is less than 'Cxx_all') and 'Cgw_TZ' and/or 'Csoil_TZ' for local decision (i.e., terminate a TZ when a TZ concentration is less than 'Cxx_TZ'). If either 'Cgw_xxx' or 'Csoil_xxx' is entered as -999 (or any negative number), the other value is internally computed (see Chapter 5 of the ER-2310 final report).

Although user can optimize both 'Nmw' and 'Ngp' or 'Nbg' simultaneously, the minimum search range for both should be bigger than 1 to use both water and soil data. Therefore, if 'Ngw' or 'Nsoil' is zero, the corresponding 'Cgw_xxx' or 'Csoil_xxx' cannot be utilized as a stop criterion.

When the oxidant concentration ('C_OX') is to be optimized, the lower and upper search bound generally ranges from 2000 mg/ L to up to 50% ~ 80% of its solubility (e.g., 50% for $KMNOP_4$ and 80% for $NaMNO_4$). It should be noted that continuous injection uses lower concentrations but longer durations than intermittent injection.

The parameter 'Srind/k0' representing the pore clogging effect by MnO_2 precipitation on permeability can be defined as follows. For a general Srind value, Srind = -5.5E-16 m^2 L/mg was taken from West and Kueper (2012). For example, Srind/k0 = 4.58E-7 L/mg when k0 = 1.2E-9 m^2 (West, M.R. and Bernard H. Kueper (2012) Numerical simulation of DNAPL source zone remediation with in situ chemical oxidation (ISCO). Adv. Water Res. 44:126-139).

When 'ISCOtype' = 0 in 'Fixed [1,1]', SCOToolkit will read Table A1-9a for pulse (intermittent) ISCO injection. 'Fixed [2×10]' values are defined followed by two lines of header (line holders for variable names, not used internally) in Table A1.9a (see the example file below).

Table A1.9a. Variables for ISCO intermittent injection

Variable	Matrix	Definition	Unit
Fixed [2×10]	ISCOtype Aiw Q_OX Nsplt ttx SlnGWmw SlnGWgp SlnSLgp SlnSLbg SlnOX Fgwmin OX2O2 O22CH Cl2CH S_CH W_CH W_Cl Avtot t0 duramax		
NODtot	paramISCO(i,1)	Natural Oxygen Demand, 0.2~200 /kg soil (g oxidant/kg soil)	g/kg
f_fast	paramISCO(i,2)	NOD fast (instant) fraction to 'NODtot', 0.02~0.7	g/g
r_slow	paramISCO(i,3)	Rate coefficient of slow NOD, 0.01~1 (L/mmol $KMmnO_4$/day)	L/mmol/day

Ntz	paramISCO(i,4)	Number of Treatment Zones	ea
fmt	paramISCO(i,5)	Mass transfer enhancement factor ($=D_{ox}/(n_{ox/CH}*D_{CH})$. See Chapter 5 of the ER-2310 final report.	-
Fover	paramISCO(i,6)	Well overlap factor ($\geq$1)	
Ninj_min	paramISCO(i,7)	Number of minimum injections	ea
Ninj_max	paramISCO(i,8)	Number of maximum injections	ea
Lx_tt	paramISCO(i,9)	Length from upstream to downstream of a TZ to compute travel distance of oxidant	m
Coxdmin	paramISCO(i,10)	Minimum oxidant concentration below which contaminant monitoring starts when the number of injections $\geq$ Ninj_min. When monitoring soil only, user can optimize this to initiate first soil monitoring since a prior injection.	mg/L
Fsl/gw	paramISCO(i,11)	A multiplier to groundwater monitoring interval ('dtgw') indicating the frequency of soil sampling.	
dtgw	paramISCO(i,12)	Groundwater monitoring interval (e.g., 90 days = quarterly)	days
Nsmp_gp	paramISCO(i,13)	Number of samples along a geoprobe vertical section per geoprobe hole per event ('Nsmp_gp' for water = 'Nsmp_gp', when water sample option is active)	ea
Nsmp_bg	paramISCO(i,14)	Number of soil samples along a vertical section per bore hole per event	ea
Srind/k0	paramISCO(i,15)	Ratio of Srind to k0, where Srind is the slope between permeability k (m^2) and MnO_2 concentration (mg/L) and k0 (m^2) is the intrinsic permeability before injection.	L/mg
Cgw_all	paramISCO(i,16)	Groundwater concentration averaged for the entire TZs to terminate ISCO_i (if negative, 'Csoil_all' should be defined)	µg/L
Csoil_all	paramISCO(i,17)	Soil concentration averaged for the entire TZs to terminate ISCO_i (if negative, it is computed from 'Cgw_all')	µg/kg
Cgw_redo	paramISCO(i,18)	Groundwater concentration of a TZ to initiate oxidant reinjection for that TZ	µg/L
Cgw_stop	paramISCO(i,19)	Groundwater concentration of a TZ to terminate the ISCO system for that TZ	µg/L
Csoil_redo	paramISCO(i,20)	Soil concentration of a TZ to initiate oxidant reinjection for that TZ	µg/kg
Csoil_stop	paramISCO(i,21)	Soil concentration of a TZ to terminate the ISCO system for that TZ	µg/kg
alpha	paramISCO(i,22)	Significant level of t-distribution to define a UCL of measured concentrations (0<alpha $\leq$ 0.5),	

TZ_j Repeat the block below with this head line as many as 'Ntz' defined in 'paramISCO'

Ftz	paramTZ(j,1)	Treatment area safety factor ($\geq$1)	
Nmw0	paramTZ(j,2)	Number of existing monitoring wells for TZ_j per event (these wells are not counted for cost).	
Nmw	paramTZ(j,3)	Number of new monitoring wells for TZ_j per event (these wells are counted for cost).	

Ngp	paramTZ(j,4)	Number of geoprobe locations per event for TZ_j (horizontal locations)	
Nbg	paramTZ(j,5)	Number of bore holes for TZ_j (horizontal locations)	
C_OXD	paramTZ(j,6)	Oxidant concentration for TZ_j (horizontal locations) per event	mg/L

TZchar Treatment zone characterization (define 'Ntz' columns followed by this comment line)

Not_used	VarISCO(1,1:Ntz)	Reserved for future update	
Area	VarISCO(2,1:Ntz)	Planar area of TZs	m^2
Thickness	VarISCO(3,1:Ntz)	Thickness of TZs	m
Width	VarISCO(4,1:Ntz)	Width of TZs	m
SL_avg	VarISCO(5,1:Ntz)	Average soil centration of TZs	µg/kg
SL_min	VarISCO(6,1:Ntz)	Minimum soil concentration of TZs	µg/kg
SL_max	VarISCO(7,1:Ntz)	Maximum soil concentration of TZs	µg/kg
CostISCO	path\file name	When 'isCost(1)'=1, a cost file should be defined. If the cost file is in the same directory, the path can be omitted (see the example file)	

It should be mentioned that if groundwater is monitored, user should provide the criteria of groundwater concentration ('Cgw_redo' and 'Cgw_stop') for reinjection and termination, respectively. Real time termination decisions for ISCO source treatment using soil and/or groundwater sample data can be implemented using the SCOToolkit Excel tool **ISCO treatment termination decisions using real time data.xlsx** (Appendix A4). An example of ISCO parameters and variables for pulse injection is as follows (File name: XXX.inp).

```
Lines 1~14
15_name   prior     prior_sd  log?   tune?  synch?    LB      UB   % header
Omitted: paramSource1 ~ paramEDEA1
 ~
paramISCO % Source 1 with Ntz=3, Srind/k0 = 4.58E-6, GW only
iType   Aiw       Q_OX  Nsplt ttx   SlnGWmw  SlnGWgp  SlnSLgp  SlnSLbo SlnOX
Fgwmin  OX2O2     O22CH Cl2CH S_CH  W_CH     W_OXD    Avtot    t_beg   duramax
    0   72.7      16.35 4     0     0.5      1.15     1.15     2.0     0.3
    2   0.211     1     4     0.15  0.166    0.158    412.5    2014    360
1NODtot     2       0.3       1       3       0         0.6     6.64
2f_fast     0.15    0.3       1       3       0         0.045   0.5
3r_slow     0.02    0.3       1       3       0         6E-3    0.066
4Ntz        3       0         0       0       0         0       0
5fmt        1.35    0         0       0       0         0       0
6Fover      1.25    0         0       0       0         0       0
7Ninjmin    1       0         0       0       0         0       0
8Ninjmax    20      0         0       0       0         0       0
9Lxtt       20      5         0       3       0         10      30
10Coxdmin   50      0         0       0       0         0       0
11Freqqsl   0       0         0       0       0         0       0
12dtmon2    90      0         0       0       0         0       0
13Nsmp_gp   0       0         0       0       0         0       0
14Nsmp_bg   0       0         0       0       0         0       0
15Srind/k0  4.58E-60        0       0       0         0       0
16GWglo     100     0         0       0       0         0       0
17SLglo     -999    0         0       0       0         0       0
18GW_redo1  200     0         1       2       0         150     500
19GW_stop1  50      0         1       2       0         10      100
20SL_redo1  -999    0         0       0       0         100     1000
```

```
21SL_stop1  -999    0         0       0       0         10      200
22alpha     0.5     0         0       0       0         0.05    0.5
% TZ1
Ftz         1.1     0         0       0       0         0       0
Nmwo1       4       0         0       0       0         0       0
Nmw1        2       0         0       2       0         0       4.4
Ngp1        0       0         0       0       0         0       0
Nbg1        0       0         0       0       0         0       0
C_OX1       10000   0         1       2       0         5E3     30E3
% TZ2
Ftz         1.1     0         0       0       0         0       0
Nmwo2       4       0         0       0       0         0       0
Nmw2        2       0         0       2       0         0       4.4
Ngp2        0       0         0       0       0         0       0
Nbg2        0       0         0       0       0         0       0
C_OX2       10000   0         1       2       0         5E3     30E3
% TZ3
Ftz         1.1     0         0       0       0         0       0
Nmwo3       4       0         0       0       0         0       0
Nmw3        2       0         0       2       0         0       4.4
Ngp3        0       0         0       0       0         0       0
Nbg3        0       0         0       0       0         0       0
C_OX3       10000   0         1       2       0         5E3     30E3
%ISCOvar    TZ_A    TZ_B    TZ_C
Not_used    2       2       2
Area        200     460     465
Thick     5.5       5.5       5.5
Width     25        60        75
SL_avg    30875     6179      949
SL_min    1E4       1E3       1E2
SL_max    1E5       1E4       1E3

costISCO  costISCOgw.dat
```

An example cost file ('costISCOgw.dat') is as follows. Unit cost parameters for the pulsed injection ISCO source treatment model from cost sensitivity analysis results can be computed using the SCOToolkit Excel tool **ISCO unit cost calcs for pulsed injection. xlsx** (Appendix A4, Chapter 5 of ER-2310 main report).

```
Item        Cost($K)   Unc       Comments
Cbase       108.163    0         % Base fixed cost
Ciw         0          0         % IW installation/IW
Cmw         2.97       0         % new MW installation
Cmass       0.0055     0         % cost per kg
Cvol        0.02076    0         % cost per m^3
Cinj        0          0         % cost per injection event
Cevnt       0          0         % cost per monitoring event
Cgpsl0      0.9        0         % first GP soil sample $K/sample
Cgpsl1      0.3        0         % from second GP soil sample $K/sample
Cbgsl0      0.0        0         %
Cbgsl1      0.0        0         %
Cgwgp0      0.0        0         %
Cgwgp1      0.0        0         %
Cgwmw0      0.55       0         % cost per MW sample for first
Cgwmw1      0.0        0         %
Coxd        0.0        0         % cost per Oxidant monitoring
Cday        0.30       0         % cost per day
Cpen        1E6        0         % cost per penalty (one time for all TZs)
```

Note: The column head line ('Item Cost($K) Unc Comments') will be skipped internally (but required). From line 2, any space or tab will be recognized as a delimiter. All text after the 'Unc' column will be skipped and thus it does not affect results.

Definitions of fixed variables for ISCO intermittent injection

1) ISCOtype: Index for ISCO type; 0 = pulse injection, 1 = continuous injection, 2 = historical injection
2) Aiw: Area of influence per one injection well (m^2) – not used in continuous ISCO
3) Q_OX: Oxidant injection rate (m^3/d) – not used in continuous ISCO
4) Nsplt: Number of split injections per TZ– not used in continuous ISCO
5) ttx: travel time multiplier (≥ 1) – not used in continuous ISCO
6) SlnGWmw: Log uncertainty (standard deviation) of water samples from monitoring wells
7) SlnGWgp: Log uncertainty (standard deviation) of water concentration from geoprobe samples
8) SlnSLgp: Log uncertainty (standard deviation) of soil concentration from geoprobe samples
9) SlnSLbg: Log uncertainty (standard deviation) of bore hole samples
10) SlnOXD: Log uncertainty (standard deviation) of oxidant samples

Note) If a concentration is averaged from multiple vertical samples, user must reduce the uncertainty of measurement (i.e., SlnSL = SlnSL0/sqrt(Ngp_v), where SlnSL0 = log uncertainty of one single measurement and Ngp_v is the number of soil samples collected vertically for that location.

11) Fgwmin: Minimum number of groundwater sampling rounds following injection before termination or reinjection decision can be made (2 or 3 is recommended)
12) OX2O2: Oxidant mass per O_2 equivalent moles (0.211 kg/mol O_2eq of $KMnO_4$ for PCE and 0.316 for TCE)
13) O22CH: O_2 equivalent moles per mole contaminant (1.5 for TCE and 1 for PCE)
14) Cl2CH: Chloride equivalent moles per mole contaminant (3 for TCE and 4 for PCE)
15) S_CH: Solubility of contaminant (kg/m^3, 1.1 for TCE and 0.15 for PCE)
16) W_CH: Molecular weight of contaminant (kg/mol, 0.13 for TCE and 0.166 for PCE)
17) W_OXD: Molecular weight of oxidant (kg/mol)
18) Avtot: Source flux transect area (m^2) – total vertical area covering all TZs. If entered as zero or negative, it will be internally computed based on the width and thickness of each TZ.
19) t0: ISCO beginning year (numeric year) – it is important when computing cost or calibrating ISCO parameters.
20) duramax: ISCO maximum operation period (months)

2) Continuous ISCO injection

When 'ISCOtype' = 1, SCOToolkit will read Table A1.9b for continuous ISCO injection. Fixed [2×10] values are defined followed by two lines of header in Table A1.9b.

Table A1.9b. Variables for ISCO continuous injection

Variable	Matrix	Definition	Unit
Fixed [2×10]	ISCOtype TypeCir dummy OXmin ttx SlnGWmw SlnGWgp SlnSLgp SlnSLbg SlnOX Foxd OX2O2 O22CH Cl2CH S_CH W_CH W_OXD Avtot t0 duramax		
NODtot	paramISCO(i,1)	Natural Oxygen Demand ranging, 0.2~200 (g oxidant/kg soil)	g/kg
f_fast	paramISCO(i,2)	NOD fast (instant) fraction to 'NODtot', 0.02~0.7	g/g
r_slow	paramISCO(i,3)	Rate coefficient of slow NOD, 0.01~1 (L/mmol $KMmnO_4$/day)	L/mmol/ day
Ntz	paramISCO(i,4)	Number of Treatment Zones	ea
fmt	paramISCO(i,5)	Mass transfer enhancement factor (=$D_{ox}/(n_{ox/CH}*D_{CH})$. See Chapter 5 of the ER-2310 final report.	-
Fox	paramISCO(i,6)	Multiplier of oxidant concentration reduction to the prior injection concentration	
Fsl/gw	paramISCO(i,7)	A multiplier to groundwater monitoring interval (dtmon) indicating the frequency of soil sampling.	
dtmon	paramISCO(i,8)	Groundwater monitoring interval if groundwater is monitored and soil sampling interval when only soil is monitored.	day
Nsmp_gp	paramISCO(i,9)	Number of samples per geoprobe location per event (Nsmp_gp for water = Nsmp_gp, when water sample option is active)	ea
Nsmp_bg	paramISCO(i,10)	Number of soil samples per bore hole per event	ea
Srind/k0	paramISCO(i,11)	Ratio of Srind to k0, where Srind is the slope between permeability k (m^2) and MnO_2 concentration (mg/L) and k0 (m^2) is the intrinsic permeability before injection.	L/mg
Cgw_all	paramISCO(i,12)	Groundwater concentration averaged for the entire TZs to terminate ISCO_i (if negative, Csoil_all should be defined)	µg/L
Csoil_all	paramISCO(i,13)	Soil concentration averaged for the entire TZs to terminate ISCO_i (if negative, it is computed from Cgw_all)	µg/kg
Cgw_TZ	paramISCO(i,14)	Groundwater concentration of a TZ to terminate the ISCO system for that TZ	µg/L
Csoil_TZ	paramISCO(i,15)	Soil concentration of a TZ to terminate the ISCO system for that TZ	µg/kg
alpha	paramISCO(i,16)	Significant level of t-distribution to define a UCL of measured concentrations (0<alpha ≤ 0.5),	
TZ_vars	Repeat the block below as many as 'Ntz' followed by this head line		
Ftz	paramTZ(j,1)	Treatment area safety factor ('Ftz' ≥ 1)	
Nmw0	paramTZ(j,2)	Number of existing monitoring wells for TZ_j per event (these wells are not counted for cost).	ea
Nmw	paramTZ(j,3)	Number of new monitoring wells for TZ_j per event (these wells are counted for cost).	ea
Ngp	paramTZ(j,4)	Number of geoprobe locations for TZ_j (horizontal locations) per event	ea

Nbg	paramTZ(j,5)	Number of soil bore holes for TZ_j (horizontal locations) per event	ea
C_OXD	paramTZ(j,6)	Oxidant concentration for TZ_j (horizontal locations) per event	mg/L
TZchar	Treatment zone characteristics (define 'Ntz' columns followed by this comment line)		
frac_lost	VarISCO(1,1:Ntz)	Fraction of oxidant lost by advection for TZs (0 to 1)	
Area	VarISCO(2,1:Ntz)	Planar area of TZs	m^2
Thickness	VarISCO(3,1:Ntz)	Thickness of TZs	m
Width	VarISCO(4,1:Ntz)	Width of TZs	m
SL_avg	VarISCO(5,1:Ntz)	Average soil centration of TZs	µg/kg
SL_min	VarISCO(6,1:Ntz)	Minimum soil concentration of TZs	µg/kg
SL_max	VarISCO(7,1:Ntz)	Maximum soil concentration of TZs	µg/kg
q_in	VarISCO(8,1:Ntz)	Injection velocity (m/d) to compute a target oxidant injection flow rate of a TZ. Injection rate will be then q_in*(net width)*(thickness) for each TZ internally.	m/d
C_add	VarISCO(9,1:Ntz)	Oxidant concentration to add to recirculated effluent for TZs	g/m^3
M_max	VarISCO(10,1:Ntz)	User specified maximum oxidant utilization for TZs (used for Option 2)	kg
Fcapture	VarISCO(11,1:Ntz)	Capturing ratio (= Effluent volume/influent volume) of TZs	
CostISCO	path\file name	When isCost(1)=1, a cost file should be defined. If the cost file is in the same directory, the path can be omitted (see the example cost file)	

Definitions of fixed variables for ISCO continuous injection

1) ISCOtype: Index for ISCO type; 0 = pulse injection, 1 = continuous injection, 2 = historical injection
2) TypeCirc: Option for a recirculation type (0, 1, or 2) if ISCOtype = 1.
3) On-month: number of active injection months
4) Off-month: number of inactive months
5) OXmin: Minimum oxidant concentration to trigger groundwater monitoring.
6) SlnGWmw: Log uncertainty (standard deviation) of water samples from monitoring wells
7) SlnGWgp: Log uncertainty (standard deviation) of water concentration from geoprobe samples
8) SlnSLgp: Log uncertainty (standard deviation) of soil concentration from geoprobe samples
9) SlnSLbg: Log uncertainty (standard deviation) of bore hole samples
10) SlnOXD: Log uncertainty (standard deviation) of oxidant samples

Note) If a concentration is averaged from multiple vertical samples, user must reduce the uncertainty of measurement (i.e., SlnSL = SlnSL0/sqrt(Ngp_v), where SlnSL0 = log uncertainty of one single measurement and Ngp_v is the number of soil samples collected vertically for that location.

11) Ngwmin: Minimum number of groundwater sampling rounds following injection before termination or reinjection decision can be made (2 or 3 is recommended)
12) OX2O2: Oxidant mass per O_2 equivalent moles (0.211 kg/mol O_2eq of $KMnO_4$ for PCE and 0.316 for TCE)
13) O22CH: O_2 equivalent moles per mole contaminant (1.5 for TCE and 1 for PCE)
14) Cl2CH: Chloride equivalent moles per mole contaminant (3 for TCE and 4 for PCE)
15) S_CH: Solubility of contaminant (kg/m^3, 1.1 for TCE and 0.15 for PCE)
16) W_CH: Molecular weight of contaminant (kg/mol, 0.13 for TCE and 0.166 for PCE)

17) W_OXD: Molecular weight of oxidant (kg/mol, 0.158 for $KMnO_4$)
18) Avtot: Source flux transect (m^2) – total vertical area of TZs. If entered as zero or negative, it will internally be computed based on the width and thickness of each TZ.
19) t0: ISCO beginning year (numeric year) – it is important when computing cost or calibrating ISCO parameters
20) duramax: ISCO maximum operation period (months)

Continuous ISCO injection generally recirculate effluents to increase the efficiency of operation. Two options of 'TypeCirc' are defined in this version. Option 1 maintains the total injected mass per time as a constant 'C_OXD*(q_in*Avert)' by adding additional oxidant (C_add) to recirculated effluent from the extraction wells. In Option 1, user will enter 'C_OXD', 'C_add', and 'q_in'. 'C_OXD' can be fixed or optimized.

Option 2, on the other hand, assumes the added mass per time is constant as 'C_OXD*(q_in*Avert)'. As 'C_OXD*(q_in*Avert)' is regardless with the oxidant concentration of effluent, 'Cadd' is not required (not used).

An example of ISCO parameters and variables for continuous injection is as follows (File name: XXX.inp)

```
Lines 1~14
15_name   prior     prior_sd  log?   tune?  synch?    LB      UB   % header
omitted: paramSource1 ~ paramEDEA1
 ~
paramISCO continuous for Source 1 with Ntz=2, Srind/k0 = 4.58E-6, GW & SL
iType   iCirc Onmon Offmon    OXmin SlnGWmw  SlnGWgp  SlnSLgp  SlnSLbo SlnOX
Ngwmin  OX2O2 O22CH Cl2CH     S_CH  W_CH     W_OXD    AVtot    t0     duramax
    1   1     4     6         500   0.5      2.0      2.0      2.0      0.25
    2   0.211 1     4         0.15  0.166    0.158    800      2014     36
1NODtot     2       0.3       1       3       0         0.6     6.64
2f_fast     0.15    0.3       1       3       0         0.045   0.5
3r_slow     0.02    0.3       1       3       0         6E-3    0.066
4Ntz        2       0         0       0       0         0       0
5fmt        1.35    0         0       0       0         0       0
6Fox        0.7     0         0       0       0         0       0
7Fsl/gw     2       0         0       0       0         0       0
8dtmon      90      0         0       0       0         0       0
9Nsmp_gp    0       0         0       0       0         0       0
10Nsmp_bg   0       0         0       0       0         0       0
11Srind/k0  4.58E-60          0       0       0         0       0
12GW_all    100     0         0       0       0         0       0
13SL_all    -999    0         0       0       0         0       0
14GW_TZ     100     0         1       2       0         10      100
15SL_TZ     -999    0         0       0       0         0       0
22alpha     0.5     0         0       2       0         0.05    0.5

% TZvar1
Ftz         1       0         0       0       0         0       0
Nmwo1       2       0         0       0       0         0       0
Nmw1        0       0         0       0       0         0       0
Ngp1        4       0         0       2       0         0.5     4.4
Nbg1        0       0         0       0       0         0       0
C_OX1       5000    0         1       2       0         1E3     30E3
% TZvar2
Ftz         1       0         0       0       0         0       0
Nmwo2       2       0         0       0       0         0       0
```

```
Nmw2          0       0          0       2       0          0       4.4
Ngp2          4       0          0       2       0          0.5     4.4
Nbg2          0       0          0       0       0          0       0
C_OX2         5000    0          1       2       0          1E3     30E3

% ISCOvar     TZ1     TZ2
1f_lost       0       0
2Area         1600    800
3Thick        10      10
4Width        80      40
5SL_avg       30875   5000
6SL_min       1E4     1E3
7SL_max       1E5     1E4
8q_in(m/d)    5       4     %based on XX PV for 4 months: this comment is skipped
9C_add(ppm)   20000   20000
10Mmax(kg)    8E5     4E5
11Fcap        1       1

costISCO1     Cost_gpsl_cont.dat
~
```

Example of a cost file ('costISCOgw.dat') is as follows. See Chapter 5 of the ER-2310 final report for the cost function. Unit cost parameters for the continuous injection ISCO source treatment model from cost sensitivity analysis results can be computed using the SCOToolkit Excel tool **ISCO unit cost calcs for continuous injection. xlsx** (Appendix A4).

```
Item        Cost($K)    Unc       Comments
Cbase       176         0         % Base fixed cost
Ciw         0           0         % IW installation/IW
Cmw         2.97        0         % new MW installation
Cmass       0.0055      0         % cost per kg
Cvol        0.02076     0         % cost per m^3
Cinj        0.04        0         % cost per m3/d (continuous injection)
Cevnt       0           0         % cost per monitoring event
Cgpsl0      0.9         0         % first GP soil sample $K/sample
Cgpsl1      0.3         0         % from second GP soil sample $K/sample
Cbgsl0      0.0         0         %
Cbgsl1      0.0         0         %
Cgwgp0      0.0         0         %
Cgwgp1      0.0         0         %
Cgwmw0      0.55        0         % cost per MW sample for first
Cgwmw1      0.0         0         %
Coxd        0.0         0         % cost per Oxidant monitoring
Cday        0.30        0         % cost per day
Cpen        5           0         % penalty cost per ppb exceeding
```

Note: The first line is for user information only and is not used by the program (but is required). From line 2 forward, spaces or tabs will be recognized as a delimiter. All text after the uncertainty column is for user comments and is not required.

3) Historical ISCO injection

Historical ISCO injection is a special module to consider periodic site reassessment. This module reads the concentrations and total liquid volume of oxidant that has been injected to each TZ by time. When 'ISCOtype' = 2 in 'Fixed [1,1]', SCOToolkit will read Table A1.9c for historical ISCO injection. Fixed [2×10] values are defined followed by two lines of note in Table A1-9c. All variables are defined in previous ISCO sections.

Definitions of fixed variables for ISCO historical injection

1) ISCOtype: Index for ISCO type; 0 = pulse injection, 1 = continuous injection, 2 = historical injection
2) dummy: Reserved for future ISCO update
3) dummy: Reserved for future ISCO update
4) dummy: Reserved for future ISCO update
5) dummy: Reserved for future ISCO update
6) dummy: Reserved for future ISCO update
7) dummy: Reserved for future ISCO update
8) dummy: Reserved for future ISCO update
9) dummy: Reserved for future ISCO update
10) dummy: Reserved for future ISCO update
11) iCal: Flag for calibrating parameters to ISCO effluent concentration (0 = no, 1 = yes). Concentration file name is listed in Line 13 in the project definition block.
12) OX2O2: Oxidant mass per O_2 equivalent moles (0.211 kg/mol O_2eq of $KMnO_4$ for PCE and 0.316 for TCE)
13) O22CH: O_2 equivalent moles per mole contaminant (1.5 for TCE and 1 for PCE)
14) Cl2CH: Chloride equivalent moles per mole contaminant (3 for TCE and 4 for PCE)
15) S_CH: Solubility of contaminant (kg/m^3, 1.1 for TCE and 0.15 for PCE)
16) W_CH: Molecular weight of contaminant (kg/mol, 0.13 for TCE and 0.166 for PCE)
17) W_OXD: Molecular weight of oxidant (kg/mol)
18) Avtot: Source flux transect (m^2) – total vertical area of TZs. If entered as zero or negative, it will internally be computed based on the width and thickness of each TZ.
19) dummy: Reserved for future ISCO update
20) duramax: ISCO maximum operation period (months)

It should be noted that if a calibration is performed for historical ISCO injection, a regular calibration (using transport solution) is not performed, and vice versa.

Table A1.9c. Variables for ISCO historical injection

Variable	Matrix	Definition	Unit
Fixed [2×10]	iscoType dummy dummy dummy dummy dummy dummy dummy dummy dummy iCal OX2O2 O22CH Cl2CH S_CH W_CH W_OXD Avtot dummy duramax		
NODtot	paramISCO(i,1)	Natural Oxygen Demand, 0.2~200 /kg soil (g oxidant/kg soil)	g/kg
f_fast	paramISCO(i,2)	NOD fast (instant) fraction to NODtot, 0.02~0.7	g/g
r_slow	paramISCO(i,3)	Rate coefficient of slow NOD, 0.01~1 (L/mmol $KMmnO_4$/day)	L/mmol/day
Ntz	paramISCO(i,4)	Number of Treatment Zone	ea
fmt	paramISCO(i,5)	Mass transfer enhancement factor ($=D_{ox}/(n_{ox/CH}*D_{CH})$. See Chapter 5 of the ER-2310 final report.	-

Srind/k0	paramISCO(i,6)	Ratio of Srind to k0, where Srind is the slope between permeability k (m^2) and MnO_2 concentration (mg/L) and k0 (m^2) is the intrinsic permeability before injection.	L/mg
ISCOinfo	path\file name	File name that contains historical injection and TZ information. If the information file is in the same directory, the path can be omitted (see the example cost file)	
CostISCO	path\file name	When isCost(1)=1, a cost file should be defined. If the cost file is in the same directory, the path can be omitted (see the example cost file)	

Example of historical ISCO input (5 TZs) is as follows (File name: XXX.inp).

```
~
Line 12 should be like: CONC   Y    N    Atlas_cal1.dat
~
15_name   prior     prior_sd  log?   tune?  synch?    LB      UB   % header
omitted: paramSource1 ~ paramEDEA1

paramISCO historical - This line is internally skipped
iType   dummy   dummy   dummy   dummy   dummy   dummy   dummy   dummy   dummy
iCal    OX2O2   O22CH   Cl2CH   S_CH    W_CH    W_OXD   Cl0     dummy   duramax
    2   0       0       0       0       0       0       0       0       0
    1   0.213   1.5     4       1.1     0.13    0.142   0       0       54
1NODtot     1           0.5     1    3    0     0.2     4
2f_fast     0.15        0       0    0    0     0       0
3r_slow     0.02        0.3     1    3    0     6E-3    0.066
4Ntz        5           0       0    0    0     0       0
5fmt        1.35        0       0    0    0     0       0
6Srind/k0   4.58E-6     0       0    0    0     0       0
Inj_His_info:    Atlas_history.dat
ISCO_Cost_file:  ISCOcost_hist.dat
```

Format for historical injection data and TZ information ('Atlas_history.dat')

TZ_j Repeat the block below with this head line 'TZ_j' as many as 'Ntz' in 'paramISCO'

Ninj	paramTZj(1)	Number of injection periods (events) to read for TZ_j	
1 2 ~ Ninj	paramTZj(1:Ninj,1:4)	(1) Start date (mm/dd/yyyy), (2) end date (mm/dd/yyyy), (3) average liquid injection rate (m^3/d) during injection period, and (4) average oxidant concentration (mg/L) during injection period. and Write (1)~(4) 'Ninj' lines.	

TZvar Include this head line (e.g., TZvar) before defining TZ variables below.

Area	VarISCO(1,1:Ntz)	Planar area of TZs	m^2
Thickness	VarISCO(2,1:Ntz)	Thickness of TZs	m
Width	VarISCO(3,1:Ntz)	Transverse width of TZs perpendicular to groundwater flow direction	m
Effluent	VarISCO(4,1:Ntz)	TZ effluent concentration from the extraction wells	µg//L
Eff/Inf	VarISCO(5,1:Ntz)	Average ratio of TZ effluent concentration to influent	-

Example file for historical injection and TZ information ('Atlas_history.dat') is as follows.

```
TZ1     % This line is read but will be ignored internally.
Ninj  2
1     7/1/2012      9/19/2012     100   17667
2     5/16/2013     8/1/2013      36    8774
TZ2
Ninj  1
1     5/16/2013     8/1/2013      33    8774
TZ3
Ninj  1
1     5/16/2013     7/19/2013     43    8774
TZ4
Ninj  3
1     7/19/2013     8/1/2013      9     8774
2     5/1/2014      8/1/2013      9     8774
3     7/19/2013     8/1/2013      9     8774
TZ5
Ninj  1
1     7/14/2014     9/12/2014     96    7066

TZvar    TZ1      TZ2      TZ3      TZ4      TZ5 -> This line is internally skipped.
Area     219.6    167.0    443.7    357.7    557.2
Thick    3.1      1.3      3.8      3.8      3.3
Width    15.2     15.2     15.2     15.2     15.2
Effppb   250.3    898.7    495.7    423.8    714.9
Eff/inf  1.7      1.7      1.7      1.7      1.7
```

Example of calibration data file ('Atlas_cal1.dat') defined in Line 12 is as follows.

```
TZid    Date          TCEppb     SlnC    Weight % This line is ignored internally.
1     7/12/2012      480.00     0.75    1
1     12/12/2012     2.00       0.75    1
1     3/6/2013       360.00     0.75    1
1     5/16/2013      610.00     0.75    1
1     9/18/2013      350.00     0.75    1
2     12/13/2013     430.00     0.75    1
2     2/28/2014      410.00     0.75    1
2     6/18/2014      400.00     0.75    1
2     9/16/2014      1.00       0.75    1
2     12/10/2014     1.00       0.75    1
3     6/24/2015      1.00       0.75    1
3     9/23/2015      1.00       0.75    1
3     12/18/2015     1.00       0.75    1
3     4/6/2016       1.00       0.75    1
3     6/29/2016      1.00       0.75    1
3     7/13/2012      570.00     0.75    1
3     12/12/2012     680.00     0.75    1
4     3/6/2013       380.00     0.75    1
4     5/16/2013      660.00     0.75    1
4     9/18/2013      820.00     0.75    1
4     12/12/2013     680.00     0.75    1
5     2/28/2014      480.00     0.75    1
5     6/18/2014      560.00     0.75    1
5     9/16/2014      820.00     0.75    1
5     12/12/2014     840.00     0.75    1
5     3/25/2015      450.00     0.75    1
```

Example of a cost file ('ISCOcost_hist.dat') is as follows.

```
Item       Cost($K)   Unc       Comments
C_all      108.163    0         % cost already paid
```

A1.7 Electron Donor Injection

A1.7.1 Reactive Barrier

The '**paramED1**' defines the parameters for reactive barriers that is usually installed immediate downgradient of contaminant sources. See Chapter 3 of the ER-2310 final report for detail description. Parameter sets should be defined as many as RBs (i.e., defined as 'EDtype' = 1) from upstream to downstream (Table A1.10).

Table A1.10. Parameters for Reactive Barrier (RB)

Variable	Matrix	Definition	Unit
RBsrc_num	RBvar{1}	Number of sources upgradient of RB through which they flow. If 'RBsrc_num' = -999 (or negative), the candidate sources will be identified internally based on the location of sources user defined.	-
RBsrc_ids	RBvar{2}(1, RBsrc_num)	List of source IDs counted in 'RBsrc_num'. If 'RBsrc_num'<0, the source IDs will be internally found.	-
ttRB	RBvar{3}(1, RBsrc_num) - reserved for future use	Maximum travel times from 'RBsrc_ids' to the monitoring well location of RB (waiting time to stop RB to consider the latest upstream source remediation. If 'RBsrc_num'<0, travel times will be internally computed).	years
CRB_locs	RBvar{4}(1:4) - reserved for future use	CRB_locs(1): location of a monitoring well for RB (1 = upgradient of the gallery, -1 = downgradient of the gallery, 0 = No monitoring) CRB_locs(2:4): Easting, northing, and depth of a monitoring well	- m
ERB	paramED1(i,1)	Efficiency of RB (from 0 to 1)	
t0	paramED1(i,2)	Starting date of RB	year
dtRB	paramED1(i,3)	Duration of operation in months (but days will be used internally).	months
xRB	paramED1(i,4)	Easting of the mid-point of RB	m
yRB	paramED1(i,5)	Northing of the mid-point of RB	m
LxRB	paramED1(i,6)	Length of RB measured toward the streamline	m
LyRB	paramED1(i,7)	Width of RB measured perpendicular to the streamline	m
Lztop	paramED1(i,8)	Distance to the top of RB from the water table	m
Lzbtm	paramED1(i,9)	Distance to the bottom of RB from the water table	m
a	paramED1(i,10)	1st order coefficient of the streamline of RB	-
b	paramED1(i,11)	2nd order coefficient of the streamline of RB	-
c	paramED1(i,12)	3rd order coefficient of the streamline of RB	-
alpha	paramED1(i,13)	Angle of initial flow direction for Gallery i (negative to clockwise). See Figure A1-1	deg
GridRB	path\file name	A file containing the grid points (E,N,Z) of computing contaminant flux pass a transect of RB. If the grid file is in the same directory of an input file, the path can be omitted.	
CostRB	path\file name	When isCost(1)=1, a cost file should be defined. If the cost file is in the same directory of an input file, the path can be omitted.	

An example of RB parameters and variables is as follows (File name: XXX.inp)

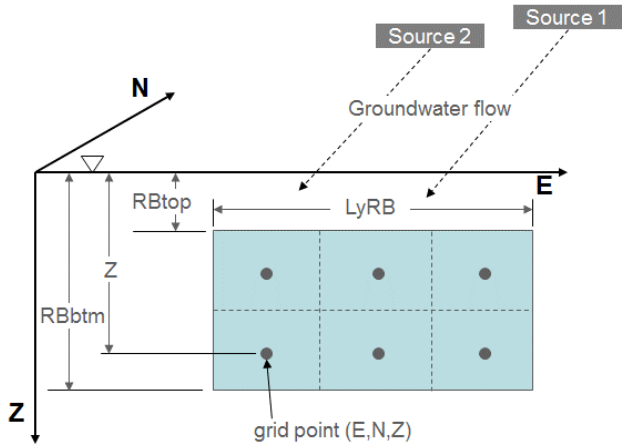


```
Lines 1~14
15_name   prior     prior_sd  log?   tune?  synch?    LB      UB   % header
omitted: paramSource1 ~ paramEDEA1

paramRB
RBsrc_num    2
RBsrc_ids    1  2
ttRB         not used currently
CRB_locs     not used currently
1ERB      0.5          0.3       0       1       0          0.1     0.99
2tRB0     2005.21      0         0       0       0          0       0
3dtRB     120          0         0       0       0          0       0
4E0_RB    57430.51     0         0       0       0          0       0
5N0_RB    503669.15    0         0       0       0          0       0
6LxRB     0.1          0         0       0       0          0       0
7LyRB     38           0         0       0       0          0       0
8RBtop    0            0         0       0       0          0       0
9RBbtm    4.88         0         0       0       0          0       0
10aRB     -0.0787      0         0       0       0          0       0
11bRB     0            0         0       0       0          0       0
12cRB     0            0         0       0       0          0       0
13alpRB   -4.5         0         0       0       0          0       0
GridRB    RB_grid.dat
costRB    costRB.dat
~
```

Efficiency is calibrated in this example.

Example of 'RB_grid.dat' to define grid points of a RB is as follows. Each line indicates (E,N,Z) of a grid point. Note the location of grid points should use the same coordinate system used for other locations (sources, EDs, MWs, etc).

```
57424.81   503676.75  1.00
57430.51   503669.15  1.00
57436.21   503661.54  1.00
57424.81   503676.75  3.00
57430.51   503669.15  3.00
57436.21   503661.54  3.00
```

Example of 'costRB.dat' is as follows. Note that cost values are site-specific.

```
Name      Cost($K)  Unc. Comments % This line is internally skipped.
Cfix_len  5         0.1  % fixed cost per width of RB ($K/m)
Cfix_etc  60        0.1  % other fixed cost per one ED site ($K/site)
Cfix_MW   10        0.1  % fixed cost per ED MW construction ($K/well)
Cop_yr    60        0.1  % general RB operating cost per RB ($K/yr)
Cop_etcS  0         0.1  % other RB operating cost ($K/yr/RB)
Cop_lenS  0.7       0.1  % annual operating cost per width ($K/m/yr)
Cop_matS  0.01      0.1  % oper. cost per kg injected material ($K/kg)
Cop_smp   2.5       0.1  % Monitoring cost per sample ($K/sample)
```

A1.7.2 Electron Donor Injection Gallery

The '**paramED3**' matrix summarized in Table A1.11 defines the properties and decision variables related to the operation of aqueous phase ED injection galleries. ED introduction is simulated as a soluble material. Injection of an ED gallery is assumed to commence on or after the date 'tWEDs' in field practices and simulations. If simulated injection rate is below a minimum injection rate ('MEDmin'), the ED gallery is inactive and cost is not counted.

Injection may be terminated at the earlier of (a) a specified elapsed duration, 'dtWEDs', or (b) when the annual average contaminant concentration in the ED gallery monitoring well (and specified compliance monitoring wells when defined in 'EDlag(2)') is less than 'CEDstp'. To determine termination of ED, the longest travel time from upstream EDs should be considered as 'EDtt_ij' that defines the estimated travel time (years) of injected ED from EDi to EDj, where EDi is always upgradient of EDj.

The number of sampling events per year for ED gallery monitoring wells, 'CEDsams', is used to adjust the level of noise for averaged measurements (noise diminishes linearly with $CEDsams^{-1/2}$).

Table A1.11 should be defined as many as ED galleries (i.e., defined as 'EDtype' = 3) *from upstream to downstream.*

Table A1.11. Parameters for ED injection Gallery.

Variable	Matrix	Definition	Unit
EDlag(1:2)		EDlag(1): Total number of upgradient ED galleries to monitor to determine termination of the current ED injection EDlag(2): Total number of compliance locations to monitor to determine termination of the current ED injection	- -
EDids		Gallery ED IDs defined in 'EDlag(1)'	-
EDtt_ij		Travel times from 'EDids' to the monitoring location (='CED_locs(3:4)') of ED	years
CED_locs(1:7 +EDlag(2))		CED_locs(1): location of a monitoring well for the ED gallery (1 = upgradient of the gallery, -1 = downgradient of the gallery, 0 = No monitoring, 3*=ED injection for historical or date-specific events)	-

		CED_locs(2): DNAPL source ID to which the ED gallery is injected to increase mass transfer (If 0, no enhanced source dissolution is simulated) CED_locs(3:5): Easting, northing, and depth of a monitoring well (depth measured from the water table)) – not required if ED is not monitored, i.e., 'CED_locs(1)'=0. CED_locs(6): ED transport solution type in 3D solution (1 = Flux, 0 = Resident).). If 2D solution is preferred, attach 2 for each option, e.g., 12 = 2D flux concentration, 02=2D resident concentration. CED_locs(7): Concentration below which waiting time is zero for the coupled compliance wells. CED_locs(8:7+EDlag(2)): ID numbers of compliance locations to monitor for terminating the current ED injection. Define as many as 'EDlag(2)'.	- m - µg/L -
JWEDs	paramED3(i,1)	Mass of injected aqueous phase ED per day	kg/d
fWEDs	paramED3(i,2)	Bio-available H-equivalent (kg) per mass (kg) of aqueous phase ED injected	-
tWEDs	paramED3(i,3)	Starting date of injection for the ED gallery, numeric year like 2017.5. If negative, 'tWEDs' is replaced by the earliest date listed in an external ED injection event file (see 'CostED/Hist' the last line of 'pareamED3').	year
dtWEDs	paramED3(i,4)	Duration of injection in months (but days will be used internally). Enter a negative number when injection terminates based on monitoring concentration ('CEDstp' in 'paramED3(i,16)') or past (or fixed) injection date).	months
xWEDs	paramED3(i,5)	Easting of the center of the ED gallery	m
yWEDs	paramED3(i,6)	Northing of the center of the ED gallery	m
LyWEDs	paramED3(i,7)	Width of The ED gallery measured perpendicular to the streamline	m
Lztop	paramED3(i,8)	Depth to the top of the ED gallery from the water table	m
Lzbtm	paramED3(i,9)	Depth to the bottom of the ED gallery from the water table	m
a	paramED3(i,10)	1st order coefficient of the streamline of the ED gallery	-
b	paramED3(i,11)	2nd order coefficient of the streamline of the ED gallery	-
c	paramED3(i,12)	3rd order coefficient of the streamline of the ED gallery	-
alpha	paramED3(i,13)	Angle of initial flow direction for the ED gallery (negative to clockwise). See Figure A1-1.	deg
MEDmin	paramED3(i,14)	Minimum injection rate per width to initiate the ED gallery. See Chapter 3 of the ER-2310 final report.	kg/d
CEDstp	paramED3(i,15)	Target concentration of a contaminant measured at a monitoring well to terminate the ED gallery (if dtWEDs is a decision variable, CEDstp will be disregarded and vice versa).	µg/L
CEDsmp	paramED3(i,16)	Number of samples per well per year for the ED gallery monitoring	ea
CostED/Hist	path\file name	When 'isCost(1)=1', a cost file name should be defined. If the cost file is in the same directory of an input file, the path can be omitted (see the example cost file)	

		- If 'CED_locs(1)' =3 and 'run_mode(1)'=1, i.e., calibration, it is a file name for historical injection events. See an example of gallery injection history. - If 'CED_locs(1)' =3 and 'run_mode(1)'=2, -2, or 3, user should define both a cost_file name and an injection event file. Any dummy string is needed for cost_file although cost is not simulated.	

Note) *: This option may not be available in a web-based preprocessor.

An example format of 'EDids' is as follows. When 'EDlag(1)' = 3 for designated upstream ED galleries 1, 2, and 4, 'EDids' will be '21␣ 22␣24' where the first digit '2' denotes that the upgradient remedial practice is ED injection (remedial actions are discriminated by 1 for source zone treatment, 2 for ED injection, and 3 for P&T), the second digit (1, 2, and 4) denotes the ID for the upgradient ED gallery, and '␣' denotes a space or tab.

An example of ED parameters and variables is as follows (File name: XXX.inp)

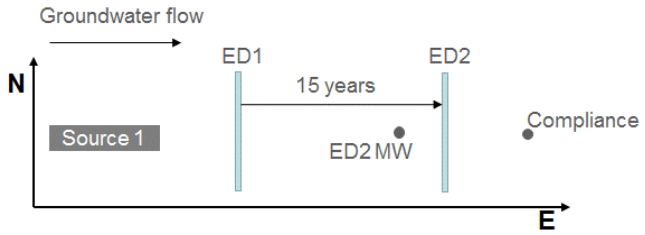


```
Lines 1~14
15_name   prior     prior_sd  log?   tune?  synch?    LB      UB   % header
Omitted: paramSource1 ~ paramEDEA1
paramSZR, paramTSR, or paramISCO - omitted if defined
paramED1
~
paramED2
ED_lag1   1  0  (consider one upstream remedial practice and no compliance)
ED_id1    21   (consider upgradient ED1)
ED_tt1    15   (wait 15 years after ED1 terminates to determine ED2 status)
CED_locs1   1       0    1423.4 962.96 5    1    5
1J_WEDs1    100       0       1       2       0       0.01    300
2f_WEDs1    0.26      0       0       0       0       0       0
3t_WEDs1    2007      0       1       2       0       2006.99   2015
4dt_WEDs1   -999      0       0       0       0       0       0
5x_WEDs1    1448.3    0       0       0       0       0       0
6y_WEDs1    960.78    0       0       0       0       0       0
7Ly_WEDs1   200       0       0       0       0       0       0
8Lztop      0         0       0       0       0       0       0
9Lzbtm      30        0       0       0       0       0       0
10a         -0.0787   0       0       0       0       0       0
11b         0         0       0       0       0       0       0
12c         0         0       0       0       0       0       0
13alp       4.5       0       0       0       0       0       0
14MEDmin1   0.01      0       0       0       0       0       0
15Num_MWs1  1         0       0       0       0       0       0
16CEDstps1  5         0       1       2       0       1       100
17CEDmin1   5         0       0       0       0       0       0
18CED_sams1 3         0       0       2       0       0.5     4.5
costED    costED2.dat
```

Example of ‘costED2.dat’ file is as follows.

```
Name      Cost($K)  Unc. Comments
Cfix_len  3.3       0.1  % fixed cost per length of gallery ($K/m)
Cfix_etc  55        0.1  % other fixed cost per one ED site ($K/site)
Cfix_MW   10        0.1  % fixed cost per ED MW construction ($K/well)
Cop_yr    61.1      0.1  % general ED operating cost per ED ($K/yr)
Cop_etcS  0         0.1  % other ED operating cost ($K/yr/gallery)
Cop_lenS  0.733     0.1  % annual operating cost per length ($K/m/yr)
Cop_matS  0.0074    0.1  % oper. cost per kg injected material ($K/kg)
Cop_smp   2.5       0.1  % ED monitoring cost per sample ($K/sample)
```

Note: As the ‘Unc.’ column is specified as 0.1, each cost will be randomly generated between 0.9 and 1.1 times ‘Cost($k)’ for MC simulations.

When ‘CED_locs(1)’ = 3, users should define a historical event file. In this case, the last line of ‘paramED’ is defined as ‘costED/Hist event-EDs.dat’ when ‘run_mode(1)’=1 for calibration and ‘costED/Hist costED2.dat event-EDs.dat’ for other run modes requiring cost calculation or just forward run. An example of ‘event-EDs.dat’ file is as follows

```
t_beg       t_end       JED(kg/d)   %it is PICT1. This line is skipped.
7/27/2006   7/30/2006   0.329
4/9/2008    4/29/2008   0.365
10/22/2009  11/20/2009  0.401
4/26/2011   5/13/2011   0.789
9/12/2014   11/3/2014   0.090
3/7/2016    5/10/2016   0.015
6/1/2017    -999*       -999**
```

Note: 1) The first line is skipped internally but required; 2) *: ‘t_end’ is determined by performance monitoring or user- defined ‘dt_WEDs’ internally; and 3) **: ‘JED(kg/d)’ is determined by user input or optimization. However, ‘-999’ is not allowed for JED when ‘run_mode(1)=1’ for calibration.

A1.8 Dissolved Plume Monitoring for Compliance

The matrix '**paramMonitor**' with dimension [num_complnc, 10] in Table A1.12 defines protocols for compliance monitoring. Note that the locations of compliance wells are not necessarily same as P&T monitoring wells. More than one compliance wells may be defined.

Table A1.12. Variables for compliance monitoring

Variable	Matrix	Definition	Unit
monLAG		Number of upgradient remediation actions to consider lag time for starting/stopping compliance monitoring i	-
monLAGids		Remediation types (1=source removal (SZR, TSR, ISCO), 2 = ED (RB or ED gallery), and 3 = P&T) and their sequential IDs to consider lag time (e.g., second TSR =12, third ED gallery =23, first P&T= 31)	-
monTT		Travel time from each remediation type to compliance location i	years
monLAY	monLay(1:4)	monLAY(1): solution type (0 = resident concentration, 1 = flux concentration) monLAY(2): compliance rule (type 'RCL' or 'EXV') monLAY(3): confidence limit when using 'RCL' (e.g., 95) monLay(4): dimension of transport solution for compliance (optional). If not entered, it follows 'run_mode(3)'. This option may not be available in the web-based preprocessor.	- - % -
Emon	paramMonitor(i,1)	Easting of the compliance location	m
Nmon	paramMonitor(i,2)	Northing of the compliance location	m
Zmon	paramMonitor(i,3)	Depth of the compliance location	m
monstart	paramMonitor(i,4)	Monitoring start date as a numeric year	year
monstop	paramMonitor(i,5)	Maximum monitoring date (= simulation termination) as a numeric year	year
MCL	paramMonitor(i,6)	Target cleanup level for the compliance location	μg/L
lookback	paramMonitor(i,7)	Lookback period to confirm no further action (NFA) or non-compliance (typically 5 years of lookback)	years
dtavg	paramMonitor(i,8)	Averaging period for concentration values (annual average is widely used, i.e., 'dtavg' = 1)	years
monFRE	paramMonitor(i,9)	Monitoring frequency (quarterly = 4 events/year)	events/year
t_pnlty	paramMonitor(i,10)	The date by which compliance criteria must be met (penalty date)	year
CostMon	path\file name	When 'isCost(1)'=1, a cost file should be defined. If the cost file is in the same directory, the path can be omitted (see the example cost file)	

To achieve the "no further action (NFA)" status, all compliance wells must achieve their target levels and maintain below these levels before the date computed by MAX[remediation termination dates + their travel time to compliance locations+ user-specified lookback period for regression]. If non-compliance criteria for one or more wells occur at any time after a specified penalty date ('t_pnlty'), the simulation still continues but a penalty cost is accrued to that

simulation. If MAX[‘monLAGids’ ending date + ‘monTT’ + ‘lookback’] exceeds the maximum simulation date (‘monstop’), the penalty cost will be incurred when 1) MAX[‘monLAGids’ ending dates] exceeds ‘monstop’ or 2) the modeled non-reacted concentration at MAX[‘monLAGids’ ending date + ‘monTT’] is greater than the target level.

One of two compliance rules can be selected: (1) the regression confidence limit (‘RCL’) rule, which requires the upper confidence limit (UCL) of measured concentrations over a lookback period (lookback) to be less than a specified target level (e.g., MCL) for compliance, or (2) the extreme value (‘EXV’) rule, which requires the maximum annual average of measured values over a lookback period to be less than MCL for compliance. For the ‘RCL’ method, the confidence limit probability level (‘monLAY(3)’) is also specified as percent (%). Details on compliance rules are found in Chapter 7 of the ER-2310 final report.

An example of compliance monitoring parameters and variables is as follows (File name: XXX.inp).

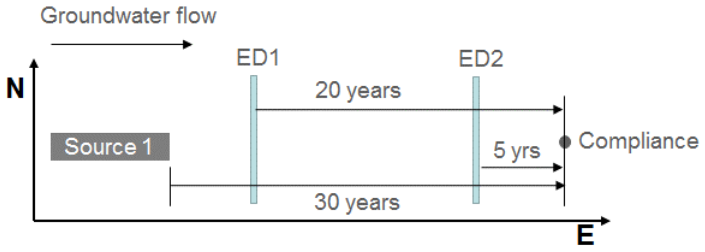


```
Lines 1~14
15_name   prior     prior_sd  log?   tune?  synch?    LB      UB   % header
Omitted: paramSource1 ~ paramEDEA1
Omitted: paramSZR1, paramED1, paramED2

paramMon1
num_lag1  3
lag_src1  11   21   22
lag_tt1   30   20   5
lay_mon1  1    RCL     95
1X_mon1      1996.2    0       0       0       0       0       0
2Y_mon1      912.84    0       0       0       0       0       0
3Z_mon1      5         0       0       0       0       0       0
4monstart1   2007      0       0       0       0       0       0
5monstop1    2050.99   0       0       0       0       0       0
6MCL1        5         0       0       0       0       0       0
7lookback1   5         0       0       0       0       0       0
8dtavg1      1         0       0       0       0       0       0
9monfre1     4         0       0       0       0       0       0
10t_pnlty1   2015.99   0       0       0       0       0       0
costMON   costMON.dat
```

Compliance monitoring costs (e.g., ‘costMON.dat’) can be defined as follows.

```
Cost name Cost($K)  Uncertainty    Comments
Ccap_well 2.97      0  %Cost.MON(1); % $K/MW (one time charge)
Ccap_etc  0         0  %Cost.MON(2); % $K for misc capital cost
Csamp     0.55      0  %Cost.MON(3); % $K/sample
Cann      2.5       0  %Cost.MON(4); % $K/year (annual cost)
Cpnlty    1E6       0  %Cost.MON(5); % Penalty cost ($K)
```

The model internally finds a monitoring start date for compliance location i using MIN[‘monSRC’ ending date + ‘monTT’, ‘EDids’ ending date’+’EDtt’] if ‘monstart’ is negative. For computational efficiency, the model starts evaluating a decision-making when the current date is on or later than [‘t_penalty’ – ‘lookback’ – ‘dtavg’ + 1]. This is meaningful because no-decision cannot be made before ‘t_penalty’ and decision need at least [‘lookback’+‘dtavg’] years of data.

The last monitoring date is determined by MIN[‘monstop’, NFA date if present]. The compliance rule allows the model to wait until MAX[‘t_pnlty’, ‘monSRC’ ending date + ‘monTT’ + ‘lookback’] before determining compliance status as far as a monitored statistics (‘RCL’ or ‘EXV’ value) meets a target level before or on ‘t_penalty’.

A1.9 Pump and Treat (P&T) Systems

The ‘**paramPT**’ matrix with dimension [‘num_pt’, 10] as shown in Table A1.13 defines P&T systems. Since the model does not explicitly simulate P&T systems, the P&T systems defined in ‘paramPT’ do not affect computed contaminant concentrations. P&T system are assumed to be initiated to control downgradient plume migration. It is assumed that no other remediation systems and no compliance wells are located downgradient of the P&T systems, and that the effects of the P&T system on upstream concentrations are negligible. The location of a P&T monitoring well upgradient of the potential P&T system is specified to control implementation (commencement) and/or termination of the P&T system. Also, any other potential remediation systems that are upgradient of the P&T system and their travel times to the P&T monitoring well should be specified if they need to be considered.

‘PTstart’ is user specified and effective in counting capital cost into net present value when ‘PTstart’ is later than earliest ‘monstart’. This means that existing P&Ts were already in operation (e.g., capital cost paid or financed) before the date of current remediation system. If PTstart is entered as negative, ‘PTstart’ is determined internally by MAX[termination dates of upstream remediation to consider + their travel times to the P&T(ptTT)].

The decision information is first reported after ‘lookPT’ years since ‘PTstart’ and the P&T system is operated until the P&T termination criteria is met, which is based on ‘EXV’ or ‘RCL’ method. Monitoring data is averaged over ‘tavgPT’ years and monitoring uncertainty is reduced by 1/sqrt(‘ptFRE’).

Table A1.13. Variables for P&T monitoring

Variable	Matrix	Definition	Unit
ptLAG		Number of upstream remediation actions to consider lag time for starting/stopping P&T system	-
ptLAGids		Remediation types (1=source removal (SZR, TSR, ISCO), 2 = ED (RB or ED gallery), and 3 = P&T) and their sequential IDs to consider lag time (e.g., second TSR =12, third ED gallery =23, first P&T= 31) upstream of the P&T system	-
ptTT_ij		Travel time from each lag source j to monitoring well	years
ptLAY	ptLAY(1:3)	ptLAY(1): solution type (0 = resident concentration, 1 = flux concentration) ptLAY(2): compliance rule (‘RCL’ or ‘EXV’)	- -

		ptLAY(3): confidence limit when using RCL (e.g., 95) ptLAY(4): dimension of transport solution for compliance (optional). If not entered, it follows 'run_mode(3)'. This option was not coded in the web-based preprocessor	% -
Ept	paramPT (i,1)	Easting of the P&T monitoring well for P&T system	m
Npt	paramPT (i,2)	Northing of the P&T monitoring well for P&T system	m
Zpt	paramPT (i,3)	Depth of the P&T monitoring well for P&T system	m
PTstart	paramPT (i,4)	Start date of P&T as a numeric year	year
PTstop	paramPT (i,5)	End date of P&T as a numeric year	year
MCLpt	paramPT (i,6)	Target concentration at P&T monitoring location to terminate P&T system	μg/L
lookPT	paramPT (i,7)	Lookback period to make P&T start/stop decisions	years
tavgPT	paramPT (i,8)	Duration for averaging concentration	years
ptFRE	paramPT (i,9)	Monitoring frequency per year	events/year
CostPT	path\file name	When 'isCost(1)'=1, a cost file should be defined. If the cost file is in the same directory, the path can be omitted (see the example cost file)	

The parameters and variables of P&T are identical to 'paramMonitor' except 'paramPT' does not have 't_penalty'. P&T system operation and monitoring costs (e.g., 'costPT.dat') may be, for example, as follows.

```
Cost name Cost($K)  Uncertainty   Comments
CPT_cap   200.97    0 % $K (one time charge)
CPT_ann   10        0 % $K/year operating cost
```

A2. How to Install/Run

A2.1 Installation of a standalone compiled executable file

1. Make a new folder with your preferred name.
2. Download the following two files in the folder created in Step 1.
   (1) Download Matlab Runtime (a set of libraries to run a complied standalone Matlab file) 'MCR_R201Xb_win64_installer.exe' (or 2014 later version) directly from Mathworks https://www.mathworks.com/products/compiler/mcr.html.
   (2) Download 'SCOToolkit_exe.zip' from http://scotoolkit.csuohio.edu/download.php and unzip.
3. Install Matlab Runtime ('MCR_R201Xb_win64_installer.exe').
4. Run 'SCOToolkit.exe'.

A2.2 Use of source codes

1. Make a new folder using your preferred name and location.
2. Download 'SCOToolkit_codes.zip' from http://scotoolkit.csuohio.edu/download.php and unzip into the folder in Step 1.
3. Run 'main.m'.

Note: Parallel computing is implemented only when the source codes were executed in the Matlab Command directly.

A2.3 Input Preparation

The model reads space- or tab- delimited ASCII files for input file and data. The model requires several files depending on the specific problem considered. It is efficient to manage projects by assigning meaningful names to input files. The main input file [*.inp] specifies which files should be loaded to simulate the defined project as shown in Tables A1.1 and A2.1. An output file [*.out] will be automatically generated with the same name as the main input file.

Table A2.1. Example of input files.

Input files	Contents	Remark
*.inp	A main input file that defines the project, model parameters, decision variables, and other auxiliary files (see Table A1.1).	Required
*.rlz	Includes parameter realizations generated based on parameter covariance. A [*.rlz] file is usually generated after calibration and its file name is same as the main input file. User can modify the file name after that.	Optional
*.gen	Includes parameter realizations generated randomly based a probability distribution function. A [*.gen] file is usually generated when user specified as 'Tune' = 3 for specific parameters, and its file name is same as the main input file. If it is generated by setting 'Tune'=3, it follows normal distribution when 'Log'=0 and log-normal distribution when 'Log'=1.	Optional
*con.dat	Includes observed concentration data for calibration or list of well locations and dates to simulate. See the file format in Table A2.3.	Optional
*flx.dat	Includes observed source flux data for calibration or list of source numbers and dates to simulate. See the file format in Table A2.4.	Optional
*mas.dat	Includes observed source mass removal data for calibration or list of source numbers and dates to simulate. See the file format in Table A2.5.	Optional

Note: User can define any file extension for any input file.

The first block of the [*.inp] file includes problem definition (see Table A1.1) followed by parameters and decision variables as shown Table A2.2.

Table A2.2. Order of modules of parameters and remediation in [*.inp].

Order	Name	Number of blocks	Remark
0	Project_Define	1	Project definition (Table A1-1)
1	paramSource	num_sources	
2	paramSourceGeom	num_sources	
3	paramAquifer	1	
4	paramED0	1	
5	paramEDEA	1	
6	paramSZR	num_SZRs	Define only when 'isSZR' = 0, 1, or 2
7	paramED	num_EDs	
8	paramMonitor	num_complnc	
9	paramPT	num_PT	

Note: Shaded blocks are mandatory and required for any simulation.

Measured contaminant concentration, source flux, and source mass removal data are entered as shown in Tables A2.3 to 2.5. FORTRAN expression formats are presented for clarity. When real measured data are entered, the model uses them as observed values during calibration. However, when they are set to -999, the model will ignore the values and simply generate predictions for

the specific dates and locations listed in [*.dat]. Mass remaining data will be automatically generated for the dates and sources specified in the mass removal data file. Note that all columns should have headers and all values in rows should be separated by space(s) or tab(s). Therefore, 'Well_ID' and 'mm/dd/yyyy' should not include a space, except 'Note' which is optional and skipped internally. The header line will be internally skipped while loading.

Table A2.3. Format of concentration data.

Well_ID	E	N	Z	mm/dd/yyyy	Conc	SlnC0	Navg	Weight	Type	Note (option)
string	real	real	real	string	real	real	real	real	real	string

Note: Weight: 1 for non-weighted observation (default). The weight is a numeric value to represent relative importance compared to 1, which is used to compute the revised SlnC = SlnC0/{Weight*sqrt(Navg)} internally, where Navg is the number of data used in averaging Conc. See Chapter 6 of the ER-2310 final report for further detail.

Type: 0 and 1 is for the groundwater concentration of resident and flux, respectively (unit: μg/L).

Type: 2, 3, and 4 is for the soil concentration of average, mobile, and immobile zone, respectively (unit: μg/kg)

Example of concentration file is as follows (File name: XXX.dat).

```
IDW     E(m)       N(m)       Z(m)    Date         TCEeq   SlnC N  W    T  Note
DM329D  125401.83  193972.0   4.72    11/10/1995   28.06   0.75 1  1.00 1  before ED
DM329D  125401.83  193972.0   4.72    3/1/1996     56.42   0.75 1  1.00 1
DM329D  125401.83  193972.0   4.72    7/23/1996    38.71   0.75 1  1.00 1
```

Note: 1) The header line (1st line) will be skipped internally (but required).
2) Any comment written in the 'Note' column will be skipped internally (not required).

Table A2.4. Format of source flux data.

Source_ID	mm/dd/yyyy	Flux	SlnJ	Weight	Note (option)
real	string	real	real	real	string

Note: The unit of 'Flux' is kg/day.

Example of flux file is as follows (File name: XXX.flx).

```
src_id date         flux(kg/d)  Sln  Weight Note
1      11/01/2003   0.754       0.1    1    source 1
2      11/01/2003   0.323       0.1    1    source 2
3      04/01/2006   0.420       0.1    1    source 3 passive
```

Note: 1) The header line (1st line) will be skipped internally (but required).
2) Any comment written in the 'Note' column will be skipped internally (not required).

Table A2.5. Format of source mass removal data.

Source_ID	mm/dd/yyyy	Mass_removal	SlnM	Weight	Note (option)
real	string	real	real	real	string

Note: The unit of 'Mass_removal' is kg. If actual mass removal data are written, they will be used as calibration data for source mass, requiring proper 'SlnM' and 'Weight' valuses.

Example of mass removal file is as follows (File name: XXX.mas).

```
IDsrc   Date        Mass_rmv    SlnM    W  Note
1       6/30/2000   -999.00     0       0
1       6/30/2005   -999.00     0       0
1       6/30/2010   -999.00     0       0  Ignore this note & next empty line.

2       6/30/2000   -999.00     0       0
2       6/30/2005   -999.00     0       0
2       6/30/2010   -999.00     0       0

3       6/30/2000   -999.00     0       0
3       6/30/2005   -999.00     0       0
3       6/30/2010   -999.00     0       0
```

Note: 1) The header line (1st line) will be skipped internally (but required).
2) This example is just to print the accumulated amount of mass removed. Therefore, 'Mass_rmv' is -9999 and thus 'SlnM' and 'W' are not used although read.
3) Any comment written in the 'Note' column will be skipped internally (not required).

The possible outputs after simulating SCOToolkit are presented in Table A2.6. The generated output files are dependent of on the tasks defined in the [*.inp] files. Examples of Table A2-6 are presented later. Mass removal is accumulated after the first source removal date and thus mass remaining data is the mass which remains after source removal for the specified dates and sources. Note that plots for source flux, mass removal, and mass remaining will add up all sources for each defined time step and the plots are exported as [*.png] and [*.eps] files. Note that the output file name ('*') is taken from the main input file name excluding its extension '*.inp'. The column "Note" in Table A2.5 will be skipped while loading. User may write one line note with unlimited length.

Table A2.6. List of generated output files.

Output files	Contents	Remark
*.out	Results after the model runs	Default
*.rlz and *.rlzh	Results for parameter realization after calibration	Default in calibration
*.gen	Results for uncorrelated (random) parameter generation	User-request
*_flx.out	Results for mass flux when specified in the [*.inp]	User-request
*_rmv.out	Results for mass removal specified in the [*.inp]	User-request
*_rmn.out	Results for mass remaining specified in the [*.inp]	User-request
*_corr.png (and .eps)	Correlation plot between the observed and simulated concentration	Default in calibration
*_con.png (and .eps)	Concentration curve from single or multiple runs with 95 and 99% confident limits	User-request
*_flxsum.png (and .eps)	Total summation of mass fluxes curve from single or multiple runs with 95 and 99% confident limits	User-request
*_rmv.png (and .eps)	Total mass removal curve from single or multiple runs with 95 and 99% confident limits	User-request
*_cost.png (and .eps)	Cost histogram from single or multiple runs with median and average	Default in computing cost

A2.3 Contact Information

1) Users may send questions or error messages to scodnapl@gmail.com.

2) If errors are encountered, it will be helpful to send the input files used.

A3. Example Input and Output Files

Example files for parameter calibration, design optimization, and simple forward runs are posted in http://scotoolkit.csuohio.edu/download.php. Examples include the demonstration remediation methods such as ED, TSR, and ISCO.

A4. Provided Excel Worksheets to Facilitate Estimation of SCOToolkit Inputs

The following Excel worksheets, which facilitate estimation of SCOToolkit inputs and real-time decision making, may be downloaded at http://scotoolkit.csuohio.edu/download.php.

ISCO treatment termination decisions using real time data.xlsx
This workbook implements real time termination decisions for ISCO source treatment using soil and/or groundwater sample data for multiple monitoring zones (MZ) within multiple treatment zones (TZ) using a rigorous statistical approach based on soil and/or groundwater sample data in a manner that provides consistent decision reliability at scales ranging from individual monitoring zones, to groups of monitoring zones (aka, treatment zones) to site-wide.

ISCO unit cost calcs for continuous injection.xlsx
This worksheet computes unit cost parameters for the continuous injection ISCO source treatment model from cost sensitivity analysis results.

ISCO unit cost calcs for pulsed injection.xlsx
This worksheet computes unit cost parameters for the pulsed injection ISCO source treatment model from cost sensitivity analysis results.

Source function parameter estimation from field data.xlsm
The purpose of this workbook is to calculate prior estimates of source parameters M_{cal}, J_{cal}, β and t_{cal} from measured source zone groundwater concentration data and soil data for input into the SCOToolkit calibration tool. These values and uncertainty estimates can be used as prior estimates for transport model calibration to monitoring well data over time.

Streamline calculation.xlsx
This worksheet fits linear or polynomial streamline functions to digitized streamline data for contaminant source locations, ED injection galleries, or reactive barriers.

Thermal treatment model calibration.xlsx
This workbook calibrates thermal model parameters to measured mass recovery data for single or multiple pdf recovery functions.

Thermal treatment termination decisions using real time data.xlsx
This workbook enables real time termination decisions to be made for thermal source treatment that allows for multiple monitoring zones (MZ) using a rigorous statistical approach based on soil and/or mass recovery measurements to provide consistent decision reliability at multiple scales. The worksheet also calibrates thermal model parameters to measured recovery data.

Thermal treatment unit cost calcs.xlsx
This worksheet computes unit cost parameters for the source zone thermal treatment model from cost sensitivity analyses.

Appendix B. List of Publications Related to Project ER-2310

Technical Reports

1. ER-1611 Final Report 'Practical Cost-Optimization of Characterization and Remediation Decisions at DNAPL Sites with Consideration of Prediction Uncertainty', https://www.serdp-estcp.org/content/download/11363/141040/file/ER-1611-FR.pdf
2. ER-2310 Final Report 'A Practical Approach for Remediation Performance Assessment and Optimization at DNAPL Sites for Early Identification and Correction of Problems Considering Uncertainty', available in Jan 2018.

Publications

1. Kim, U., J.C. Parker, and R.C. Borden (2018) Stochastic Cost-optimization and Risk Assessment of In-situ Chemical Oxidation for Dense Nonaqueous Phase Liquid (DNAPL) Source Remediation. *Stochastic Environmental Research and Risk Assessment*. In revision.
2. Parker, J., U. Kim, A. Fortune, S. Griepke, and J. Galligan (2017) Data Analysis and Modeling to Optimize Thermal Treatment Cost and Performance. *Ground Water Monitoring and Remediation* 37(1): 51-66. DOI: 10.1111/gwmr.12199.
3. Parker, J. and U. Kim (2015) An Upscaled Approach for Transport in Media with Extended Tailing due to Back-Diffusion Using Analytical and Numerical Solutions of the Advection Dispersion Equation. *Journal of Contaminant Hydrology* 182: 157-172. DOI: 10.1016/j.jconhyd.2015.09.008.
4. Kim, U., J. Parker, P. Kitanidis, M. Cardiff, X. Liu, and J. Gillie (2013) Stochastic Cost Optimization of DNAPL Remediation - Field Application. *Environmental Modeling & Software* 46: 12-20. DOI:10.1016/j.envsoft.2012.05.003.
5. Parker, J., U. Kim, P. Kitanidis, M. Cardiff, X. Liu, and G. Beyke (2012) Stochastic Cost Optimization of DNAPL Remediation - Method Description and Sensitivity Study. *Environmental Modeling & Software* 38: 74-88. DOI:10.1016/j.envsoft.2012.05.002.
6. Lee, J., X. Liu, P.K. Kitanidis, U. Kim, J. Parker, A. Bloom, and R. Lyon (2012) Cost Optimization of DNAPL Remediation at Dover Air Force Base Site. *Ground Water Monitoring & Remediation* 32(2): 48-56. DOI: 10.1111/j1745–6592.2011.01382.x.
7. Liu, X., J. Lee, P.K. Kitanidis, J. Parker, and U. Kim (2012) Value of Information as a Context-specific Measure of Uncertainty in Groundwater Remediation. *Water Resources Management* 26(6): 1513-1535. DOI: 10.1007/s11269-011-9970-3.
8. Parker, J., U. Kim, M. Widdowson, P. Kitanidis, and R. Gentry (2010) Effects of Model Formulation and Calibration Data on Uncertainty in Predictions of DNAPL Source Dissolution Rate. *Water Resources Research* 46: W12517. DOI: 10.1029/2010WR009361.
9. Parker, J., U. Kim, P. Kitanidis, M. Cardiff, and X. Liu (2010) Stochastic Cost Optimization of Multi-strategy DNAPL Site Remediation. *Groundwater Monitoring & Remediation* 30(3): 65-78. DOI: 10.1111/j1745–6592.2010.001287.x.

10. Cardiff, M., X. Liu, P.K. Kitanidis, J. Parker, and U. Kim (2010) Cost Optimization of DNAPL Source and Plume Remediation Under Uncertainty Using a Semi-Analytic Model. *Journal of Contaminant Hydrology* 113(1-4): 25-43. DOI: 10.1016/j.jconhyd.2009.11.004.

Presentations

1. Kim, U. and J. Parker (2016) Periodic application of stochastic cost optimization methodology to achieve remediation objectives with minimized life cycle cost. Fall Meeting, *American Geophysical Union*, Dec 12-16, San Francisco, CA.
2. Kim, U., J. Parker, and R.C. Borden (2015) Cost and Performance Assessment of In-Situ Chemical Oxidation for Intermittent and Continuous Oxidant Injection. Fall Meeting, *American Geophysical Union*, Dec 14-18, San Francisco, CA.
3. Kim, U. and J. Parker (2015) Cost Optimization of Groundwater Remediation Considering Prediction Uncertainty. Cleveland Water Alliance Regional Innovation Showcase, *AWT 2015 Training Seminars*, April 8-12. Cleveland, OH.
4. Parker, J.C., U. Kim, R. Borden, and A. Fortune (2015) An Integrated Approach to Multi-Strategy DNAPL Remediation Considering Uncertainty Using Stochastic Cost Optimization. *REMTEC 2015 Meeting*, March 2-4, Westminster, CO.
5. Kim, U., J. Parker, and R.C. Borden (2014) Optimal Design and Operation of In-Situ Chemical Oxidation Using Stochastic Cost Optimization Toolkit. Fall Meeting, *American Geophysical Union*, Dec 15-19, San Francisco, CA.
6. Parker, J.C., U. Kim, R. Borden, A. Fortune, D. Becker, P. Hunter, and D. Waddill (2014) A Practical Approach for Remediation Performance Assessment and Optimization at DNAPL Sites for Early Identification and Correction of Problems. *Chlorinated Solvents in Groundwater Technical Exchange Meeting*, Dec 10-12, Fort Myers, Arlington, VA.
7. Kitanidis, P., J. Parker, U. Kim, X. Liu, and J. Lee (2010) Context-Specific Quantification of Uncertainty, Value of Information, and Total-Cost Optimization of DNAPL Site Remediation. *SERDP Annual Meeting*, Nov 30-Dec 2, Washington D.C.
8. Parker, J., U. Kim, P. Kitanidis, and X. Liu (2010) Practical Cost-Optimization of Remediation and Monitoring Decisions at DNAPL Sites with Consideration of Prediction Uncertainty. *SERDP Annual Meeting*, Nov 30-Dec 2, Washington D.C.
9. Parker, J., P. Kitanidis, U. Kim, X. Liu, M. Cardiff, and M. Widdowson (2009) DNAPL Source Strength vs. Time Model Formulation, Calibration and Uncertainty. *SERDP Annual Meeting*, Dec 1-3, Washington D.C.
10. Parker, J., P. Kitanidis, U. Kim, X. Liu, and M. Cardiff (2009) Cost Optimization of DNAPL Site Remediation with Consideration of Prediction Uncertainty. *SERDP Annual Meeting*, Dec 1-3, Washington D.C.